Marqueurs pathologiques et pistes thérapeutiques dans la Sclérose Latérale Amyotrophique Sporadique

Philippe Codron

THESE DE DOCTORAT

UNIVERSITE D'ANGERS
COMUE UNIVERSITE BRETAGNE LOIRE

ÉCOLE DOCTORALE N° 605
Biologie Santé
Spécialité : Neurosciences

Par
Mr Philippe CODRON

Marqueurs Pathologiques et Pistes Thérapeutiques dans la Sclérose Latérale Amyotrophique Sporadique

Pathological Markers and Therapeutic Prospects in Sporadic Amyotrophic Lateral Sclerosis

Thèse présentée et soutenue à Angers, le 3 Octobre 2019
Unité de recherche : UMR CNRS 6015 INSERM 1083

Rapporteurs avant soutenance :

M. William CAMU,
Professeur des Universités, Université de Montpellier, France.

M. Jean-Philippe CAMDESSANCHE,
Professeur des Universités, Université de St Etienne, France.

Composition du Jury :

M. Jean-Pierre JULIEN (Président du Jury),
Professeur des Universités, Université Laval, Qc, Canada.

Mme Mathilde DUCHESNE,
Maître de conférences, Université de Limoges, France.

M. William CAMU,
Professeur des Universités, Université de Montpellier, France.

M. Jean-Philippe CAMDESSANCHE,
Professeur des Universités, Université de St Etienne, France.

M. Christophe VERNY,
Professeur des Universités, Université d'Angers, France

Directeur de thèse : M. Arnaud CHEVROLLIER,
Maître de conférences (HDR), Université d'Angers, France.

Co-encadrant : M. Julien CASSEREAU,
Maître de conférences, Université d'Angers, France.

UNIVERSITE BIOLOGIE BRETAGNE SANTE LOIRE

université angers

THESE DE DOCTORAT

UNIVERSITE D'ANGERS
COMUE UNIVERSITE BRETAGNE LOIRE

ÉCOLE DOCTORALE N° 605
Biologie Santé
Spécialité : Neurosciences

Par
Mr Philippe CODRON

Marqueurs Pathologiques et Pistes Thérapeutiques dans la Sclérose Latérale Amyotrophique Sporadique

Pathological Markers and Therapeutic Prospects in Sporadic Amyotrophic Lateral Sclerosis

Thèse présentée et soutenue à Angers, le 3 Octobre 2019
Unité de recherche : UMR CNRS 6015 INSERM 1083

Rapporteurs avant soutenance :

M. William CAMU,
Professeur des Universités, Université de Montpellier, France.

M. Jean-Philippe CAMDESSANCHE,
Professeur des Universités, Université de St Etienne, France.

Composition du Jury :

M. Jean-Pierre JULIEN (Président du Jury),
Professeur des Universités, Université Laval, Qc, Canada.

Mme Mathilde DUCHESNE,
Maître de conférences, Université de Limoges, France.

M. William CAMU,
Professeur des Universités, Université de Montpellier, France.

M. Jean-Philippe CAMDESSANCHE,
Professeur des Universités, Université de St Etienne, France.

M. Christophe VERNY,
Professeur des Universités, Université d'Angers, France

Directeur de thèse : M. Arnaud CHEVROLLIER,
Maître de conférences (HDR), Université d'Angers, France.

Co-encadrant : M. Julien CASSEREAU,
Maître de conférences, Université d'Angers, France.

Remerciements

ENGAGEMENT DE NON PLAGIAT

Je soussigné Mr Philippe CODRON déclare être pleinement conscient que le plagiat de documents ou d'une partie d'un document publiée sur toutes formes de support, y compris l'internet, constitue une violation des droits d'auteur ainsi qu'une fraude caractérisée.

En conséquence, je m'engage à citer toutes les sources que utilisées pour écrire ce rapport ou mémoire.

A Angers le 03/06/2019

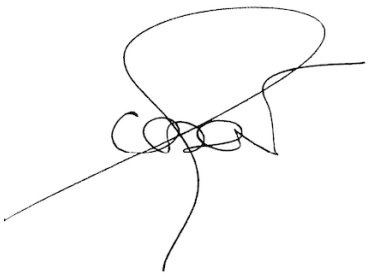

AVANT-PROPOS

Ce travail de thèse est l'aboutissement de trois années passionnantes dédiées à la recherche en neurosciences sur la Sclérose Latérale Amyotrophique (SLA), s'inscrivant dans un cursus médical et scientifique initié en 2011 au CHU d'Angers. Dès le début de mon internat au sein du service de Neurologie du Pr Christophe Verny, mon intérêt s'est porté vers les maladies neuromusculaires, sujet de ma thèse de médecine dirigée par le Dr Julien Cassereau. J'ai dans ce cadre été formé au diagnostic et à la prise en charge des neuropathies périphériques, des myopathies et de la SLA dans le centre de référence des maladies neuromusculaires et le centre SLA du CHU d'Angers, second centre SLA créé en France en 1991 par le Pr Jean Émile.

La réalisation d'une année de Master 2 en 2014 (Université Pierre et Marie Curie, Sorbonne Université, Paris) a permis mon initiation aux neurosciences et à la méthode scientifique. J'ai dans ce cadre effectué un travail de recherche au sein de l'équipe Mitolab (Dr Guy Lenaers) de l'UMR CNRS 6015 INSERM 1083 (Dr Daniel Henrion) à Angers, structure dédiée à l'étude des anomalies du métabolisme énergétique et de la dynamique mitochondriale dans les maladies neurodégénératives. Encadré par le Dr Arnaud Chevrollier, j'ai été formé aux techniques de culture cellulaire et de microscopie live et en immunofluorescence en réalisant un travail de modélisation du réseau mitochondrial de fibroblastes de patients atteints de maladie de Charcot-Marie-Tooth 2A.

La fin de mon internat a été consacrée à l'apprentissage des techniques de préparation et de lecture de prélèvements nerveux, musculaires et cérébraux au sein du service de neuropathologie et neurobiologie du CHU d'Angers, dirigé par le Dr Franck Letournel. L'activité de ce service fondé en 1986 par le Pr Frédéric Dubas est consacrée au diagnostic biologique et histologique des maladies neuromusculaires et neurodégénératives. La recherche y occupe également une place importante, la biocollection du service comptant plus de 500 cerveaux et moelles épinières de patients provenant de Maine-et-Loire, Loire-Atlantique, Mayenne, Sarthe et Indre-et-Loire, dont 50 patients atteints de SLA.

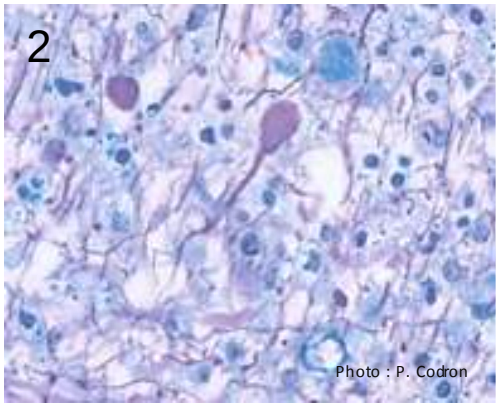

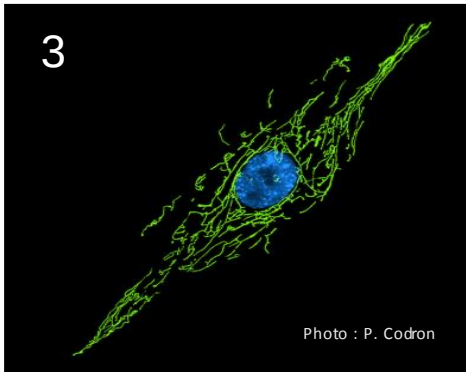

(1) Centre Hospitalo-Universitaire d'Angers. Le service de Neurologie dirigé par le Pr Christophe Verny, comprend - entre autres unités - un centre de référence des maladies neuromusculaires et un centre SLA (Dr Julien Cassereau). (2) Exemple d'analyse de tissu cérébral après coloration effectuée au sein du service de neurobiologie et neuropathologie clinique dirigé par le Dr Franck Letournel. (3) L'étude en vidéo-microscopie de l'architecture et de la dynamique mitochondriale du réseau mitochondrial après marquage des mitochondries (en vert) et du noyau (en bleu) est l'une des techniques utilisées au sein de l'UMR CNRS 6015 INSERM 1083 (4).

Ma thèse d'université sur la SLA a débuté en 2016. Ce travail a été dirigé par le Dr Arnaud Chevrollier et co-encadré par le Dr Julien Cassereau. Ma première année (2016-2017), financée par l'université d'Angers (Médaille d'Or) et le CHU d'Angers (Appel d'Offre interne), a été consacrée à l'analyse de l'ultrastructure et du métabolisme de fibroblastes de patients atteints de SLA sporadique. Ce travail m'a permis de conforter mes connaissances en biologie cellulaire et en physique optique, et de contribuer à la mise en place des techniques de microscopie super-résolution STORM au sein du laboratoire. Ce projet a également permis de réunir plusieurs chercheurs de notre laboratoire, cliniciens et biologistes, autour d'une thématique commune, la Sclérose Latérale Amyotrophique, et d'établir des partenariats nationaux et internationaux avec des équipes de recherche travaillant sur la maladie.

Ma seconde année de thèse (2017-2018) financée par un poste d'Accueil Inserm, a été pour moi l'occasion d'effectuer une mobilité internationale au sein d'une équipe de recherche prestigieuse travaillant sur différentes stratégies thérapeutiques pour le traitement de la SLA. Grâce à l'aimable invitation du Pr Jean-Pierre Julien (Institut CERVO, Qc, Canada) j'ai eu la chance de contribuer à la mise au point d'une nouvelle approche thérapeutique basée sur l'administration d'une immunothérapie ciblant la protéine TDP-43. Durant cette année j'ai pu m'initier à l'expérimentation animale, tout en confortant mes compétences en préparation et analyse de tissu cérébral et médullaire en immunofluorescence. Cette mobilité au Québec a également été l'occasion de vivre une année riche en expériences, découvertes et rencontres.

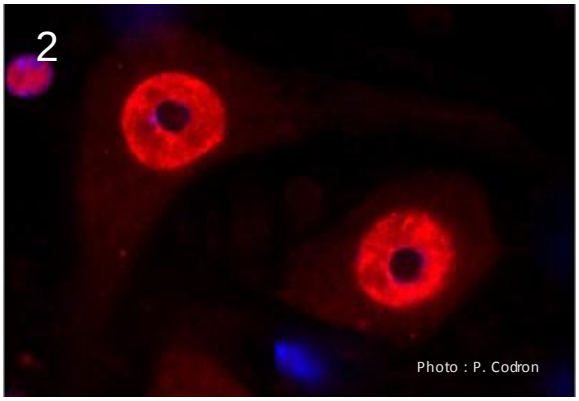

(1) Centre de Recherche CERVO, Québec, Canada. L'axe Neurosciences Intégratives et Thérapies Expérimentales est dirigé par le Pr Jean-Pierre Julien. (2) L'étude de la protéine TDP-43 (en rouge) au sein des motoneurones spinaux par immunofluorescence est l'une des techniques utilisées pour évaluer l'efficacité des nouvelles approches thérapeutiques testées sur modèles animaux transgéniques.

De retour en France au sein de l'équipe Mitolab - UMR CNRS 6015 – INSERM 1083 pour ma troisième année de thèse (2018-2019) également financée par un poste d'accueil Inserm, j'ai pu initier un travail de recherche portant sur la mise au point d'une technique d'imagerie super-résolutive par microscopie STORM sur tissu cérébral et médullaire, dans le but d'améliorer la caractérisation des lésions histologiques présentées par les patients atteints de SLA. Ce projet à l'interface entre la neurologie, la neuropathologie et l'imagerie cellulaire, est le résultat de la mise en commun des connaissances acquises tout au long de mon cursus. Ce travail a permis de créer un partenariat avec l'équipe du Pr Charles Duyckaerts (Institut du Cerveau et de la Moelle épinière, INSERM U1127, CNRS UMR7225, Université Pierre et Marie Curie, Sorbonne Universités, Paris, France), et de conforter les collaborations nationales et internationales existantes.

Ce manuscrit s'ouvre sur une introduction générale, suivie de trois chapitres correspondant aux trois projets menés aux cours de cette thèse. Chaque partie fait l'objet d'une introduction spécifique, puis les objectifs du travail et le contexte de sa réalisation sont présentés succinctement. Les principaux résultats sont ensuite discutés et des perspectives de recherche sont proposées. L'ensemble de ce travail fait enfin l'objet d'une conclusion générale.

SOMMAIRE

CHAPITRE 3 : PISTES THERAPEUTIQUES.

Injection intrathécale d'une immunoglobuline monoclonale dirigée contre le domaine RRM1 de la protéine TDP-43

UNIVERSITE BIOLOGIE
BRETAGNE SANTE
LOIRE

université
angers

INTRODUCTION

INTRODUCTION

1. LA SCLEROSE LATERALE AMYOTROPHIQUE

La sclérose latérale amyotrophique (SLA), ou maladie de Charcot, est une pathologie neurodégénérative affectant les motoneurones du cortex moteur, des noyaux du tronc cérébral, et de la corne antérieure de la moelle épinière (Kiernan et al., 2011). La maladie touche entre 5 et 10 personnes pour 100 000 dans le monde, près de 7 000 patients en sont atteints en France (Chió et al., 2013 ; Marin et al. 2014). Dans 90% des cas, la SLA est dite sporadique (sSLA), sans cause étiologique connue. Toutefois, certains gènes de susceptibilité (plus de 120 identifiés à ce jour) tels que *SMN* (survie des motoneurones) *VEGF* (vascular endothelial growth factor), *ANG* (angiogénine), *APOE* (Apolipoproteine E) ou encore *NFH* (neurofilament heavy chain) pourraient augmenter le risque de survenue de SLA (Corcia et al., 2014 ; Wang MD et al., 2017). De même, certains facteurs environnementaux tels qu'un traumatisme du système nerveux central (SNC), une activité physique soutenue, un tabagisme actif, un déficit en vitamine D, ou encore une exposition aux métaux lourds, pesticides ou solvants, pourraient favoriser le développement de la maladie (Camu et al., 2014 ; Wang et al., 2017). La survenue de la SLA sporadique serait ainsi conditionnée par l'association d'une susceptibilité polygénique et l'exposition à différents facteurs de risque environnementaux. Dans 10% des cas, la SLA est héréditaire (fSLA), conséquence de la transmission de mutations pathogènes portant sur des gènes connus depuis de nombreuses années (*SOD1*) ou de découverte plus récente (*C9orf72, TARDBP, FUS*).

La SLA débute en moyenne à l'âge de 60 ans. Les patients atteints de la maladie présentent un déficit moteur diffus d'aggravation progressive, associé à des troubles de la phonation et de la déglutition. Le diagnostic de la SLA est avant tout clinique et électrophysiologique, reposant sur l'existence d'une atteinte motoneuronale dans différents territoires spinaux, bulbaires et corticaux (EFNS Task Force, 2012). La médiane de survie des patients est de 20 à 36 mois après le début des symptômes (Chiò et al., 2009). Il existe une grande variabilité phénotypique chez les patients, qui porte sur plusieurs aspects cliniques. La localisation centrale ou périphérique de l'atteinte peut tout d'abord varier, avec un spectre allant d'une atteinte exclusivement centrale appelée sclérose latérale primitive (SLP), aux formes périphériques pures appelées atrophies musculaires progressives (AMP). De même la topographie du déficit moteur peut différer d'un patient à l'autre, les symptômes pouvant

prédominer au niveau des membres (formes spinales) ou à l'étage oro-pharyngé (formes bulbaires), avec toutefois une épargne oculomotrice et sphinctérienne constante. Des signes cliniques non moteurs peuvent également être présents, tels que des troubles cognitifs (près de 50% des patients), une dysautonomie, un syndrome extrapyramidal, des symptômes douloureux ou encore des troubles de l'équilibre (Phukan et al., 2011 ; Swinnen et Robberecht, 2014). Plus généralement, 30 à 60% des patients peuvent présenter un syndrome hypermétabolique, défini par une augmentation des dépenses énergétiques de repos, à l'origine d'un déclin accéléré des fonctions motrices et de la survie (Jésus et al., 2018 ; Steyn et al., 2018). Enfin la durée d'évolution de la maladie est très variable d'un patient à l'autre, pouvant aller de quelques mois à plusieurs dizaines d'années (Swinnen et Robberecht, 2014).

Le seul traitement médicamenteux disponible à ce jour en France pour ralentir l'évolution de la maladie est le Riluzole, décrit pour diminuer de 38,6 % le taux de décès des patients à 1 an et allonger de la durée de vie sans trachéotomie (Bensimon et al., 1994 ; Lacomblez et al., 1996). La prise en charge repose par ailleurs en grande partie sur la mise en place de traitements symptomatiques et fonctionnels (antalgie, kinésithérapie, ergothérapie, orthophonie, ventilation non invasive), permettant une amélioration de la survie et de la qualité de vie des patients (Radunović et al., 2007). La création de centres de référence à partir de 1990 a permis d'harmoniser le diagnostic et la prise en charge des patients en France.

2. NEUROPATHOLOGIE ET PISTES ETIOPATHOGENIQUES

Les mécanismes physiopathologiques à l'origine de la neurodégénérescence motoneuronale observée dans la SLA restent encore incertains malgré les avancées considérables opérées dans le champ de la recherche en neuroscience ces vingt dernières années. Les premières hypothèses ont émergé à partir de l'observation des lésions présentes au sein du système nerveux central des patients décédés de la maladie (Gray et al., 2013).

2.1. Observations Générales

L'examen macroscopique de l'encéphale et de la moelle prélevés post mortem chez les patients atteints de SLA met en évidence une atrophie des circonvolutions précentrales, un effacement des pyramides bulbaires, ainsi qu'une diminution du calibre de la moelle épinière (Figure 1a). Ces

observations sont associées à une atrophie des nerfs crâniens moteurs et des racines spinales ventrales, plus prononcée aux étages correspondant aux signes cliniques.

L'étude microscopique des coupes histologiques du cortex de l'aire précentrale retrouve une raréfaction des neurones pyramidaux de la couche V (cellules de Betz). Aux niveaux bulbaire et médullaire, une dégénérescence du faisceau cortico-spinal peut être présente, traduisant l'atteinte des motoneurones corticaux (Figure 1b). A ces étages, une raréfaction des motoneurones périphériques peut également être observée, au niveau de la corne antérieure de la moelle et des noyaux moteurs du tronc cérébral. Les neurones restants apparaissent basophiles et atrophiques, témoignant d'une souffrance cellulaire pré-apoptotique, ou hypertrophiques et ballonnés avec en leur sein des inclusions hyalines éosinophiles appelées corps de Bunina (denses) ou inclusions Skein-like (plus diffuses et réticulées) (Figure 1c). Ces lésions de neurodégénérescence sont accompagnées d'une activation astrocytaire et microgliale réactionnelle (Figure 1d,e). Il n'existe pas au niveau du tissu musculaire des patients de signe pathologique spécifique de la SLA : un regroupement de fibres anguleuses et de petite taille peut être observé, témoin de la dégénérescence des neurones périphériques.

La répartition topographique de la perte motoneuronale est relativement bien corrélée aux manifestations cliniques présentées par les patients (Gray et al., 2013). Ainsi, l'atteinte sera plus prononcée au niveau du tronc cérébral et de la moelle épinière chez les patients atteints de formes bulbaires et spinales, et plus marquée au niveau du cortex moteur chez les patients présentant majoritairement des symptômes pyramidaux. De même, les noyaux oculomoteurs du tronc cérébral et le noyau sacré d'Onufrowicz sont généralement préservés, reflet de l'absence d'atteinte oculomotrice et sphinctérienne observée dans la maladie. Enfin, chez les patients présentant des symptômes non-moteurs associés, des lésions de neurodégénérescence similaires peuvent être retrouvées au niveau du néocortex des régions préfrontales, des tracti cérébelleux, du mésencéphale ou encore des noyaux végétatifs.

Si l'ensemble de ces signes anatomopathologiques traduit l'existence d'une atteinte neurodégénérative affectant préférentiellement les neurones moteurs encéphaliques et médullaires, ils ne permettent toutefois pas de préjuger des mécanismes à l'origine de la perte neuronale.

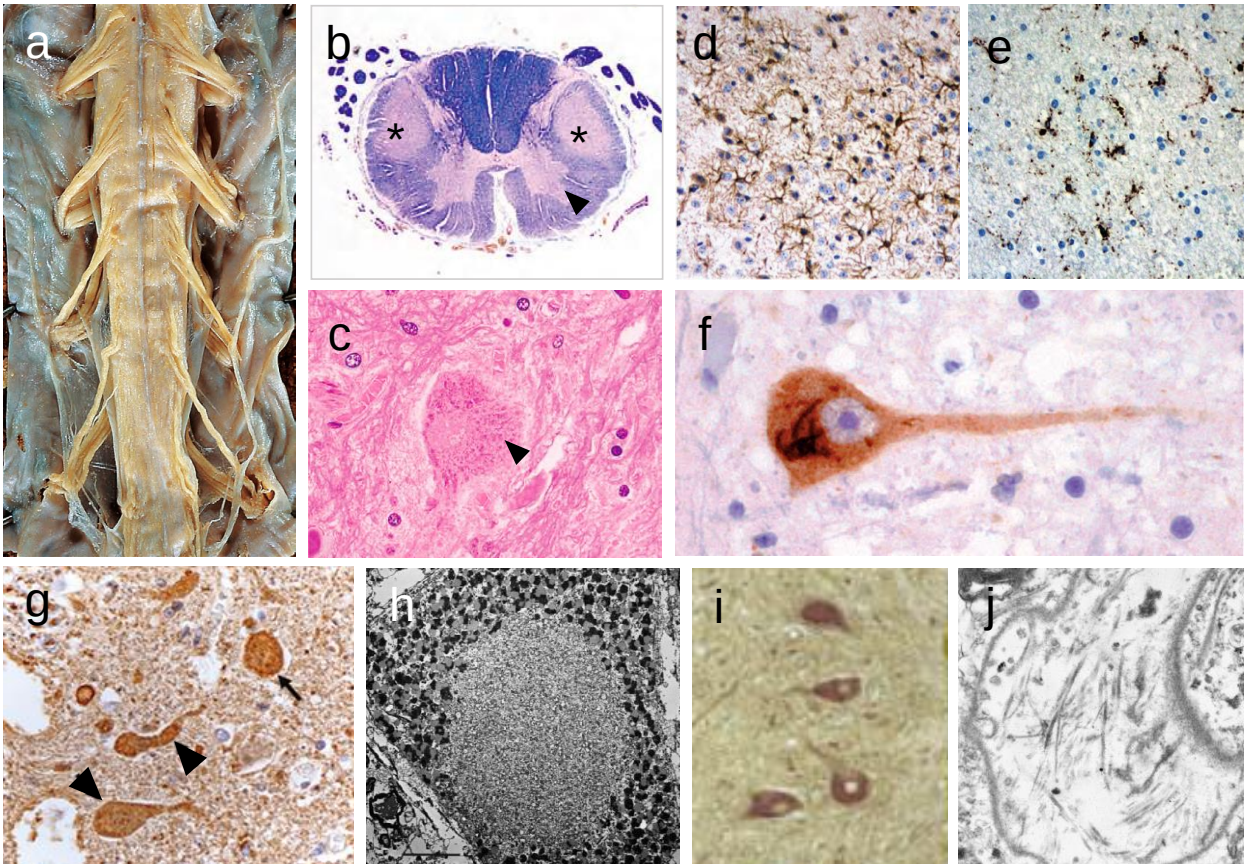

Figure 1. Marqueurs histopathologiques de la Sclérose Latérale Amyotrophique. (a) Étude macroscopique d'une moelle cervicale de patient atteint de SLA, révélant une diminution du calibre de la moelle associée à une atrophie des racines antérieures. (b) L'examen microscopique de la moelle épinière retrouve à faible grossissement une dégénérescence des tracti pyramidaux latéraux (astérisques), ainsi qu'une perte motoneuronale au niveau de la corne antérieure (pointe de flèche). (c) Les motoneurones restants étudiés en coloration Hématéine-Éosine apparaissent hypertrophiques, avec au sein de leur cytoplasme des inclusions hyalines éosinophiles (pointe de flèche). (d,e) La perte motoneuronale est accompagnée d'une astrocytose (d) et d'une microgliose (e), révélées par immunohistochimies dirigées contre les protéines GFAP et Iba1. (f) Les motoneurones corticaux et médullaires présentent au sein de leur cytoplasme des inclusions marquées positivement en immunohistochimie dirigée contre l'ubiquitine, traduisant la présence d'agrégats protéiques. (g) L'étude des neurofilaments permet d'en observer l'accumulation au sein des corps cellulaires des neurones (pointes de flèche), mais également au sein de segments axonaux ballonnés appelés sphéroïdes (flèche) traduisant une perturbation du transport axonal. (h) Analyse au microscopie électronique à transmission (MET) d'un motoneurone révélant une fragmentation du réseau mitochondrial. (i) Immunohistochimie dirigée contre la 3-nitrotyrosine, marqueur du stress oxydant, mettant en évidence une élévation de ce dernier au sein des motoneurones médullaires. (j) Étude de la matrice extra-cellulaire d'une section de moelle épinière de patient atteint de SLA en microscopie électronique à transmission : les fibres de collagène sont orientées de façon anarchique et forment des agrégats hétérogènes. (Sources Images : Beal et al., 1997 ; Ono et al., 1998 ; Sasaki et al., 2007 ; Ellison et al., 2012 ; Codron et al., 2016).

2.2. Observations spécifiques : émergence des premières pistes

Les avancées opérées ces 20 dernières années dans le champ de l'imagerie cellulaire ont permis de progresser dans notre compréhension des mécanismes étiopathogéniques impliqués dans la SLA, grâce à la caractérisation de lésions spécifiques de la maladie.

2.2.1. Maintenance protéique

La dégradation des protéines altérées, mal repliées ou agrégées est une fonction essentielle pour les cellules non proliférantes telles que les neurones. Des agrégats de protéines ubiquitinylées peuvent être observés au sein du cytoplasme des neurones de patients atteints de certaines pathologies neurodégénératives telles que la maladie d'Alzheimer et la maladie de Parkinson, traduisant un dépassement des mécanismes de maintenance protéique neuronale dans ces maladies. L'aspect ballonné des motoneurones des patients atteints de SLA et la présence d'inclusions hyalines cytoplasmiques ont conduit à suspecter l'existence de mécanismes similaires dans la maladie.

En condition physiologique, les protéines ou agrégats protéiques à dégrader au sein d'une cellule son marqués par un signal de reconnaissance constitué par l'adjonction de plusieurs molécules d'ubiquitines par les enzymes E1, E2, E3. Les protéines marquées par une chaîne d'au moins quatre molécules d'ubiquitine sont dirigées vers l'une des deux principales voies de dégradation en fonction de leur nature et de leur taille (Komatsu et al.,2007 ; Tanaka et al., 2014).

Les peptides et protéines de taille intermédiaire sont conduits au protéasome, complexe enzymatique cytosolique dont la fonction principale est la dégradation des protéines mal repliées, dénaturées ou en fin de vie. Ce complexe possède en son centre une cavité cernée par quatre anneaux, formant un espace clos pour la dégradation des protéines par ses protéases (Figure 2a).

Les structures plus volumineuses telles que les polypeptides, agrégats protéiques, macromolécules ou organites, sont quant à elles éliminées par autophagie guidée par les récepteurs LC3 et P62, Optineurine et TBK1. Ce processus est initié par la constitution d'une vacuole appelée autophagosome par une double membrane phospholipidique (phagophore), qui capte les constituants du cytoplasme à dégrader. L'autophagosome fusionne ensuite avec un lysosome, vésicule dédiée aux mécanismes de dégradation riche en hydrolases actives à pH acide (lipases, protéases, nucléases) (Figure2b).

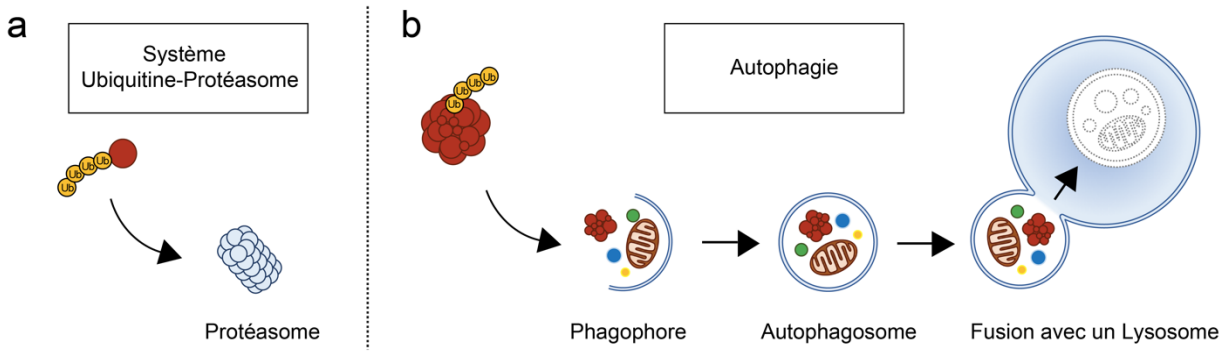

Figure 2. Principales voies de dégradation protéique au sein d'une cellule en condition physiologique. (a) Les protéines de taille intermédiaire sont marquées par ubiquitination (Ub) et dirigées vers le protéasome, complexe polypeptidique dédié à l'élimination des protéines anormales ou en fin de vie. (b) Les macromolécules, agrégats protéiques et fragments d'organites plus volumineux sont quant à eux captés lors de la constitution d'autophagosomes pour permettre leur dégradation après fusion avec un lysosome. (P. Codron)

Le marquage des inclusions hyalines présentes au sein des motoneurones des patients atteints de SLA par immunohistochimie dirigée contre l'ubiquitine a fait émerger l'hypothèse d'un dépassement des voies de l'homéostasie protéique dans la maladie, à l'origine de l'accumulation d'agrégats cytotoxiques (Figure 1f) (Neumann et al., 2006). Un travail complémentaire de review sur l'homéostasie protéique et le rôle de la protéine ubiquiline 2 dans la SLA est reporté en Annexe (Travail Complémentaire n°1, Renaud et al., 2019)

2.2.2. Anomalies du Cytosquelette

Le cytosquelette des neurones est composé de trois principales structures, classées selon leur diamètre : les microtubules (15 nm), les filaments intermédiaires (10 nm) et les microfilaments d'actine (6 nm). Les filaments intermédiaires (FI) sont les éléments du cytosquelette les plus abondants au sein des neurones matures. Ils sont composés de différentes sous-unités protéiques codées par des gènes distincts : α-internexine, peripherine, neurofilament light chain (NFL), neurofilament medium chain (NFM), et neurofilament heavy chain (NFH). La composition des FIs (sous unités) et leurs modifications post traductionnelles varient selon le type de neurone, leur localisation (centrale ou périphérique) et leur maturité. Ces deux éléments déterminent leurs propriétés structurelles et métaboliques (interactions protéiques) au sein de la cellule. Les FIs contribuent à l'organisation de l'architecture cellulaire, à la croissance radiale des axones et au trafic intracellulaire et axonal.

Les analyses en immunohistochimie portant sur les filaments intermédiaires des motoneurones de patients atteints de SLA ont révélé l'existence d'une désorganisation et d'une accumulation de ces derniers au sein du corps cellulaire des neurones (Munoz et al., 1988 ; Troost et al., 1992). Ces anomalies étaient également présentes au niveau de segments axonaux appelées sphéroïdes, traduisant une altération du trafic intracellulaire et axonal (Figure 1g). S'il est difficile de déterminer si les altérations de l'architecture du cytosquelette et du transport axonal sont une cause ou une conséquence du stress motoneuronal observés dans la SLA, ces anomalies participent indiscutablement aux processus de neurodégénérescence à l'origine de la maladie. Un travail complémentaire de review portant sur l'implication des neurofilaments dans la physiopathologie de la SLA est disponible en Annexe (Travail Complémentaire n°2, Codron et al., 2016).

2.2.3. Métabolisme énergétique mitochondrial

Les mitochondries sont des organites intracellulaires tubulaires constitués d'une membrane externe et d'une membrane interne, délimitant deux compartiments, l'espace inter-membranaire et la matrice mitochondriale. Elles possèdent leur propre génome, l'ADN mitochondrial (ADNmt), codant pour des sous unités de protéines mitochondriales, des acides ribonucléiques ribosomiques et des acides ribonucléiques de transfert. Toutefois les protéines mitochondriales sont en grande majorité codées par le génome nucléaire puis acheminées vers les mitochondries.

La principale fonction des mitochondries est la production d'énergie sous forme d'adénosine triphosphate (ATP). Le catabolisme des nutriments (glucides, acides aminés et acides gras) et le cycle de Krebs fournissent les substrats nécessaires au fonctionnement des quatre complexes protéiques de la chaîne respiratoire au niveau de la membrane interne pour permettre la synthèse d'ATP par l'ATP synthase (Figure 3a).

Au sein des cellules, les mitochondries sont organisées en réseau dynamique, dont la morphologie et la distribution varient selon le type cellulaire et les conditions métaboliques (Griparic et Van der Bliek, 2001). L'architecture du réseau repose sur l'équilibre entre deux processus fonctionnels : la fusion mitochondriale qui favorise les échanges nucléiques et protéiques entre les mitochondries, et la fission mitochondriale qui permet l'élimination de fragments mitochondriaux non fonctionnels, le plus souvent par autophagie, alors appelée mitophagie (Karbowski et Youle, 2003) (Figure 3b-d). Les mitochondries sont par ailleurs en mouvement constant au sein d'une cellule, se déplaçant le long des microtubules via les protéines de la famille des kinésines et des dynéines. Ce transport

permet de répartir le réseau mitochondrial de façon homogène afin de répondre aux demandes énergétiques de la cellule. Ce processus est capital pour les neurones compte tenu de leurs nombreux prolongements : les mitochondries sont transportées le long des microtubules de façon antérograde du corps cellulaire vers les synapses afin d'apporter l'énergie dans les parties les plus distales de l'axone, puis retournent vers le soma par transport rétrograde pour être régénérées ou dégradées (Miller et Sheetz, 2004).

Plus généralement, il existe une relation directe et bidirectionnelle entre la structure du réseau mitochondrial et la fonction énergétique (Koopman et al., 2005 ; Pich et al., 2005 ; Benard et al., 2007). Ainsi, l'architecture du réseau mitochondrial d'une cellule est un indicateur de son état métabolique, la survenue d'un stress mitochondrial primitif ou secondaire conduisant à la fragmentation du réseau et à l'induction des voies de l'apoptose.

Les motoneurones, ayant une demande énergétique élevée et de nombreux prolongements, sont particulièrement sensibles aux perturbations du métabolisme et de la dynamique mitochondriale. Des altérations fonctionnelles mitochondriales ont été mises en évidence au sein des neurones moteurs périphériques de la moelle épinière des patients atteints de SLA, avec en particulier une diminution d'activité enzymatique des complexes de la chaine respiratoire mitochondriale (Borthwick et al., 1999 ; Wiedemann et al., 2002). Ces anomalies sont associées à une fragmentation du réseau mitochondrial des motoneurones de la corne antérieure des patients, observable en microscopie électronique à transmission (MET), probable conséquence d'un stress cellulaire ou mitochondrial (Figure 1h) (Sasaki et al., 2007). Enfin, la désorganisation du cytosquelette des motoneurones et les anomalies du transport axonal participent assurément aux altérations de la dynamique mitochondriale observée chez les patients.

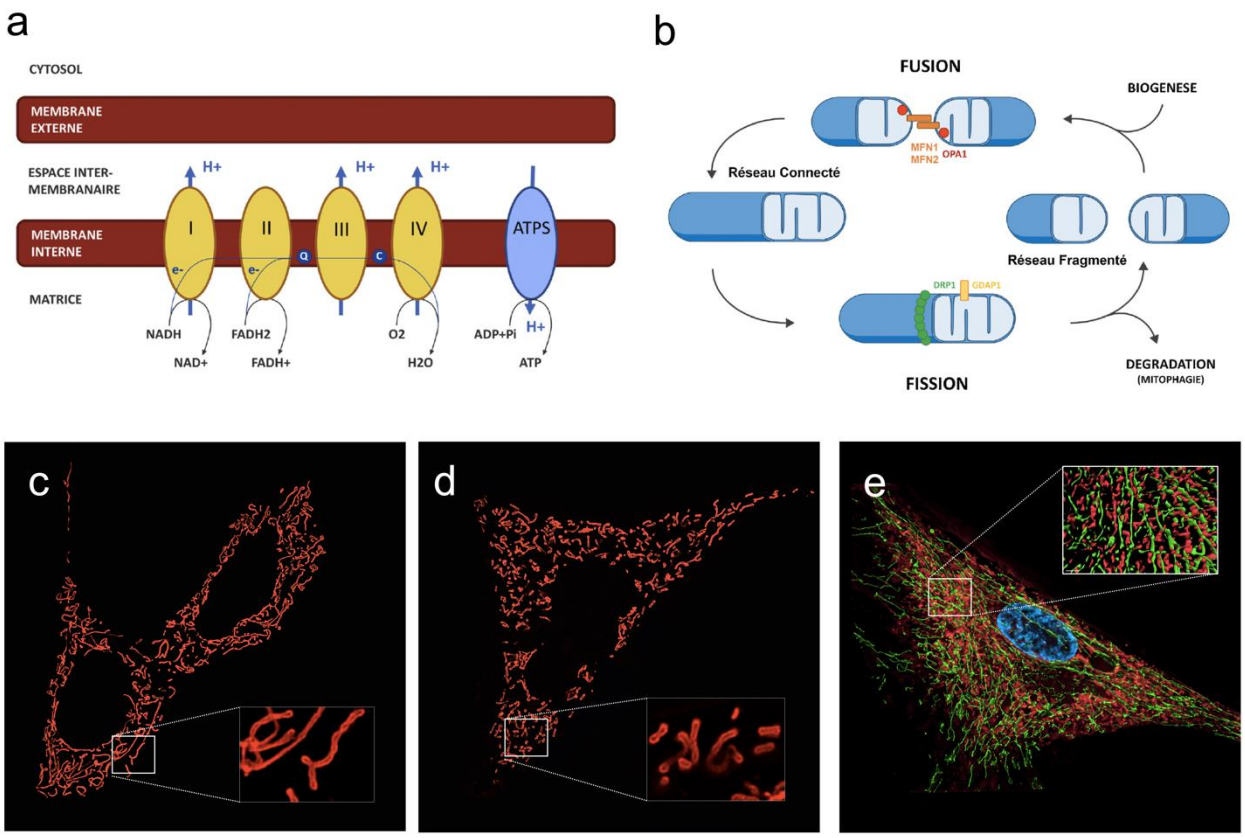

Figure 3. Métabolisme énergétique et dynamique mitochondriale. (a) Le catabolisme des nutriments et l'activité du cycle de Krebs fournissent à la chaîne respiratoire mitochondriale des équivalents réduits sous forme de NADH et de FADH2. Le NADH cède ses électrons (e-) au complexe I (NADH-ubiquinone oxydoréductase) et le FADH2 au complexe II (succinate-ubiquinone oxydoréductase). Les électrons sont ensuite transportés jusqu'au complexe III (ubiquinone-cytochrome *C* oxydoréductase) par l'ubiquinone (Q). Les électrons sont finalement pris en charge par le cytochrome C (C) puis libérés au niveau du complexe IV (cytochrome C oxydase), où ils sont utilisés pour la réduction du dioxygène (O2) en eau (H2O). Le transfert des électrons s'accompagne d'un pompage de protons (H+) de la matrice mitochondriale vers l'espace inter-membranaire au niveau des complexes I, III et IV, à l'origine d'un gradient de pH. La résultante de ce gradient électrochimique est la force proton-motrice, qui permet la production d'ATP par l'ATP synthase. (b) Les mitochondries sont organisées en réseau dynamique dont l'équilibre repose sur les phénomènes de fusion et fission. Les protéines MFN1 et MFN2 initient la fusion en accolant les membranes externes adjacentes, puis la protéine OPA1 guide la fusion des membranes internes. La protéine GDAP1 participe à l'initiation du processus de fission, aboutissant au recrutement de la mécano-enzyme DRP1 au niveau des sites de scission où elle agit par constriction du tubule mitochondrial. (c,d) Marquage du réseau mitochondrial chez des fibroblastes embryonnaires murins (MEF) en culture. A l'état basal physiologique, le réseau mitochondrial apparaît tubulaire et connecté (c). En cas de stress cellulaire ou mitochondrial, le réseau se fragmente, les mitochondries sont de petites taille et isolées (d). (e) Co-marquage du réseau mitochondrial (rouge), du réticulum endoplasmique (vert) et du noyau (bleu) chez un fibroblaste en culture. Le réseau mitochondrial est en constante interaction avec le réticulum endoplasmique au niveau des MAMs (mitochondria associated membranes), participant à l'homéostasie calcique intracellulaire. (Schémas : Cassereau et Codron, 2016. Images : P. Codron).

2.2.4. Homéostasie calcique et Excitotoxicité

Une élévation des concentrations intracellulaires en Calcium a également été rapportée au sein des motoneurones des patients atteints de SLA (Siklos et al., 1996). Cette observation pourrait être la conséquence d'une excitotoxicité neuronale. Au sein des neurones, l'homéostasie calcique est assurée par les interactions entre le réticulum endoplasmique et le réseau mitochondrial (Figure 3e). Dans le cadre de la SLA, une altération de la recapture astrocytaire du glutamate au niveau synaptique serait à l'origine d'une entrée massive de calcium par ouverture des récepteurs glutamatergiques. Le dépassement des voies du maintien des concentrations calciques intracellulaires aboutirait à l'induction de la mort neuronale par ouverture des pores membranaires mitochondriaux et au relargage du cytochrome C dans le cytosol (Leigh et Meldrum, 1996 ; Appel et al., 2001). Par ailleurs, si les mécanismes d'action du Riluzole sont encore aujourd'hui incertains, son action sur le métabolisme du glutamate conforte l'hypothèse de la participation d'une toxicité médiée par ce neurotransmetteur dans la SLA.

2.2.5. Stress Oxydant

Le stress oxydant, ou stress oxydatif, est secondaire à la présence au sein d'une cellule d'espèces réactives de l'oxygène (ROS) telles que l'anion superoxyde (O2•–) et le radical hydroxyle (HO•). Ces composés radicalaires instables porteurs d'un électron dit célibataire non apparié sont vecteurs d'une importante toxicité de par leur réactivité vis-à-vis des protéines, des lipides et des nucléotides avoisinants. S'il existe une production physiologique de ROS au sein des cellules, principalement liée à l'activité de la chaine respiratoire mitochondriale, celle-ci est contrôlée par un système de détoxification basé sur l'activité d'enzymes telles que la superoxyde dismutase, la catalase, et la glutathion peroxydase (Boveris et Chance, 1973). Ainsi, la présence d'un stress oxydant au sein d'une cellule traduit une augmentation de la concentration en ROS et/ou un dépassement des systèmes antioxydants.

Les ROS en excès altèrent directement la structure des molécules intracellulaires (protéines, lipides et acides nucléiques) par le biais de leur électron célibataire. Ils sont notamment responsables d'une altération de la structure des protéines par oxydation des résidus cystéine, pouvant entrainer une désorganisation du cytosquelette et la constitution d'agrégats protéiques intracellulaires (Iguchi et al., 2012). Les ROS peuvent par ailleurs altérer les propriétés de la membrane plasmique et des membranes des organites intracellulaires par peroxydation des lipides (Chen JJ et al., 1995). De

même, le stress oxydant peut être responsable d'un stress mitochondrial à l'origine d'une altération du métabolisme énergétique et d'une fragmentation du réseau mitochondrial (Fridovich, 1997). Enfin, les ROS sont vecteurs de mutations de l'ADN nucléaire et mitochondrial.

Plusieurs études ont mis en évidence une élévation des marqueurs de stress oxydant au sein des neurones moteurs du cortex et de la moelle épinière de patients atteints de SLA (Figure 1i) (Beal et al., 1997 ; Ferrante et al., 1997). De plus, l'effet du traitement antioxydant par Edaravone sur l'évolution de la maladie de certains sous-groupes de patients conforte l'hypothèse de l'implication des ROS dans le développement de la SLA (ALS 19 Study Group, 2017). Toutefois, il reste difficile de déterminer si les processus de neurodégénérescence à l'origine de la maladie sont la cause ou la conséquence d'un stress oxydant.

2.2.6. Neuroinflammation

Le cerveau a longtemps été considéré comme un organe immunoprivilégié, l'étanchéité de la barrière hémato-encéphalique (BHE) empêchant toute pénétration d'agents infectieux et cellules immunitaires circulants. Il est aujourd'hui admis qu'il existe au sein du SNC un système de défense médié par des signaux pro-inflammatoires et des cellules immunitaires, dont la dynamique complexe se distingue des processus inflammatoires périphériques. Au sein du neuropile, les cellules microgliales et les astrocytes expriment des récepteurs PRR (pattern-recognition receptors), qui permettent l'identification de débris endogènes (corps apoptotiques, agrégats protéiques, organites sénescents) et de structures pathogènes (agents infectieux, toxines, corps étrangers) (Tang et al., 2012 ; Lee H et al., 2013). La stimulation de ces récepteurs entraine l'activation de cascades de signalisation qui modifient le phénotype des cellules microgliales, qui deviennent hypertrophiques et amiboïde, prolifèrent, et sécrètent de nombreux facteurs de signalisation.

La détection d'agents pathogènes par les récepteurs PRR entraine l'activation des cellules microgliales dans un état de « défense », stimulant les processus de phagocytose et la sécrétion de cytokines pro-inflammatoires (TNF-α, IFN-γ, IL-6, IL-1β) qui attirent les cellules microgliales voisines et ouvrent les portes de la BHE aux cellules de défense circulantes (lymphocytes, monocytes et granulocytes). D'autres facteurs participent au stress inflammatoire, telles que la production de ROS et le relargage de glutamate respectivement responsables d'un stress oxydant et d'une excitotoxicité, ainsi que la sécrétion de métalloprotéinases matricielles à l'origine d'un remaniement du neuropile. Dans ce contexte, les neurones jouent un rôle immunomodulateur en

freinant l'inflammation locale, en inhibant les kinases et facteurs de transcription pro-inflammatoires tels que MAPK (mitogen-activated protein kinase), c-myc, Nrf2 (nuclear factor erythroid 2-related factor 2) et NFκB (nuclear factor kappa-light-chain-enhancer of activated B cells), et en sécrétant des facteurs solubles inhibiteurs de l'activation microgliale tel que le TGF-β (transforming growth factor-β) (Renaud et al., 2015). Cette modulation est primordiale pour leur survie, l'exposition prolongée aux facteurs pro-inflammatoires étant délétère pour les neurones et les oligodendrocytes au faible potentiel de régénération.

Dans certaines conditions, les cellules microgliales peuvent s'activer dans un état « réparateur », favorisant la détersion de structures endogènes sénescentes ou d'agrégats protéiques au sein du neuropile, le remodelage matriciel, et la sécrétion de facteurs trophiques stimulant la différenciation de cellules souches en oligodendrocytes, astrocytes, et neurones (Eggen et al., 2013).

L'activation microgliale et l'élévation des facteurs pro-inflammatoires observées au sein de la moelle épinière des patients atteints de SLA pourrait être secondaire à un emballement des mécanismes neuroinflammatoires, à l'origine des processus de neurodégénérescence (Kuhle et al., 2009). Un défaut d'activation microgliale dans un état « réparateur » pourrait également être à l'origine d'une accumulation d'agrégats protéiques et de corps apoptotiques au sein du SNC, contribuant au stress motoneuronal et à la propagation des lésions.

2.2.7. Anomalies de la Matrice Extra-cellulaire

Enfin, la mise en évidence en microscopie électronique à transmission d'une désorganisation des fibres de collagène au sein de section de moelle épinière de patients atteints de SLA pose la question du rôle d'un remaniement de la matrice extra-cellulaire dans la survenue de la maladie (Figure 1j) (Ono et al., 1998). Celui-ci pourrait être lié à un défaut de sécrétion astrocytaire du collagène, aux mécanismes inflammatoires locaux, à la présence de ROS au sein du neuropile ou encore à une activité anormale des métalloprotéinases matricielles (MMPs) (Lim et al. 1996).

A partir de l'ensemble de ces observations, plusieurs pistes physiopathologiques se sont progressivement construites. L'identification parallèle des gènes impliqués dans certaines formes familiales de maladies du motoneurone, l'étude des modèles animaux porteurs de ces mutations, et les effets de certains traitements sur l'évolution de la maladie ont permis de progressivement renforcer ces hypothèses (Figure 4) (Tableau 1).

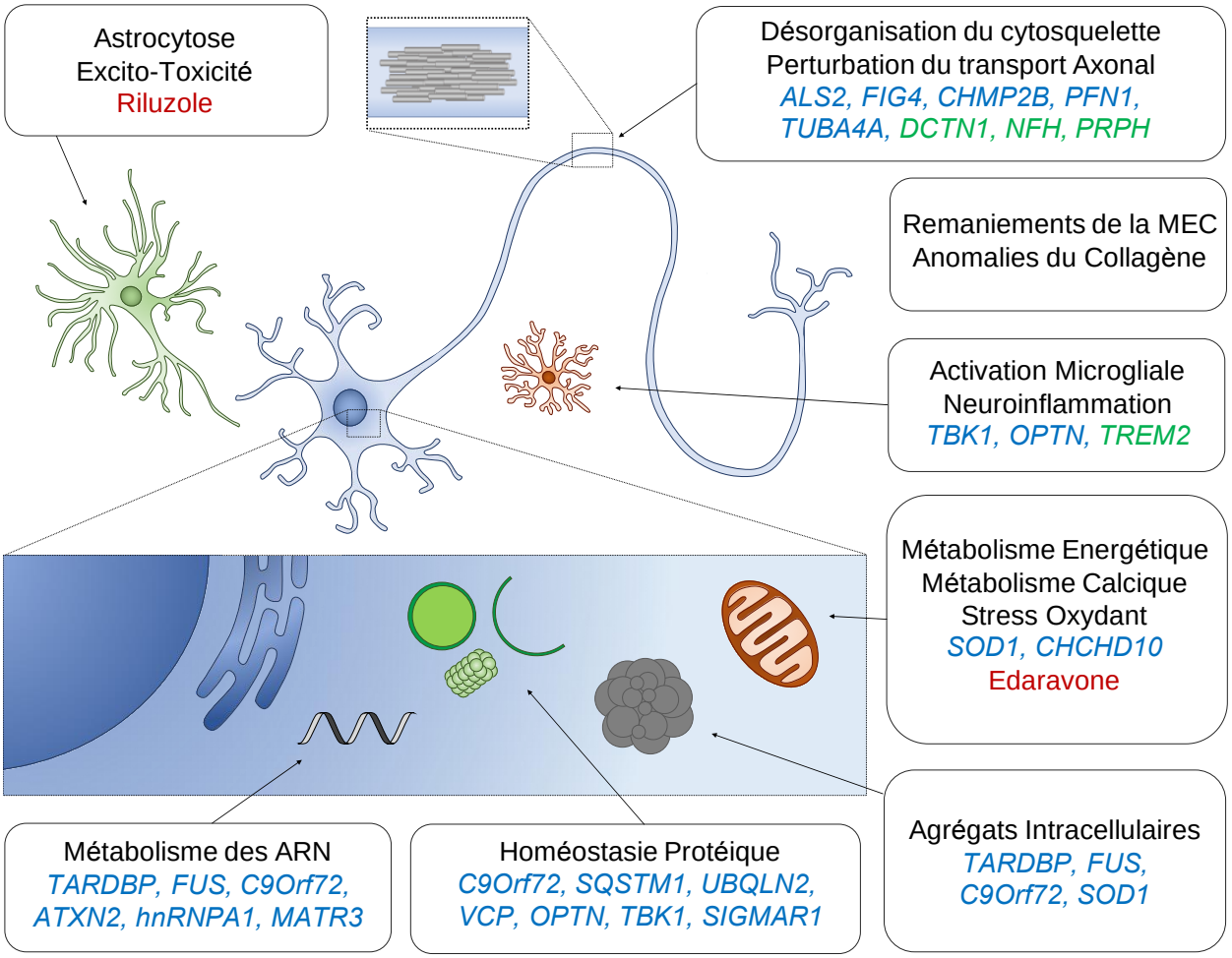

Figure 4. Principales pistes physiopathologiques dans la SLA. Ces hypothèses reposent sur l'observation neuropathologique de tissu cérébral et médullaire de patients atteints de la maladie (noir), l'identification de gènes impliqués dans certaines formes familiales de maladies du motoneurone (bleu) et de gènes de susceptibilité (vert), et les effets de certains traitements sur l'évolution de la maladie (rouge). ARN : acide désoxyribonucléique. MEC : matrice extra-cellulaire. (P. Codron).

Tableau 1. Principaux gènes dont la pathogénicité a été établie dans les formes familiales de SLA.

Gène (protéine)	Fonction	Transmission	Références
SOD1 (superoxide dismutase 1)	Stress Oxydant	AD-AR	Siddique et al., 1991 Rosen et al., 1993
FUS (RNA-binding protein FUS)	Métabolisme des ARN	AD-AR	Kwiatkowski et al., 2009 Vance et al., 2009
TARDBP (TAR DNA-binding protein 43)	Métabolisme des ARN	AD	Kabashi et al., 2008 Sreedharan et al., 2008
C9orf72 (guanine nucleotide exchange C9orf72)	Métabolisme des ARN	AD	DeJesus et al., 2011 Renton et al., 2011

AD : autosomique dominant. AR : autosomique récessif. ARN : Acide Ribonucléique. XL : Liée à l'X.

3. TDP-43, UN ACTEUR CENTRAL DANS LA MALADIE

L'année 2006 marque un tournant dans le champ de la recherche sur la SLA grâce à l'identification de la protéine Transactive Response DNA-binding protein-43 (TDP-43) au sein des agrégats protéiques présents dans le cytoplasme des motoneurones (Arai et al., 2006 ; Neuman et al., 2006). En effet, en condition physiologique TDP-43 est majoritairement localisée au sein du noyau des neurones (Figure 5a). Sa délocalisation nucléaire et son accumulation intracytoplasmique sont observées chez la quasi-totalité des patients atteints de SLA sporadique ou familiale, faisant de cette lésion un marqueur pathologique de la maladie (Mackenzie et al., 2010) (Figure 5b-e). Ces agrégats sont constitués de protéine TDP-43 ubiquitinylée et hyperphosphorylée, mais également de fragments de son extrémité C-terminale (CTF) de 35 kDa et 25 kDa. L'identification deux ans plus tard de formes familiales de SLA liées à des mutations du gène *TARDBP* codant cette protéine (plus de 60 à ce jour) a par la suite renforcé l'hypothèse de son rôle central dans la physiopathologie de la maladie (Gitcho et al., 2008 ; Kabashi et al., 2008 ; Sreedharan et al., 2008).

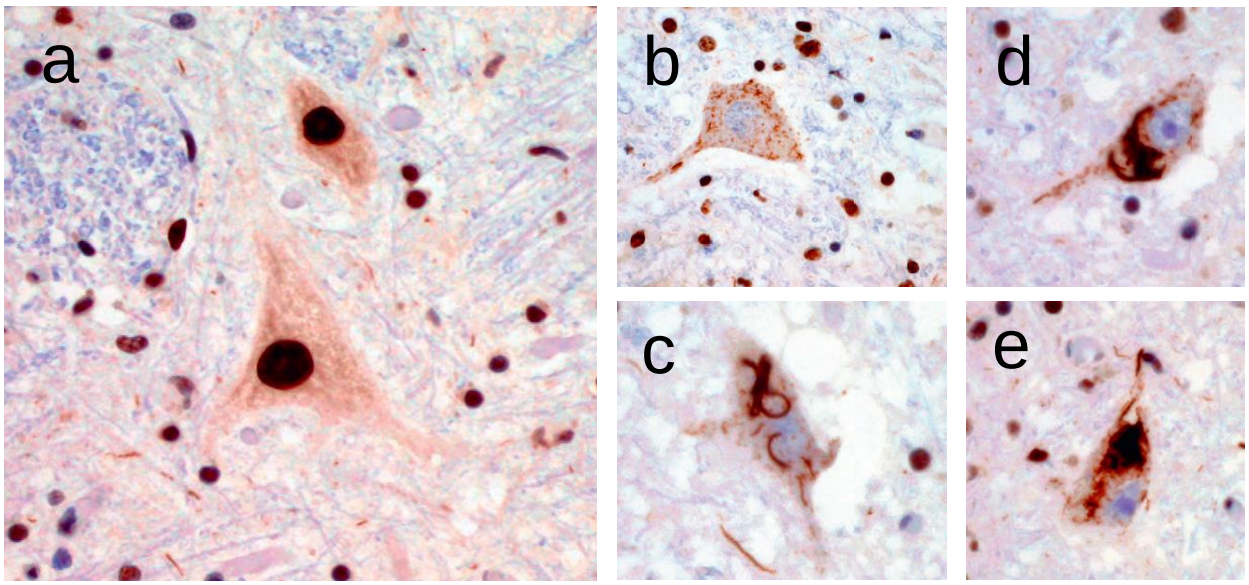

Figure 5. Accumulation cytosolique de la protéine TDP-43 dans la SLA. Étude de sections médullaires de sujet contrôle (a) et de patients atteints de SLA (b-e) après immunomarquage dirigé contre TDP-43. La protéine TDP-43 normalement majoritairement nucléaire (a) est relocalisée et agrégée dans le cytoplasme des neurones moteurs des patients, avec un aspect pouvant être punctiforme (b), filamenteux (c), ou plus dense (d,e). (Images : Ellison et al., 2012).

3.1. Structure et fonction

TDP-43 est une protéine ubiquitaire de 43 kDa appartenant à la famille des RNA-binding-proteins (RBPs). Les 414 acides aminés qui la composent sont codés par le gène *TARDBP* (OMIM#605078) situé sur le chromosome 1. TDP-43 possède deux domaines de liaison aux acides ribonucléiques (RNA recognition motifs RRM1 et RRM2), des domaines d'import (NLS) et d'export nucléaire (NES), et des domaines d'adressages mitochondriaux (M1, M3, M5). Ses extrémités N et C terminales sont quant à elles dédiées aux interaction protéine-protéine (Figure 6a). En effet, TDP-43 est présente à l'état physiologique sous forme d'homodimère ou d'oligomère, et interagit constamment avec de nombreux partenaires protéiques (Shiina et al., 2010 ; Afroz et al., 2017).

La principale fonction de TDP-43 est dédiée au métabolisme des ARN, avec une activité portant sur plus de 30% du transcriptome cellulaire total (Figure 6b) (Tollervey et al., 2011 ; Xiao et al., 2011). Au sein du noyau, TDP-43 se lie aux ARN messagers (ARNm) émergents de l'ARN polymérase II afin de moduler leur transcription, initier leur épissage et assurer leur stabilisation, transport et traduction en dehors du noyau (Buratti et Baralle, 2001). TDP-43 joue également un rôle dans la biogénèse des ARN non codants (ARNnc) tels que les micro-ARN (miARN) et les ARN longs non codants (lncARN), qui permettent la modulation de l'expression de certaines protéines et voies cellulaires. Au sein des mitochondries, TDP-43 inhibe la traduction d'ARN mitochondriaux codant pour des sous-unités du complexe I de la chaine respiratoire (Wang W et al., 2016). Enfin, en conditions de stress cellulaire, TDP-43 participe à la formation des granules de stress (SG) au sein du cytosol des cellules. Ces granules composés de RBPs (Ataxin 2, TIA1, TIAR) et d'ARNm se constituent lors de la survenue d'un stress oxydant, hypoxique ou thermique, avec pour objectif la séquestration transitoire des ARNm d'entretien pour favoriser la traduction des ARNm codant pour les protéines de réponse au stress (Bentmann et al., 2013).

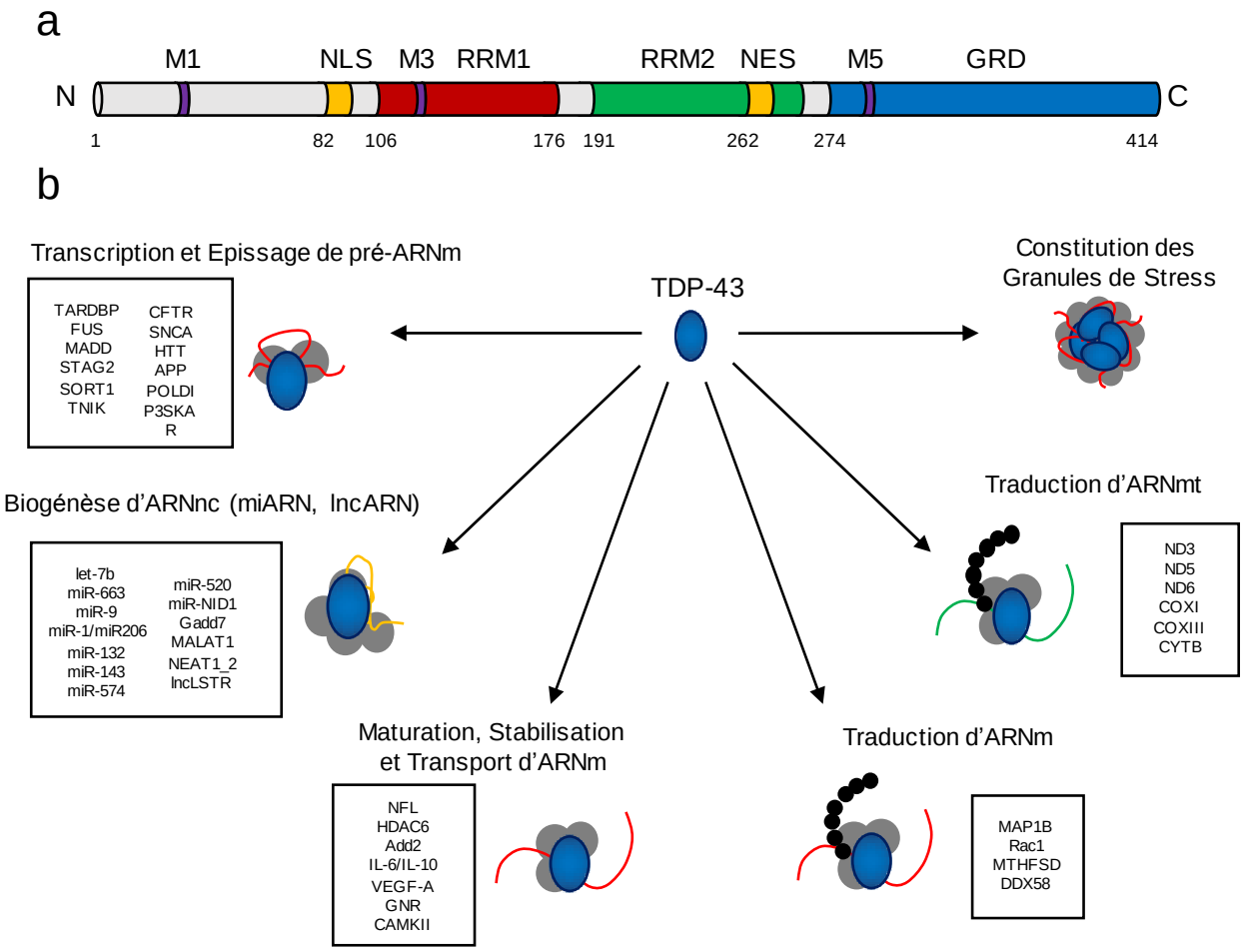

Figure 6. Structure et fonctions de la protéine TDP-43. (a) Structure de TDP-43. RRM : RNA recognition motifs. GRD : Glycin Rich Domain. NLS : nuclear localization sequence. NES : nuclear export sequence. M1, M3, M5 : séquences d'adressage mitochondrial (b) Principales fonctions de TDP-43. ARNm : ARN messager. ARNmt : ARN mitochondrial. ARNnc : ARN non codant. miARN : micro-ARN. lncARN : ARN longs non codants. (Adapté de Ratti et Buratti, 2016).

3.2. Agrégats cytoplasmiques de TDP-43 : gain de fonction cytotoxique

Les mécanismes à l'origine de la constitution d'agrégats de protéine TDP-43 au sein des motoneurones restent débattus. Les modifications conformationnelles de TDP-43 responsables de son accumulation pourraient être la conséquence de modifications post traductionnelles de son domaine RRM1 au niveau du cytosol après exposition à un stress oxydant (Chang et al., 2013 ; Shodai et al., 2013). La protéine anormale agirait ensuite sur un modèle prion-like via son extrémité C terminale riche en glycine, en transmettant ces anomalies structurelles aux protéines TDP-43 voisines et en favorisant la constitution d'inclusions cytoplasmiques (Furukawa et al., 2011 ; Guo et al., 2011 ; Nonaka et al., 2013). Ces phénomènes seraient accompagnés par un dépassement des mécanismes d'homéostasie protéique (système ubiquitine-protéasome, autophagie) empêchant

l'élimination des protéines anormales et des agrégats (Scotter et al., 2014). Les inclusions protéiques de TDP-43 pathologique pourraient ensuite être transmises aux cellules voisines au sein du SNC, par relargage post apoptotique des agrégats, ou par transmission plus directe médiée par microvésicules, exosomes ou nanotubes (Feiler et al., 2015 ; Iguchi et al., 2016). L'arrivée des protéines toxiques au sein des cellules hôtes serait alors à l'origine d'une nouvelle cascade pathologique, participant à la diffusion de la maladie dans le SNC des patients.

A l'échelle cellulaire, la première conséquence de l'élévation des concentrations cytoplasmiques de TDP-43 serait un dérèglement du métabolisme des ARNm au sein du cytosol (transport, stabilisation, traduction). La constitution d'inclusions protéiques serait en outre responsable d'une cytotoxicité cellulaire par désorganisation de l'architecture cytoplasmiques et perturbation des cascades cellulaires internes (Zhang et al., 2009 ; Guo et al., 2011 ; Fang YS et al., 2014). De plus, une augmentation de la localisation mitochondriale de la protéine entrainerait une inhibition de la traduction des ARNmt codant pour le complexe I de la chaine respiratoire à l'origine d'une altération du métabolisme énergétique et une augmentation de la production de radicaux libres oxydants (Onesto et al., 2016 ; Wang W et al., 2016). Ce stress mitochondrial serait également responsable d'une fragmentation du réseau mitochondrial et d'un déséquilibre de l'homéostasie calcique par altération des échanges avec le réticulum endoplasmique (Wang W et al., 2013 ; Stoica et al., 2014).

Enfin, l'accumulation intracytoplasmique de TDP-43 serait à l'origine d'une hyper-activation des voies de la neuroinflammation, via l'interaction directe entre le domaine RRM1 de TDP-43 et la sous unité p65 du facteur de transcription pro-inflammatoire NFkB (Swarup et al., 2011).

3.3. Déplétion nucléaire : perte de fonction physiologique

La seconde conséquence de la relocalisation nucléo-cytoplasmique de TDP-43 est la diminution de sa concentration intranucléaire. Cette déplétion peut être le fruit d'une sortie active du noyau en réponse à un stress persistant, d'une ségrégation cytoplasmique empêchant tout renouvellement de la fraction nucléaire, ou d'une perturbation du trafic nucléo-cytoplasmique secondaire à la désorganisation de l'ultrastructure cellulaire.

La première conséquence directe serait une perte de la fonction nucléaire de TDP-43, participant aux phénomènes de cytotoxicité par dérèglement du métabolisme des ARN cibles (Kraemer et al., 2010 ; Polymenidou et al., 2011 ; Wu LS et al.2012 ; Iguchi et al., 2013 ; Yang C et al., 2014 ; White et al., 2018). L'altération du métabolisme des ARNm du gènes codant pour les chaines légères des

neurofilaments (NFL) pourrait par exemple concourir à la désorganisation de l'architecture du cytosquelette observée au sein des motoneurones (Strong et al., 2007). De même, un dérèglement de l'expression des gènes *ATG7* (autophagy related 7), *TFEB* (transcription factor EB) et *HDAC6* (histone deacetylase 6) participerait au phénomène de dépassement des voies de l'homéostasie protéique et de la réponse au stress (Kim SH et al., 2010). Une anomalie portant sur l'expression des gènes *IL6* (interleukine 6) et *GRN* (granuline) pourrait également jouer un rôle dans l'activation de la neuroinflammation (Lee S et al., 2015).

Enfin, TDP-43 étant impliquée dans la régulation de sa propre expression, une perte de ce rétrocontrôle entrainerait une surexpression cellulaire de TDP-43, amplifiant l'accumulation de la protéine au sein du cytoplasme (Ayala et al., 2011 ; White et al., 2018).

Les hypothèses portant sur les mécanismes à l'origine de la pathogénicité de la protéine TDP-43 dans la SLA sont représentées sur la Figure 7.

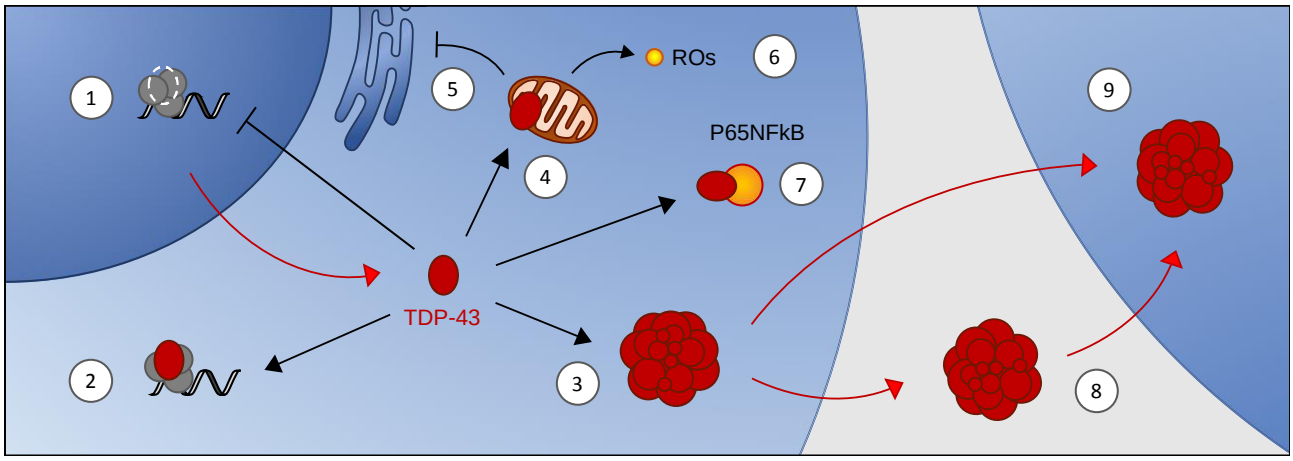

Figure 7. Principales hypothèses actuelles portant sur les mécanismes de pathogénicité de TDP-43 dans la SLA. La relocalisation de la protéine TDP-43 du noyau vers le cytoplasme a plusieurs conséquences à l'échelle cellulaire. Sa déplétion nucléaire (1) et son accumulation cytoplasmique (2) seraient à l'origine d'une altération du métabolisme des ARN aboutissant à une dérégulation de voies cellulaires et un déséquilibre de sa propre expression. La constitution d'agrégats cytosoliques hyperphosphorylés et ubiquitinylés de la protéine (3) serait par ailleurs à l'origine d'une toxicité cellulaire. L'accumulation de TDP-43 au sein des mitochondries (4) serait responsable d'une altération du métabolisme énergétique, d'une désorganisation du réseau mitochondrial, d'anomalies de l'homéostasie calcique (5), et de la production de radicaux libres oxydants (ROS) (6). Par ailleurs, l'interaction directe de TDP-43 avec la sous unité P65 du complexe NFkB via son domaine RMM1 aboutirait à une hyper-activation pathologique des voies de la neuroinflammation (7). Enfin, les agrégats toxiques de protéine TDP-43 seraient transmis directement ou indirectement aux cellules voisines (8,9), concourant à la propagation de la pathologie au sein du SNC des patients. (P. Codron).

4. SOD1 ET FUS, POSSIBLES ACTEURS COMPLEMENTAIRES DANS LA SLA SPORADIQUE

Le gène *SOD1* (OMIM#147450), codant pour la protéine Cu/Zn-binding superoxide dismutase 1 (SOD1), a été le premier gène décrit comme étant responsable de formes familiales de SLA (Rosen et al. 1993). SOD1 est une métalloenzyme de 32 kDa dont le rôle principal est la transformation des radicaux superoxydes toxiques O2•– en peroxyde d'hydrogène H2O2, principalement au niveau du cytosol et de l'espace inter-membranaire mitochondrial des cellules (Rotunno et al., 2013). Plus de 170 mutations du gène *SOD1* ont été rapportées à ce jour, responsables d'environ 20% des cas de SLA familiales, soit près de 2% de l'ensemble des patients atteints SLA. Les mécanismes physiopathologiques impliqués dans ces formes particulières de la maladie semblent liés à un gain de fonction de la protéine SOD1 mutée conduisant à la formation d'agrégats toxiques cytosoliques (Rotunno et al., 2013).

Ces dernières années, plusieurs hypothèses ont émergé quant à l'implication de la protéine SOD1 sauvage dans la physiopathologie des formes sporadiques de SLA, c'est à dire en l'absence de variant pathogène du gène *SOD1*. En effet, il a été observé que cette protéine en condition oxydante peut elle aussi subir une modification de sa conformation et s'organiser en agrégats toxiques (Rakhit et al., 2004 ; Ezzi et al., 2007 ; Bosco et al., 2010). Ces résultats ont été confortés par l'observation d'inclusions de protéine SOD1 au sein des motoneurones spinaux de sujets atteints de SLA sporadique (Bosco et al., 2010 ; Forsberg et al., 2010 ; Paré et al., 2018). Toutefois, des études similaires menées sur tissu médullaire de patients n'ont pas permis de retrouver ces agrégats (Liu et al., 2009 ; Kerman et al., 2010 ; Da Cruz et al., 2017). Si ces résultats contradictoires peuvent être le fait de différences portant sur les protocoles d'immunomarquage employés et les anticorps utilisés, ils suggèrent toutefois l'existence probable de différences conformationnelles entre les inclusions de protéine SOD1 observées dans les formes sporadiques et familiales de la maladie, résultants de mécanismes pathogéniques distincts. De plus, l'absence d'agrégats de protéine TDP-43 au sein des motoneurones des patients porteurs d'une mutation du gène SOD1 est un élément supplémentaire de distinction physiopathologique entre les formes sporadiques et familiales de la maladie (Mackenzie et al., 2007).

Dans le même esprit, les résultats d'une étude récente posent la question de l'implication dans la sSLA d'une autre protéine dont la mutation est responsable de fSLA (Tyzack et al. 2019). FUS est une protéine nucléaire dont la structure et la fonction sont proches de celles de TDP-43. La relocalisation cytoplasmique de cette protéine n'était jusqu'alors observée que dans les formes liées aux

mutations du gène *FUS* (OMIM#137070), soit environ 5% des formes familiales de SLA (Kwiatkowski et al., 2009 ; Vance et al., 2009). Dans cette étude, les analyses en immunomarquage réalisées sur tissu médullaire de patients atteints de SLA sporadique ont permis de révéler une accumulation cytosolique de la protéine au sein des neurones, soulevant la question de la participation de FUS dans la dégénérescence motoneuronale observée dans la maladie.

Si l'implication des protéines SOD1 et FUS sauvages dans la physiopathologie de la de SLA sporadique reste débattue (anomalies primitives toxiques ou marqueurs secondaires non pathogènes), cette question est centrale dans le champ de la recherche sur la SLA car elle conditionne le développement et l'extension aux formes sporadiques de protocoles de recherche aujourd'hui réservés aux formes familiales de la maladie.

5. ENJEUX DE LA RECHERCHE ET PROBLEMATIQUES DE LA THESE

La recherche clinique sur la SLA a été marquée ces 20 dernières années par une multitude d'essais négatifs (Mitsumoto et al., 2014). Deux constats peuvent en partie expliquer les résultats de ces études et les difficultés à faire émerger de nouvelles pistes thérapeutiques.

D'une part, les mécanismes physiopathologiques à l'origine de la dégénérescence motoneuronale dans la SLA demeurent mal compris malgré l'importance des avancées opérées ces dernières années. Ces difficultés sont à certains égards liées à l'absence de modèle d'étude fiable de la SLA sporadique. Si les souris transgéniques *SOD1* présentent une atteinte motoneuronale marquée et une espérance de vie courte, leur utilisation ne permet pas de modéliser fidèlement la forme sporadique de la maladie (Gurney et al., 1994). En effet, la présentation clinico-histologique des formes familiales liées aux mutations du gène *SOD1* est singulière, avec en particulier une absence de pathologie TDP-43 au niveau du SNC. De plus, les fSLA *SOD1* représentent seulement 2% de l'ensemble des patients atteints de SLA. Enfin, les échecs des essais thérapeutiques orientés par les résultats d'études pré-cliniques sur ces modèles témoignent de leurs limites. Plus récemment, de nouveaux modèles in vitro et in vivo de SLA ont été générés par inhibition ou surexpression de la protéine TDP-43 sauvage ou mutée (Hergesheimer et al., 2019). Si leur étude constitue un apport considérable dans le champ de la recherche sur la SLA, l'hétérogénéité de leurs phénotypes et l'incomplète reproduction des mécanismes impliqués dans la physiopathologie de la maladie

rendent encore nécessaire la genèse de nouveaux modèles pour avancer dans la compréhension de la maladie et faire émerger des pistes thérapeutiques novatrices.

D'autre part, l'absence de biomarqueur diagnostique et pronostique spécifique de la maladie et la grande hétérogénéité clinique des patients rendent difficile la construction et l'interprétation des essais thérapeutiques. En effet, il est à ce jour impossible au moment du diagnostic de prédire l'évolution de paramètres tels que la topographie de l'atteinte, le développement de signes associés et la durée d'évolution de la maladie. Ainsi, l'administration d'un même traitement à un groupe hétérogène de patients pourra masquer un possible effet bénéfique sur un sous-groupe atteint d'une forme particulière de SLA. Si les récents résultats d'études portant sur le dosage des neurofilaments light chain (NFL) et heavy chain phosphorylés (pNFH) dans le sang et le LCR semblent indiquer l'utilisation de ces biomarqueurs de neurodégénérescence pour conforter le diagnostic de SLA et estimer l'évolution clinique et le pronostic des patients (Gagliardi et al., 2019 ; Thouvenot et al., 2019), leur absence de spécificité pour la maladie reste cependant une limite (Khalil et al., 2018). L'identification de biomarqueurs fiables et spécifiques de la maladie et de ses sous-types reste donc un enjeu capital pour avancer dans la compréhension de la physiopathologie de la SLA, mieux diagnostiquer la maladie en pratique clinique, et homogénéiser les groupes de patients dans les essais pour se diriger vers une médecine personnalisée.

Ces dernières années, les efforts dans le champ de la recherche sur SLA se sont donc concentrés sur quatre enjeux majeurs :

- Élucider les mécanismes physiopathologiques à l'origine de la SLA.

- Générer de nouveaux modèles d'étude de la maladie.

- Identifier des biomarqueurs de la SLA et de ses différents sous-types.

- Faire émerger des pistes thérapeutiques novatrices.

Dans ce travail, nous avons cherché à apporter des éléments de réponse à certains de ces grands axes actuels de la recherche.

Le premier projet de ce travail de thèse a porté sur l'optimisation de l'analyse histologique des lésions neuronales observées dans les maladies neurodégénératives grâce à la mise au point d'une nouvelle technique d'imagerie cellulaire permettant l'analyse de tissu cérébral, médullaire et musculaire de patients à l'échelle nanométrique. Nos premiers résultats obtenus à partir de la banque de cerveaux du département de Neuropathologie du CHU d'Angers ont permis de caractériser avec précision les agrégats protéiques observés dans certaines pathologies neurologiques, ouvrant un nouveau champ pour l'exploration de tissus de patients atteints de SLA. L'utilisation de cette technique pourrait permettre de caractériser avec précision l'architecture et la composition des lésions observées dans la maladie et d'émettre de nouvelles hypothèses sur les mécanismes physiopathologiques à l'origine de la dégénérescence motoneuronale.

Le second travail de cette thèse a porté sur la recherche de marqueurs biologiques de la SLA, en étudiant des fibroblastes en culture issus de prélèvements cutanés. Grâce à l'expertise de l'équipe UMR CNRS 6015 INSERM 1083 (Angers), nous avons analysé l'ultrastructure cellulaire, le métabolisme énergétique et protéique, l'architecture du réseau mitochondrial, et la réponse au stress d'une biocollection de fibroblastes issus de patients atteints de SLA sporadique et de sujets controles constituée prospectivement. Nos données ont permis d'objectiver chez ces cellules une altération de certaines voies métaboliques, ainsi qu'une augmentation de la synthèse du collagène.

Enfin, la 3ème approche expérimentale de cette thèse a été menée au sein de l'équipe du Professeur Jean-Pierre JULIEN (Institut CERVO, Qc, Canada) qui développe des thérapeutiques innovantes dans le domaine de la SLA. Nous avons plus particulièrement étudié l'adressage et l'action d'anticorps monoclonaux ciblant les agrégats de protéine TDP-43 au niveau du système nerveux central de souris transgéniques porteuses de la mutation TDP-43^{A315T}. Nos résultats obtenus par immunomarquages fluorescents et études histologiques ont montré l'efficacité de l'adressage du traitement ainsi qu'une diminution de la charge lésionnelle centrale. Sur la base de ces résultats, des projets complémentaires ont été initiés dans la perspective de tester l'efficacité de cette nouvelle approche chez l'homme.

CHAPITRE 1

COMPREHENSION DES MECANISMES PHYSIOPATHOLOGIQUES

Analyse d'agrégats protéiques pathologiques du système nerveux central par microscopie super-résolutive STORM

Années :

- 2018-2019

Laboratoire d'accueil :

- UMR CNRS 6015 INSERM 1083, Angers, France

Financement :

- Poste d'Accueil Inserm 2017-2019
- Appel d'Offre Interne CHU Angers 2016

Imaging Human Brain at the Nanoscale Level

with Super-Resolution Microscopy

Philippe CODRON[1,2,3,*], Franck LETOURNEL[1,2], Serge MARTY[4], Laurence RENAUD[5], Christophe VERNY[1,3], Guy LENAERS[3], Charles DUYCKAERTS[4], Jean-Pierre JULIEN[5,6], Julien CASSEREAU[1,3], Arnaud CHEVROLLIER[3]

1. Service de Neurologie, Centre Hospitalier Universitaire d'Angers, Angers, France.
2. Service de Neurobiologie et Neuropathologie, Centre Hospitalier Universitaire d'Angers, Angers, France.
3. Équipe Mitolab, Institut MITOVASC, INSERM U1083, CNRS 6015, Université d'Angers, Angers, France.
4. Institut du Cerveau et de la Moelle épinière, INSERM U1127, CNRS UMR7225, Paris, France.
5. CERVO Brain Research Centre, 2601 Chemin de la Canardière, Québec, QC, Canada.
6. Department of Psychiatry and Neuroscience, Université Laval, Québec, QC, Canada.

ANALYSE D'AGREGATS PROTEIQUES PATHOLOGIQUES DU SYSTEME NERVEUX CENTRAL PAR MICROSCOPIE SUPER-RESOLUTIVE STORM

1. INTRODUCTION A LA MICROSCOPIE SUPER-RESOLUTIVE

1.1. Limites de l'imagerie optique conventionnelle

La description histopathologique des lésions observées au sein du cerveau et de la moelle épinière des patients atteints de SLA reste un élément central dans le champ de la recherche sur les formes sporadiques la maladie. Cette approche anatomo-clinique a permis d'avancer dans la compréhension des mécanismes physiopathologiques à l'origine de son développement, depuis les premières observations macroscopiques par Jean-Martin Charcot au XIXe siècle jusqu'à l'identification plus récente du rôle de la protéine TDP-43 par immunohistochimie. Toutefois, malgré les avancées opérées au cours des dernières décennies dans le champ de l'imagerie optique, les limites résolutives imposées par la diffraction de la lumière restent une barrière à la caractérisation précise des structures intraneuronales.

La résolution spatiale, ou pouvoir séparateur, désigne la capacité d'un système optique à distinguer deux points contigus pour qu'ils soient correctement discernés. Selon un principe établi en 1873 par Ernst Abbe, il est impossible pour un microscope optique conventionnel (microscope en épifluorescence et microscope confocal) de distinguer deux structures lumineuses ponctuelles séparées par une distance inférieure à la moitié de la longueur d'onde de la lumière émise, soit environ 250 nm dans le spectre visible (Abbe, 1873). Ce phénomène est lié à la diffraction des photons : pour un système optique sans aberration, l'image d'un point lumineux pour une ouverture circulaire est un disque de plusieurs centaines de nanomètres aux contours flous et auréolé de cercles concentriques de plus faible luminosité, appelé tache d'Airy (Figure 8a). Si deux sources lumineuses sont trop proches (< 250 nm) leurs aires de diffraction se confondent dans le même halo empêchant leur distinction (Figure 8b). Cette barrière résolutive prend toute son importance en imagerie cellulaire, discipline basée sur l'étude de structure de l'ordre de quelques dizaines de nanomètres marquées par des sondes ou des anticorps émettant un signal fluorescent (pouvant être considérés comme sources lumineuses ponctuelles).

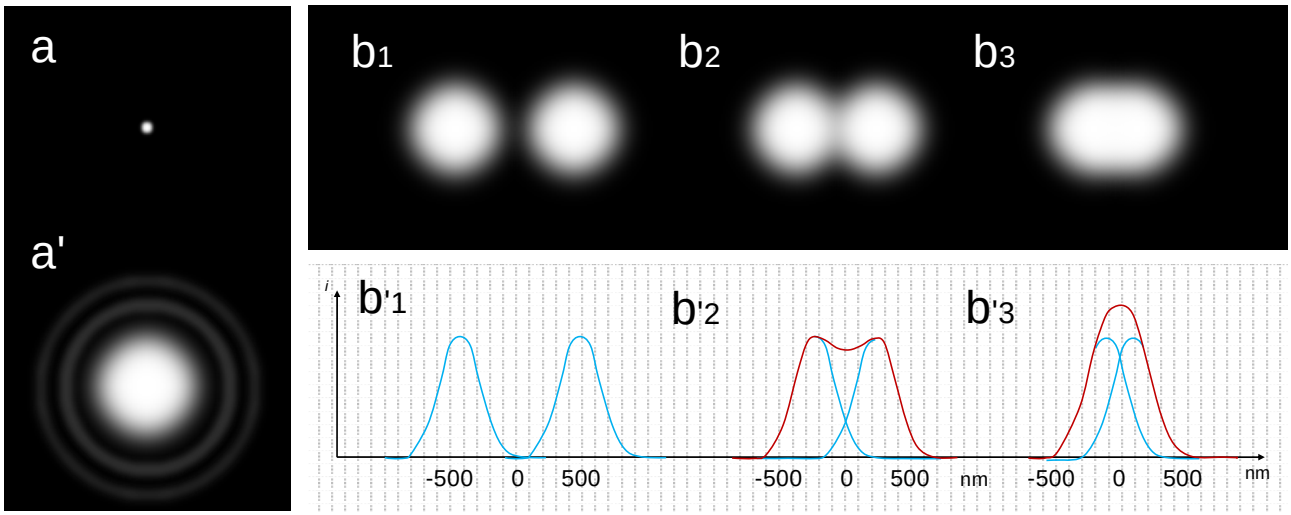

Figure 8. Limites résolutives liées à la diffraction de la lumière. (a) Pour un système optique sans aberration, l'image d'une source lumineuse ponctuelle (a) est un disque de plusieurs centaines de nanomètres aux contours flous (a'), conséquence de la diffraction des photons émis. (b) Ce phénomène limite les possibilités résolutives des microscopes conventionnels, deux sources lumineuses séparées d'une distance inférieure à 250nm étant impossible à distinguer quel que soit le système optique utilisé (b3). *i* : intensité. nm : nanomètres. (P. Codron).

1.2. Principe de l'imagerie STORM

Afin de surmonter cette barrière, des approches dites « super-résolutives », ou nanoscopiques, se sont développées ces dernières années (Sigal et al., 2018 ; Schermelleh et al., 2019). Le prix Nobel de Chimie a été décerné en 2014 aux Docteurs Eric Betzig, Stefan Hell et William Moerner pour leurs travaux dans ce domaine. L'une de ces techniques, appelée stochastic optical reconstruction microscopy (STORM) repose sur le principe de détection en molécule unique.

L'échantillon analysé est baigné dans un tampon aux propriétés oxydo-réductrice et exposé à un faisceau d'excitation laser en champ large à haute intensité. Dans ces conditions, certains fluorochromes organiques photoconvertibles (Cy5, Alexa 647, Atto655, Alexa 532) ont la propriété de passer dans un état de clignotement. Cette activation temporelle stochastique des fluorochromes permet une séparation spatiale de leurs taches d'Airy, de telle sorte qu'elles ne se recouvrent pas (Figure 9a). Les acquisitions sont répétées dans le temps (toutes les 40 ms environ), entre 5 000 et 25 000 images sont acquises au total. Les taches d'Airy sont individualisées sur chaque image, et la localisation des molécules émettrices est déterminée avec précision par fit gaussien. En utilisant une approche basée sur le principe du pointillisme, chaque point source détecté sur les milliers d'images acquises est représenté par un pixel sur une image de reconstruction.

La résolution finale de l'image est de l'ordre de 20 nm, proche de celle d'un microscope électronique à transmission, tout en conservant les avantages de l'analyse spécifique de protéines cibles propres à l'immunomarquage (Figure 9b).

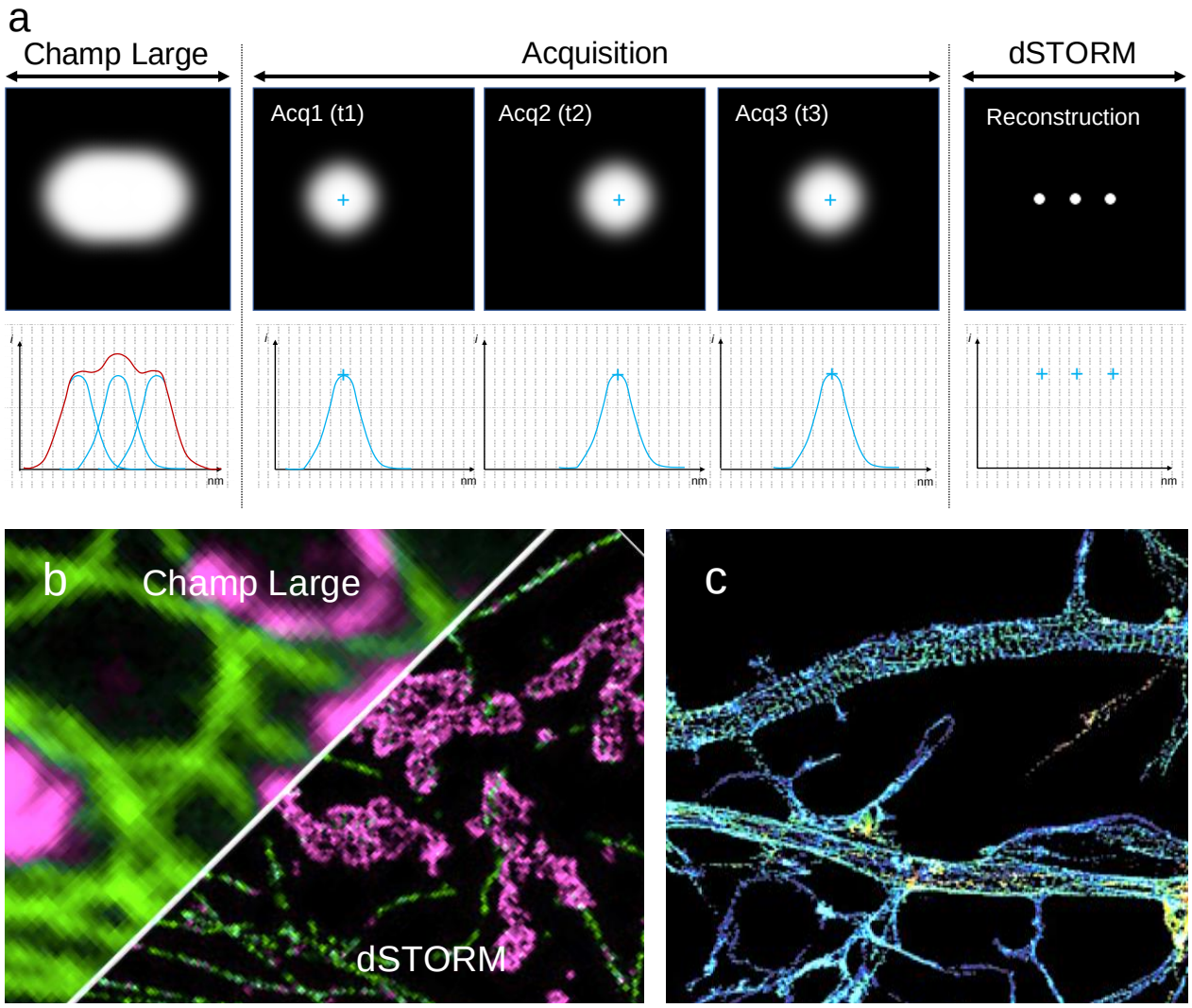

Figure 9. Principe d'acquisition d'une image super-résolutive en utilisant la technologie STORM. (a) L'image d'une structure marquée par 3 fluophores en microscopie conventionnelle (Champ Large) est la somme des aires d'Airy de ces derniers, ne permettant pas de les distinguer s'ils sont trop rapprochés. Lors d'une acquisition STORM, les fluorochromes passent dans un état de clignotement permettant de séparer leurs aires d'Airy dans le temps (t1, t2, t3) (Acquisition). Le centre de chaque aire, correspondant à la localisation de la molécule fluorescente, est déterminé par fit gaussien (croix bleue) et marqué par un pixel sur une image de reconstruction. La répétition des acquisitions (Acq1, Acq2, Acq3) permet de s'assurer de détecter toutes les molécules fluorescentes afin d'obtenir d'une image super-résolue (reconstruction) en utilisant le principe du pointillisme. (b) La résolution nanométrique permet une définition précise des organites intracellulaires. Exemple d'images obtenues après marquage des mitochondries (magenta) et des microtubules (vert) au sein d'une cellule en culture. (c) L'utilisation de la technique STORM en neurosciences a permis de caractériser l'architecture périodique du cytosquelette des axones (microfilaments d'actine d'un neurone en culture). (Schéma : P. Codron, images : huanglab.ucsf.edu ; Xu et al., 2013).

La mise au point de cette nouvelle technologie a constitué une avancée considérable dans le domaine de l'imagerie optique et des neurosciences, permettant par exemple de caractériser l'architecture périodique du cytosquelette des axones, et l'organisation interne des protéines synaptiques (Figure 9c) (Dani et al., 2010 ; Xu et al., 2013). Toutefois son utilisation reste pour le moment limitée à l'étude de modèles cellulaires en culture, empêchant son application à l'approche anatomo-clinique par analyse tissulaire.

2. MISE EN PLACE DE L'ETUDE

2.1. Problématique et objectifs

L'objectif de ce travail était de mettre au point un protocole d'analyse de tissu cérébral par microscopie super-résolutive STORM et d'utiliser cette technique sur des échantillons cérébraux et médullaires prélevés chez des patients atteints de maladies neurodégénératives afin de caractériser à l'échelle nanoscopique la composition et l'architecture des agrégats protéiques présents au sein des neurones. Notre perspective était d'employer cette approche sur des prélèvements issus de patients atteints de SLA afin de tenter de caractériser avec précision l'architecture et la composition des lésions observées dans la maladie, et d'émettre de nouvelles hypothèses sur les mécanismes physiopathologiques à l'origine de la dégénérescence motoneuronale.

2.2. Contexte méthodologique et stratégie expérimentale

Depuis 2010, nous travaillons avec le Dr Arnaud CHEVROLLIER à la mise en place des techniques d'imagerie super-résolutive STORM sur lignées cellulaires au sein de l'UMR CNRS 6015 INSERM 1083 (Angers), en ciblant plus particulièrement l'étude de l'architecture du cytosquelette et du réseau mitochondrial dans les maladies neurodégénératives (Figure 10) (Codron et al., 2016 ; Codron et al., 2018).

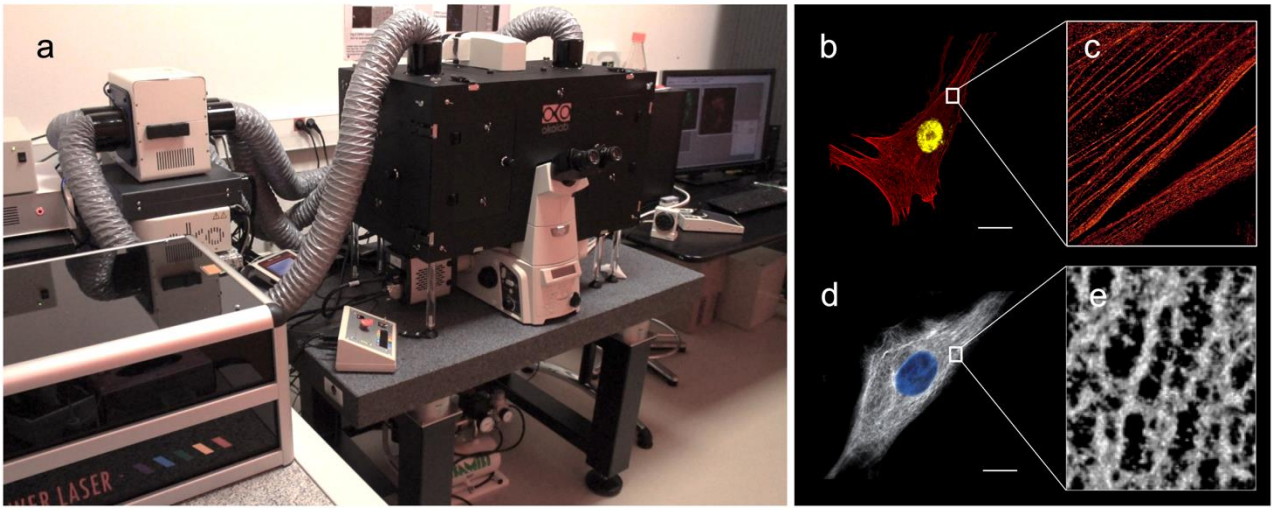

Figure 10. Système optique et exemples d'acquisition STORM du laboratoire UMR CNRS 6015 INSERM 1083, Angers. (a) microscope inversé NIKON ECLIPSE Ti-E (Nikon Instruments Europe, Amsterdam, The Netherlands) équipé d'un objectif CFI SR APO TIRF 100X ON1.49, d'un système Perfect Focus, d'un module ILas2 (Roper Scientific, Martinsried, Germany) et d'une caméra Evolve 128TM EMCCD 512 x 512 (Photometrics, Tucson, AZ, USA). (b) Microscopie conventionnelle en champ large sur fibroblaste de peau, noyau marqué en jaune et microfilaments d'actine en rouge. Barre d'échelle 10µm. (c) Étude des microfilaments d'actine à l'échelle nanoscopique en microscopie super résolution STORM. Le diamètre d'un microfilament d'actine est d'environ 10nm. (d) Microscopie conventionnelle en champ large sur fibroblaste de peau fixé, noyau marqué en bleu et filaments intermédiaires (vimentine) en blanc. Barre d'échelle 10µm. (e) Étude des filaments intermédiaires en microscopie super résolution STORM. (Images P. Codron – A. Chevrollier).

Pour ce projet, nous avons couplé notre expertise développée dans ce domaine à l'expérience acquise au sein du service de neuropathologie du CHU d'Angers afin de mettre au point une technique de préparation et d'analyse de coupes histologiques de tissu cérébral par microscopie STORM. La résolution des images a été comparée à celles obtenues sur les mêmes tissus à partir de techniques de microscopie optique conventionnelle et électronique, en partenariat avec l'UMR CNRS 7225 - INSERM 1127 (Institut du Cerveau et de la Moelle épinière, Université Pierre et Marie Curie, Sorbonne Universités, Paris, France). Des techniques complémentaires ont été développées afin de permettre des acquisitions en double couleur et en 3 dimensions. Enfin, nous avons utilisé cette nouvelle approche pour caractériser à l'échelle nanoscopique les lésions intra- et extra-neuronales caractéristiques de maladies neurodégénératives.

Les résultats de ce travail sont rapportés dans l'article suivant.

Article N°1

Manuscrit en préparation (*Nature Neuroscience*)

Imaging Human Brain at the Nanoscale Level with Super-Resolution Microscopy

Philippe CODRON[1,2,3,*], Franck LETOURNEL[1,2], Serge MARTY[4], Laurence RENAUD[5], Christophe VERNY[1,3], Guy LENAERS[3], Charles DUYCKAERTS[4], Jean-Pierre JULIEN[5,6], Julien CASSEREAU[1,3], Arnaud CHEVROLLIER[3]

1. Service de Neurologie, Centre Hospitalier Universitaire d'Angers, Angers, France.
2. Service de Neurobiologie et Neuropathologie, Centre Hospitalier Universitaire d'Angers, Angers, France.
3. Équipe Mitolab, Institut MITOVASC, INSERM U1083, CNRS 6015, Université d'Angers, Angers, France.
4. Institut du Cerveau et de la Moelle épinière, INSERM U1127, CNRS UMR7225, Paris, France.
5. CERVO Brain Research Centre, 2601 Chemin de la Canardière, Québec, QC, Canada.
6. Department of Psychiatry and Neuroscience, Université Laval, Québec, QC, Canada.

Imaging Human Brain at the Nanoscale Level with Super-Resolution Microscopy

Philippe CODRON[1,2,3,*], Franck LETOURNEL[1,2], Serge MARTY[4], Laurence RENAUD[5], Christophe VERNY[1,3], Guy LENAERS[3], Charles DUYCKAERTS[4], Jean-Pierre JULIEN[5,6], Julien CASSEREAU[1,3], Arnaud CHEVROLLIER[3]

1. Service de Neurologie, Centre Hospitalier Universitaire d'Angers, Angers, France.
2. Service de Neurobiologie et Neuropathologie, Centre Hospitalier Universitaire d'Angers, Angers, France.
3. Équipe Mitolab, Institut MITOVASC, INSERM U1083, CNRS 6015, Université d'Angers, Angers, France.
4. Institut du Cerveau et de la Moelle épinière, INSERM U1127, CNRS UMR7225, Sorbonne Universités, Paris, France.
5. CERVO Brain Research Centre, 2601 Chemin de la Canardière, Québec, QC, Canada.
6. Department of Psychiatry and Neuroscience, Université Laval, Québec, QC, Canada.

Corresponding Author

Dr Philippe CODRON

Service de Neurologie, Centre Hospitalier Universitaire d'Angers, 4 rue Larrey, 49933 Angers, France

Équipe Mitolab, Institut MITOVASC, INSERM U1083, CNRS 6015, Université d'Angers, 4 rue Larrey, 49933 Angers, France

Tel : +33 2 41 35 46 13

Mail : philippe.codron@inserm.fr

Abstract:

The development of STochastic Optical Reconstruction Microscopy (STORM) has contributed recently to major advances in the field of cell neuroscience. Here, we extended this technique to neuropathological tissue preparations to perform 2D-, 3D- and two-color STORM on human neocortex, white matter and brainstem samples. In particular, we imaged pathological protein aggregates in tissues from patients affected with neurodegenerative diseases, to visualize the architecture of Amyloid-β, Tau and Lewy pathologies with unprecedented details. Thus, this approach opens further gates to a more comprehensive understanding of the human brain organization and revelations about the underlying mechanisms responsible for common neurological diseases.

Keywords:

STORM, Tau, Amyloid-β, Lewy body, Neuropathology, Neuroscience.

Imaging Human Brain at the Nanoscale Level with Level with Super-Resolution Microscopy

Introduction

Advances in neuroscience are closely linked to the progresses made in optical brain imaging. The invention of the microscope in the 17th century first allowed the characterization of the human brain at the cellular level and the emergence of clinical neurology, neurosurgery and psychiatry in the 18th and 19th centuries. Likewise, the understanding and classification of neurodegenerative disorders have benefited from the development of immunostaining techniques and multichannel fluorescence imaging in the second part of the 20th century. However, despite these advances, the diffraction barrier (~ 250 nm) remains a resolution limit for conventional light microscopy, hindering the precise characterization of subcellular structures.

In the recent years, super-resolution microscopy techniques overcame this limit by using different concepts[1]. One of them, called STochastic Optical Reconstruction Microscopy (STORM), is based on single molecule localization by stochastic excitation of photo-switchable fluorescent molecules[2]. By improving the resolution barrier towards the nanometer scale (~20-50 nm), STORM allows the visualization of nanoscopic structures while retaining the advantages of optical microscopy such as sample preparation, molecular identification through immunostaining, and multicolor imaging[3]. This led in the field of neuroscience to the characterization of the periodic structure of axonal cytoskeleton in neurons[4] and to the outlining of the spatial organization of synaptic proteins[5]. However, to date, the use of STORM microscopy was restricted to cultured cells and rodent brain, while so far no experiment on human cortex has been reported.

In this study, we performed STORM on human brain structures combining cellular microscopy protocols with neuropathology tissue preparation techniques. Using an astigmatism-based imaging method and photo-switchable fluorophores, we performed 2D-, 3D- and two-color STORM to characterize pathological structures in brain samples from patients with common age-related neurodegenerative diseases.

Results

Super-resolution imaging of human brain samples

To assess STORM technique on human brain tissue, we first aimed to image a well-defined histological structure as axon tracts from the neocortex. Prefrontal cortex samples of control subjects were immunostained using an anti-neurofilament primary antibody and a secondary antibody conjugated with the photo-switchable fluorophore Alexa Fluor (AF) 647. Coverslips with immunostained brain sections were bathed in a switching buffer and placed on the stage of an inverted motorized microscope equipped with a high-power laser module, a Total Internal Reflection Fluorescence (TIRF) system, and an Electron Multiplying Charge Coupled Device (EMCCD) single-photon sensitive camera (Fig. 1a).

STORM is based on separating stochastically the emission of photo-switchable fluorescent molecules in time, so that each individual emitter can be distinguished from the others that reside within the same diffraction-limited volume. For each acquisition, thousands of frames are recorded and each frame is computationally processed to detect activated fluorescent molecules, determine their center position, and report it as a single pixel on a corresponding reconstruction picture. The final super-resolved STORM image is obtained by merging all the reconstruction pictures in a single overlap image (Fig.1b, Supplementary Video 1). The total acquisition and reconstruction time for one super-resolved image lasts from 5 to 10 minutes, depending on the number of acquired frames.

Using this technique, we imaged neurofilaments in axons with high resolution. Although neurofilament fibrils (~10 nm) could not be defined as well as when using Transmission Electron Microscopy (TEM), the axon caliber was significantly decreased compared the one found using conventional fluorescence microscopy (Supplementary Fig. 1). For the same prefrontal axons, the diameter in longitudinal sections and the area in transversal sections were more than 50% smaller when measured with STORM than with conventional fluorescence microscopy ($p<0.001$) (Fig. 1c-e). In contrast, there was no significant difference regarding these parameters from prefrontal cortex samples of an age-matched control subject, measured with STORM or TEM ($p= 0.441$ diameters, $p = 0.596$ areas). Thus, STORM provides a powerful tool to image human brain samples and a reliable method to measure histological structures at the nanoscale level.

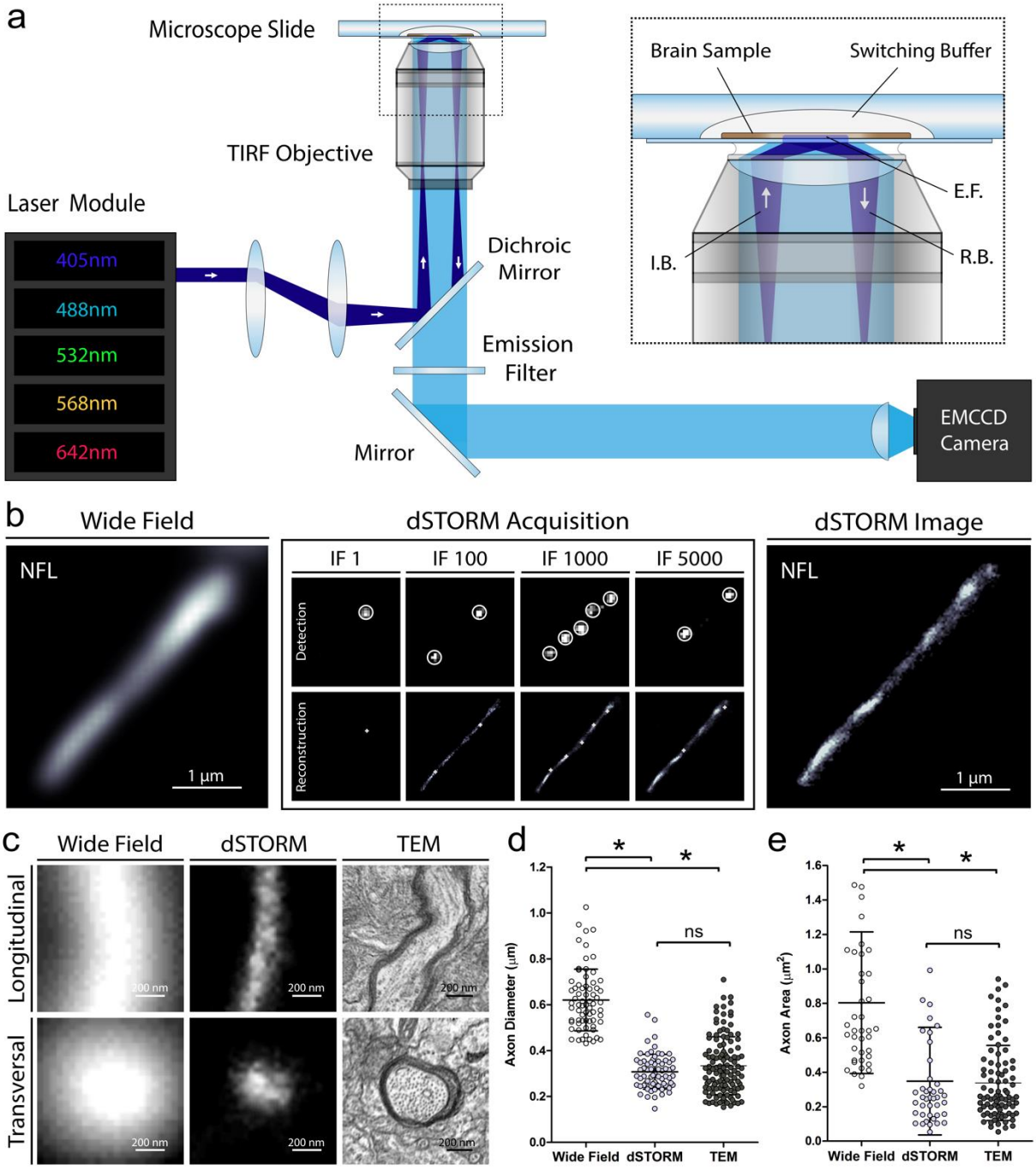

Fig. 1. Super-resolution imaging of human brain samples. a, Schematic of the optical setup used for STORM imaging. I.B. = incident beam, E.F = evanescent field, R.B. = reflected beam. b, STORM acquisition of a cortical axon in a human brain section immunostained for neurofilaments (NF): a conventional fluorescence microscopy image was first acquired (left), excitation power was then strongly increased to induce fluorophore blinking and thousands of frames were recorded (center – up). Each frame was computationally processed to detect activated fluorescent molecules and report their center position as single pixels on a corresponding reconstruction picture (center – down). The final STORM image was obtained by merging all the reconstruction pictures in a single overlap image (right). IF = imaging frame. c, Representative images of longitudinally and transversally sectioned prefrontal cortex axons acquired with conventional fluorescence microscopy, STORM, and Transmission Electron Microscopy (TEM). d,e, Axon diameters (longitudinal sections) and areas (transversal sections) measured in human brain using conventional fluorescence microscopy, STORM, and TEM. Error bars indicate means with standard deviations. * p<0.001.

3D-STORM and two-color STORM imaging of human brain samples

As three-dimensional and multichannel imaging provide fundamental insights into the architectural organization of nanoscale structures, we assessed STORM to image human brain sections, using an astigmatism-based method allowing a three-dimensional detection of individual fluorophore[6]. After setting a cylindrical lens in the detection path of the microscope, the z coordinate of each fluorescent molecule was determined from the ellipticity of its image. Prefrontal cortex samples of control subjects were immunostained for Neurofilaments, and after reconstruction, axons were visualized in 3D with high resolution and an imaging depth of ~0.5 µm (Fig. 2a). The cylindrical shape of the axon tracts was discernible and both longitudinal and transversal sections of the 3D modelled axon were similar in size to those obtained with 2D-STORM.

Then, to assess two-color STORM imaging on cortex samples, we immune-stained human brain sections with two primary antibodies detecting nearby structures, the Bassoon and Homer 1 proteins from the synapses, and used secondary antibodies conjugated with the photoswitchable fluorophores AF 647 and AF 532. In conventional fluorescence microscopy, Bassoon and Homer 1 signals appeared diffuse and overlapping, and the synaptic clefts could not be precisely defined (Fig. 2b). In contrast, the two-color STORM imaging allowed to distinct pre- and postsynaptic protein clusters separated by the synaptic cleft, and to precise the exact size, orientation and organization of the synapses. Interestingly, multichannel imaging combining conventional fluorescence microscopy and STORM was also achievable, allowing super-resolution imaging of brain structures using both photoswitchable and non-photoswitchable fluorophores. Although less specific than two-color STORM, this technique can provide valuable information about the layout of adjacent structures, as for example myelin sheath around axonal tracts (Fig. 2c). Together, these results demonstrate the possibility to perform 3D and two-color STORM imaging with a nanoscale resolution on human brain samples.

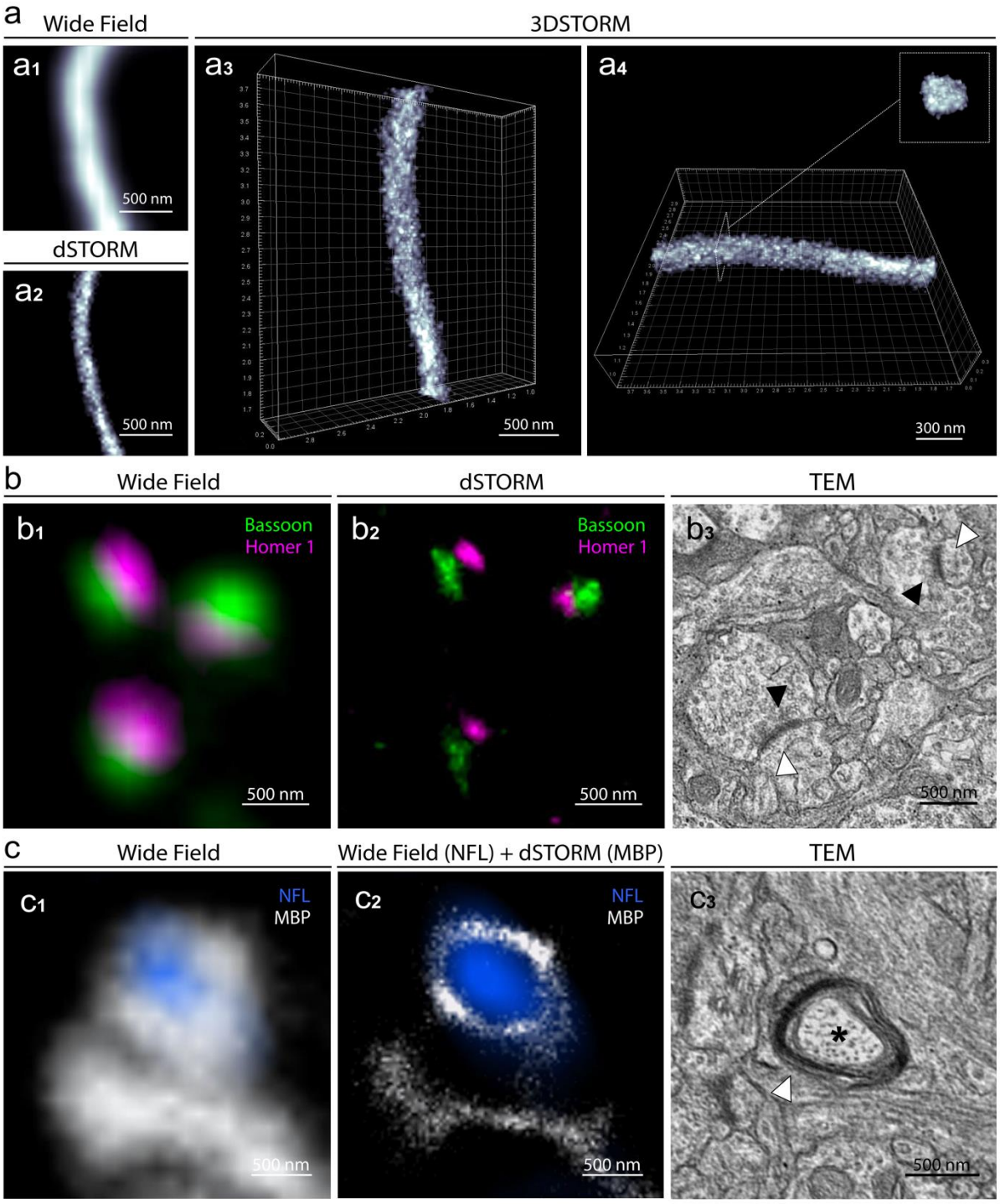

Fig. 2. 3D-STORM and two-color STORM images of physiological structures in human brain. a1, Conventional fluorescence microscopy image of a longitudinally sectioned axon immunostained for neurofilament (NF) in prefrontal cortex. a2, STORM image of the same area. a3,a4, 3D-STORM reconstruction of the acquired axon, allowing a three-dimensional analysis of the structure at the nanoscale level. b1, Conventional fluorescence microscopy image of pre- and post-synaptic proteins Bassoon and Homer 1 in prefrontal cortex. b2, Two-color STORM image of the same area resolving distinct synaptic clusters. b3, Comparative TEM image of 2 synapses with pre- (black arrowheads) and post- (white arrowheads) synaptic compartments. c1, Conventional fluorescence microscopy image of axonal NFs and oligodendrocyte Myelin Basic Protein (MBP) in peri-ventricular white matter. c2, Image of the same area combining conventional fluorescence microscopy (NF) and STORM (MBP). c3, Comparative TEM image of a transversally sectioned axon (asterisk) surrounded by oligodendrocyte processes and myelin sheath (white arrowhead).

Super-resolution imaging of Aβ and Tau Pathology

Understanding the pathophysiology of neurodegenerative disorders to identify novel therapeutic prospects is a major challenge. As each of these diseases is defined by specific intra- or extra-cellular protein aggregates in distinctive anatomical brain regions, valuable insights will be provided by the precise characterization of the corresponding lesions. To this end, we focused on imaging Amyloid-β (Aβ), Tau and α-synuclein aggregates with STORM in samples from patients with parkinsonism and dementia.

Alzheimer's disease (AD) is the leading cause of dementia, with hallmarks of the disease consisting in the presence of extracellular deposits of Aβ peptides called senile plaques, and intracellular aggregates of hyperphosphorylated tau protein (pTau) called neurofibrillary tangles (NFT), essentially in the hippocampus, entorhinal cortex and neocortex[7]. As aggregate size can measure up to 100 µm, keeping an overall view of the whole lesions is critical to study Aβ and Tau pathology in the brain, while high resolution imaging is required to characterize the nanoscale organization of the misfolded proteins.

Towards this goal, we imaged by STORM entire senile plaques and degenerating neurons together with performing observations at a nanoscale resolution. Tissue samples from the prefrontal, parietal and temporal cortex of AD patients were immunostained for Aβ and pTau (Ser202, Thr205). Auto-fluorescence quenchers were used to reduce the signal of lipofuscin, an autofluorescent pigment present in senescent neurons[8]. Lipofuscin signal was specifically detectable in neuron, but did not preclude STORM acquisitions. STORM images of ~30 µm diameter senile plaques and ~15 µm degenerating neurons with NFTs were acquired. While the Aβ fibrils and the paired helical filaments of Tau could not be identified as with TEM, the STORM images provided highly resolving details of the nanoscale distribution and size of Aβ peptides and pTau aggregates (Fig 3a,b). Aβ fibrils were highly reticulated and cross-linked in the extracellular matrix (Fig. 3a), while NFTs appeared denser, with both a honeycombed structure in the soma and a filamentous organization in the axon (Fig. 3b). These observations emphasize that STORM provides great insights in studying Aβ and Tau aggregates in brain samples from AD patients, which will contribute to a better understanding of their formation and generation of neuronal lesions.

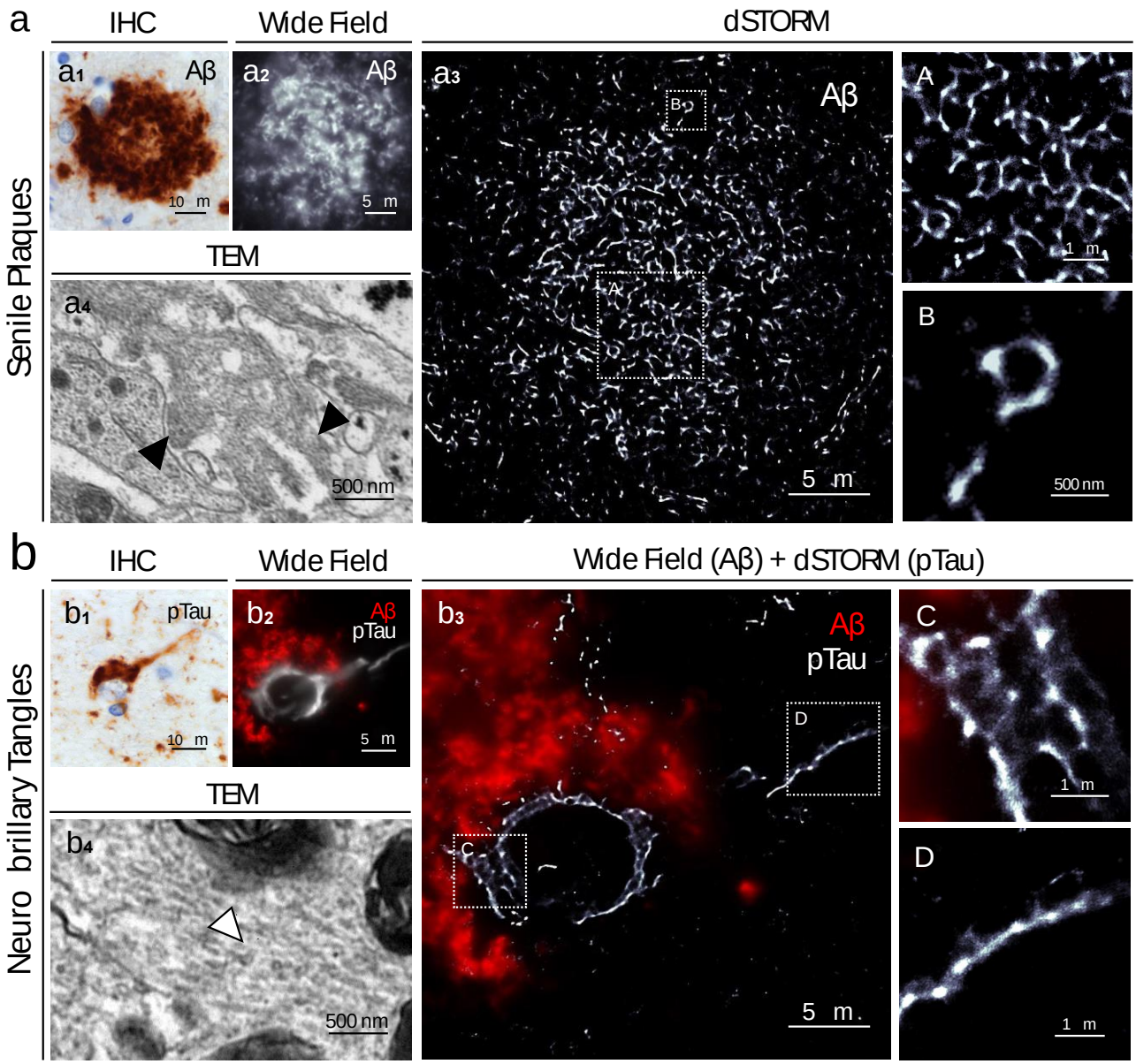

Fig. 3. Super-resolution images of senile plaques and neurofibrillary tangles in AD brain samples. a1, Representative image of a senile plaque in the neocortex of a patient affected with AD (immunohistochemical detection of Aβ). a2, Conventional fluorescence microscopy image of a whole senile plaque in a neocortex section immunostained for Aβ. a3, STORM image of the same area. The high-magnification views of marked regions show fine details of the nanoscale distribution and size of Aβ. a4, Comparative TEM image of Aβ fibrils (black arrowheads) in a senile plaque. b1, Representative image of neurofibrillary tangles in the neocortex of a patient affected with AD (immunohistochemical detection of pTau). b2, Conventional fluorescence microscopy image of neurofibrillary tangles within the soma of a whole degenerating neuron surrounded by Aβ deposition in a neocortex section. b3, Same area imaged by combining conventional fluorescence microscopy and STORM. The high-magnification views of marked regions show the honeycombed structure of pTau aggregates in the soma and a filamentous organization in the axon. b4, Comparative TEM image of Tau filaments (white arrowhead) in neurofibrillary tangles.

Super-resolution imaging of Lewy Pathology

Parkinson's disease (PD) and dementia with Lewy bodies (DLB) are two neurodegenerative diseases characterized by the presence of intra-neuronal α-synuclein immuno-reactive inclusions, called Lewy bodies (LB)[9]. The structure of LBs varies depending on their localization within the central nervous system. Two main types of LB can be defined: typical Lewy bodies (TLB) mainly found in the soma of the brainstem neurons, spherical with a pale core surrounded by a dense halo when studied in immunohistochemistery, and smaller cortical Lewy bodies (CLB), usually lacking the central core and peripheral halo, mainly detected in the axons of the neocortex (Fig. 4a). Accumulation of α-synuclein in dystrophic axons called Lewy neurites (LN) can also be observed. To date, the structure of LBs remains unclear, as the resolution of conventional fluorescence microscopy is too low to characterize their internal architecture and TEM does not provide sufficient information about protein content and organization.

In order to characterize LB pathogenicity at the nanoscale level with a molecular staining approach, we performed STORM imaging using brain samples from PD and DLB patients. Neocortex from prefrontal and temporal samples and *substancia nigra* (brainstem) sections were immune-stained with α-synuclein (phospho S129) antibodies and images of TLBs, CLBs and LNs were acquired. The pale core and the dense halo of TLBs were observed both with conventional and super-resolution imaging, although only the STORM images defined precisely their internal organization (Fig. 4a). The pale core appeared empty, while the halo was made of an α-synuclein reticulated corona. Likewise, STORM imaging of CLBs revealed a dense honeycomb structure that could not be detected by conventional fluorescence microscopy (Fig. 4a). Finally, two-color STORM imaging of LB showed a central core of aggregated pTau surrounded by reticulated α-synuclein (Fig. 4b). In contrast, LNs were composed of α-synuclein dense aggregates bounded by neurofilaments (Fig. 4c). These very first STORM images of α-synuclein aggregates hold great promise for characterizing the composition, organization and diffusion of Lewy pathologies in human brain and discovering the pathophysiological processes involved in α-synucleinopathies.

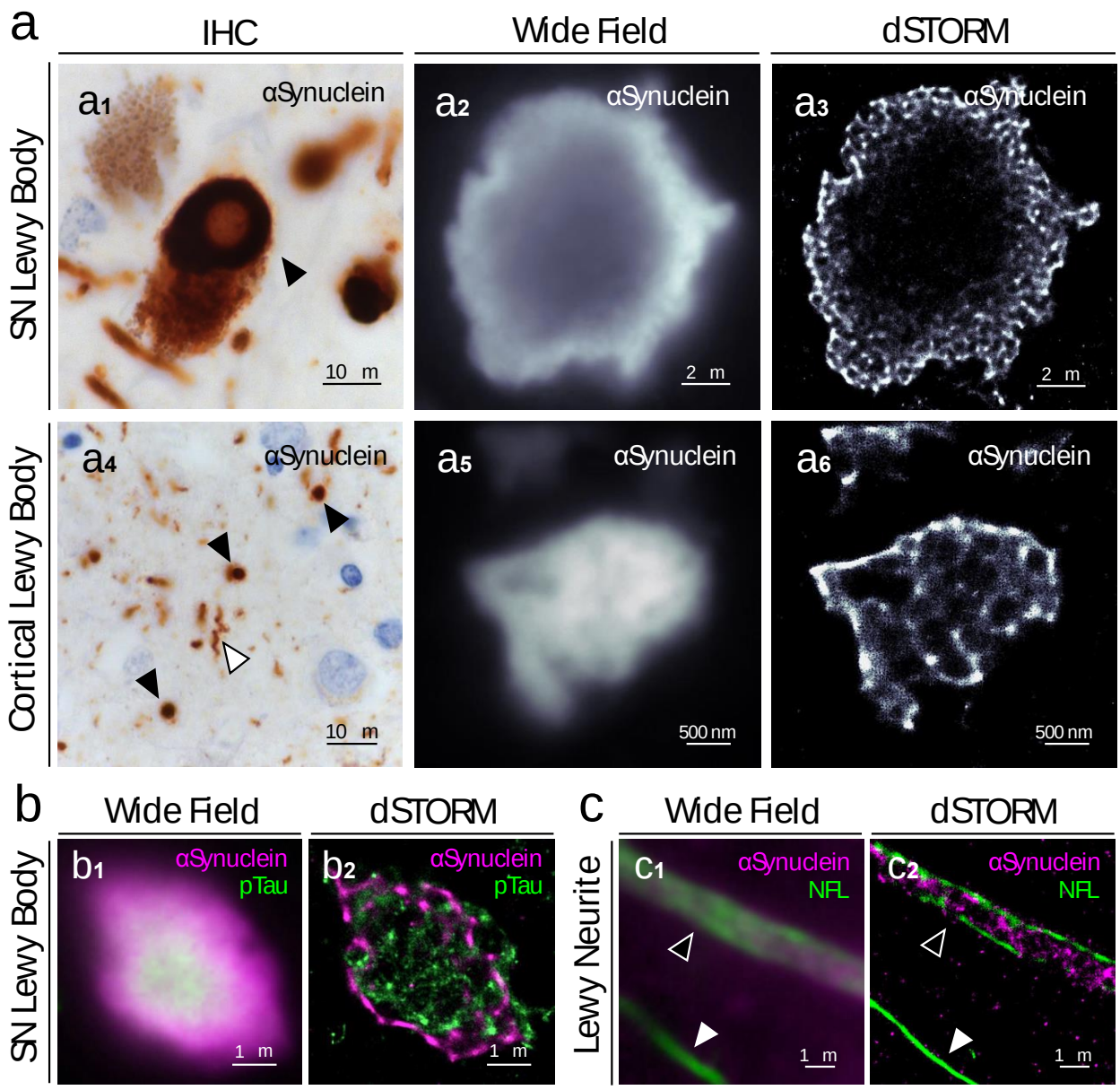

Fig. 4. Super-resolution images of Lewy bodies in PD and DLB brain samples. a1, Representative image of a typical Lewy body (black arrowhead) in the *substantia nigra* of a patient affected with PD (immunohistochemical detection of α-synuclein). a2, Conventional fluorescence microscopy image of a typical Lewy body in a *substantia nigra* section immunostained for α-synuclein. a3, STORM image of the same area resolving distinctly the α-synuclein reticulated corona of the Lewy body. a4, Representative image of cortical Lewy bodies (black arrowheads) and Lewy neurite (White arrowhead) in the neocortex of a patient affected with PD. a5, Conventional fluorescence microscopy image of a cortical Lewy body in a neocortex section immunostained for α-synuclein. a6, STORM image of the same area revealing the dense honeycomb organization of the Lewy body. b1, Conventional fluorescence microscopy image of a typical Lewy body immunostained for α-synuclein and pTau. b2, Two-Color STORM image of the same area showing a central core of aggregated pTau surrounded by reticulated α-synuclein. c1, Conventional fluorescence microscopy image of a Lewy neurite (black arrowhead) immunostained for α-synuclein and neurofilaments (NF). c2, Two-Color STORM image of the same area showing α-synuclein dense aggregates bounded by neurofilaments. Note the unaffected axon with normal caliber (white arrowhead).

Discussion

In this work, we combined approaches used for cellular imaging to neuropathological techniques in order to develop a reliable STORM protocol for observing human control and pathological brain samples. This allowed to characterize with a nanometer-scale precision the architecture of physiological structures in human cortex and white matter, such as axons, oligodendrocytes processes, and pre- and post-synaptic compartments. In addition, for the very first time, we imaged Aβ, Tau and Lewy aggregates with unprecedented details from brain samples of patients affected with neurodegenerative disorders.

Until now, the only approach to image nanoscopic brain structures relied on TEM. While TEM imaging is time consuming, requires ultrathin tissue sections and stringent sample preparation, and limits its focus on restricted areas, STORM imaging retains the advantages of conventional fluorescence microscopy with respect to sample preparation, specificity of the molecular labelling, 3D acquisitions and multi-channel observations across large areas. The tissue preparation technique developed in this work for STORM brain tissue observations is time-saving and easily reproducible, as it is inspired by the protocols used routinely for conventional fluorescence microscopy. Moreover, it can be used on any brain tissue sample stored in a Brain Bank, with reagents and antibodies commonly employed in neuropathology departments and neuroscience research laboratories. Finally, the acquisition and reconstruction of a STORM image takes only a few minutes.

Nevertheless, while attractive, performing STORM on human brain samples requires adjustments to generate high resolution final images. Regarding sample preparation, the first issue is the presence of sample-induced aberrations that can distort and blur single-molecule emission patterns, in particular when performing 3D acquisition. In this work, we selected to use <5 μm tissue sections to limit the impact of optical artifacts on the final image. Imaging thicker brain sections can be considered, however it should require complementary techniques such as adaptive optics (AO)-based correction or self-interferences (SELFI) method to avoid excessive aberrations[10,11]. Sample preparation is also critical. First, the signal of auto-fluorescent materials must be reduced using quenchers. Likewise, the fluorophores must have high photoswitching kinetics and sufficient brightness to be detected properly. In this work, we chose to use AF 647 and AF 532 as they exhibit excellent photoswitching characteristics and have long wavelength excitation and emission, allowing deep tissue penetration and limiting background signal from tissue autofluorescence. The sizes of the antibodies used for immunostaining has also to be adapted to those of the analyzed nano-structures, as the combination of a primary and a secondary antibody can reach up to 30 nm distance. Nevertheless, we selected conventional immunostaining with antibodies routinely used in neuropathology departments, because they are accessible and commonly employed both in neuroscience research and clinicopathological practice. But the immunostaining protocol can involve fluorescent probes or primary antibodies conjugated with fluorophores to increase the accuracy of the measurements. Finally, the background fluorescence generated

by fluorophores located outside the focal plane must be reduced to its minimum. To meet this imperative, we used TIRF illumination[12], with the incident beam reflected at the coverslip and the sample excited by the resulting evanescent wave, thus providing effective optical-sectioning and background reduction. However, as TIRF illumination is limited to a depth of a few micrometers, other approaches should be considered for imaging thicker tissue sections, such as light-sheet illumination or tissue clearing[13].

To conclude, STORM imaging of human tissue samples will provide valuable data about the organization and composition of physiological and pathological brain structures. In particular, the ultrastructural imaging of Aβ, pTau and α-synuclein pathological samples will further contribute to a more comprehensive understanding of the progressive mechanisms involved in AD, PD and DLB. Moreover, inferring correlations between clinical diagnosis and high-resolution imaging should further highlight ultrastructural differences between lesions, identify factors contributing to clinical heterogeneity, and define subclasses of diseases, precluding future therapeutic routes. Finally, the easiness of sample preparation should open a straightforward extension of this approach to study the pathological lesions of other neurodegenerative disorders such as Frontotemporal Lobar Dementia, Amyotrophic Lateral Sclerosis, Huntington disease, or Multiple Sclerosis, with promising new avenues to the current challenges in neuroscience.

Acknowledgements

The authors acknowledge the donors and their families. We are grateful to Khalid Hamid El Hachimi for providing us biopsies for electron microscopy. This work was supported by the University Hospital of Angers (Grant N° 2016-A01425-46) and by the Institut National de la Santé et de la Recherche Médicale (INSERM Research Fellow 2017–2019).

Author Contributions

P.C. initiated and led all aspects of the project, conducted the experiments, analyzed data and wrote the manuscript. A.C. and F.L. supervised the project. A.C. optimized the imaging protocol. F.L., L.R., C.D. and J.P.J. helped in developing the tissue preparation method. S.M. conducted TEM acquisitions. P.C., F.L., S.M., L.R., C.V., G.L., C.D., J.-P.J., J.C. and A.C. proofread the manuscript and agreed on its final version.

Competing Interests

The authors declare no competing interests.

References

1. Schermelleh, L. et al. Super-resolution microscopy demystified. Nat Cell Biol. **21**,72-84 (2019).

2. Rust, M. J., Bates, M. & Zhuang, X. Sub-diffraction-limit imaging by stochastic optical reconstruction microscopy (STORM). Nat. Methods **3**, 793–795 (2006).

3. Sigal, Y. M., Zhou, R. & Zhuang, X. Visualizing and discovering cellular structures with super-resolution microscopy. Science **361**, 880-887 (2018).

4. Xu, K., Zhong, G. & Zhuang, X. Actin, spectrin, and associated proteins form a periodic cytoskeletal structure in axons. Science **339**, 452-6 (2013).

5. Dani, A. et al. Superresolution imaging of chemical synapses in the brain. Neuron **68**, 843-856 (2010).

6. Huang, B. et al. Three-dimensional super-resolution imaging by stochastic optical reconstruction microscopy. Science **319**, 810-813 (2008).

7. Montine, T. J. et al. National Institute on Aging-Alzheimer's Association guidelines for the neuropathologic assessment of Alzheimer's disease: a practical approach. Acta Neuropathol. **123**, 1-11 (2012).

8. Hainsworth, A. H. et al. Super-resolution imaging of subcortical white matter using stochastic optical reconstruction microscopy (STORM) and super-resolution optical fluctuation imaging (SOFI). Neuropathol Appl Neurobiol. **44**, 417-426 (2018).

9. Braak, H. & Del Tredici, K. Invited Article: Nervous system pathology in sporadic Parkinson disease. Neurology. **70**, 1916-1925 (2008).

10. Bon, P. et al. Self-interference 3D super-resolution microscopy for deep tissue investigations. Nat Methods **15**, 449-454 (2018).

11. Mlodzianoski, M. J. et al. Active PSF shaping and adaptive optics enable volumetric localization microscopy through brain sections. Nat Methods **15**, 583-586 (2018).

12. Boulanger, J. et al. Fast high-resolution 3D total internal reflection fluorescence microscopy by incidence angle scanning and azimuthal averaging. Proc Natl Acad Sci USA **111**, 17164-17169 (2014).

13. Gustavsson, A. K., Petrov, P. N. & Moerner, W. E. Light sheet approaches for improved precision in 3D localization-based super-resolution imaging in mammalian cells. Opt Express. **26**, 13122-13147 (2018).

Methods

Tissue samples

All post mortem brain samples used for STORM imaging were obtained from the Neurodegenerative Diseases Brain Bank of Angers University Hospital. Four patients with neurodegenerative disorders and 3 age-matched control subjects were chosen by screening archived histological sections. Samples from prefrontal cortex, parietal cortex, temporal cortex, peri-ventricular white matter, and *substantia nigra* were considered. Patient and control characteristics are reported in Supplementary Table 1.

Immunostaining

Cryopreserved brain samples were used for STORM imaging (samples bathed 30 seconds into iso-pentane immersed in liquid nitrogen during brain autopsy and stored dry at -80°C). Tissue samples were cryo-sectioned at −20 °C into 5 µm thick sections using a Leica CM3050 S cryostat (Leica Biosystems, Wetzlar, Germany). Each frozen section was retrieved onto 22x22 mm N°1 cover glasses (Paul Marienfeld, Lauda-Königshofen, Germany), air-dried for 45 minutes. After three washes in phosphate buffered saline (PBS) (PAN-Biotech, Aidenbach, Germany) the sections were blocked and permeabilized in 0.1% triton X-100 and 5 % bovine serum albumin (BSA) (Sigma-Aldrich, Saint-Louis, MO, USA) in PBS for 1 h at room temperature (RT). The sections were then washed and incubated over night at 4 °C with primary antibodies diluted in blocking solution. The next day, the sections were washed and incubated with appropriate AF-conjugated secondary antibodies (Thermo Fisher Scientific, Waltham, MA, USA) diluted in blocking solution for 2 hours at RT. Finally, DNA was counterstained with Hoechst 33342 (Thermo Fisher Scientific, Waltham, MA, USA) diluted in PBS (1:200) for 5 minutes at RT. Sudan Black B (Sigma-Aldrich, Saint-Louis, MO, USA) or TrueBlack® (Biotium, Fremont, CA, USA) were used to quench lipofuscin autofluorescence following manufacturer's instructions. Antibodies and reagents references and dilutions are reported in Supplementary Table 2.

STORM Acquisition

For super resolution imaging, the cavity of a clean single depression slide (Paul Marienfeld, Lauda-Königshofen, Germany) was filled with 50 µl of switching buffer (Abbelight, Paris, France), and covered by a coverslip, the sample side facing downward. Excess buffer was carefully wiped away, and the coverslip was sealed on its slide with the two-component silicone-glue Twinsil® (Picodent, Wipperfürth, Germany). After a drying time of 10 minutes, the device was placed on the stage of an inverted motorized microscope NIKON ECLIPSE Ti-E (Nikon Instruments Europe, Amsterdam, The Netherlands) equipped with a CFI SR APO TIRF 100X ON1.49 objective, a Perfect Focus System, and a Total Internal Reflection Fluorescence (TIRF) ILas2 module (Roper Scientific, Martinsried, Germany). Image sequences were acquired with a single-photon sensitive camera Evolve 128TM EMCCD 512 x 512 imaging array, 16 x 16 µm pixels (Photometrics, Tucson, AZ, USA). Acquisitions were performed at fixed temperature 25°C (Okolab NA, Pozzuoli, Italy). Phase contrast

was first used for orientation and focus adjustment. The TIRF angle was then adjusted for each channel to reduce the background excitation. The region of interest was defined using the 647 nm and 532 nm laser line, and the 488 nm laser line was used to assess the autofluorescence signal. Prior to STORM imaging, a multichannel conventional fluorescence microscopy image was acquired for subsequent comparison with STORM image. The excitation power of either 647 nm or 532 nm laser line was then strongly increased (~50 to 100 mW before the objective lens) to induce fluorophore blinking and preform STORM imaging. The em-gain of the camera was set to high amplification to optimize the signal-to-noise ratio. Images were acquired with an integration time of 30 ms per frame. The total acquisition time points for each sequence was adapted to the observed structure and to the labelling density (5,000 to 20,000 frames).

Image reconstruction

The center positions of the fluorophores were determined by fitting of 2D Gaussian function with parameters of microscope's point spread function (PSF) using WaveTracer software (Roper Scientific, Martinsried, Germany). Imaris 8.0 software (Bitplane, Zurich, Switzerland) was used for image processing and visualization. More than 300 STORM images have been acquired and analyzed in total.

Immunohistochemistry

Formalin-fixed tissue samples were embedded in paraffin and cut at 4 µm using a Leica RM125 microtome (Leica Biosystems, Wetzlar, Germany). Sections were collected on slides and immunostained using a fully automated IHC stainer Leica-BOND III (Leica Biosystems, Wetzlar, Germany). Finally, samples were analyzed under a Zeiss Axioscop40 microscope equipped with an Axio-cam MRC5 camera, using AxioVisio 4.6 software (Carl Zeiss, Oberkochen, Germany).

Electron microscopy

Brain cortical samples from the middle frontal gyrus of the right hemisphere were collected between 1974 and 1986[15]. Biopsies were immediately fixed in Karnovsky's solution, postfixed in osmium, and embedded in Araldite. Samples from a 38-year-old male subject who suffered a brain hemorrhage were used as control (laboratory identification #927). Samples from a 58-year-old male patient affected with a familial form of AD (M146L mutation of the *PSEN1* gene) were used to study neurofibrillary tangles and senile plaques (laboratory identification #1507). Seventy-nm-thick ultrathin sections were collected on copper grids, and contrasted by incubation with 5 % uranyl acetate followed by lead citrate for 5 min each. Sections were analyzed with a Hitachi HT 7700 (Elexience, Verrieres le Buisson, France) electron microscope. More than 80 TEM images have been analyzed in total for each sample.

Statistical analysis

Statistical analyses were conducted using PRISM software version 5.0 for Windows (GraphPad, La Jolla, CA). Comparisons of means were performed using Student's t-test for two groups analysis, and one-way analysis of variance (ANOVA) for multiple groups analysis, after verifying the Normal distribution and the homoscedasticity of data using Shapiro–Wilk's test. In the absence of Normal distribution, the nonparametric Mann–Whitney U-test was used. Differences were considered to be significant at $p<0.01$.

Ethical considerations

Brain tissue samples were stored in the Biological Resource Centre « Neurodegenerative disorders » (national identifier BB-0033-00038) after being authorized by the Regional Ethics Committee West II (declaration number DC-2011-146). The study protocol has been declared to the French commission for information technology and civil liberties (declaration number ar19-0012v0). An anonymous database and a list of correspondence have been generated and stored on a hard disk of the University Hospital of Angers with restricted access.

Reporting Summary.

Further information on research design is available in the Nature Research Reporting Summary linked to this article.

Data availability

The data sets generated and analyzed during the current study are available from the corresponding author on reasonable request.

References

14. Braak, H. et al. Staging of brain pathology related to sporadic Parkinson's disease. Neurobiol Aging. **24**, 197-211 (2003).

15. Androuin, A. et al. Evidence for altered dendritic spine compartmentalization in Alzheimer's disease and functional effects in a mouse model. Acta Neuropathol. **135**, 839-854 (2018).

Supplementary data

Supplementary Figure

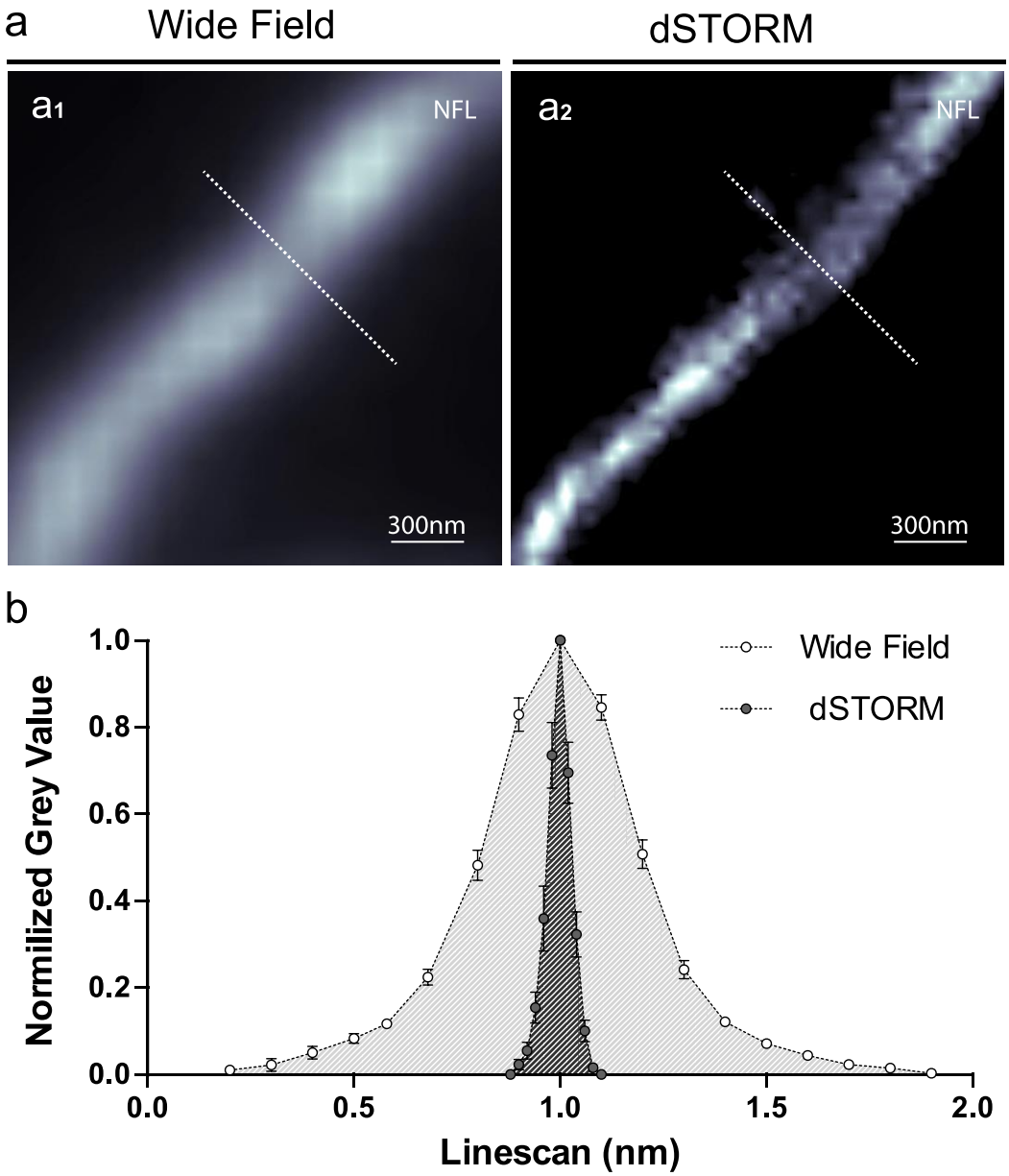

Supplementary Fig. 1. Comparison of conventional fluorescence and STORM imaging of axonal processes. a1, Conventional fluorescence image of a longitudinally sectioned axon immunostained for neurofilaments (NF) in prefrontal cortex. a2, STORM image of the same area. b, Representation of the cross-sectional profiles (dotted lines in a) through axonal process. Error bars indicate mean with standard error, n=8 measures per image.

Supplementary Movie

Supp Movie 1. Super-resolution imaging of human brain samples with STORM. STORM imaging of a cortical axon in a human brain section immunostained for neurofilaments.

Supplementary Tables

Supplementary table 1: Controls and patients clinical and pathological characteristics.

Identifier	Gender	Age	Clinical information	Tau and Aβ pathology[7]	Lewy pathology[14]
17N00233	M	25	Control (BH)	-	-
18N00117	F	48	Control (AMOF)	-	-
18N00032	M	70	Control (AMOF)	-	-
18N00040	F	86	Dementia	A3-B3-C3	-
18N00132	F	66	Dementia	A4-B5-C3	-
18N00068	F	58	Parkinsonism	A4-B5-C3	Stage 4
17N00238	M	74	Parkinsonism	A2-B3-C3	Stage 5

AMOF: Acute Multiple Organ Failure, BH Brain Hemorrhage.

Supplementary table 2: Antibodies and reagents.

Primary antibodies	Host	Company	Catalog Number	Dilution
Alpha-synuclein (phospho S129)	Rabbit	Abcam	ab209422	1:1000
Bassoon	Rabbit	Synaptic Systems	141003	1:250
Beta Amyloid	Rabbit	Abcam	ab2539	1:1000
Beta Amyloid	Mouse	Dako-Agilent	M0872	1:1000
Homer 1	Mouse	Synaptic Systems	160011	1:500
Myelin Basic Protein	Rabbit	Dako-Agilent	A0623	1:250
Neurofilament	Mouse	Monosan	MON3004-1	1:1000
Phospho-Tau (Ser202, Thr205)	Mouse	Thermo Fisher	MN1020	1:1000
Secondary antibodies	**Host**	**Company**	**Catalog Number**	**Dilution**
Alexa Fluor 532 anti-Mouse IgG	Goat	Thermo Fisher	A-11002	1:2500
Alexa Fluor 647 anti-Mouse IgG	Goat	Thermo Fisher	A-21235	1:2500
Alexa Fluor 532 anti-Rabbit IgG	Goat	Thermo Fisher	A-11009	1:2500
Alexa Fluor 647 anti-Rabbit IgG	Goat	Thermo Fisher	A-21244	1:2500

Reagents or Resources	Company	Catalog Number
Abbelight smart kit STORM	Abbelight	SMART KIT-1
Bovine Serum Albumin	Sigma-Aldrich	A6003
Fluoromount-G®	Southern Biotech	0100-01
Hoechst 33342	Thermo Fisher Scientific	H3570
Microscope cover glasses	Paul Marienfeld	0102052
Microscope slide with single cavity	Paul Marienfeld	1320000
Paraformaldehyde	Sigma-Aldrich	P6148
Phosphate Buffered Saline	Pan Biotech	P04-53500
Sudan Black B	Sigma-Aldrich	199664
Triton X-100	Sigma-Aldrich	T9284
TrueBlack®	Biotium	CAT#23007
Twinsil®	Picodent	CAT#13001000

3. DISCUSSION ET PERSPECTIVES

3.1. Principaux résultats de l'étude

Dans ce travail nous avons mis au point une technique novatrice d'analyse super-résolutive de tissu cérébral humain en utilisant une approche pluridisciplinaire. La résolution des images est élevée, proche de celles obtenues en microscopie électronique, et les techniques complémentaires en double couleur et 3D-STORM permettent une analyse plus complète de la composition et de l'architecture des structures étudiées.

Le développement de la technique de microscopie super-résolutive STORM constitue une avancée considérable dans le domaine de la microscopie optique. Si le matériel nécessaire à la réalisation des acquisitions était initialement onéreux et son utilisation particulièrement complexe, la commercialisation des outils d'imagerie super-résolution par différents constructeurs a permis ces dernières années une démocratisation de la technique et son utilisation par de nombreuses équipes de recherche. Les fabricants proposent désormais des modules complémentaires qu'il est possible d'implémenter directement sur un statif déjà disponible, diminuant ainsi les couts d'acquisition. De plus, certains constructeurs proposent des appareils et réactifs clé-en-main, facilitant d'autant plus la mise en place du dispositif au sein d'une unité de recherche. Enfin des logiciels open source intuitifs permettant une reconstruction fiable d'images super-résolues sont disponibles en téléchargement libre.

Sur un plan pratique, si les temps d'acquisition et de reconstruction des images sont plus importants qu'en imagerie optique conventionnelle (environ 10 minutes pour l'obtention d'une image STORM), ce délai reste raisonnable en regard du gain résolutif permis par la technique. Dans cette étude nous avons choisi d'employer un protocole classique d'immunomarquage basée sur l'utilisation d'anticorps primaires ciblant une protéine spécifique de structure, et un anticorps secondaire couplé à un fluorochrome permettant la révélation du premier. Nous nous sommes par ailleurs attachés à utiliser des anticorps communs, utilisés en routine dans les services d'anatomopathologie et les laboratoires de recherche en neurosciences, afin de favoriser la diffusion de la technique. Toutefois ce choix méthodologique diminue sensiblement la résolution des images acquises : en effet, le complexe antigène + anticorps primaire + anticorps secondaire peut mesurer jusqu'à 30 nm, de par la taille des immunoglobulines utilisées. Si cette distance est négligeable en microscopie conventionnelle, elle peut gêner les mesures et études en colocalisation lors d'une acquisition en nanoscopie. Nous travaillons actuellement sur la mise au point de techniques de préparation

permettant de réduire la taille du complexe de marquage, en utilisant des anticorps primaires directement couplés à un fluorochrome, des immunoglobulines recombinantes de plus petite taille (fragments Fab, fragments monocaténaires), et des sondes fluorescentes. Cette stratégie permettra d'obtenir un signal au plus proche de la structure et diminuer les artéfacts de marquage.

La technique d'imagerie STORM présentée dans cet article permet l'analyse d'échantillons de tissu cérébral de patients à l'échelle nanoscopique. L'extension et l'adaptation de ce protocole à d'autres types de tissus peuvent être envisagées, ouvrant de nombreuses perspectives dans les champs de la recherche et du diagnostic : échantillons issus de modèles animaux ou végétaux, biopsie de patient ou encore matériel autopsique. Il est toutefois important de considérer qu'une connaissance des principes fondamentaux de physique optique et d'imagerie cellulaire, ainsi qu'une formation à la discipline anatomopathologique (préparation d'échantillons et lecture de lames) sont nécessaires pour permettre l'acquisition d'images STORM sur coupes tissulaires, pouvant ainsi constituer une limite technique.

3.2. Perspectives en recherche

3.2.1. Analyse des lésions motoneuronales dans la SLA à l'échelle nanométrique

Dans cette étude, les délais d'accès aux tissus cérébraux et médullaires de patients atteints de SLA stockés au sein du Centre de Ressources Biologiques (CRB) du CHU d'Angers suivant l'émission de l'autorisation de Comité de Protection des Personnes (CPP) n'ont pas rendu possible l'utilisation ces prélèvements pour ce projet. La technique a donc été initialement mise au point sur des échantillons de patients et sujets contrôles déjà accessibles au sein du laboratoire au moment de la délivrance des autorisations administratives et éthiques. Les résultats obtenus pour l'analyse d'agrégats protéiques dans les maladies d'Alzheimer et de Parkinson nous incitent à poursuivre ce travail et utiliser l'imagerie STORM pour caractériser la composition et l'architecture des lésions observées au sein du SNC des patients atteints de SLA.

En effet, si les observations anatomo-histologiques ont indiscutablement permis d'émettre des hypothèses quant aux mécanismes de neurodégénérescence impliqués dans la SLA, les contraintes résolutives et techniques des approches d'imagerie cellulaire conventionnelles rendent difficile l'obtention de nouvelles données pathologiques.

Cette limite est d'abord présente à l'échelle cellulaire, dans les analyses morphologiques visant à caractériser avec précision la localisation des agrégats protéiques au sein des neurones et leurs

rapports aux autres structures intracellulaires. Une étude récente portant sur la présence d'agrégats intra-mitochondriaux de protéine TDP-43 avait utilisé une approche en immunofluorescence conventionnelle en double marquage sur tissu médullaire de patient (Figure 11a) (Wang et al., 2016 *sup data*). Si les résultats obtenus permettent de suspecter une proximité des agrégats protéiques et des mitochondries au sein des motoneurones, la localisation exacte de TDP-43 autour ou au sein de cet organite reste à définir. Une analyse en imagerie double couleur STORM ciblant TDP-43 et différents marqueurs mitochondriaux (membrane externe, membrane interne, matrice) permettrait ainsi de confirmer et de préciser à l'échelle nanoscopique la localisation intra-mitochondriale de ces inclusions. Plus généralement, une telle approche permettrait d'étudier les rapports des agrégats protéiques avec les différents organites intracellulaires des motoneurones (lysosomes, peroxysomes, noyau).

A l'échelle moléculaire, les limites résolutives des systèmes optiques et les difficultés techniques de l'imagerie électronique empêchent la caractérisation précise de la constitution et de l'architecture des agrégats intraneuronaux. Une étude en immunofluorescence utilisant une acquisition en triple marquage TDP-43, périphérine et ubiquitine suivie d'un traitement numérique par déconvolution des images obtenues afin d'en augmenter la résolution, avait permis d'observer une organisation en bulbe d'oignon des agrégats (Figure 11b) (Sanelli et al., 2007). La protéine TDP-43 étant située en périphérie de ces inclusions, les auteurs avançaient l'hypothèse d'une implication plus importante de la périphérine, située plus au cœur des agrégats, dans les mécanismes physiopathologiques à l'origine de la maladie. Toutefois, compte tenu de la possible construction d'artéfacts numériques résultant de l'application d'algorithmes de déconvolution aux images acquises par système optique, l'utilisation d'une imagerie STORM (double couleur et 3D) plus résolutive et basée sur la détection directe du signal fluorescent permettrait un complément d'analyse plus précis mais également plus fiable.

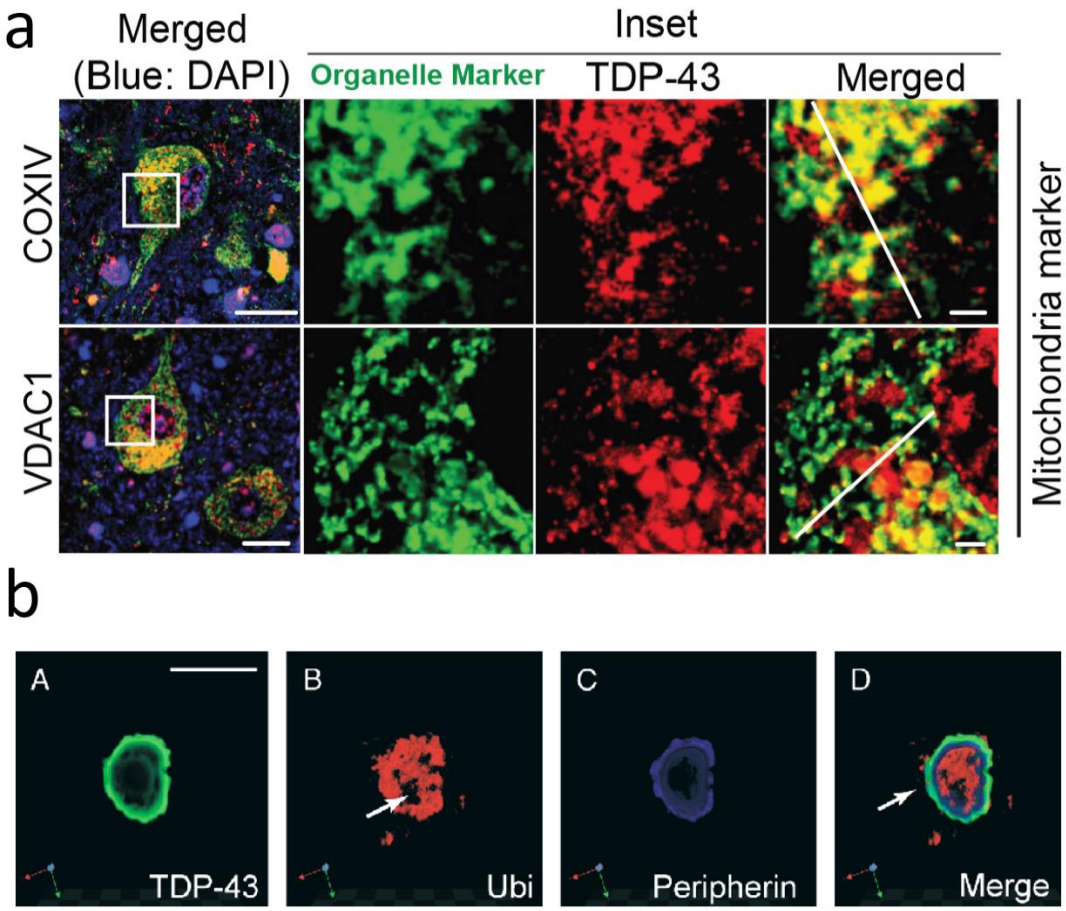

Figure 11 : Limites techniques actuelles rencontrées en imagerie optique conventionnelle pour l'étude des rapports et de l'ultrastructure des agrégats protéiques intraneuronaux chez les patients atteints de SLA. a. Travaux de Wang et al., 2016 (*supp data*) : si la superposition (jaune) des signaux émis par l'immunomarquage ciblant TDP-43 (rouge) et des deux marqueurs mitochondriaux (COXIV et VDAC1, en vert) permet de suspecter une proximité des agrégats protéiques avec les mitochondries au sein des motoneurones, la localisation exacte de TDP-43 autour ou au sein de cet organite reste à définir. Barres d'échelle 20 µm (2 µm inset) b. Travaux de Sanelli et al., 2007 : l'utilisation d'algorithmes de déconvolution permet d'augmenter numériquement la résolution d'images acquises en immunofluorescence et étudier l'ultrastructure et la composition des agrégats intraneuronaux. Toutefois la possible présence d'artéfacts construits doit être prise en compte dans l'interprétation des images obtenues. Barre d'échelle 10 µm.

Dans cette optique, un travail préliminaire a été effectué sur tissu cérébral (cortex moteur) de sujets contrôles afin d'évaluer les possibilités d'utilisation de cette technique pour l'étude des agrégats de TDP-43 à l'échelle nanoscopique. Un immunomarquage dirigé contre les protéines TDP-43 (Proteintech 10782-2-AP, 1:750) et Lamine A/C (Novocastra NCL-LAM-C/C, 1:2000) a été réalisé. Les premières images obtenues nous ont permis de confirmer la possibilité de retenir cette méthode pour l'étude de TDP-43 en STORM, et d'observer avec précision la distribution de la protéine au sein du noyau des neurones en conditions normales (Figure 12a).

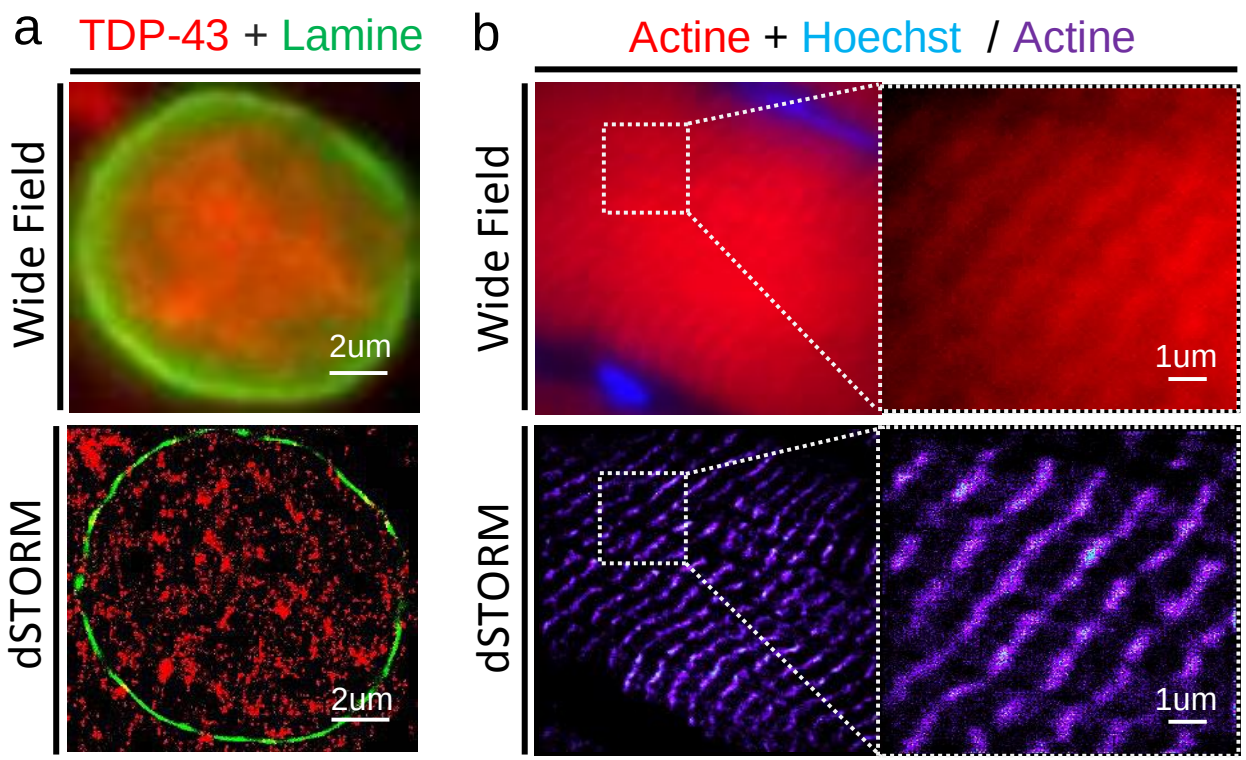

Figure 12. Protocole d'imagerie STORM sur tissu cérébral et musculaire. (a) Acquisition en Champ Large (Wide Field) et STORM d'un noyau de motoneurone central (cortex moteur de sujet contrôle). Immunomarquage dirigé contre les protéines TDP-43 et Lamine A/C. (b) Acquisition en Champ Large et STORM de myofibrilles au sein d'un myocyte en coupe longitudinale (biopsie musculaire de sujet contrôle). Marquage de l'actine par sonde Phallotoxine-647. (Images : P. Codron).

3.2.2. Protocole d'analyse du tissu musculaire en microscopie STORM

Nous avons également adapté les techniques de préparation et lecture afin de permettre l'analyse en microscopie STORM de tissu musculaire provenant de biopsies effectuées en ambulatoire chez des patients atteints de maladies neuromusculaires. Nous avons ainsi pu obtenir des images super-résolutives de myofibrilles de fibres musculaires en utilisant un marquage de l'actine par Phallotoxine-647 (Thermo-Fisher Scientific) (Figure 12b,c). Ainsi, l'étude des structures intra- et inter-myofibrillaires des fibres musculaires squelettiques prélevées chez des patients atteints de SLA sporadique pourrait mettre en lumière des lésions auparavant indétectables en microscopie optique conventionnelle.

4. CONCLUSION ET OUVERTURE

Un projet de recherche financé par le CHU d'Angers (appel d'offre interne 2019) débutera au mois de Novembre 2019, avec pour objectif l'analyse en microscopie super-résolutive STORM de coupes histologiques cérébrales et médullaires de patients atteints de SLA sporadique. Nous utiliserons les échantillons de cerveau de patients issus de la Biocollection du service de neuropathologie du CHU d'Angers comptant plus de 50 cerveaux et moelles épinières de patients atteints de SLA. Nous étudierons avec précision l'architecture des lésions présentes au sein des motoneurones des patients, en nous intéressant plus particulièrement aux agrégats de protéine TDP-43, aux anomalies du cytosquelette et à l'architecture du réseau mitochondrial. Des échantillons de sujets contrôles, dont l'étude histologique n'a pas permis de retrouver de signes de neurodégénérescence active, seront utilisés comme contrôle. Un travail complémentaire portant sur des biopsies musculaires sera également effectué, afin de tenter d'identifier des anomalies ultrastructurelles au sein des myofibrilles des patients. L'utilisation de l'imagerie STORM pour l'analyse d'échantillons cérébraux et médullaires prélevés chez des patients atteints de SLA pourrait permettre de caractériser à l'échelle nanoscopique la composition et l'architecture des lésions observées au sein des motoneurones et d'améliorer nos connaissances sur les mécanismes physiopathologiques à l'origine de la maladie. Les corrélations clinico-histologiques obtenues par une approche translationnelle pourront également permettre de détacher différents profils de patients.

CHAPITRE 2

MODELES ET BIOMARQUEURS

Étude de l'ultrastructure et du métabolisme de fibroblastes en culture issus de patients atteints de SLA sporadique

Années :

- 2016-2017

Laboratoire d'accueil :

- UMR CNRS 6015 INSERM 1083, Angers, France

Financement :

- Médaille d'Or Université d'Angers 2016-2017
- Appel d'Offre Interne CHU Angers 2016

Primary fibroblasts derived from sporadic amyotrophic lateral sclerosis patients do not show ALS cytological lesions

P. Codron[1,2,3], J. Cassereau[1,2], P. Vourc'h[4,5], C. Veyrat-Durebex[2], H. Blasco[2,4,5], S. Kane[2], V. Procaccio[2], F. Letournel[3], C. Verny[2], G. Lenears[2], P. Reynier[2], A. Chevrollier[2]

1. Department of Neurology, ALS Center, University Hospital of Angers, Angers Cedex 9, France
2. MitoLab Unit, MITOVASC Institute, CNRS 6015, INSERM U1083, University of Angers, Angers Cedex 9, France
3. Department of Neurobiology and Neuropathology, University Hospital of Angers, Angers Cedex 9, France
4. Department of Biochemistry and Molecular Biology, University Hospital of Tours, Tours Cedex 1, France
5. School of Medicine, INSERM U930, François-Rabelais University, Tours Cedex 1, France

ÉTUDE DE L'ULTRASTRUCTURE ET DU METABOLISME DE FIBROBLASTIQUES EN CULTURE ISSUS DE PATIENTS ATTEINTS DE SLA SPORADIQUE

1. PRELEVEMENTS CUTANES ET FIBROBLASTES EN CULTURE

1.1. La biopsie cutanée pour l'étude des maladies neurodégénératives

Si l'approche anatomo-clinique a indiscutablement joué un rôle central dans l'émergence des hypothèses portant sur la physiopathologie de la SLA, son caractère observationnel post-mortem empêche l'approche interventionnelle permise par les expérimentations in vitro et in vivo. Toutefois, l'impossibilité d'obtenir des lignées primaires neuronales de patients, les difficultés techniques et les coûts engagés pour la genèse de cellules souches pluripotentes induites (iPSC), et l'absence de modèle cellulaire ou animal reproduisant fidèlement les mécanismes de neurodégénérescence en œuvre dans la maladie constituent des limites certaines.

Ces dernières années, un nombre croissant de travaux a porté sur l'étude des anomalies cutanées présentées par les patients porteurs de maladies neurodégénératives. En effet, en raison de l'origine embryonnaire ectodermique commune de la peau et du système nerveux, certaines lésions proches de celles observées au sein du SNC peuvent être détectées au niveau cutané par analyses histologiques. La réalisation d'une biopsie cutanée - peu invasive - offre en outre la possibilité de générer des cultures de fibroblastes dérivant directement des patients. Ces cellules dont le phénotype se rapproche en certains points de celui des astrocytes et des neurones (Janmaat et al., 2015) permettent une approche translationnelle particulièrement intéressante pour l'identification et l'étude de marqueurs biologiques du vivant des patients (del Hoyo et al., 2006 ; Auburger et al., 2012 ; Mocali et al., 2014 ; Khan et al., 2015 ; Codron et al., 2016).

1.2. Applications dans le domaine de la SLA

Dans le champ de la recherche sur la SLA, les études histologiques menées depuis 2010 sur tissu cutané de sujets atteints de la maladie ont révélé des anomalies similaires à celles observées au niveau de la moelle épinière des patients, telles qu'une augmentation de l'expression de la protéine TDP-43 (Suzuki et al., 2009), une fragmentation du réseau mitochondrial (Rodrígez et al., 2012), une augmentation des marqueurs de l'inflammation (Fukazawa et al., 2013, Ono et al., 2001) et de l'expression des protéines de l'homéostasie telles que l'Ubiquitine (Watanabe et al., 2010) et la VCP

(Ishikawa et al., 2012), et une augmentation des taux de collagénases et métalloprotéinases (Fullmer et al., 1966 ; Fang L et al., 2009) associée à une désorganisation du collagène (Ono et al., 1988, Kolde et al., 1996).

Compte tenu de ces résultats, un nombre croissant d'études a porté sur des fibroblastes en culture obtenus à partir de prélèvements cutanés de patients atteints de SLA. Ces travaux ont principalement été menés sur des fibroblastes issus de patients atteints de formes familiales de la maladie. En effet, ces cellules exprimant naturellement des mutations pathogènes, elles constituent un bon modèle d'étude de la fSLA. Les principaux résultats de ces études sont reportés dans le Tableau 2.

Tableau 2. Principaux résultats des études menées sur des fibroblastes en culture générés à partir de prélèvements cutanés de patients atteints de SLA familiale. (P. Codron)

Auteurs	**Mutations (patients)**	**Principaux Résultats**
Bartolome et al., 2013	VCP^{R155C} (n=1), VCP^{R155H} (n=1), VCP^{R191Q} (n=1)	Abaissement du potentiel de membrane mitochondrial, diminution de la production d'ATP.
Schwartz et al., 2014	FUS^{H517Q} (n=1), $FUS^{M511Nfs*6}$ (n=1)	Agrégats intranucléaires de la protéine FUS, hyperphosphorylation de l'ARN-polymérase II.
Allen et al., 2014	$SOD1^{I113T}$ (n=3)	Diminution de production d'ATP par phosphorylations oxydatives et augmentation des voies de la glycolyse.
Bannwarth et al., 2014	CHCHD10 (n=1)	Diminution de production d'ATP par phosphorylations oxydatives, diminution de la consommation en dioxygène, fragmentation du réseau mitochondrial.
Yu et al., 2015	FUS^{R521C} (n=1), FUS^{R514G} (n=1)	Relocalisation cytosolique de la protéine FUS.
Yang S et al., 2015	$UBQLN2^{T487I}$ (n=1),$TDP\text{-}43^{M337V}$ (n=2)	Présence d'agrégats cytosoliques ubiquitinylés de TDP-43 après traitement par MG132 (inhibition de l'UPS), Sodium Arsenite et H2O2 (induction d'un stress oxydant).
Sabatelli et al., 2015	$TDP\text{-}43^{A382T}$ (n=2), $TDP\text{-}43^{G294V}$(n=1), $SOD1^{L84F}$ (n=1), $SOD1^{D90A}$(n=1) $SOD1^{G93D}$(n=1), $SOD1^{E133del}$(n=1), FUS^{R521C} (n=1), $FUS^{c*59G>A}$ (n=1), C9ORF72 expansions (n=3)	Présence d'agrégats cytosoliques de TDP-43 chez les fibroblastes porteurs de mutations sur les gènes *TARDBP*, *FUS* et *C9Orf72*. Diminution de l'expression de la protéine chez les fibroblastes porteurs d'une mutation sur le gène *SOD1*.
Onesto et al., 2016	$TDP\text{-}43^{A382T}$ (n = 3) C9ORF72 expansions (n = 4)	Absence de relocalisation cytosolique ou mitochondriale de TDP-43. Fragmentation du réseau mitochondrial. Élévation du potentiel de membrane mitochondrial associée à une augmentation de la consommation d'ATP, du stress oxydant et de la mitophagie chez les fibroblastes *C9Orf72*.
Orrù et al., 2016	$TDP\text{-}43^{A382T}$ (n= 2)	Diminution du nombre de stress granules et de la viabilité cellulaire chez les fibroblastes porteurs de la mutation après induction d'un stress oxydant par Sodium Arsenite.

1.3. Enjeux pour la recherche sur la SLA sporadique

Les résultats de ces travaux nous ont amenés à envisager l'utilisation de fibroblastes issus de patients atteints de sSLA pour l'étude de la forme sporadique de la maladie. En effet, compte tenu de l'absence de mutation impactant directement la machinerie cellulaire chez ces cellules, la mise en évidence d'anomalies caractéristiques de la SLA traduirait l'existence de mécanismes pathogènes systémiques telles qu'une susceptibilité polygénique ou l'exposition à des facteurs environnementaux. Ainsi, la présence d'altérations chez ces cellules pourrait amener à conforter le fibroblaste comme modèle d'étude primaire de la SLA sporadique, et la caractérisation de ces anomalies pourrait permettre d'améliorer notre compréhension de la physiopathologie de la maladie. De plus, la mise en perspective des phénotypes cellulaires avec les paramètres cliniques des patients (âge, forme de la maladie, durée d'évolution) par une approche translationnelle permettrait d'identifier de potentiels marqueurs biologiques diagnostiques et pronostiques de la maladie observables du vivant des patients, particulièrement utiles en pratique clinique.

2. MISE EN PLACE DE L'ETUDE

2.1. Problématique et objectifs

Dans ce second travail nous avons cherché à caractériser le phénotype cellulaire de fibroblastes issus de patients atteints de SLA sporadique, en nous intéressant plus particulièrement aux signatures pathologiques centrales de la maladie. Notre objectif était de mettre en évidence la présence d'agrégats cytoplasmiques de protéine TDP-43, une désorganisation du cytosquelette, une fragmentation du réseau mitochondrial, et une altération du métabolisme énergétique et de la réponse au stress oxydant.

2.2 Contexte méthodologique et stratégie expérimentale

Ce projet a été financé conjointement par l'Université d'Angers (bourse d'étude) et le CHU d'Angers (appel d'offre interne 2016). L'inclusion des sujets (patients et témoins) a été réalisée prospectivement au sein du centre SLA du CHU d'Angers à partir du 1er décembre 2016 après validation du protocole de recherche par l'ANSM et le CPP Ouest 2. Un examen neurologique et un

prélèvement cutané ont été effectués lors d'une consultation avec l'investigateur principal pour l'ensemble des sujets participant à la recherche après signature d'un consentement éclairé. Les critères d'inclusion ont été définis à priori pour les patients (SLA cliniquement définie selon les critères d'El Escorial révisés - Airlie House, absence de comorbidité ou traitement susceptible de perturber le métabolisme énergétique ou protéique) et témoins (examen neurologique normal, absence de comorbidité ou traitement susceptible de perturber le métabolisme énergétique ou protéique). Les fibroblastes obtenus à partir de la biopsie de peau ont été amplifiés et cryo-congelés lors des premiers passages. La caractérisation génétique des patients a été réalisée au CHU de Tours (Laboratoire de Neurogénétique et Métabolomique, UMR INSERM U930, Tours), afin de s'assurer de l'absence de mutations sur les gènes responsables des formes familiales de SLA. La cinétique de croissance des cellules a été étudiée grâce au système IncuCyte® permettant le relevé automatisé de la confluence cellulaire au sein d'un incubateur. La localisation de la protéine TDP-43, l'architecture du cytosquelette et la dynamique du réseau mitochondrial ont été étudiées par microscopie à épifluorescence et super-résolution STORM. La production de radicaux libres oxydants a été quantifiée par microscopie à l'aide de sondes fluorescentes sensibles aux ROS. Enfin, la constitution de granules de stress a été étudiée par immunofluorescence après induction d'un stress oxydant par Sodium Arsenite.

Un travail complémentaire portant plus spécifiquement sur le métabolisme énergétique et lipidique de ces fibroblastes a été réalisé en parallèle par le Dr VEYRAT-DUREBEX au sein du laboratoire en utilisant des techniques d'oxygraphie, de métabolomique, de lipidomique et de séquençage de l'ADNmt. Ce travail a été effectué en partenariat avec l'UMR INSERM U930 de Tours et les Centres de Référence SLA de Tours et Limoges.

Les résultats de ces travaux sont rapportés dans l'article suivant (Codron et al.2018) et dans l'article complémentaire n°1 situé en annexe (Veyrat-Durebex et al., 2018).

Article N°2

Published in

Amyotrophic Lateral Sclerosis and Frontotemporal Degeneration

Volume 19, 2018 - Issue 5-6

Primary fibroblasts derived from sporadic amyotrophic lateral sclerosis patients do not show ALS cytological lesions

P. Codron[1,2,3], J. Cassereau[1,2], P. Vourc'h[4,5], C. Veyrat-Durebex[2], H. Blasco[2,4,5], S. Kane[2], V. Procaccio[2], F. Letournel[3], C. Verny[2], G. Lenears[2], P. Reynier[2], A. Chevrollier[2]

1. Department of Neurology, ALS Center, University Hospital of Angers, Angers Cedex 9, France
2. MitoLab Unit, MITOVASC Institute, CNRS 6015, INSERM U1083, University of Angers, Angers Cedex 9, France
3. Department of Neurobiology and Neuropathology, University Hospital of Angers, Angers Cedex 9, France
4. Department of Biochemistry and Molecular Biology, University Hospital of Tours, Tours Cedex 1, France
5. School of Medicine, INSERM U930, François-Rabelais University, Tours Cedex 1, France

Amyotrophic Lateral Sclerosis and Frontotemporal Degeneration, 2018; 1–11

RESEARCH ARTICLE

Primary fibroblasts derived from sporadic amyotrophic lateral sclerosis patients do not show ALS cytological lesions

PHILIPPE CODRON[1,2,3], JULIEN CASSEREAU[1,2], PATRICK VOURC'H[4,5], CHARLOTTE VEYRAT-DUREBEX[2], HÉLÈNE BLASCO[2,4,5], SELMA KANE[2], VINCENT PROCACCIO[2], FRANCK LETOURNEL[3], CHRISTOPHE VERNY[2], GUY LENEARS[2], PASCAL REYNIER[2] & ARNAUD CHEVROLLIER[2]

[1]*Department of Neurology, ALS Center, University Hospital of Angers, Angers Cedex 9, France,* [2]*MitoLab Unit, MITOVASC Institute, CNRS 6015, INSERM U1083, University of Angers, Angers Cedex 9, France,* [3]*Department of Neurobiology and Neuropathology, University Hospital of Angers, Angers Cedex 9, France,* [4]*Department of Biochemistry and Molecular Biology, University Hospital of Tours, Tours Cedex 1, France, and* [5]*School of Medicine, INSERM U930, François-Rabelais University, Tours Cedex 1, France*

Abstract

Objective: Sporadic amyotrophic lateral sclerosis (sALS) is a fatal neurodegenerative disorder affecting upper and lower motor neurons. In view of the heterogeneous presentation of the disease, one of the current challenges is to identify diagnostic and prognostic markers in order to diagnose sALS at early stage and to stratify patients in trials. In this study, we sought to identify cytological hallmarks of sALS in patient-derived fibroblasts with the aim of finding new clinical-related markers of the disease. *Methods*: Primary fibroblasts were prospectively collected from patients affected with classical, rapid, and slow forms of sALS. TDP-43 localization, cytoskeleton distribution, mitochondrial network architecture, and stress granules formation were analyzed using 3D fluorescence microscopy and new super-resolution imaging. Intracellular reactive oxygen species (ROS) production was assessed using live imaging techniques. *Results*: Six sALS patients (two classical, two rapid, and two slow) and four age-matched controls were included. No difference in fibroblasts cell growth, morphology, and distribution was noticed. The analysis of TDP-43 did not reveal any mislocalization nor aggregation of the protein. The cytoskeleton was harmoniously distributed among the cells, without any inclusion noticed, and no difference was observed regarding the mitochondrial network architecture. Basal ROS production and response to induced stress were similar among patient and control fibroblasts. *Conclusions*: ALS cytological lesions are absent in patient-derived fibroblasts and thus cannot contribute as diagnostic nor prognostic markers of the disease.

Keywords: *Amyotrophic lateral sclerosis*, *primary skin fibroblasts*, *TDP-43*, *cytoskeleton*, *mitochondria*, *oxidative stress*, *stress granules*

Introduction

Amyotrophic lateral sclerosis (ALS) is a neurodegenerative disorder affecting upper and lower motor neurons in the cortex, brainstem and spinal cord (1). Ninety percent of the ALS cases are sporadic (sALS), whereas 10% are hereditarily transmitted (fALS). The disease is responsible for a progressive paralysis leading to death within 2–5 years after the symptom onset, usually from respiratory failure. Clinical manifestations of ALS can vary widely from one patient to another in terms of location of onset, rate of progression, and associated non-motor involvement (2). Common pathophysiologic processes are nevertheless supported by the presence of constant postmortem lesions in degenerating motor neurons: intracytoplasmic inclusions of ubiquitinated 43 kDa TAR DNA-binding protein (TDP-43) (3), intermediate filaments aggregates (4), mitochondria structural alterations (5,6), and elevated markers of oxidative stress (7).

To date, the only treatment available for ALS is the Riluzole, with a modest efficiency on the progression of the disease (8). Indeed, despite the advances in understanding the pathophysiology of ALS in the last two decades, most therapeutic trials remained negative (9). Finding human-based study

Correspondence: Philippe Codron, Department of Neurology, ALS Center, University Hospital of Angers, 4 rue Larrey, 49933 Angers Cedex 9, France. Tel: +33 2 41 35 79 33. Fax: +33 2 41 35 51 18. E-mail: Philippe.Codron@chu-angers.fr

(Received 28 November 2017; revised 5 January 2018; accepted 9 January 2018)

ISSN 2167-8421 print/ISSN 2167-9223 online
DOI: 10.1080/21678421.2018.1431787

models of the disease with the aim of better characterizing its pathophysiology and identifying novel therapeutic prospects is a central issue. Furthermore, as patients may need personalized medicine in view of their heterogeneous clinical presentation, another current challenge is to identify clinical-related markers in order to diagnose ALS at the very early stage, and to stratify patients in trials on the basis of their clinical profile and prognosis.

In recent years, there has been increasing concerns about the use of primary skin fibroblasts as a study model of ALS, following the publication of studies highlighting the presence of histologic alterations in patients' skin (10–12). As fibroblasts are directly derived from patients and share embryologic origins with neurons, they provide an interesting translational model in neurosciences. Fibroblasts have thus been used in many studies assessing the pathogenicity of ALS-associated mutations in familial cases, such as in *C9Orf72* and *TARDBP* (13–16), *FUS* (17,18), *SOD1* (19), *CHCHD10* (20), *UBQLN2* (21), and *VCP* (22). Indeed, the natural expression of the mutated protein in these cells lines resulted in specific biological and/or ultrastructural alterations in standard culture conditions. Nevertheless, despite the potential multigenic origin of the sporadic form of the disease, only a few studies investigated the phenotype of sALS patient fibroblasts. Recently, five studies using transcriptomic, proteomic, and respirometry techniques highlighted the presence of biological alterations in sALS patient fibroblasts regarding energy metabolism, stress–response, and RNA processing (23–27).

We prospectively collected primary skin fibroblasts from patients affected with classical, rapid, and slow forms of sporadic amyotrophic lateral sclerosis (sALS) in order to identify histopathological hallmarks of ALS, with the aim of finding new clinical-related markers and providing a study-model of ALS lesions.

Materials and methods

Patients inclusion

Sporadic ALS patients were included prospectively in the ALS center of the University Hospital of Angers from November 2016 to May 2017. Diagnosis of ALS was made according to revised El Escorial/Airlie House Criteria (28). Patients were screened for *C9ORF72*, *SOD1*, *FUS*, and *TARDBP* mutation. Strict inclusion criteria were defined in order to avoid bias related to age, medical history, treatments, toxic exposure, and severity of the disease. Patients with age <19 or >80, other relevant medical history or treatment, body mass index <19 or >25, alcoholic or tobacco consumption, professional toxic exposure, ALS Functional Rating Scale (ALSFRS) score <30, cognitive impairment, and transient or permanent noninvasive ventilation therapy, gastrostomy or tracheotomy were excluded from the study. Patients were classified as having one of the following clinical courses of the disease: *classical*, *rapid* (<18 months and aggressive form), or *slow* (>8 years and slow evolution). Healthy age- and sex-matched subjects without relevant medical history or toxic exposure were included prospectively as controls.

Cell culture

Patients and controls primary fibroblasts were derived from skin biopsies after obtaining written consent. Amplifications were performed from passage 1 to 5, allowing cell cryoconservation of eight samples per cell line. Fibroblasts were cultured in Dulbecco's minimum essential medium in the presence of 10% fetal calf serum (FCS), 1% uridine, and 1% pyruvate, in a humidified atmosphere (95% air, 5% CO_2) at 37 °C. Monolayers of primary fibroblasts were routinely maintained in T75 flasks. All experiments were conducted on cells with similar passage numbers, ranging from 6 to 20, in order to avoid artifacts due to senescence.

Cell growth assay

Approximately, 10,000 fibroblasts per well were seeded on a 12-well chamber slide (Cellstar, Greiner, Monroe, NC) and placed in a cell incubator equipped with a microscope gantry connected to a networked external hard drive (IncuCyte ZOOM® system Essen Biosciences, Ann Arbor, MI). Four phase-contrast automated images per well were acquired every 10 hours during 90 hours with a 10× objective. Cell growth was automatically calculated at each time point using the relative cell density (ratio of the occupied area to the total area of the acquired regions).

Immunofixation

Approximately, 30,000 fibroblasts were seeded in 22 mm borosilicate glass coverslips (Dutscher D.) in a humidified atmosphere (95% air, 5% CO_2) at 37 °C for at least 24 hours. Cells were then fixed with 4% paraformaldehyde for 15 min at room temperature. After three washes in phosphate buffered saline (PBS), cells were blocked and permeabilized in 0.1% triton X-100 and 5% bovine serum albumin in PBS for 1 h at room temperature. Cells were then washed and incubated over night at 4 °C with primary antibodies, depending on the immunolabeling: rabbit anti-TDP-43 (Proteintech 10782-2-AP, Rosemont, IL, 1:2000), mouse anti-pTDP-43 Ser409/410 (Cosmobio CAC-TIP-PTD-M0, Tokyo, Japan, 1:25,000), mouse anti-vimentin (Sigma V6630, Kawasaki, Japan, 1:1000), mouse anti-α-tubulin (Sigma T9026, Kawasaki, Japan, 1:500), mouse anti-ATP-synthase (ThermoFisher

A21351, Waltham, MA, 1:5000), mouse anti-TIAR (BD Transduction Labs 610352, Franklin Lakes, NJ, 1:1000). Finally, cells were washed in PBS and incubated with Alexa Fluor conjugated secondary antibodies (Invitrogen, Carlsbad, CA, 1:10,000). For actin imaging, cells were incubated with Alexa Fluor 647 Phalloidin (ThermoFisher, Waltham, MA, 1:40) 20 minutes at room temperature after immunofixation. DNA was counterstained with Hoechst 33342 (ThermoFisher H3570, Waltham, MA, 1:200). For the assessment of stress response, fibroblasts were exposed to 1 mM sodium arsenite (Sigma-Aldrich, St. Louis, MO) for 60 min at 37 °C before fixation.

3D fluorescence microscopy

For fluorescence imaging, coverslips were mounted in housing and placed on the stage of an inverted wide-field microscope ECLIPSE Ti-E (Nikon, Tokyo, Japan) equipped with a 100× oil immersion objective (Nikon Plan Apo100x, Tokyo, Japan, N.A. 1.45) and an Andor NEO sCOMS camera controlled by Metamorph® 7.7 software (Molecular Devices, Sunnyvale, CA). A precision, piezoelectric driver mounted underneath the objective lens allowed faster Z-step movements, keeping the sample immobile while shifting the objective lens. Twenty-one image planes were acquired along the Z-axis at 0.1 µm increments. More than 3500 images were acquired and analyzed in total. Imaris 8.0® software (Bitplane, Zurich, Switzerland) was used for 3D processing and morphometric analysis. For mitochondrial network characterization, acquired images were iteratively deconvolved using Huygens Essential® software (Scientific Volume Imaging, Hilversum, The Netherlands), with a maximum iteration scored 50 and a quality threshold at 0.01. The cell volume and mitochondrial network were modeled in 3D, and thresholds were defined in order to classify mitochondria depending on their volume: $<5\ \mu m^3$ (fragmented), $<100\ \mu m^3$ (normal size), and $>100\ \mu m^3$ (overfused).

Super resolution microscopy (dStorm)

For super resolution imaging, coverslips were mounted in an Attofluor™ cell chamber (ThermoFisher, Waltham, MA), bathed in a standardized super-resolution buffer (Smart Kit, Abbelight, Paris, France), and placed on the stage of an inverted motorized microscope NIKON ECLIPSE Ti-E equipped with a CFI SR APO TIRF 100X ON1.49 objective and a Perfect Focus System (Nikon Instruments Europe, Amsterdam, The Netherlands), allowing long acquisition in oblique illumination mode. Acquisitions were performed at fixed temperature 25 °C in order to reduce microscope drift (Okolab NA, Pozzuoli, Italy). A microscope equipped with a TIRF module, based on the ILas2 module (Roper Scientific, Martinsried, Germany), was used for direct stochastic optical reconstruction microscopy (dStorm). A 642 nm laser was used to excite fluorescence and switch Alexa-647 to the dark state. dSTORM images were acquired using a Photometrics Evolve 512×512 backthinned EM-CCD with 16 micron pixels and analyzed with MetaMorph Imaging Software, MetaSeries version 7.8.2 (Molecular Devices, Sunnyvale, CA) using a 10 ms exposure time. Series of 12,000 images were taken at a frequency of 20 Hz. Images were reconstructed and analyzed in real-time using the integrated WaveTracer (Roper Scientific, Martinsried, Germany).

Reactive oxygen species (ROS) detection

For intracellular ROS detection in cells, approximately 50,000 fibroblasts per well were seeded on a two-well chamber slide (Labtek, Nunc International, Penfield, NY) in a humidified atmosphere (95% air, 5% CO_2) at 37 °C for at least 24 hours. Cells were then incubated for 30 minutes with 5 µM CellROX Orange® (Molecular Probes, Eugene, OR). After loading, the cells were thoroughly washed and bathed with DMEM without red phenol, 1% FCS, 1% uridine, and 1% pyruvate. Fluorescent live-images were acquired with an inverted microscope ECLIPSE Ti-E (Nikon, Tokyo, Japan), equipped with 20× objective and an airtight heating system (Okolab NA, Pozzuoli, Italy). Measurements were performed at fixed temperature 37 °C in order to minimize cell stress. At least 200 cells were analyzed for each line. Acquisition, reconstruction and analyses of images were proceeded using Metamorph® 7.7 software.

Statistical analysis

The study protocol was developed in collaboration with the methodology and statistics department of Angers University Hospital. Statistical analyses were carried out using PRISM software version 5.0 for Windows (GraphPad, La Jolla, CA). Comparisons of means were performed using Student's *t*-test for two groups analysis, and the one-way analysis of variance (ANOVA) for multiple groups analysis, after verifying the normal distribution and the homoscedasticity of data using Shapiro–Wilk's and Bartlett's tests. Comparisons of percentages were performed using Fischer's test. Differences were considered to be significant at $p < 0.05$.

Ethical considerations

The study protocol has been registered on ClinicalTrials.gov (NCT02969759) and approved by the Regional Ethics Committee West II (Authorization Number 2016/36) and the French Health Products Safety Agency (2016-102600243).

An anonymous database and a list of correspondence have been generated and stored on a hard disk of the University Hospital of Angers with restricted access.

Results

Patients

Six sALS patients (two *classical*, two *rapid*, and two *slow*) with a mean age of 63.8 (±7.3 SD) and four control subjects with a mean age of 59.7 (±12.7 SD) have been included. There was no significant difference between patient and control groups regarding age ($p = 0.76$) and sex ($p = 1$). The mean severity of the disease assessed by the ALSFRS score was 38/48 (±4 SD). None of the patients carried a known ALS-associated mutation. Clinical characteristics of patients and controls are summarized in Table 1.

Cell proliferation

As cell growth is a general indicator of cells functioning, we monitored fibroblasts proliferation over the time. The cell growth, calculated from the cell density at each time point, was similar among patients and controls fibroblasts, with 100% confluence reached after 90 hours of proliferation (Supplemental Figure 1). Furthermore, no difference in fibroblasts morphology or distribution within the wells was noticed between the lines.

TDP-43 localization

We aimed to characterize the ultrastructural architecture of sALS patient fibroblasts focusing on TDP43 distribution in order to highlight potential relocation or aggregation. 3D fluorescence imaging was performed on fixed and immunostained cells. The analysis of TDP-43 distribution did not reveal any mislocalization nor protein inclusion in patient and control fibroblasts (Figure 1(a–g)). TDP-43 was mainly intranuclear, and no significant difference was found between the lines with regard to the nucleocytoplasmic ratio of the fluorescence signal ($p = 0.22$) (Figure 1(h,i)). Similar findings were obtained regarding the phosphorylated form of TDP-43 (Figure 1(j–m)).

Cytoskeleton architecture

Our analysis of vimentin distribution did not show any disorganization nor aggregation of intermediate filaments in patient fibroblasts using both 3D fluorescence microscopy and new super-resolution imaging (Figure 2). Likewise, microtubules and actin were well distributed among the cells, without any inclusion noticed (Figure 3).

Mitochondrial network organization

In fibroblasts, mitochondria are organized in a large connected network. We did not observe any difference between patients and controls fibroblasts regarding the overall organization of the mitochondrial networks (Figure 4(a–g)). After 3D modelization of mitochondria and cell volumes (Figure 4(h)), the mitochondria/cell ratio was calculated for each cell and found similar among patient and control fibroblasts ($p = 0.59$) (Figure 4(i)). In order to characterize the mitochondrial network architecture, mitochondria were then divided into three groups depending on their volume range: $<5\,\mu m^3$ (fragmented), $<100\,\mu m^3$ (normal size), and $>100\,\mu m^3$ (overfused) (Figure 4(j)). No difference was observed regarding the mitochondrial distribution between patients and controls cells (Figure 4(k)).

Reactive oxygen species production and stress granules formation

As the increase of oxidative stress markers in the central nervous system is another hallmark of ALS, we acquired fluorescent live-images of cultured fibroblasts after CellROX® staining. Intracellular

Table 1. Clinical characteristics of patients and controls.

	Age at biopsy	Sex	Duration of disease (months)	Clinical course	Other medical history	Treatment	Toxic exposure	Score ALSFRS	Death during the study (months after biopsy)
ALS_1	65	M	18	Classical	None	None	No	43/48	–
ALS_2	62	F	24	Classical	None	Riluzole, antidepressant	No	40/48	–
ALS_3	54	F	6	Rapid	None	None	No	31/48	3
ALS_4	60	F	16	Rapid	Thyroidectomy	Riluzole, levothyroxine	No	38/48	5
ALS_5	76	M	96	Slow	None	None	No	40/48	–
ALS_6	66	M	144	Slow	Benign head trauma, pulmonary embolism	Riluzole, baclofen	No	38/48	–
Ctrl_1	52	M	–	–	Anxiety syndrome	Antidepressant	No	–	–
Ctrl_2	72	F	–	–	High blood pressure	Antihypertensive treatment	No	–	–
Ctrl_3	69	M	–	–	None	None	No	–	–
Ctrl_4	46	F	–	–	None	None	No	–	–

ALFRS: ALS Functional Rating Scale.

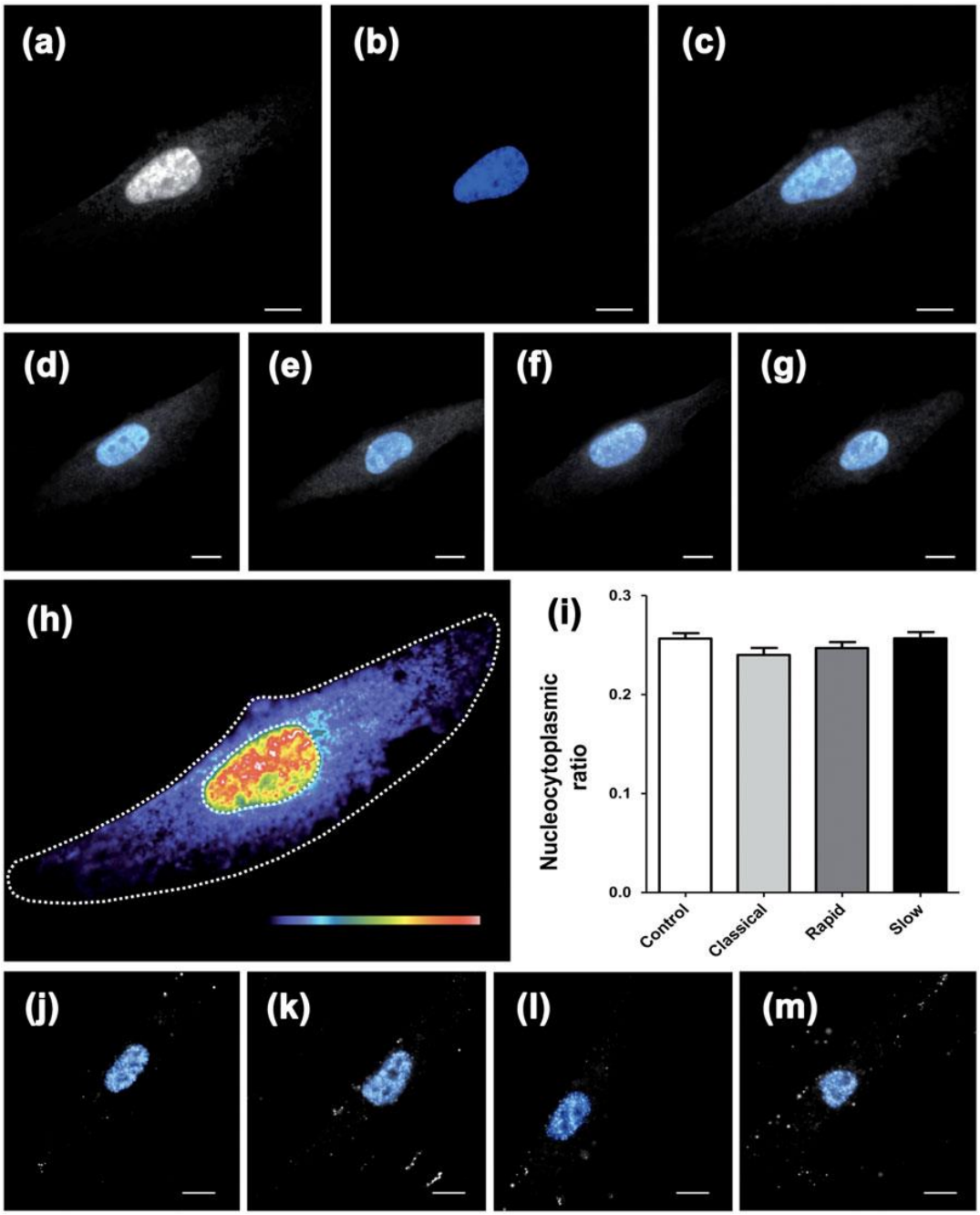

Figure 1. TDP-43 and pTDP-43 are not mislocalized nor aggregated in sALS patient fibroblasts. 3D fluorescence imaging was performed on fixed and immunostained fibroblasts with sequential analysis of TDP-43 (a), Hoechst 33342 (b), and Merge (c). Representative images of fibroblasts from each group are shown in d (*control*), e (*classical*), f (*rapid*), and g (*slow*). The nucleocytoplasmic ratio of the protein was calculated on the basis of the fluorescence intensity distribution within each cell (h). Histograms display the mean calculated nucleocytoplasmic ratio for each group, error bars indicate the standard deviation (i). Analyses of pTDP-43 and Hoechst 33342 were also performed, representative merged images of fibroblasts from each group are shown in j (*control*), k (*classical*), l (*rapid*), and m (*slow*). Scale bars 10 μm.

ROS levels determined from the mean signal intensity per cell were similar among patients and controls fibroblasts ($p = 0.73$) (Figure 5(a,b)). We then assessed the fibroblasts response to oxidative stress exposure using sodium arsenite. After treatment, cells were fixed and immunostained with antibodies against TIAR, a stress-granule marker, and TDP-43. The stress response was similar among patients and controls fibroblasts, with formation of numerous and evenly distributed stress granules. Furthermore, TDP-43 remained intranuclear without any additional inclusion noticed both in patients and controls fibroblasts (Figure 5(c–j)).

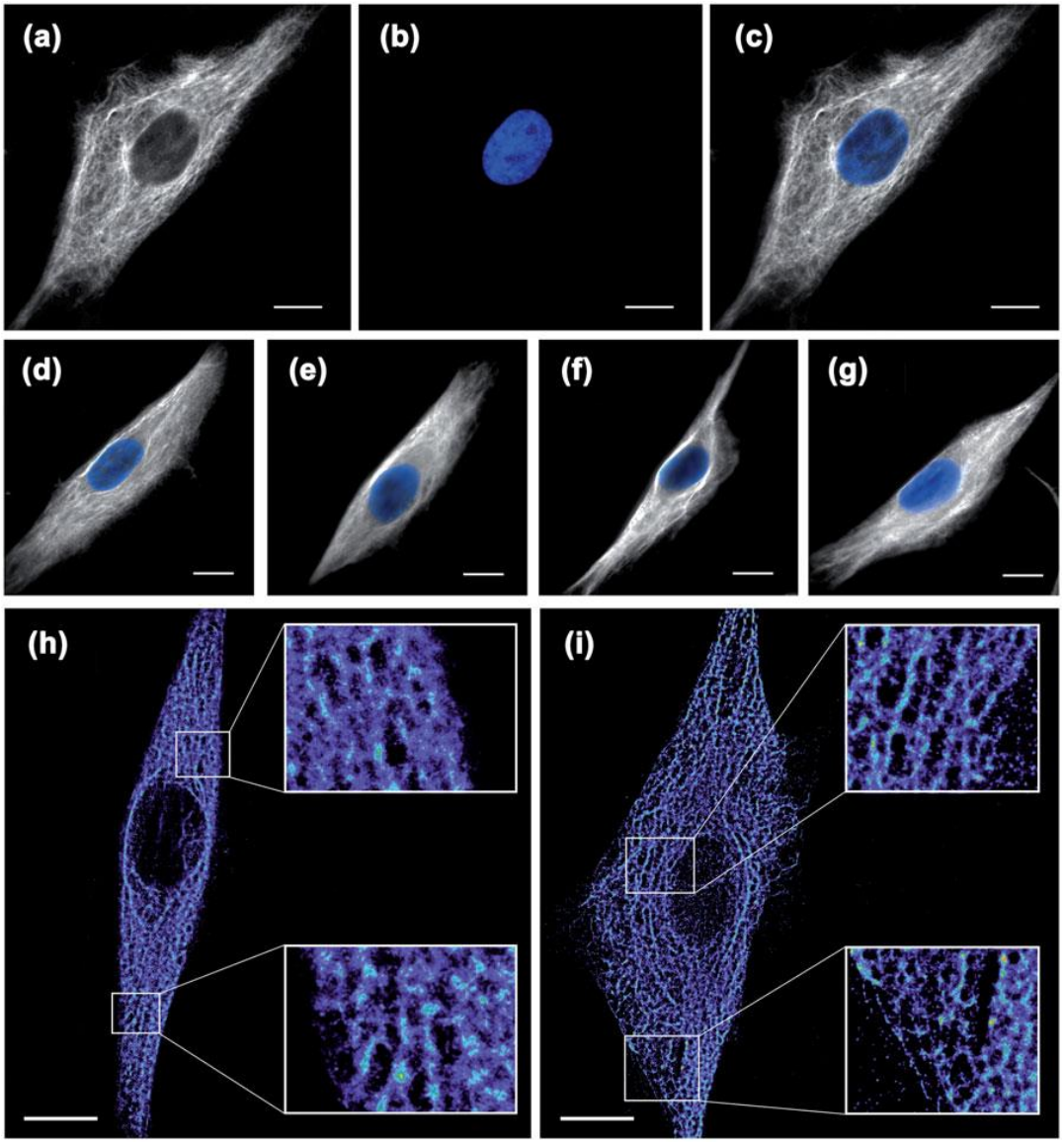

Figure 2. Intermediate filaments network is normal in sALS patient fibroblasts. 3D fluorescence imaging was performed on fixed and immunostained fibroblasts with sequential analysis of intermediate filaments (a), Hoechst 33342 (b), and Merge (c). Representative images of fibroblasts from each group are shown in d (*control*), e (*classical*), f (*rapid*), and g (*slow*). Intermediate filaments architecture was also assessed using Super Resolution imaging (dStorm). Series of 12,000 images were taken at a frequency of 20 Hz, representative reconstructed images are shown in h (*control*) and i (*patient*). Scale bars 10 μm.

Discussion

Our study on sALS primary patient fibroblasts based on strict clinical inclusion criteria and the use of high resolution techniques showed the absence of ultrastructural alterations in the disease condition. To our knowledge, this is the first prospective study investigating specifically and simultaneously several morphological parameters of sALS patient fibroblasts on the basis of ALS cytological lesions observed in motor neurons, although some of them were separately assessed in few studies.

Cytoplasmic relocation and aggregation of ubiquitinated and phosphorylated TDP-43 is a major component of the lesions found in neuronal cells both in sporadic and familial forms of ALS (3), with the exception of *SOD1*-linked fALS (29). It is still unclear whether the physiopathological mechanism leading to neuronal degeneration is a cytoplasmic toxicity of aggregated TDP-43 or its nuclear loss of function. In our study, we did not observe mislocalization or inclusion of both TDP-43 and phospho-TDP-43 in patients and controls fibroblasts. Likewise, in two previous studies, Sabatelli et al. (six sALS cases) and Paré et al. (six sALS cases) did not report TDP-43 relocation or aggregation in cultured patient fibroblasts, using immunoblotting and immunofluorescence techniques (16,30). Conversely, we did not find

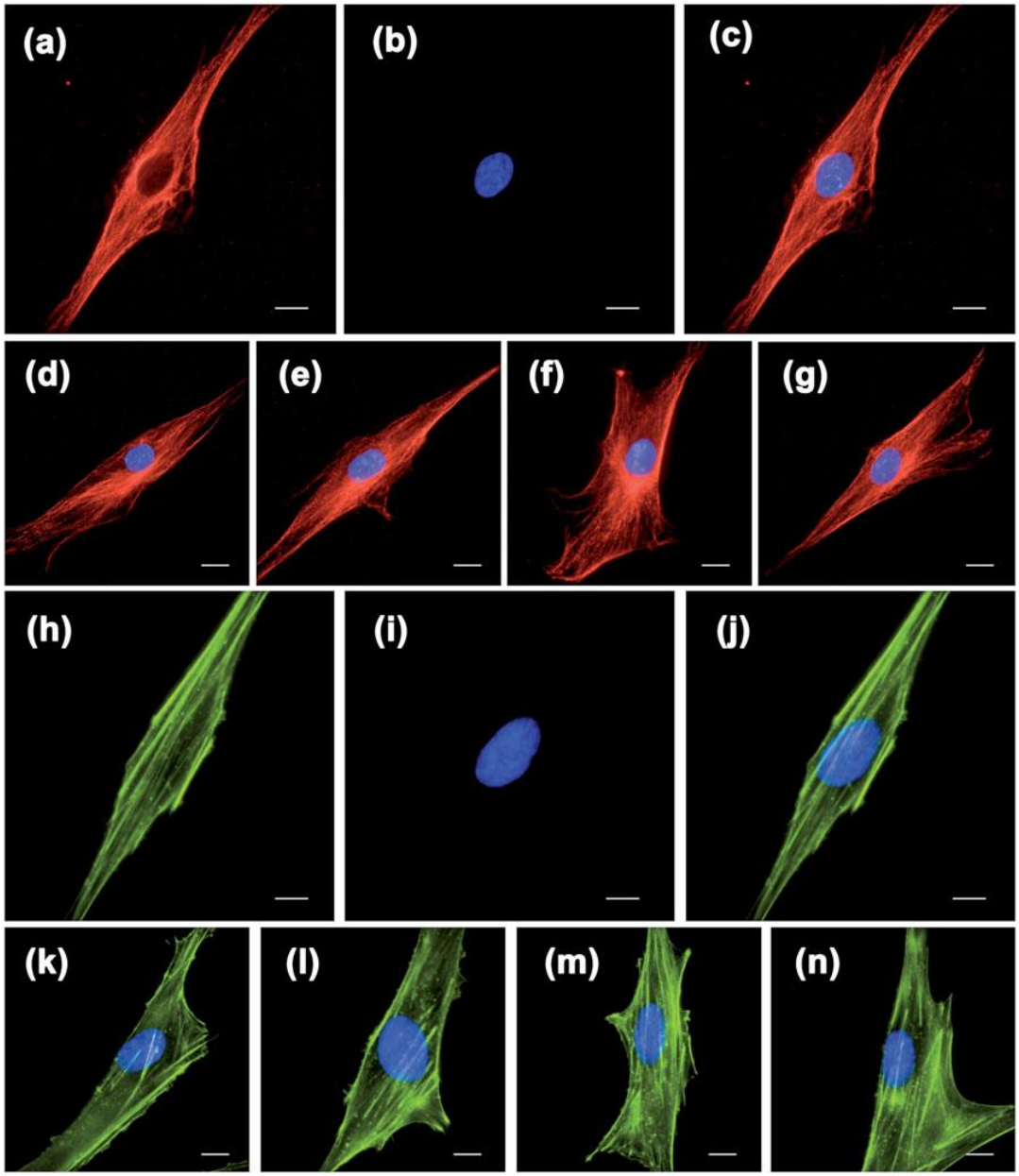

Figure 3. Microtubules and microfilaments architectures are not altered in sALS patient fibroblasts. 3D fluorescence imaging was performed on fixed and immunostained fibroblasts with sequential analysis of α-tubulin (a), Hoechst 33342 (b), and Merge (c). Representative images of fibroblasts from each group are shown in d (*control*), e (*classical*), f (*rapid*), and g (*slow*). A similar protocol was used to analyze actin microfilaments organization within the patients and controls cells (h–j). Representative images of fibroblasts from each group are shown in k (*control*), l (*classical*), m (*rapid*), and n (*slow*). Scale bars 10 µm.

abnormalities regarding the phosphorylated form of the protein reported in the first study, although we used the same antibody (16). Interestingly in the second study, the generation of a tissue engineered skin model using a 3D culture technique resulted in cytoplasmic TDP-43 lesions in sALS patient fibroblasts which were not observed in controls (30). Furthermore, some aspects of TDP-43 proteinopathy can be observed in induced pluripotent stem cells (iPSCs) derived from sALS patient fibroblasts and differentiated in motor neurons (31). Thus, these results suggest that the use of such a set of techniques may be necessary to induce TDP-43 inclusions in fibroblasts derived from sALS patients.

The accumulation of intermediate filaments in the perikarya and axons of motor neurons is another histopathological hallmark of ALS, even though it is still uncertain if these aggregates are a cause or a consequence of the disease (32). To our knowledge, the cytoskeleton of ALS patient fibroblasts has never been investigated to date, both for sporadic and familial forms of the disease. Bundles and ovoid aggregate of vimentin have been recently highlighted in fibroblasts derived from patients with giant axonal

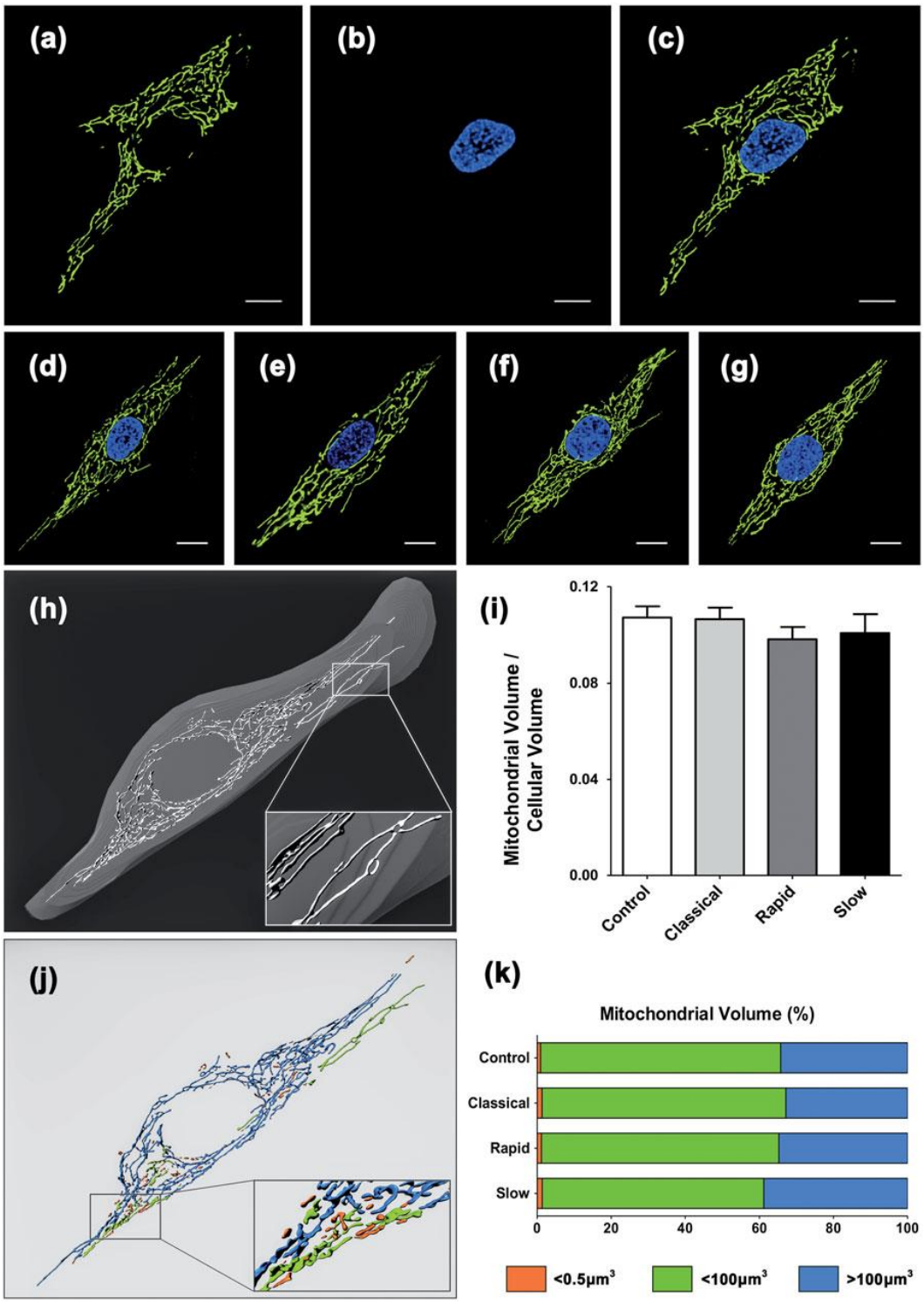

Figure 4. Mitochondrial connection and volume are similar among patients and controls fibroblasts. 3D fluorescence imaging was performed on fixed and immunostained fibroblasts with sequential analysis of ATP-synthase (a), Hoechst 33342 (b), and Merge (c) after iterative deconvolution. Representative images of fibroblasts from each group are shown in d (*control*), e (*classical*), f (*rapid*), and g (*slow*). The cell volume and mitochondrial network were modeled in 3D using Imaris® software (Bitplane) (h). Histograms display the mean mitochondrial volume per cellular volume ratio for each group, error bars indicate the standard deviation (i). Mitochondria were then divided into three groups depending on their volume: 55 μm^3 (fragmented), 5100 μm^3 (normal size), and 4100 μm^3 (overfused) (j).

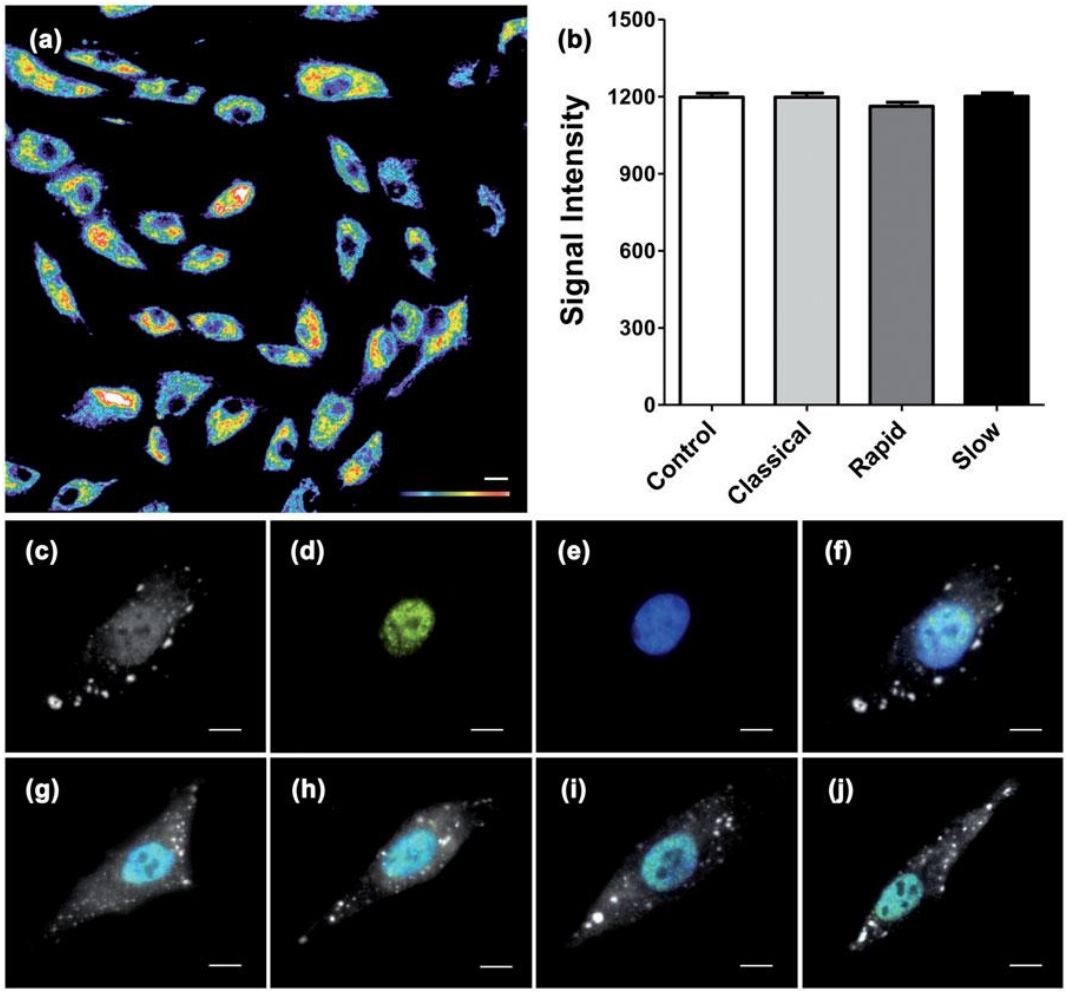

Figure 5. Reactive oxygen species production and oxidative stress response are similar between patients and controls fibroblasts. Fluorescent live-images of fibroblasts were acquired after CellROX staining for intracellular reactive oxygen species detection (a). Histograms display the mean signal intensity per cell for each group, error bars indicate the standard deviation (b). For the assessment of stress response, fibroblasts were exposed to 1 mM sodium arsenite for 60 min at 37 °C before fixation. 3D fluorescence imaging was then performed on immunostained fibroblasts with sequential analysis of TIAR (c), TDP-43 (d) Hoechst 33342 (e), and Merge (f). Representative images of fibroblasts from each group are shown in g (*control*), h (*classical*), i (*rapid*), and j (*slow*).

neuropathy, an autosomal-recessive disorder inducing aggregates of intermediate filaments in neurons (33). Although we did not find cytoskeleton alteration in sALS patient fibroblasts in our study, it would be interesting to explore this parameter in familial ALS patient fibroblasts showing ultrastructural and metabolic alterations, in order to find if they are accompanied by intermediate filaments aggregation.

Mitochondria are thought to have a major role in the occurrence of ALS through multiple pathways. Indeed, alterations of mitochondrial morphology and metabolism are present in the central nervous system of ALS patients (5,34), and mutations in genes coding for mitochondrial proteins can lead to fALS (20). Significant differences regarding mitochondrial membrane potential and oxygen consumption rates were reported in seven *TARDBP* and *C9ORF72* mutated fibroblasts grown in galactose medium, accompanied by a fragmentation of the mitochondrial network (13). Likewise, an increase of the mitochondrial metabolism in fibroblasts derived from a large cohort of sALS patients was highlighted in a recent study, thanks to the use of a new machine learning approach, but fibroblasts' mitochondrial architecture was not assessed (27). In another study investigating mitochondrial metabolism in six sALS patient fibroblasts, while changes in mitochondrial respiration rates were also noticed, no significant difference was reported in mitochondrial network complexity between affected and control individuals, both in standard and glucose-free conditions (23). In our study, we did not observe any mitochondrial network alteration in patient fibroblasts. Thus, while mitochondrial metabolism appears to be modified in fibroblasts derived from sALS patients, these changes do not affect mitochondrial morphology.

SOD1 was the first gene reported to cause familial forms of ALS (35). This gene encodes the Cu/Zn-binding superoxide dismutase protein, a homodimeric metalloenzyme that catalyzes the dismutation of the toxic superoxide anion $O_2^{\bullet -}$ to O_2 and H_2O_2. This linkage highlighted the potential role of free radical toxicity in the disease, supported later by studies reporting elevated markers of oxidative stress in the cortex and spinal cord of ALS patients (7,36). In our study, the ROS level measured in cultured sALS fibroblasts did not differ from controls in basal culture conditions. This observation is in line with two previous studies which investigated respectively 5 and 10 ALS cases and reported the lack of evidence of oxidative stress in patient fibroblasts (37,38). Since our results did not point out an alteration of the ROS homeostasis in physiological conditions, we decided to challenge cells by inducing an oxidative stress using sodium arsenite, in order to assess the cellular response and the potential mislocalization of TDP-43. However, we did not find any difference between patients and controls fibroblasts regarding stress granules formation and TDP-43 location. Likewise, in a previous study assessing stress response after sodium arsenite exposure, TDP-43 remained in the nucleus and stress granule formation was not reduced in two sALS patient fibroblasts (14).

Conclusions

Despite the use of strict prospective inclusion criteria and high-resolution techniques, the cultured fibroblasts derived from patients affected with different forms of sporadic ALS did not show any ultrastructural alteration compared to controls. The parameters analyzed in our study thus cannot contribute as diagnostic nor prognostic markers of the disease. 3D culture techniques and the use of iPSC to generate neuronal cells appear to be more promising ways to investigate these features.

Acknowledgements

The authors acknowledge the patients and healthy subjects who participated in the study, and Dr A.-V. Fayolle for critical reading and comments on the manuscript.

Declaration of interest

The authors report no conflicts of interest.

This work was supported by the University Hospital of Angers (Grant N°. 2016-A01425-46) and by the Institut National de la Santé et de la Recherche Médicale (INSERM Research Fellow 2017–2019).

ORCID

PHILIPPE CODRON http://orcid.org/0000-0003-1745-8299

References

1. Kiernan MC, Vucic S, Cheah BC, Turner MR, Eisen A, Hardiman O, et al. Amyotrophic lateral sclerosis. Lancet. 2011;377:942–55.
2. Swinnen B, Robberecht W. The phenotypic variability of amyotrophic lateral sclerosis. Nat Rev Neurol. 2014;10:661–70.
3. Neumann M, Sampathu DM, Kwong LK, Truax AC, Micsenyi MC, Chou TT, et al. Ubiquitinated TDP-43 in frontotemporal lobar degeneration and amyotrophic lateral sclerosis. Science. 2006;314:130–3.
4. Munoz DG, Greene C, Perl DP, Selkoe DJ. Accumulation of phosphorylated neurofilaments in anterior horn motoneurons of amyotrophic lateral sclerosis patients. J Neuropathol Exp Neurol. 1988;47:9–18.
5. Sasaki S, Iwata M. Mitochondrial alterations in the spinal cord of patients with sporadic amyotrophic lateral sclerosis. J Neuropathol Exp Neurol. 2007;66:10–6.
6. Wang W, Wang L, Lu J, Siedlak SL, Fujioka H, Liang J, et al. The inhibition of TDP-43 mitochondrial localization blocks its neuronal toxicity. Nat Med. 2016;22:869–78.
7. Ferrante RJ, Browne SE, Shinobu LA, Bowling AC, Baik MJ, MacGarvey U, et al. Evidence of increased oxidative damage in both sporadic and familial amyotrophic lateral sclerosis. J Neurochem. 1997;69:2064–74.
8. Miller RG, Mitchell JD, Moore DH. Riluzole for amyotrophic lateral sclerosis (ALS)/motor neuron disease (MND). Cochrane Database Syst Rev. 2012;3:CD001447.
9. Mitsumoto H, Brooks BR, Silani V. Clinical trials in amyotrophic lateral sclerosis: why so many negative trials and how can trials be improved? Lancet Neurol. 2014;13:1127–38.
10. Oketa Y, Higashida K, Fukasawa H, Tsukie T, Ono S. Abundant FUS-immunoreactive pathology in the skin of sporadic amyotrophic lateral sclerosis. Acta Neurol Scand. 2013;128:257–64.
11. Suzuki M, Mikami H, Watanabe T, Yamano T, Yamazaki T, Nomura M, et al. Increased expression of TDP-43 in the skin of amyotrophic lateral sclerosis. Acta Neurol Scand. 2010;122:367–72.
12. Watanabe T, Okeda Y, Yamano T, Ono S. An immunohistochemical study of ubiquitin in the skin of sporadic amyotrophic lateral sclerosis. J Neurol Sci. 2010;298:52–6.
13. Onesto E, Colombrita C, Gumina V, Borghi MO, Dusi S, Doretti A, et al. Gene-specific mitochondria dysfunctions in human TARDBP and C9ORF72 fibroblasts. Acta Neuropathol Commun. 2016;4:47.
14. Orrù S, Coni P, Floris A, Littera R, Carcassi C, Sogos V, et al. Reduced stress granule formation and cell death in fibroblasts with the A382T mutation of TARDBP gene: evidence for loss of TDP-43 nuclear function. Hum Mol Genet. 2016;25:4473–83.
15. Renton AE, Majounie E, Waite A, Simón-Sánchez J, Rollinson S, Gibbs JR, et al. A hexanucleotide repeat expansion in C9ORF72 is the cause of chromosome 9p21-linked ALS-FTD. Neuron. 2011;72:257–68.
16. Sabatelli M, Zollino M, Conte A, Del Grande A, Marangi G, Lucchini M, et al. Primary fibroblasts cultures reveal TDP-43 abnormalities in amyotrophic lateral sclerosis patients with and without SOD1 mutations. Neurobiol Aging. 2015;36:2005.e5–e13.

17. Schwartz JC, Podell ER, Han SSW, Berry JD, Eggan KC, Cech TR. FUS is sequestered in nuclear aggregates in ALS patient fibroblasts. Mol Biol Cell. 2014;25:2571–8.
18. Yu Y, Chi B, Xia W, Gangopadhyay J, Yamazaki T, Winkelbauer-Hurt ME, et al. U1 snRNP is mislocalized in ALS patient fibroblasts bearing NLS mutations in FUS and is required for motor neuron outgrowth in zebrafish. Nucleic Acids Res. 2015;43:3208–18.
19. Allen SP, Rajan S, Duffy L, Mortiboys H, Higginbottom A, Grierson AJ, et al. Superoxide dismutase 1 mutation in a cellular model of amyotrophic lateral sclerosis shifts energy generation from oxidative phosphorylation to glycolysis. Neurobiol Aging. 2014;35:1499–509.
20. Bannwarth S, Ait-El-Mkadem S, Chaussenot A, Genin EC, Lacas-Gervais S, Fragaki K, et al. A mitochondrial origin for frontotemporal dementia and amyotrophic lateral sclerosis through CHCHD10 involvement. Brain. 2014;137:2329–45.
21. Deng H-X, Chen W, Hong S-T, Boycott KM, Gorrie GH, Siddique N, et al. Mutations in UBQLN2 cause dominant X-linked juvenile and adult-onset ALS and ALS/dementia. Nature. 2011;477:211–5.
22. Bartolome F, Wu H-C, Burchell VS, Preza E, Wray S, Mahoney CJ, et al. Pathogenic VCP mutations induce mitochondrial uncoupling and reduced ATP levels. Neuron. 2013;78:57–64.
23. Allen SP, Duffy LM, Shaw PJ, Grierson AJ. Altered age-related changes in bioenergetic properties and mitochondrial morphology in fibroblasts from sporadic amyotrophic lateral sclerosis patients. Neurobiol Aging. 2015;36:2893–903.
24. Kirk K, Gennings C, Hupf JC, Tadesse S, D'Aurelio M, Kawamata H, et al. Bioenergetic markers in skin fibroblasts of sporadic amyotrophic lateral sclerosis and progressive lateral sclerosis patients. Ann Neurol. 2014;76:620–4.
25. Narayan M, Seeley KW, Jinwal UK. Identification of Apo B48 and other novel biomarkers in amyotrophic lateral sclerosis patient fibroblasts. Biomark Med. 2016;10:453–62.
26. Raman R, Allen SP, Goodall EF, Kramer S, Ponger L-L, Heath PR, et al. Gene expression signatures in motor neurone disease fibroblasts reveal dysregulation of metabolism, hypoxia-response and RNA processing functions. Neuropathol Appl Neurobiol. 2015;41:201–26.
27. Konrad C, Kawamata H, Bredvik KG, Arreguin AJ, Cajamarca SA, Hupf JC, et al. Fibroblast bioenergetics to classify amyotrophic lateral sclerosis patients. Mol Neurodegener. 2017;12:76.
28. Brooks BR, Miller RG, Swash M, Munsat TL, World Federation of Neurology Research Group on Motor Neuron Diseases. El Escorial revisited: revised criteria for the diagnosis of amyotrophic lateral sclerosis. Amyotroph Lateral Scler Other Motor Neuron Disord. 2000;1:293–9.
29. Mackenzie IRA, Bigio EH, Ince PG, Geser F, Neumann M, Cairns NJ, et al. Pathological TDP-43 distinguishes sporadic amyotrophic lateral sclerosis from amyotrophic lateral sclerosis with SOD1 mutations. Ann Neurol. 2007;61:427–34.
30. Paré B, Touzel-DeschÊnes L, Lamontagne R, Lamarre M-S, Scott F-D, Khuong HT, et al. Early detection of structural abnormalities and cytoplasmic accumulation of TDP-43 in tissue-engineered skins derived from ALS patients. Acta Neuropathol Commun. 2015;3:5.
31. Burkhardt MF, Martinez FJ, Wright S, Ramos C, Volfson D, Mason M, et al. A cellular model for sporadic ALS using patient-derived induced pluripotent stem cells. Mol Cell Neurosci. 2013;56:355–64.
32. Codron P, Cassereau J, Eyer J, Letournel F. Neuronal intermediate filaments in amyotrophic lateral sclerosis. In: Foyaca-Sibat H, ed. Update on amyotrophic lateral sclerosis. InTech; 2016.
33. Lowery J, Jain N, Kuczmarski ER, Mahammad S, Goldman A, Gelfand VI, et al. Abnormal intermediate filament organization alters mitochondrial motility in giant axonal neuropathy fibroblasts. Mol Biol Cell. 2016;27:608–16.
34. Wiedemann FR, Manfredi G, Mawrin C, Beal MF, Schon EA. Mitochondrial DNA and respiratory chain function in spinal cords of ALS patients. J Neurochem. 2002;80:616–25.
35. Rosen DR, Siddique T, Patterson D, Figlewicz DA, Sapp P, Hentati A, et al. Mutations in Cu/Zn superoxide dismutase gene are associated with familial amyotrophic lateral sclerosis. Nature. 1993;362:59–62.
36. Beal MF, Ferrante RJ, Browne SE, Matthews RT, Kowall NW, Brown RH. Increased 3-nitrotyrosine in both sporadic and familial amyotrophic lateral sclerosis. Ann Neurol. 1997;42:644–54.
37. Jansen GA, Wanders RJ, Jöbsis GJ, Bolhuis PA, de Jong JM. Evidence against increased oxidative stress in fibroblasts from patients with non-superoxide-dismutase-1 mutant familial amyotrophic lateral sclerosis. J Neurol Sci. 1996;139(Suppl):91–4.
38. Sala G, Trombin F, Mattavelli L, Beretta S, Tremolizzo L, Andreoni S, et al. Lack of evidence for oxidative stress in sporadic amyotrophic lateral sclerosis fibroblasts. Neurodegener Dis. 2009;6:9–15.

Supplementary material available online

3. DISCUSSION ET PERSPECTIVES

3.1. Principaux résultats de l'étude

3.1.1. Ultrastructure, métabolisme et réponse au stress des fibroblastes

Cette étude est la première à avoir analysé de façon spécifique et simultanée différents paramètres pathologiques propres à la SLA sporadique chez des fibroblastes issus de patients prélevés prospectivement. Malgré une inclusion basée sur des critères stricts et l'utilisation de techniques hautement résolutives, ce travail n'a pas permis de mettre en évidence de différence significative entre les fibroblastes de patients atteints de sSLA et les contrôles. Le faible nombre de sujets, bien que dans la moyenne pour ce type de travail, a pu diminuer la puissance de notre étude. Toutefois l'absence de tendance observée malgré une bonne représentativité des différentes formes de la maladie exclue toute possibilité de retenir ces paramètres comme potentiels biomarqueurs de SLA sporadique en pratique clinique.

Les analyses en oxygraphie et le séquençage de l'ADN mitochondrial réalisés en parallèle par le Dr Veyrat-Durebex sur ces cellules n'ont pas mis en évidence d'anomalie du métabolisme énergétique mitochondrial ni d'altérations de l'ADNmt. En revanche, l'utilisation d'une approche multi-omique a permis d'identifier plusieurs signatures métaboliques et lipidiques, portant en particulier sur les voies du métabolisme des purines et pyrimidines et les taux de phosphatidylcholine et phosphatidylethanolamine. Si ces signatures métaboliques ne semblent pas suffisantes pour être responsables à l'échelle cellulaire d'altérations ultrastructurelles compte tenu des résultats obtenus dans notre étude, elles ont permis de discriminer efficacement les patients atteints de sSLA des sujets contrôles, constituant ainsi de potentiels biomarqueurs de la maladie.

3.1.2. Données Bibliographiques

Durant la réalisation de ces deux projets, plusieurs travaux portant sur des fibroblastes en culture issus de patients atteints de SLA sporadique ont été publiés, permettant une mise en perspective de nos résultats avec les données de la littérature. Deux études ayant analysé chacune la localisation intracellulaire de TDP-43 chez des fibroblastes issus de 6 patients atteints de SLA sporadique par imagerie cellulaire et immunoblot ont conforté nos résultats en ne mettant pas en évidence de relocalisation cytoplasmique de la protéine chez ces cellules (Sabatelli et al., 2016 ; Paré et al., 2016). De même, deux études portant respectivement sur la production de ROS (nombre de patients n=10) et la réponse au stress oxydant (n=2) n'avaient pas retrouvé de différence significative avec les

contrôles (Sala et al., 2009 ; Orrù et al., 2016). Enfin, une étude portant sur le métabolisme énergétique de fibroblastes de patients atteints de sSLA (n=12) n'avait pas permis d'objectiver d'atteinte de l'activité enzymatique des complexes de la chaine respiratoire mitochondriale, de mutation de l'ADNmt ni de production excessive de ROS (Bradley et al., 2009). Toutefois, les auteurs d'une étude plus récente (n=6) ont identifié une diminution de la respiration mitochondriale à l'état basale (Allen et al., 2015), tandis que deux autres études (n=50, n=171) mettaient en évidence un état hypermétabolique des cellules de patients associant une stimulation des voies de la glycolyse et des phosphorylations oxydatives mitochondriales avec élévation du potentiel de membrane (Kirk et al., 2014 ; Konrad et al., 2017). L'hétérogénéité de ces derniers résultats peut être liée à certaines différences portant sur les populations de patients étudiées. En effet, les techniques d'analyse du métabolisme mitochondrial sont particulièrement sensibles aux caractéristiques cliniques des patients, telles que l'âge, le sexe, la durée évolution de la maladie, l'existence d'une atteinte respiratoire, la prise de traitements, ou encore la présence de comorbidités associées. Ces paramètres n'ayant pas fait l'objet d'analyses complémentaire correctives dans ces études, ils peuvent être au moins en partie à l'origine de certaines des différences observées. Il est également intéressant de noter que deux de ces travaux portaient sur de larges effectifs. Il est probable que compte tenu du nombre important de sujets inclus, une proportion de patients hypermétaboliques proche de celle observée dans les études cliniques ait été analysée, déplaçant les résultats d'ensemble vers la significativité en cas d'altérations importantes du métabolisme énergétique chez ces sujets (aucune de ces études n'a pris en compte le statut métabolique des patients inclus).

La dissociation entre ultrastructure et métabolisme observée dans ces travaux amène à privilégier une approche fonctionnelle lors de l'étude de fibroblastes de patients atteints de SLA. L'une des raisons de cette dissociation pourrait être le trop faible impact des modifications métaboliques sur la croissance et l'ultrastructure cellulaires. L'absence de marqueurs pathologiques au sein des fibroblastes pourrait également provenir de la trop grande différence phénotypique entre ces derniers et les motoneurones. Ces dernières années, plusieurs approches expérimentales ont vu le jour pour permettre d'obtenir des lignées neuronales ou gliales à partir de fibroblastes de peau. Ces méthodes de conversion, par le biais d'iPSC (Burkhardt et al., 2013 ; Fujimori et al., 2018 ; Sun et al., 2018) ou plus directes (Meyer et al., 2014), ont permis de mettre en évidence des anomalies métaboliques et morphologiques (dont la présence d'inclusions protéiques) chez les neurones obtenus. D'un apport considérable, les contraintes matérielles, techniques et financières de ces approches constituent toutefois une limite à leur mise en place au sein d'une équipe de recherche.

3.2. Perspectives en recherche

3.2.1. Paramètres énergétiques et hypermétabolisme clinique

Les résultats de nos travaux amènent plusieurs perspectives d'études complémentaires. Il apparaît tout d'abord intéressant de tenter de déterminer si les anomalies du métabolisme énergétique constatées dans certaines études chez les fibroblastes de patients atteints de SLA sont en lien avec l'existence d'un syndrome hypermétabolique clinique, et si ces anomalies sont responsables d'une altération de paramètres ultrastructurels tels qu'observés au sein des motoneurones. La construction d'une étude prospective s'attachant à caractériser le statut métabolique des sujets lors de l'inclusion permettrait d'apporter certains éléments de réponse. La mise en évidence d'anomalies spécifiques chez les sujets atteints de SLA présentant un syndrome hypermétabolique permettrait d'ouvrir de nouvelles pistes de réflexion physiopathologique et de détacher des profils clinico-biologiques de patients susceptibles de répondre à certaines approches thérapeutiques. Un exemple de schéma d'étude est proposé Figure 13.

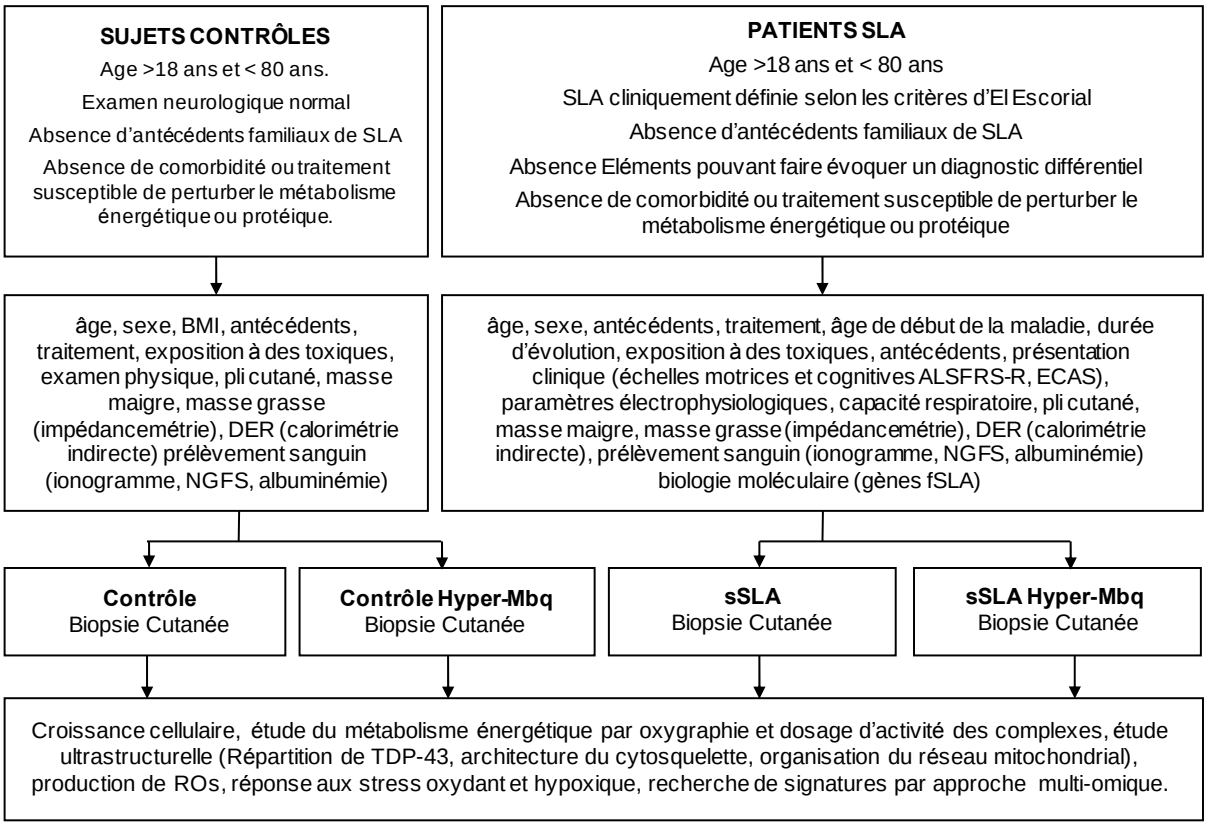

Figure 13. Schéma d'étude proposé pour l'analyse du métabolisme énergétique, de l'organisation ultrastructurelle et de la réponse au stress de fibroblastes issus de patients atteints de sSLA en fonction de leur statut métabolique. ALSFRS : Amyotrophic Lateral Sclerosis Functional Rating Scale. ECAS : Edinburgh Cognitive and Behavioural ALS Screen. DER : dépense énergétique de repos. Mbq : Métabolique. ROS : radicaux libres oxydants. (P. Codron).

3.2.2. Métabolisme du collagène

Une seconde piste de réflexion porte sur le métabolisme du collagène. En effet, la production et l'architecture du collagène sont deux marqueurs pathologiques altérés à la fois au sein du SNC et du tissu cutané des patients atteints de SLA sporadique (Ono et al., 1998, Ono et al., 2001). Cette observation peut être le fait d'anomalies primitives de synthèse du collagène par les cellules matricielles, ou de la production anormale de facteurs de dégradation de ce dernier (collagénases, métalloprotéinases). Une première étude portant sur l'analyse de biopsies de peau en culture avait permis d'observer une activité collagénolytique importante chez environ 60% des échantillons provenant de patients atteints de SLA (Fullmer et al., 1966). Cette activité était également observée chez près de 40% des fragments issus de patients atteints de maladies neurodégénératives ou neuromusculaires autres. Une seconde étude portant sur la production de facteurs collagénolytiques par des biopsies de peau et des fibroblastes en culture n'avait toutefois pas permis de mettre en évidence de différence entre les échantillons provenant de patients et de contrôles (Beach et al., 1986). Plus récemment, l'étude des taux de métalloprotéinase au sein du tissu cutané a permis d'objectiver une augmentation de l'expression de MMP9 chez les patients atteints de SLA (Fang L et al., 2009). L'origine de cette augmentation, également objectivée au niveau du SNC des patients (Lim et al., 1996), et son rôle dans la physiopathologie de la SLA restent débattus. S'agissant de la synthèse et la structure du collagène, si des anomalies ont été caractérisées dans plusieurs études portant sur des prélèvements cutanés et médullaires de patients atteints de SLA, ces paramètres n'ont à notre connaissance jamais été étudiés chez des fibroblastes en culture.

Dans un travail préliminaire conduit au sein du laboratoire Mitolab UMR CNRS 6015 INSERM 1083, nous avons effectué des analyses sur les fibroblastes issus de 4 patients atteints de sSLA (2 formes classiques, 1 forme rapide, 1 forme lente) et 4 contrôles ajustées en âge et sexe. En utilisant une technique de coloration au Sirius Red/Fast Green, qui permet de marquer spécifiquement les collagènes d'un échantillon, nous avons étudié la morphologie et la production de collagène dans ces cellules.

L'étude morphologique des collagènes produits par les fibroblastes issus de sujets contrôles et de patients SLA après marquage au Sirius Red n'a pas mis en évidence de différence notable entre les cellules en culture, ne retrouvant notamment pas d'agrégats intra- ou extra-cellulaires (Figure 14a,b). En revanche, l'analyse du rapport collagène total / protéines totales (Co/P) après 72 heures de culture a révélé une augmentation significative de la production de collagène chez les

fibroblastes issus de patients atteints de SLA (p<0,0001) (Figure 14c). Cette augmentation était proportionnelle à la durée d'évolution de la maladie (p=0,0006) (Figure 14d). Enfin, les analyses quantitatives du collagène effectuées au sein de coupes histologiques de moelles épinières cervicales ont permis de mettre en évidence une augmentation similaire du rapport Co/P chez un patient atteint de SLA par rapport à un sujet contrôle (p=0,0175) (Figure 14e-g). Les méthodes et résultats de ce travail sont détaillés dans le travail complémentaire n°3 situé en Annexe.

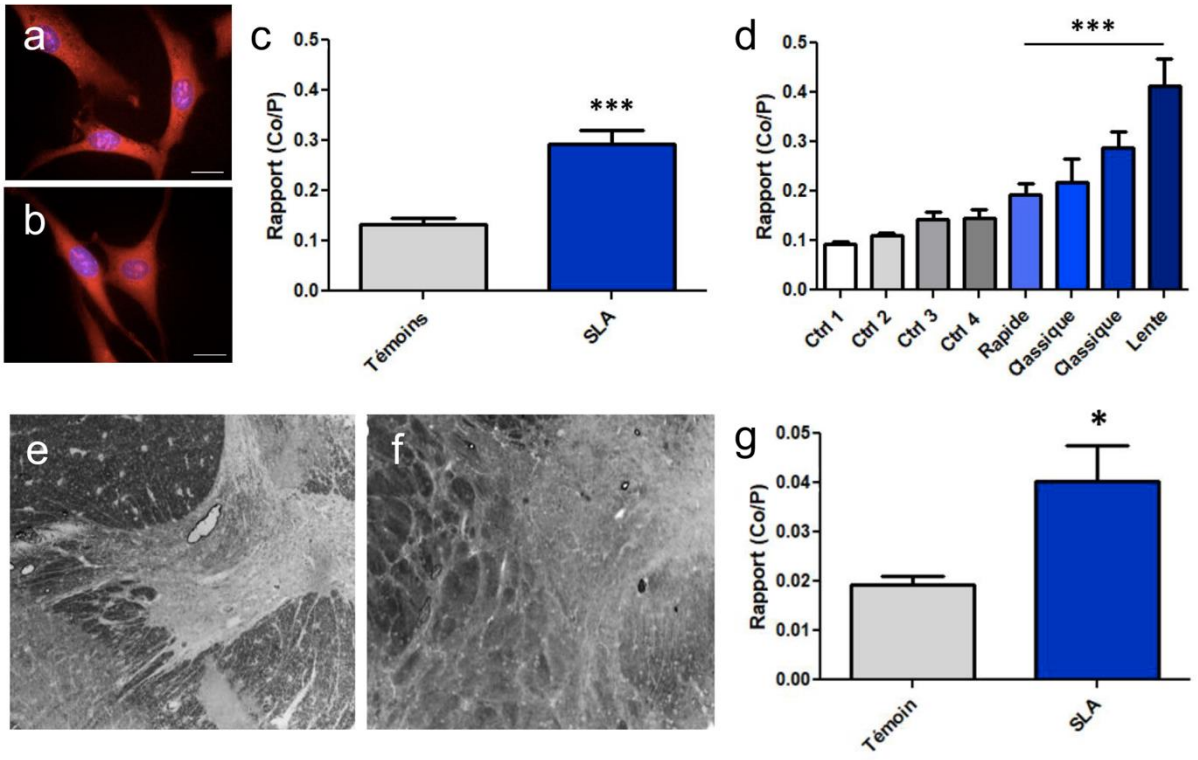

Figure 14. Production de collagènes par les fibroblastes de patients atteints de SLA. (a,b) Étude morphologique des collagènes produits par les fibroblastes issus de sujets contrôles (a) et de patients SLA (b) après marquage au Sirius Red (rouge) et Hoechst (bleu) (barre d'échelle 10 µm). (c,d) Mesures spectrométriques du rapport Collagène total / Protéines totales (Co/P) après 72 heures de culture. Analyse globale (c) et détaillée par sujet (d). (e,f) Coupes histologiques de cornes antérieures de moelle épinière cervicale de sujet contrôle (e) et de patient SLA (f). Mesures spectrométriques du rapport Co/P au sein de ces coupes. Barres d'erreur : déviations standards. * p<0,01 ***p<0,0001. (A. Bodin, P. Codron).

Ces premiers résultats mettent en avant une augmentation de la production de collagène par les fibroblastes en culture issus de patients atteints de SLA sporadique, à l'image de l'élévation des taux de collagène observée aux niveaux cutané et médullaire dans la maladie. S'il est aujourd'hui encore difficile d'émettre des hypothèses physiopathologiques quant à cette augmentation périphérique

compte tenu du peu d'études réalisées sur ce sujet, deux pistes de réflexion peuvent être avancées : ces anomalies pourraient être le reflet d'un remaniement matriciel central et périphérique, conséquence d'un stress systémique actif à la fois au niveau du SNC (neuroinflammation, stress oxydant, mort neuronale) et au niveau cutané. Ces résultats peuvent également faire évoquer un rôle pathologique propre du collagène dans la SLA, actif au niveau du SNC et dont les effets pourraient être observés au niveau cutané compte tenu de l'origine embryonnaire commune de ces deux tissus.

4. CONCLUSION ET OUVERTURE

A notre connaissance, il s'agit des premières analyses portant sur la synthèse du collagène par des fibroblastes en culture issus de patients atteints de SLA. Ces résultats préliminaires obtenus à partir d'un petit effectif de patients incitent à poursuivre ce travail. Une étude sera réalisée au sein de notre laboratoire Mitolab UMR CNRS 6015 INSERM 1083 dans le cadre d'un Master 2 à partir du mois de Janvier 2020, sur un nombre de patients et sujets contrôles plus importants. Les techniques de coloration au Sirius Red / Fast Green seront complétées par une quantification spécifique de la production des différents types de collagène (I, III, VI), de la fibronectine, de l'élastine et des métalloprotéinases par western Blot. De même, l'architecture et la composition de la matrice extra-cellulaire générée par les fibroblastes seront étudiées par immunofluorescence, microscopie super-résolutive STORM et microscopie électronique à balayage. Des études similaires seront effectuées sur des échantillons de moelle épinière de patients SLA et de sujets contrôles conservés au sein de la banque de cerveaux du service de Neuropathologie du CHU d'Angers. Enfin, une approche translationnelle s'attachera à mettre en perspective les résultats obtenus avec les paramètres cliniques des patients.

Si ces travaux confirment nos premiers résultats, la production de collagène par les fibroblastes en culture pourrait devenir un marqueur diagnostique et pronostique de la sSLA identifiable du vivant des patients, particulièrement utile dans la pratique clinique et la construction des essais thérapeutiques. De plus, ces cellules pourraient permettre d'étudier le rôle du métabolisme du collagène dans la physiopathologie de la maladie et de tester des molécules candidates afin d'ouvrir de nouvelles pistes thérapeutiques.

CHAPITRE 3

PISTES THERAPEUTIQUES

Injection intrathécale d'une immunoglobuline monoclonale dirigée contre le domaine RRM1 de la protéine TDP-43

Années :

- 2017-2018

Laboratoire d'accueil :

- CERVO Brain Research Institute, Québec City G1J 2G3, Canada.

Financement :

- Poste d'Accueil Inserm 2017-2019
- Canadian Institutes of Health Research (CIHR)

Lumbar intrathecal injections of monoclonal immunoglobulin against TDP-43 reduce proteinopathy and NFκB activation in a FTLD/ALS mouse model

S. Pozzi[1●], P. Codron[1,2●], L. Renaud[1], G. Soucy[1], C. Bareil[1], J-P. Julien[1,3 *]

1. CERVO Brain Research Institute, Québec City G1J 2G3, Canada.

2. UMR CNRS 6015, INSERM U1083, University of Angers, Angers Cedex 9, France.

3. Department of Psychiatry and Neuroscience, University of Laval, Québec City G1V 0A6, Canada.

● These authors contributed equally to this work.

INJECTION INTRATHECALE D'UNE IMMUNOGLOBULINE MONOCLONALE DIRIGEE CONTRE LE DOMAINE RRM1 DE LA PROTEINE TDP-43

1. IMMUNOTHERAPIE ET SLA

1.1. Utilisation d'anticorps pour le traitement des maladies neurodégénératives

Les avancées opérées dans la compréhension des mécanismes physiopathologiques à l'origine des maladies neurologiques ont mené ces dernières années au développement de nouvelles approches thérapeutiques ciblant plus spécifiquement certaines voies impliquées dans les processus de neurodégénérescence. Parmi elles, l'immunothérapie repose sur l'utilisation d'anticorps dirigés contre les agrégats protéiques toxiques intra- ou extra-cellulaires, afin de diminuer leur pathogénicité et favoriser leur dégradation.

L'immunisation « active » par vaccination a été la première stratégie à être testée. Cette approche est basée sur l'administration d'un peptide immunogène dans le but d'induire la production d'anticorps endogène dirigés contre un antigène cible. Les premiers résultats obtenus sur modèles animaux dans le cadre de la recherche sur la maladie d'Alzheimer se sont révélés particulièrement prometteurs (Schenk et al., 1999 ; Bard et al., 2000 ; Morgan et al., 2000). Cependant, la survenue d'effets indésirables graves lors des premiers essais cliniques, en particulier de méningo-encéphalites auto-immunes, a par la suite mené à la prudence quant à son utilisation (Nicoll et al., 2003 ; Orgogozo et al., 2003 ; Gilman et al., 20015).

Des stratégies d'immunisation dites « passives », reposant sur l'expression transgénique d'anticorps ou leur administration directe, ont été développées par la suite (Figure 15). Si l'infection virale (virus adéno-associé (AAV) ou Lentivirus porteur de transgènes codant pour les anticorps) ne nécessite qu'une seule injection, l'impossibilité de contrôler l'expression du transgène et l'absence de réversibilité en cas de survenue d'effet indésirable rendent difficile son utilisation en pratique clinique. Les approches par administration directe (ARNm ou anticorps) permettent un meilleur contrôle du traitement, au prix d'une répétition des injections.

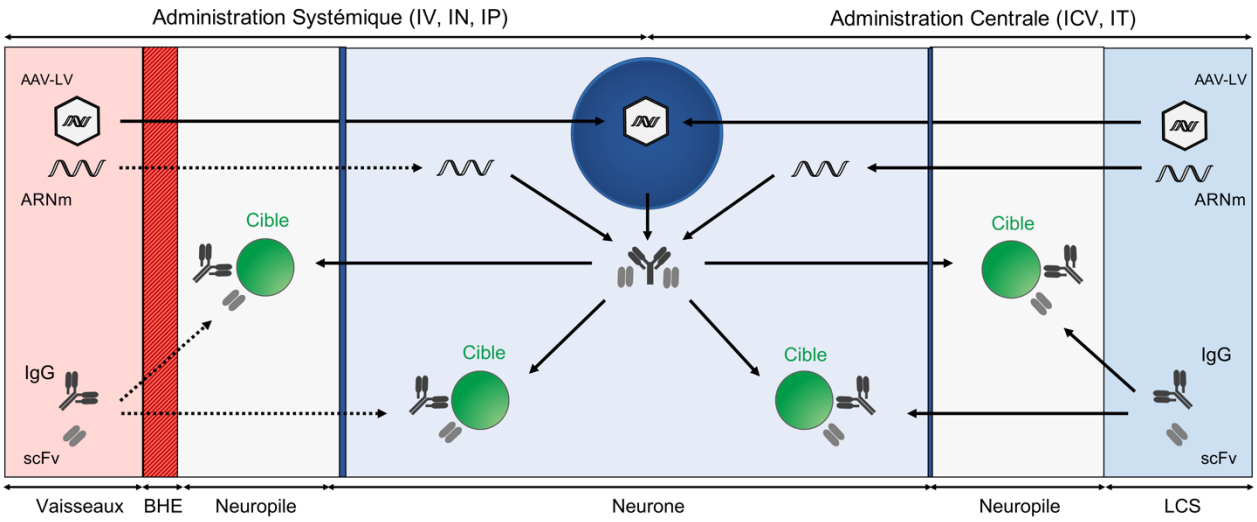

Figure 15. Techniques d'immunisation passive dirigée contre un antigène central (cible). AAV : adeno associated virus. BHE : barrière hémato-encéphalique. ICV : intra cérébroventriculaire. IgG : Immunoglobuline G. IP : intrapéritonéale. IN : intranasale. IT : intrathécale. IV : intraveineuse. LCS : liquide cérébro-spinal. LV : Lentivirus. scFv : single chain variable fragment. (P. Codron)

1.2. Stratégies thérapeutiques

Plusieurs paramètres conditionnent l'efficacité d'une immunothérapie et l'éventuelle survenue d'effets secondaires. Le type d'anticorps utilisé et les propriétés inhérentes à sa structure jouent tout d'abord un rôle central. Deux types d'anticorps sont principalement employés : les immunoglobulines G (IgG) composés de deux chaines lourdes et deux chaines légères, et les fragments monocaténaires recombinants (scFv) constitués de deux régions variables de chaînes lourdes et légères d'immunoglobulines connectées par un peptide de liaison. Les scFv sont plus petits, simples à générer par lignées d'hybridomes ou à administrer par transgénèse (alors appelés intrabodies), mais leur demi-vie est plus courte et ils ne peuvent interagir avec les récepteurs aux fragments Fc (FcR) des neurones et phagocytes pour leur internalisation et/ou dégradation.

Le choix de l'antigène est également un élément crucial : l'anticorps doit cibler un épitope pathogène accessible au sein de cellules en souffrance, avec une forte affinité, une grande spécificité et une faible immunogénicité (développement d'une immunité dirigée contre l'immunothérapie). En effet, l'interaction d'un anticorps peu spécifique avec des protéines de maintenance physiologiques sera à l'origine d'effets secondaires (Rosenmann et al., 2006). A l'inverse, un anticorps fortement immunogène ayant un accès restreint à son épitope aura peu d'effets thérapeutiques.

Enfin, la voie d'administration conditionne en grande partie l'efficacité du traitement. En effet, si les AAV et Lentivirus passent aisément la barrière hémato-encéphalique (BHE) et infectent spécifiquement les cellules cibles lorsqu'ils sont injectés par voie systémique, les ARNm et les anticorps ont un très faible pouvoir de diffusion au sein du SNC (seulement 0.1% de passage de la BHE pour les IgG en l'absence de lésion) (Poduslo et al., 1994). Afin d'améliorer leur biodisponibilité, des méthodes d'administration centrale peuvent être envisagées, au prix d'un plus grand risque iatrogène : administration intra-cérébroventriculaire (ICV) ou intrathécale (IT), par injections répétées ou par l'intermédiaire de pompes automatisées sous cutanées.

1.3. Cibles antigéniques dans la SLA

Dans le champ de la recherche sur la SLA, les stratégies thérapeutiques par immunothérapie active et passive ont principalement été étudiées sur modèle murin *SOD1*, en ciblant la forme native, mutée ou agrégée de la protéine SOD1 (Tableau 3). Les traitements ont dans l'ensemble permis une amélioration clinique et pathologique chez les souris. Toutefois, compte tenu de la forme particulière de la maladie, représentant seulement 2% des patients atteints de SLA et n'impliquant pas de pathologie TDP-43, il est difficile d'envisager l'utilisation de tels traitements pour la prise en charge des patients atteints de la forme sporadique de la maladie.

Le développement récent de modèles murins transgéniques surexprimant la protéine TDP-43 (native ou mutée), plus représentatifs de la sSLA, a fait émerger la possibilité de la mise au point de traitements par immunothérapie ciblant cette protéine.

Tableau 3. Principaux résultats des études évaluant l'efficacité d'une immunothérapie dans la SLA. (P. Codron).

Auteurs	Modèle(s)	Approche	Cible	Clinique	Neuropathologie
Urushitani et al., 2006	$SOD1^{G37R}$ $SOD1^{G93A}$	Immunisation active (Vaccination)	$SOD1^{G37R}$ $SOD1^{G93A}$	Amélioration des performances motrices, allongement de l'espérance de vie, diminution de la perte de poids. Absence d'ES.	Présence d'anticorps endogènes. Diminution de la perte motoneuronale, de la charge lésionnelle SOD1, et de la neuroinflammation.
Gros-Louis et al., 2010	$SOD1^{G93A}$	Administration ICV d'immunoglobulines	Agrégats SOD1	Amélioration des performances motrices, allongement de l'espérance de vie, diminution de la perte de poids. Absence d'ES.	Présence d'anticorps exogènes. Diminution de la perte motoneuronale, de la charge lésionnelle SOD1, et de l'activation astrocytaire.
Takeuchi et al., 2010	$SOD1^{G93A}$	Immunisation active (Vaccination)	$SOD1^{WT}$ $SOD1G^{93A}$	Amélioration des performances motrices, allongement de l'espérance de vie, diminution de la perte de poids. Absence d'ES.	Présence d'anticorps endogènes. Diminution de la perte motoneuronale et de la charge lésionnelle SOD1, modulation de la neuroinflammation.
Liu et al., 2012	$SOD1^{G37R}$ $SOD1^{G93A}$	Immunisation active (Vaccination)	Agrégats SOD1	Amélioration des performances motrices, allongement de l'espérance de vie, diminution de la perte de poids. Absence d'ES.	Présence d'anticorps endogènes. Diminution de la perte motoneuronale, de la charge lésionnelle SOD1 et de l'activation gliale, modulation de la neuroinflammation.
Patel et al., 2014	$SOD1^{G93A}$	Expression transgénique de scFv (AAV médiée, injection intrathécale)	Agrégats SOD1	Amélioration des performances motrices, allongement de l'espérance de vie, diminution de la perte de poids. Absence d'ES. Effets corrélés avec les taux intrathécaux de scFv.	Expression du transgène par les motoneurones. Diminution de la perte motoneuronale, du stress neuronal, de la charge lésionnelle SOD1 et de l'activation gliale.
Sábado et al., 2015	$SOD1^{G93A}$	Immunisation active (Vaccination)	Agrégats SOD1	Détérioration des performances motrices, absence d'effet sur l'espérance de vie et la perte de poids.	Augmentation de la charge lésionnelle SOD1, dépôts immuns, augmentation de l'activation microgliale et de la neuroinflammation.
Dong et al., 2018	$SOD1^{G93A}$	Administration IN de scFv	Agrégats SOD1	Amélioration des performances motrices, allongement de l'espérance de vie, diminution de la perte de poids. Absence d'ES.	Diminution de la perte motoneuronale, de la charge lésionnelle SOD1 et de l'activation gliale, modulation de la neuroinflammation et des voies de l'apoptose.
Maier et al., 2018	$SOD1^{G37R}$ $SOD1^{G93A}$	Administration ICV et IP d'immunoglobulines	Agrégats SOD1	Amélioration des performances motrices, allongement de l'espérance de vie, diminution de la perte de poids. Absence d'ES.	Présence d'anticorps exogènes. Diminution de la perte motoneuronale, de la charge lésionnelle SOD1 et de l'activation gliale.
Ghadge et al., 2019	$SOD1^{G93A}$	Expression transgénique de scFv (AAV médiée, injection intraveineuse)	$SOD1^{WT}$	Amélioration des performances motrices, allongement de l'espérance de vie, diminution de la perte de poids. Absence d'ES.	Expression du transgène par les motoneurones spinaux. Diminution de la perte motoneuronale, de la charge lésionnelle SOD1 et de l'activation gliale.

ES : effet secondaire. ICV : intra-cérébroventriculaire. IN : intranasale. IP : intrapéritonéale. scFv : single chain variable fragment

2. MISE EN PLACE DE L'ETUDE

2.1. Problématique et objectifs

L'objectif de ce projet était de mettre au point une immunothérapie ciblant les agrégats pathologiques de protéine TDP-43 au sein du système nerveux central afin de limiter leur cytotoxicité, empêcher leur propagation, et favoriser leur dégradation.

2.2. Contexte méthodologique et stratégie expérimentale

Compte tenu de l'expression ubiquitaire de TDP-43, la mise au point d'une immunothérapie dirigée contre cette protéine dans la SLA doit s'attacher à cibler spécifiquement les neurones affectés par la pathologie, afin de limiter les potentiels effets secondaires systémiques. De plus, de par son rôle central dans le métabolisme des ARN, les anticorps doivent, une fois captés par les neurones moteurs, n'interagir qu'avec la fraction pathogène cytoplasmique de la protéine et ne pas entraver sa fonction physiologique nucléaire.

Dans ce contexte, nous avons porté le choix de notre épitope sur le domaine RRM1 de TDP-43 (Figure 6a). En effet, ce site d'interaction nucléotidique étant masqué par l'ARN lors de l'activité physiologique de la protéine au sein du noyau, une immunothérapie dirigée contre RRM1 permettrait de cibler spécifiquement les protéines non fonctionnelles, majoritairement cytoplasmiques et extra-cellulaires. De plus, prévenir les modifications post-traductionnelles de ce domaine - en particulier l'oxydation - permettrait de contenir les phénomènes de modifications conformationnelles de TDP-43 médiées par RRM1 à l'origine de la constitution d'agrégats (Chang et al., 2013 ; Shodai et al.,2013). Enfin, bloquer l'interaction du domaine RRM1 avec la sous unité p65 de la protéine NFkB limiterait l'activation pathologique de cette voie de la neuroinflammation (Swarup et al., 2011).

Dans un premier travail mené par le Dr Pozzi au sein de l'équipe du Professeur Jean Pierre Julien (institut CERVO, Qc, Canada), nous avons mis au point une immunothérapie reposant sur l'injection ICV et IT d'AAV porteurs de transgènes codant pour des scFv dirigées contre le domaine RRM1 de la protéine TDP-43. Le traitement de souris transgéniques surexprimant les protéines mutées TDP-43^{A315T} et TDP-43^{G348C} a permis une amélioration des fonctions motrices et cognitives des animaux à 2 et 4 mois. L'étude histologique et biochimique des tissus médullaires et corticaux prélevés post mortem a permis de confirmer l'expression des transgènes par les motoneurones et microgliocytes

infectés, et d'observer une diminution de la perte motoneuronale, de la charge lésionnelle TDP-43, de l'activation astrocytaire et microgliale, et des marqueurs de la neuroinflammation. L'ensemble des résultats de ce travail est reporté dans l'article complémentaire n°2 situé en annexe (Pozzi et al., 2018).

Au vu des données de cette première étude, nous avons cherché à poursuivre ces travaux en travaillant à la mise au point d'une approche d'immunothérapie par injection directe d'immunoglobulines monoclonales, plus susceptible d'être secondairement employée dans le cadre de protocoles de recherche clinique compte tenu de la possibilité de contrôler les doses administrées et de suspendre le traitement en cas de survenue d'effet indésirable. Nous avons d'abord sélectionné puis généré une immunoglobuline G2A murine (mIgG2A) dirigée contre le domaine RRM1 de TDP-43 produite par une lignée clonale d'hybridomes, nommée E6. Nous avons ensuite analysé les effets de cet anticorps in vitro sur des lignées neuronales en culture surexprimant TDP-43. Enfin, nous avons étudié les paramètres cliniques, biochimiques et histopathologiques de souris transgéniques surexprimant la mutation TDP-43^{A315T} traitées pendant 5 semaines par immunothérapie administrée par voie systémique, intra-cérébroventriculaire et intrathécale. Les résultats de ce travail sont reportés dans l'article suivant.

Article N°3

Manuscrit en préparation

Lumbar intrathecal injections of monoclonal immunoglobulin against TDP-43 reduce proteinopathy and NFκB activation in a FTLD/ALS mouse model

S. Pozzi[1●], P. Codron[1,2●], L. Renaud[1], G. Soucy[1], C. Bareil[1], J-P. Julien[1,3] *

1. CERVO Brain Research Institute, Québec City G1J 2G3, Canada.

2. UMR CNRS 6015, INSERM U1083, University of Angers, Angers Cedex 9, France.

3. Department of Psychiatry and Neuroscience, University of Laval, Québec City G1V 0A6, Canada.

● These authors contributed equally to this work.

Lumbar intrathecal injections of monoclonal immunoglobulin against TDP-43 reduce proteinopathy and NFκB activation in a FTLD/ALS mouse model

S. Pozzi[1●], P. Codron[1,2●], L. Renaud[1], G. Soucy[1], C. Bareil[1], J-P. Julien[1,3 *]

1. CERVO Brain Research Institute, Québec City G1J 2G3, Canada.

2. UMR CNRS 6015, INSERM U1083, University of Angers, Angers Cedex 9, France.

3. Department of Psychiatry and Neuroscience, University of Laval, Québec City G1V 0A6, Canada.

● These authors contributed equally to this work.

* Corresponding Author

Corresponding Author

Pr. Jean-Pierre Julien

Department of Psychiatry and Neuroscience, Faculty of Medicine, Laval University

CERVO Brain Research Centre, 2601 Chemin de la Canardière, Québec, Québec G1J 2G3, Canada.

E-mail: jean-pierre.julien@fmed.ulaval.ca.

Lumbar intrathecal injections of monoclonal immunoglobulin against TDP-43 reduce proteinopathy and NFκB activation in a FTLD/ALS mouse model

INTRODUCTION

Transactive response DNA-binding protein 43 (TDP-43), encoded by *TARDBP* gene, is a DNA/RNA binding protein predominantly located in the nucleus of cells under physiological conditions. Accumulation of misfolded TDP-43 in the cytosol of degenerating neurons is a pathological hallmark of amyotrophic lateral sclerosis (ALS) and frontotemporal lobar degeneration (FTLD), suggesting a central role for TDP-43 in the pathogenesis of these two devastating diseases[1,2]. Further support is provided by the fact that *TARDBP* mutations are responsible for familial forms of ALS and FTLD[3,4]. However, despites the advances in understanding TDP-43 pathology in the last decade, it remains unclear whether neurodegeneration is caused by a loss of function of the protein due to its nuclear depletion, or by a direct toxicity of cytosolic aggregates. Furthermore, it also remains challenging to link TDP-43 proteinopathy to the other pathological processes observed in the diseases such as neuronal excitotoxicity, cytoskeleton disorganisation, mitochondrial dysfunction, axonal transport impairment, oxidative stress and neuroinflammation. All these uncertainties partly explain the difficulties to develop therapeutic strategies and the current lack of curative therapy for ALS and FTLD[5].

In recent years, there has been increasing concerns about the use of monoclonal antibodies targeting pathological proteins as a treatment for neurodegenerative disorders (reviewed in [6]). The principle of this approach is to block the toxicity and spreading of misfolded proteins, and to promote their degradation. With the aim of conducting such procedure in ALS and FTLD, we generated a monoclonal antibody directed against the RNA recognition motif 1 (RRM1) domain of TDP-43. This epitope was specifically chosen as it is masked under physiological condition in the nucleus of the cells, and is directly involved in TDP-43 misfolding in ALS and FTLD[7]. Moreover, RRM1 domain interacts with p65 subunit of nuclear factor κB (NFκB), activating its pathological pro-inflammatory activity[8]. In this study, we aimed to assess the tendency of the generated anti-TDP-43 antibody to decrease TDP-43 proteinopathy in vitro and in vivo in ALF/FTLD models.

RESULTS

1. Generation and characterization of E6 antibody directed against TDP-43 RRM1 domain

A monoclonal full-length mouse IgG2A (mIgG2A) named E6 directed against the RRM1 domain of TDP-43 (Fig. 1a) was used for experiments. A monoclonal mIgG2A reactive with the G1 protein of La Crosse Virus (bunyavirus vector of La Crosse encephalitis through mosquito bite in human) named 807.3 was used as a control. The antibodies were secreted by hybridoma cell line clones, purified, and stored at -80°C. The ability of E6 to recognize TDP-43 was first tested using immunoblot techniques. E6 antibody was able to detect human recombinant TDP-43 N-terminal peptide (1-206 amino acids containing RRM1) applied on a dot blot membrane, whereas no reaction occurred with 807.3 antibody (Fig. 1b). E6 reaction was lower when compared to a commercial anti-human TDP-43 (Abnova, Taipei City, Taiwan). No cross-reaction with BSA was observed for both E6 and 807.3. The antigen affinity of E6 for TDP-43 was subsequently investigated using a sandwich ELISA assay. As for dot-blot experiments, E6 antibody was able to recognize human recombinant TDP-43 but with a lower affinity than the commercial anti-human TDP-43, whereas 807.3 antibody showed the same absorbance as PBS (Fig. 1c). These results indicate that E6 was specifically directed against TDP-43 N-terminal fragment.

Since RRM1 domain is masked under physiological condition in the nucleus, immunofluorescence microscopy was performed after exposing fixed cells and tissues to antibodies with the aim of knowing if E6 was able to target only the cytosolic RNA/DNA-free fraction of TDP-43. E6 and 807.3 antibodies were conjugated to fluorophore Alexa-488 (E6-488 and 807.3-488) to allow their direct detection and to avoid nonspecific fluorescence signal. A mainly cytosolic fluorescence was observed in cells after exposing fixed HEK-293 cells to E6-488, whereas no signal was detected after control 807.3-488 exposure (Fig. 1d). Similar results were obtained with brain and spinal cord sections from TDP-43A315T transgenic mice, and human brain sections from a control subject and a patient affected with ALS/FTD (Supp Fig.1). Although these results suggested that E6 was able to recognize cytosolic but not nuclear TDP-43, the analyse of E6 and cytosolic TDP-43 colocalization was constrained by the strong nuclear signal of TDP-43 under physiological condition. The same experiment was thus performed on fixed pre-apoptotic HEK-293 cells overexpressing human TDP-43 (hTDP-43) with total cytosolic relocation of the protein. The signal of E6-488 colocalized with the signal of cytosolic TDP-43, whereas no signal was detected in fixed cells after 807.3-488 exposure (Fig. 1e). Collectively, these data indicate that E6 antibody was specific to the cytosolic fraction of TDP-43.

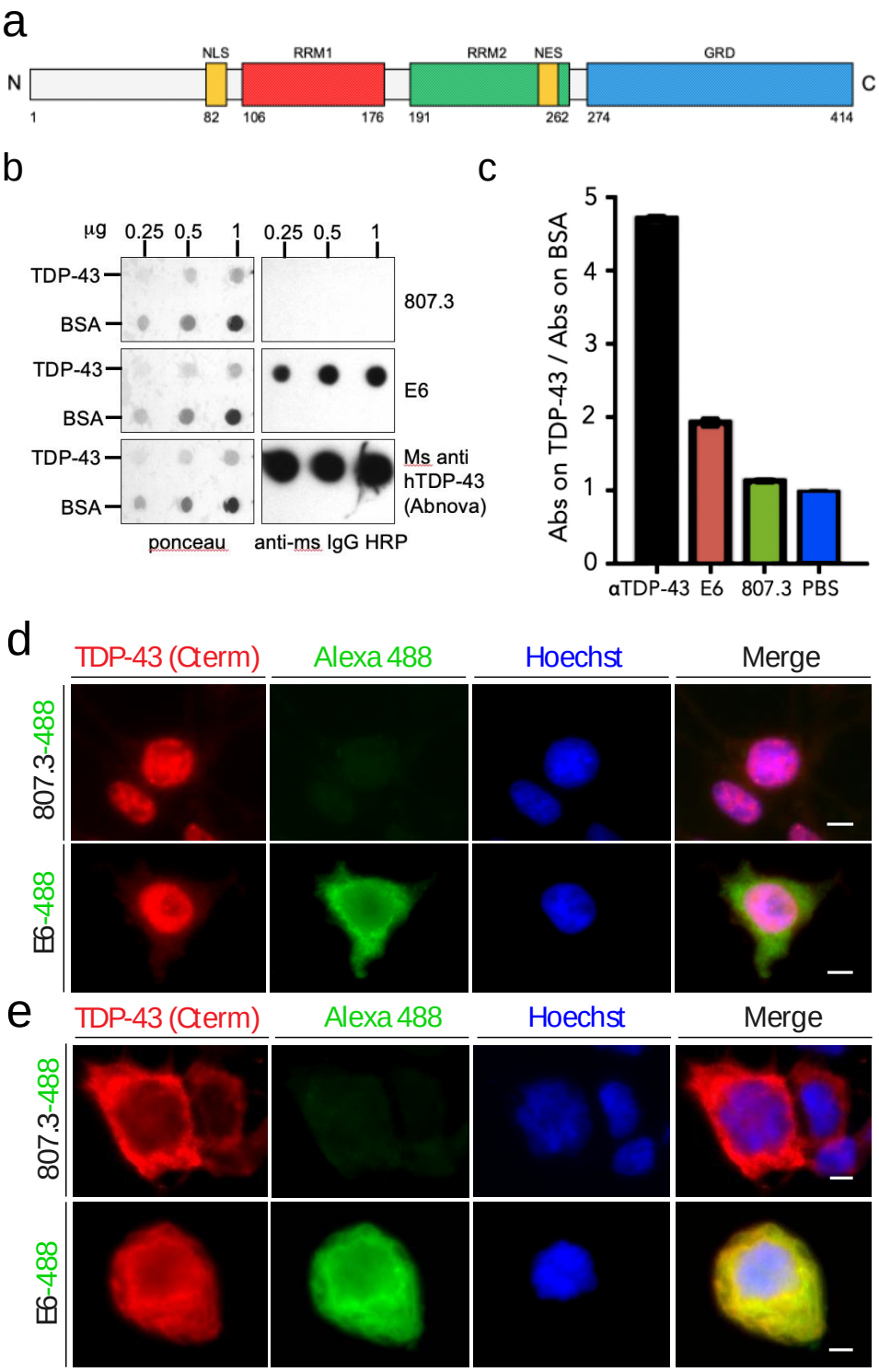

Figure 1. Characterization of E6 monoclonal antibody directed against TDP-43 RRM1 domain. (a) Schematic representation of human TDP-43 structure. NLS: nuclear localization sequence, RRM: RNA recognition motif, NES: nuclear export signal, GRD: glycine rich domain. (b) Immunoblot performed after exposing different amounts of human recombinant hTDP-43 or BSA to 807.3 control antibody, E6 antibody or commercial mouse anti-TDP-43 antibody (Abnova, Taipei City, Taiwan). Ponceau was used as loading reference. (c) ELISA assessing the affinity of E6 for human recombinant TDP-43 compared to control 807.3 antibody and commercial mouse anti-TDP-43 antibody (means ±SD from n=3 independent experiments). (d,e) Immunofluorescence performed on fixed HEK-293 cells in standard conditions (d) or after inducing a strong overexpression of hTDP-43 with cytoplasmic delocalization of the protein (e). Commercial anti-TDP-43 (Cterm) and 807.3-488 or E6-488 were used as primary antibodies. Scale bar 5µm.

2. Neuronal cells spontaneously internalize E6 into cytosol in vitro

Neuronal cells are known to be able to uptake immunoglobulins, primarily through clathrin-dependent Fc gamma receptor endocytosis[9]. Once in the cytosol of the neurons, these antibodies can interact with intracellular epitopes. To determine whether E6 was able to penetrate living neurons, mouse neuroblastoma cells (Neuro2A) were used as an in vitro model of neuronal cells. N2A cells were treated 24 hours with either free Alexa-488, 807.3-488, or E6-488, and fluorescence microscopy was performed after fixation. Although no signal was observed in free Alexa-488 treated cells, both 807.3-488 and E6-488 antibodies were detectable in the cytosol of the cells (Fig. 2a). Interestingly, no signal was detected in the nucleus of both 807.3-488 and E6-488 treated cells. Performing the same experiment in cells expressing an endosome marker highlighted that 807.3-488 and E6-488 antibodies were internalized through endocytosis (Fig. 2b). Together, these results indicate that neuronal cells spontaneously uptake antibodies present in their medium, and that once internalized, the antibodies remain in the cytosol of the cells.

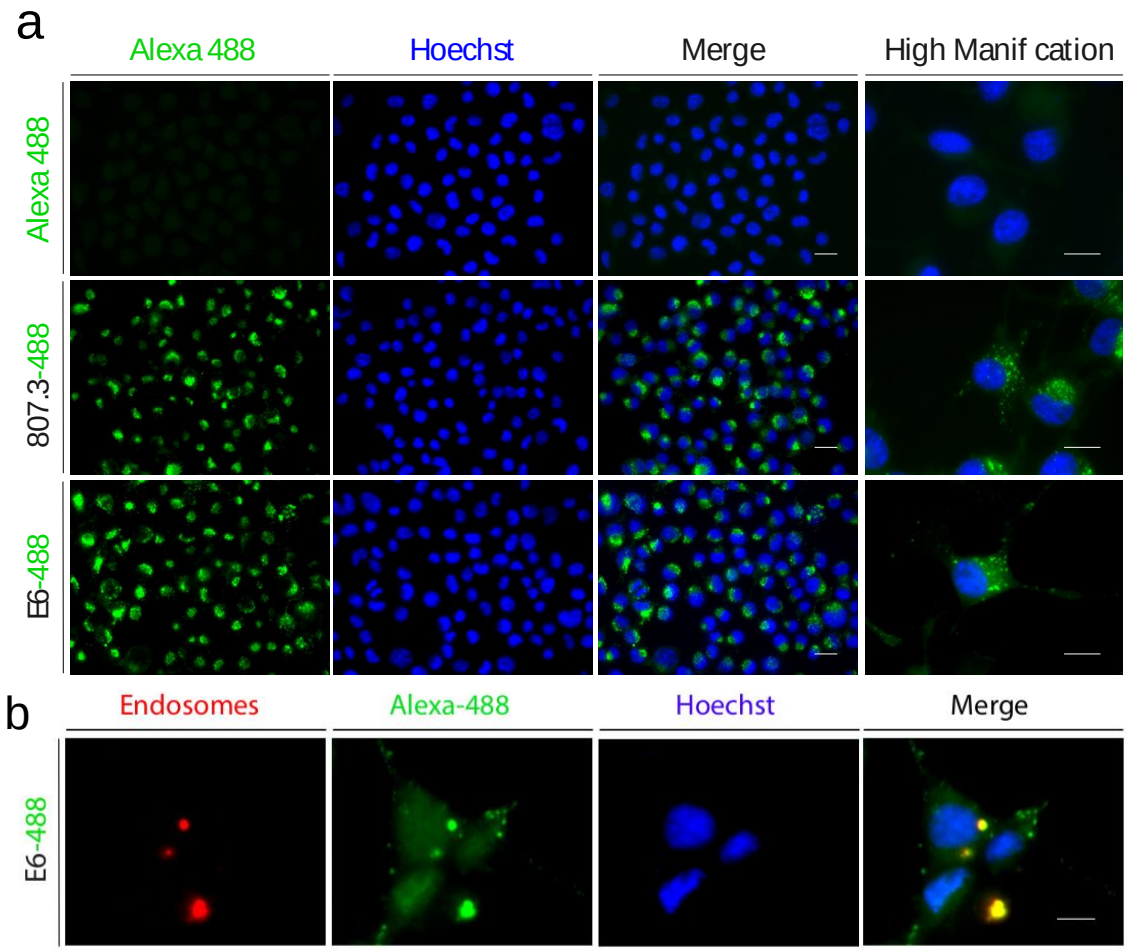

Figure 2. E6 is spontaneously internalized in cytosol by cultured neuronal cells. (a) Immunofluorescence analysis of N2A cells treated 48h with free Alexa-488, 807.3-488 control antibody or E6-488 antibody. Scale bar 20 µm. (d) Immunofluorescence analysis of N2A cells transfected with an endosome marker (red) and treated 48 h with E6-488 antibody. Scale bar 20 µm.

3. E6 targets cytosolic misfolded TDP-43 in neuronal cells in vitro

To further assess the effects of E6 antibody in vitro and its ability to target cytosolic aggregates of TDP-43, N2A cells overexpressing hTDP-43 were treated 24 hours with either free Alexa-488, 807.3-488, or E6-488, and fluorescence microscopy was performed after fixation. When present in the cytoplasm of the cells after being uptaken, E6-488 signal strongly colocalized with TDP-43 aggregates (Fig. 3a). By contrast, 807.3-488 signal did not overlap with TDP-43 cytosolic aggregates. Finally, as previously, no signal was detected in free Alexa-488 treated cells. As decreasing TDP-43 activity in cells is toxic, we aimed to assess if the action of E6 on cytosolic TDP-43 was deleterious to the cells. N2A cells in basal condition and N2A cells overexpressing hTDP-43 were treated with 24 hours with either PBS, 807.3, or E6, and cell viability was assessed by MTS assay (Promega, Madison, WI, USA). No difference was observed between the cell lines regarding the viability. These results suggest that when uptaken by neuronal cells, E6 antibody targets cytosolic abnormal aggregated TDP-43 with no major toxic effect.

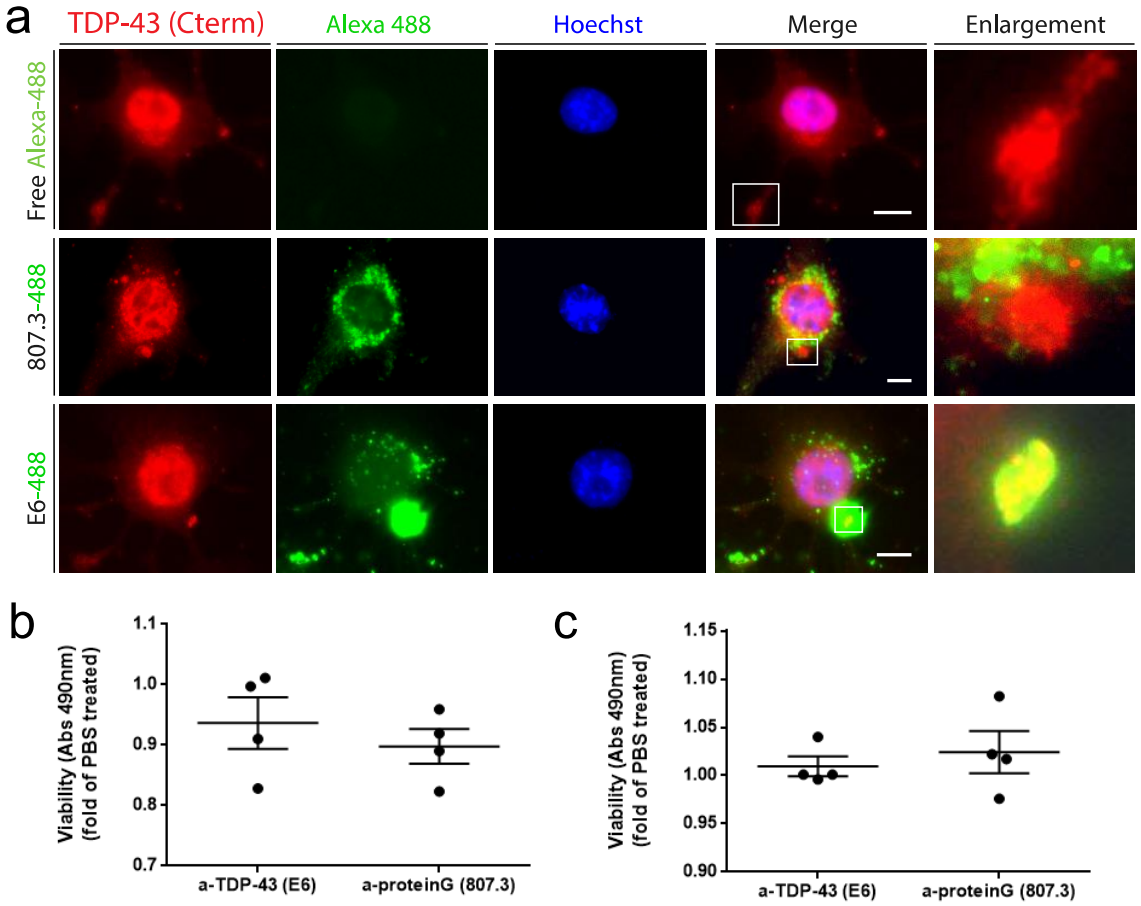

Figure 3. E6 selectively interacts with cytosolic misfolded TDP-43 in cultured neuronal cells. (a) Immunofluorescence analysis of the interaction between free Alexa-488, 807.3-488 or E6-488 antibody and cytosolic TDP-43 aggregates in N2A cells overexpressing hTDP-43, 48h after treatment. Scale bar 10 µm. (b,c) Viability of N2A cells expressing TDP-43 in basal conditions (b) or overexpressing hTDP-43 (c) 48h after treatment with PBS, 807.3 or E6. (mean ±SD from 4 independent experiments).

4. E6 is internalized by CNS neuronal and microglial cells in vivo

Given the ability of neuronal cells to spontaneously uptake E6 antibody in vitro, we next asked whether E6 could reach central nervous system (CNS) cells when administered in vivo. We thus treated transgenic mice expressing genomic fragments encoding mutated human TDP-43^{A315T} [10] with either 0.9% saline, 807.3 or E6 solutions using different procedures to assess the CNS bioavailability of our antibody.

Repeated intranasal and intraperitoneal administrations (twice a week) were first tested with the aim of assessing a systemic delivery procedure. After 2 weeks of treatment, no antibody could be detected in the brains and spinal cords of the mice treated either intranasally or intraperitoneally (Supp Fig. 2a), highlighting the high selectivity of the undamaged blood-brain barrier towards circulating antibodies. Systemic administration of the antibodies was thus excluded for further in vivo investigations.

A direct and continuous administration of the treatment in the CNS of the mice for 28 days was subsequently tested using an osmotic minipump system (Alzet, Cupertino, CA, USA). Unfortunately, the implanted device induced a local sterile inflammatory reaction in the brain of all the treated mice, regardless of the administered solution (Supp Fig. 2b,c). The high amount of endogenous antibodies in the cerebral parenchyma and the strong microglial activation precluded the assessment of E6 effects in the brain. This technique was thus also excluded for in vivo experiments.

Finally, repeated lumbar intrathecal administrations of the treatment (twice a week for 2 weeks) were tested. mIgG2A were detected by immunofluorescence microscopy in the 3 portions of the spinal cords of the animals treated with antibodies, whereas no immunostaining was observed in the CNS of the 0.9% saline treated mice (Fig. 4a). Although a weak staining was also detectable in the brainstem nuclei (data not shown), no signal was found in the cerebellum and the brain of the mice. At high magnification, both E6 and 807.3 were found to be mainly uptaken by neurons and microglial cells and remained mainly cytosolic with no overlap with nuclear TDP-43 (Fig. 4b). Taken together, these results suggest that when administered directly in the CNS in vivo through repeated intrathecal injections, E6 is uptaken by neurons and microglia and remains in the cytosol of these cells.

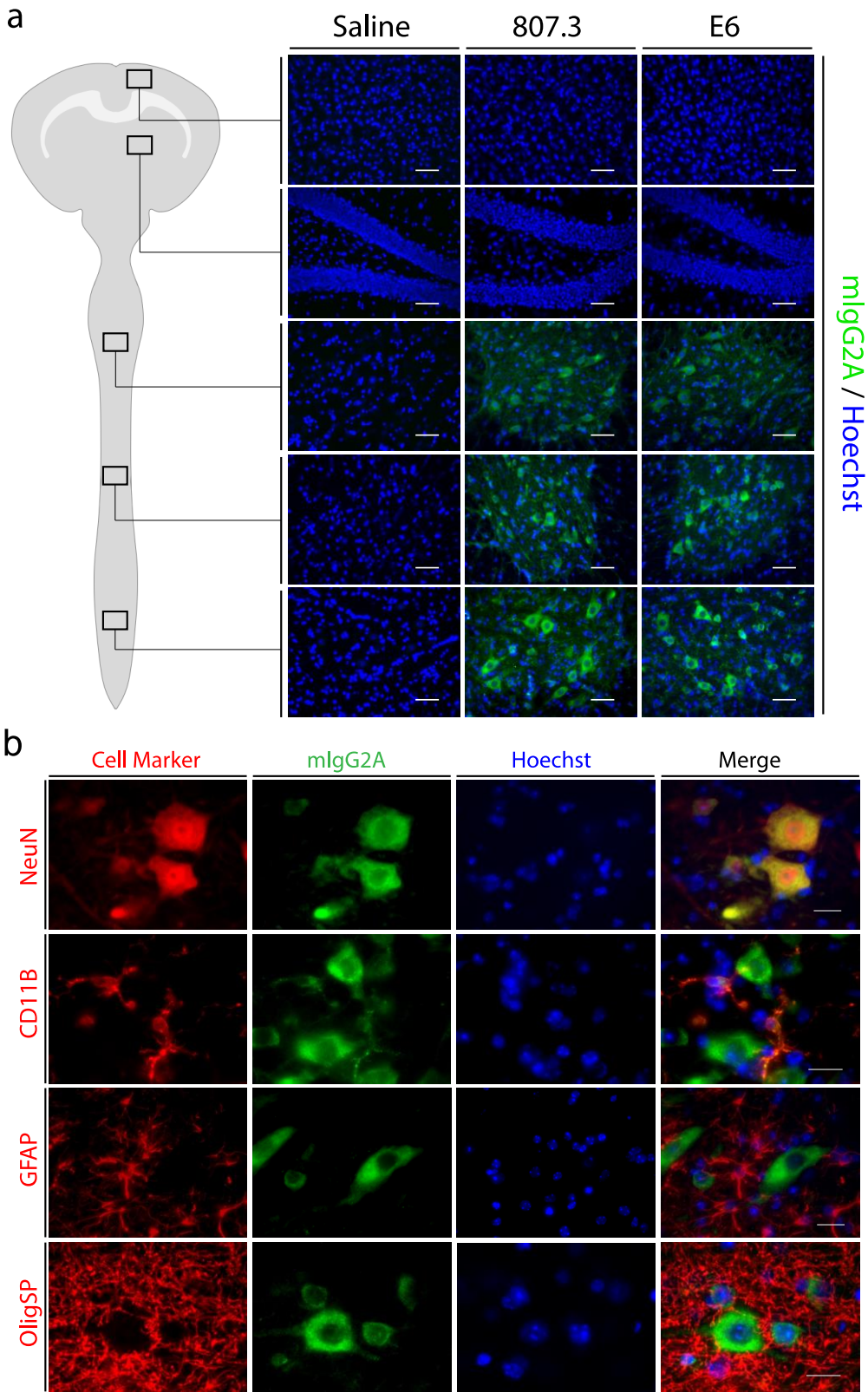

Figure 4. Repeated intrathecal injections allow endocytosis of E6 by motor neurons and microglia. (a) Representative images of mIgG2A immunofluorescence detection in spinal cords (anterior horn of lumbar, thoracic and cervical regions) and brains (hippocampus and motor cortex) of mice 2 weeks after treatment with saline 0.9%, 807.3 or E6. Scalebar 50µm. (b) Representative high magnification images of mIgG2A immunofluorescence detection in neurons (NeuN), microglial cells (CD11B), astrocytes (GFAP) and oligodendrocytes (OligSP) in anterior horn of lumbar spinal cords of mice treated with 807.3 and E6. Scalebar 20µm.

5. E6 treatment is not Toxic in vivo

With the aim of assessing the effects of intrathecal treatment with E6 in vivo, 30 TDP-43^{A315T} transgenic mice at 9 months of age were divided into 3 groups (n=10, 7 males and 3 females per group) comparable with regards to body weight, motor and cognitive performances ($p>0.05$ for all these parameters). Mice were treated for 5 weeks with repeated lumbar intrathecal injections of 0.9% saline (control saline group), 807.3 antibody (control mIgG2A group), or E6 antibody (experimental group) (Fig. 5a). Motor (accelerating rotarod and grid test) and cognitive performances (novel object recognition test and passive avoidance test) were regularly blindly collected according to the schedule depicted on Fig. 5a. After 5 weeks, mice were sacrificed for pathological analyses. Collected tissues were either frozen or fixed depending on the planned experiments (biochemistry or immunofluorescence).

No adverse effect, neurological symptom, weight loss or premature death occurred in mice throughout the course of the study, strengthening the absence of toxicity of E6 previously observed in vitro. No significant difference was observed between the 3 groups with regard to both motor and cognitive performances (Fig. 5b-d). Finally, no difference was noticed between the 3 groups with regard to the morphology and number of peripheral motor neurons in the anterior horn of the spinal cord (Fig. 5e,f). Together, these results support the absence of toxicity of E6 treatment, both at body and cellular levels.

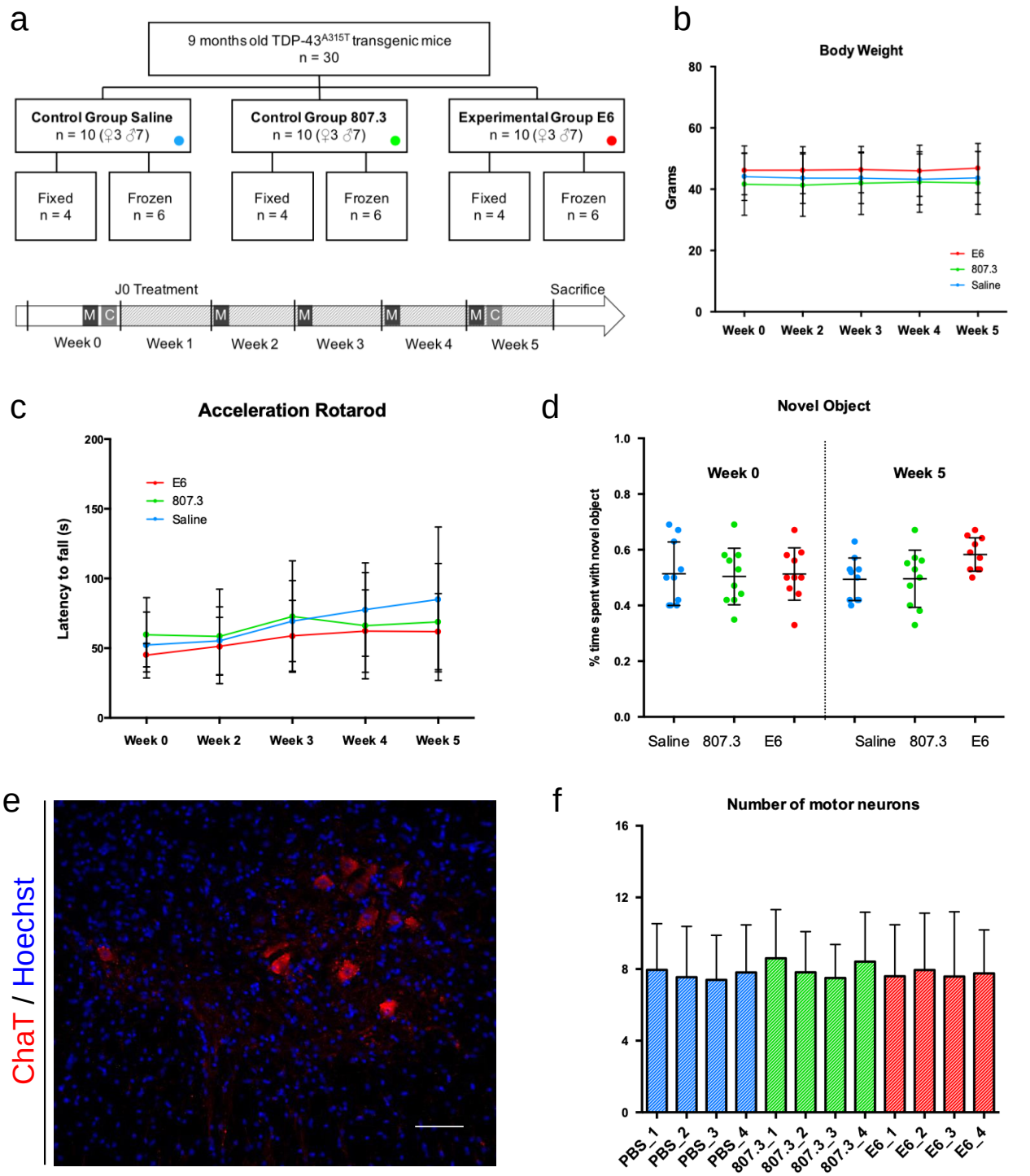

Figure 5. Absence of toxicity of E6 intrathecal treatment in mice. (a) Flow chart of the therapeutic assay conducted in mice to study the effects of intrathecal treatment in vivo (up), and schedule of blind collection of mice's motor and cognitive performances (down). (b) Body weight of mice evolution during the treatment period (mean ±SD from all the 10 mice per group; p=0.74). (c) Accelerating Rotarod performances of mice during the treatment period (mean ±SD from all the 10 mice per group; p=0.82). The slight improvement observed in all groups over time is due to learning and adaptation. (d) Novel object recognition performances of mice during the treatment period (mean ±SD from all the 10 mice per group; p=0.29). (e,f) Representative image of ChaT immunofluorescence staining in the anterior horn of lumbar spinal cords of treated mice for motor neurons counting (mean ±SD from >15 spinal cord sections per mouse; p=0.98). Scalebar 25µm.

6. E6 reduces TDP-43 proteinopathy in vivo

To assess the effects of E6 on TDP-43 level and distribution in CNS cells, protein fractions were prepared from the frozen lumbar spinal cords and nucleocytoplasmic ratio was measured in neurons using immunofluorescence microscopy. Western-blot analysis of pan TDP-43 (Cterm) highlighted a trend towards a decrease of TDP-43 levels in the spinal cord of the E6 treated mice (Figure 6a,b). Furthermore, high magnification immunofluorescence quantification of TDP-43 (Cterm) in motor neurons revealed a ~25% increase of the nucleocytoplasmic ratio of TDP-43 in the E6 group when compared to 0.9% saline and 807.3 groups (Figure 6c,d).

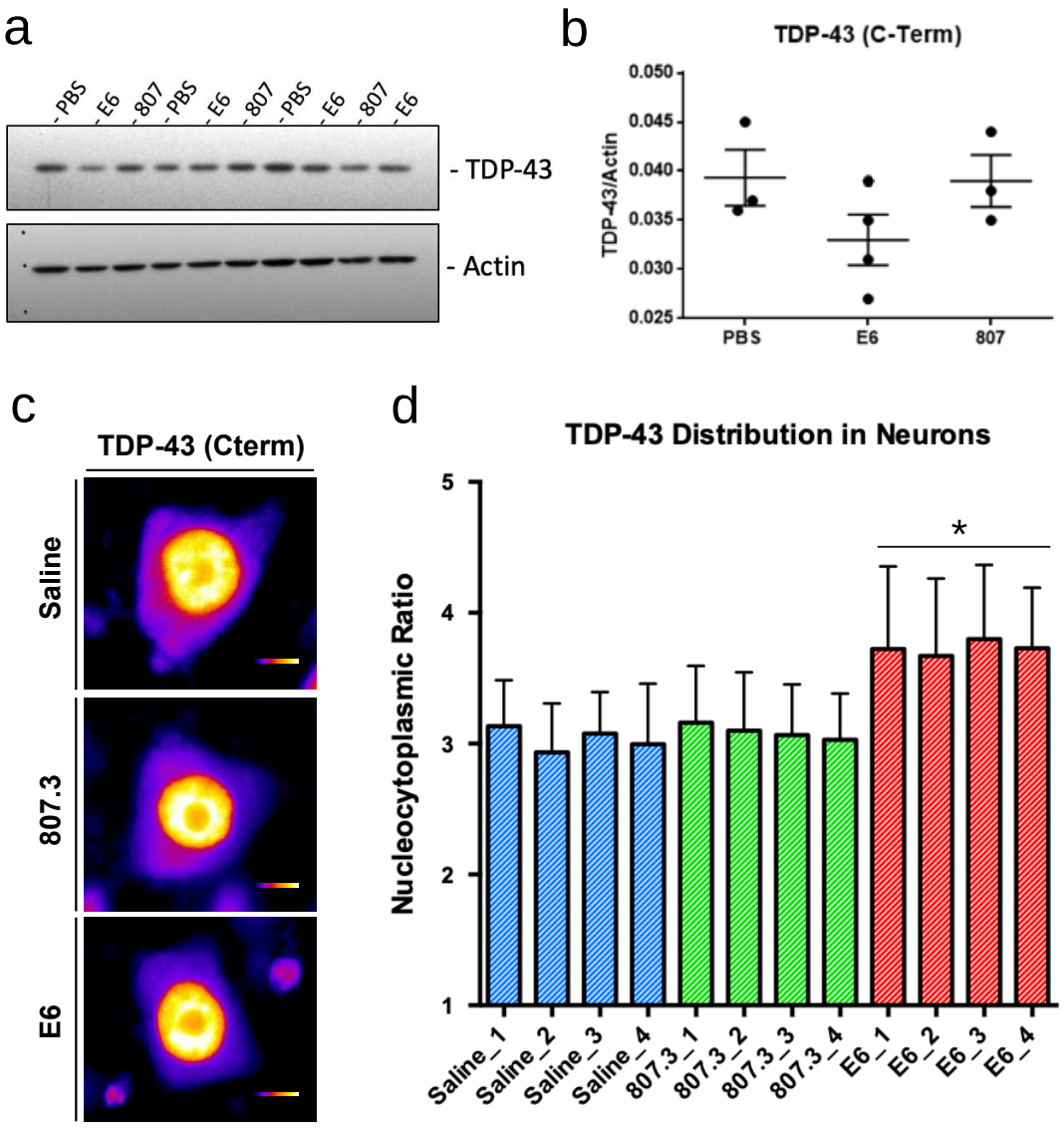

Figure 6. E6 reduces TDP-43 proteinopathy in vivo. (a,b) Western blot analysis of TDP-43 (Cterm) levels in lumbar spinal cords of mice. Actin was used as loading reference for analysis (mean ±SD from n=3 independent experiments; p=0.22) (c,d) Representative images of TDP-43 (Cterm) immunofluorescence staining in lumbar motor neurons of mice (signal intensity). The ratio between measured nuclear and cytosolic intensities was calculated for each cell (mean ±SD from >80 motor neurons analysed per mouse; pairwise comparisons, * $p < 0.01$). Scalebar 10µm, colour scale ranging from 0 to 400 intensity units.

A microglial activation was also noticed in the lumbar spinal cord of the E6 treated mice, measured by a ~15% increase of the CD11B area fraction in immunofluorescence (Fig. 7e,f). No difference was observed for GFAP analyses (Fig. 7e,g). These data indicate that E6 treatment increases TDP-43 nucleocytoplasmic ratio in motor neurons. This process is associated with a microglial activation that may contribute to TDP-43 elimination.

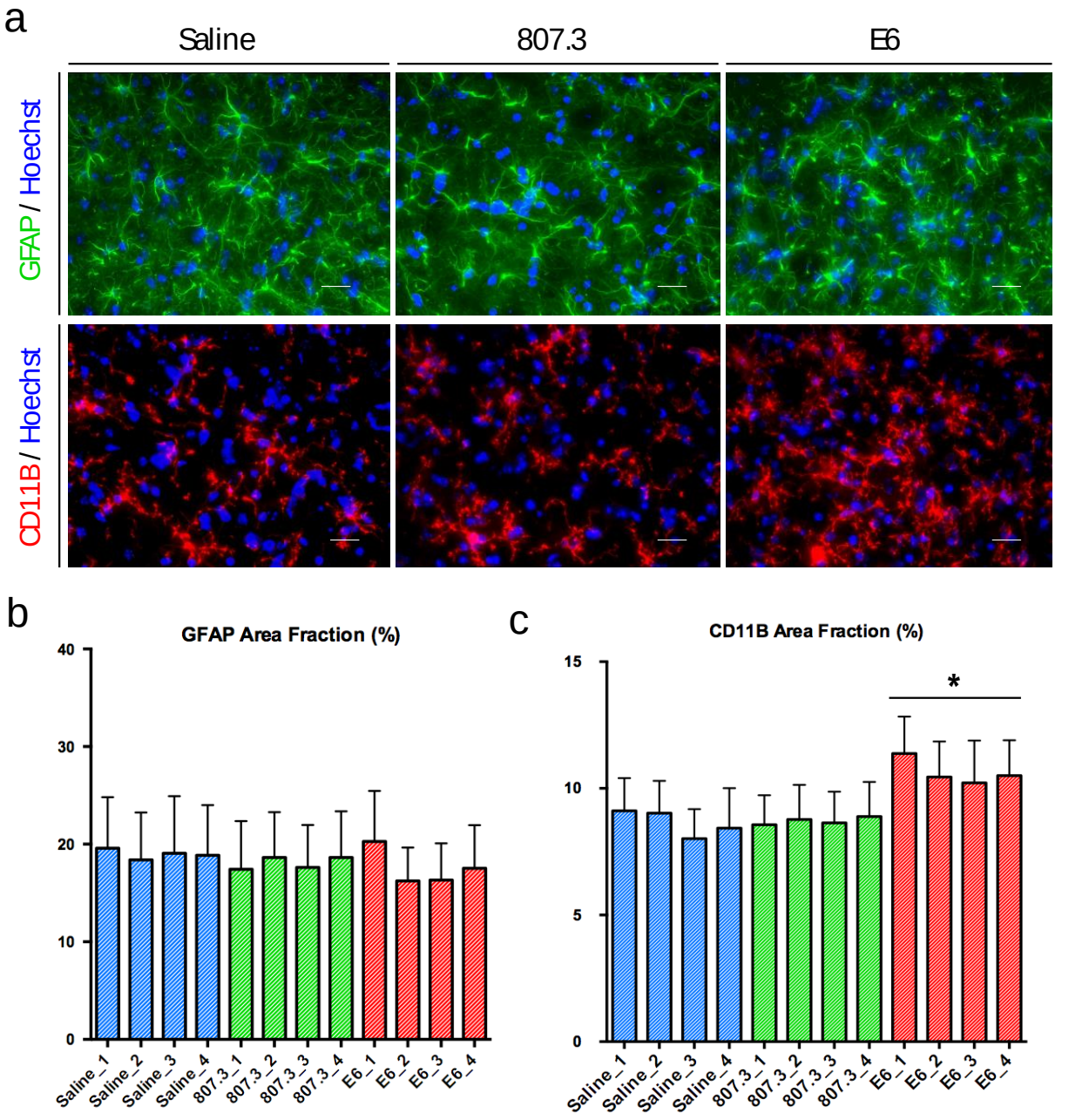

Figure 7. E6 induces microglial but not astroglial activation in vivo. (a) Representative images of GFAP and CD11B immunofluorescence staining in anterior horn of lumbar spinal cords of mice. (b,c) Quantification of astrocytes (b) and microglial cells (c) area fraction. (means ±SD, >20 images per animal, p=0.87 GFAP, * p<0.001 CD11B). Scale bars: 20 µm.

7. E6 reduces p65/NFκB activation in vivo

In ALS/FTLD, the RRM1 domain of TDP-43 interacts with p65 subunit of NFκB factor, activating the pro-inflammatory p65/NFκB pathway[8]. We thus aimed to determine whether E6 antibody was able to disrupt this interaction in the CNS of the treated mice by analysing p65 and its activated-form acetylated-p65 (ac.p65). Immunofluorescence staining of ac.P65 in the anterior horn of E6 treated mice showed a lower nuclear signal in motor neurons that had high levels of E6 in their cytoplasm compared to the others (Fig. 8a). High magnification immunofluorescence was performed to allow quantified analysis, highlighting a ~15% reduction of the ac.P65 nuclear signal in the motor neurons of E6 treated mice when compared to the two other groups (Fig. 8b,c). These results were consistent with a downregulation of p65/NFκB pathway by E6 in vivo.

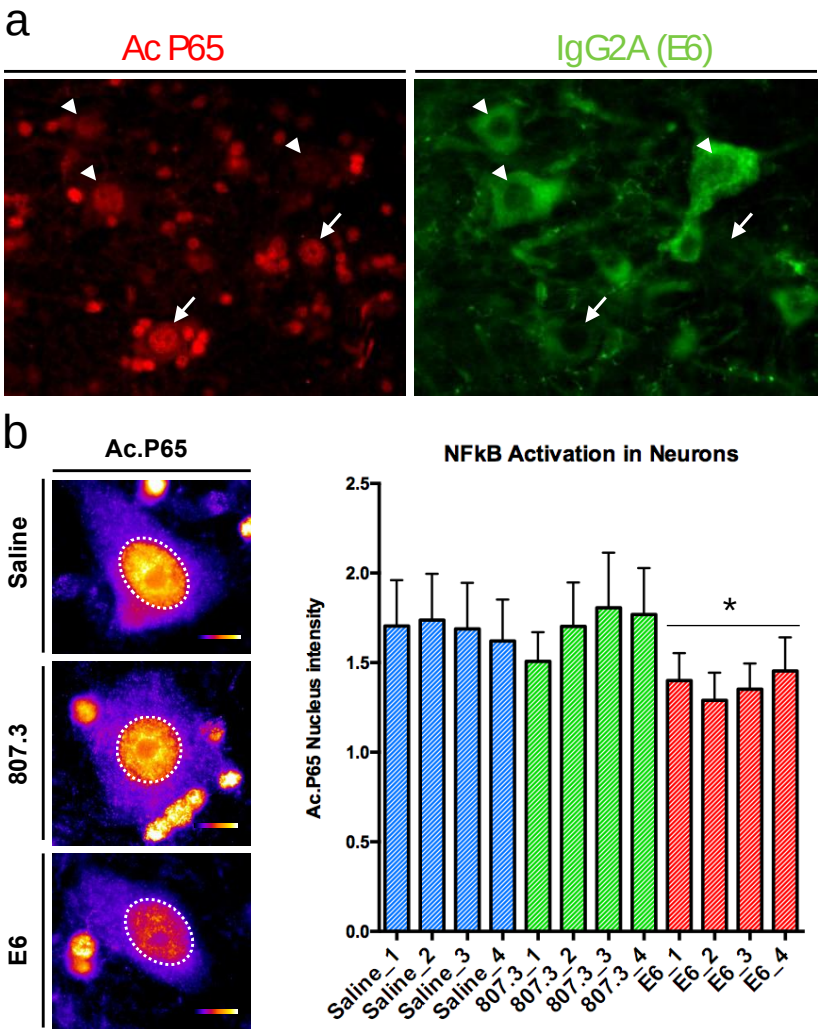

Figure 8. E6 reduces NFκB activation in vivo. (a) Representative image of acetylated P65 (ac.P65) immunofluorescence staining in anterior horn of lumbar spinal cords of mice treated with E6. Ac.P65 staining was lower in the nucleus of motor neurons that had high levels of E6 in their cytoplasm (arrowheads) compared to the others (arrows). (b,c) Representative images of ac.P65 immunofluorescence staining in lumbar motor neurons of mice. Ac.P65 nucleus total intensity was measured for each motor neuron (mean ±SD from >80 motor neurons analysed per mouse; *p<0.01). Scalebar 10µm, colour scale ranging from 0 to 400 intensity units.

DISCUSSION

In this study, we were able to reduce TDP-43 mislocalization and NFκB pathological activation in the spinal cord of TDP-43^{A315T} transgenic mice using direct administration of a monoclonal immunoglobulin against TDP-43. To the best of our knowledge, this is the first study to assess the effects of a full-length antibody specific to cytosolic TDP-43 both in vitro and in vivo.

Over the past decade, there has been increasing concerns about the use of monoclonal antibodies in neurodegenerative disorders, with the aim of targeting misfolded intra- or extra-cellular proteins, such as amyloid-ß peptide, tau, or alpha-synuclein (reviewed in [11]). In the field of ALS/FTLD, immunotherapies against SOD1 protein, involved in familial forms of the disease, have been developed and tested on cellular and mouse models with encouraging results[12–18]. However, applying such strategy for TDP-43 targeting must be cautious, given the severe consequences observed when TDP-43 is depleted in cellular and animal models[19–21]. Thus, the antibody must specifically target pathological cytosolic aggregates of TDP-43 in cells, without interfering with the physiological nuclear activity of the protein. Considering this crucial fact, we chose to generate a monoclonal antibody directed against the RRM1 domain of TDP-43, as this epitope is masked under physiological condition in the nucleus, and is involved in cytosolic TDP-43 misfolding in FTLD/ALS. Performing direct administration of full-length antibodies was motivated by fast and simple production process, and the presence of Fc fragment allowing internalization by neurons[9]. Moreover, in contrast with AAV mediated therapy, direct administration of monoclonal immunoglobulins allows adaptation and/or cessation of treatment in case of side effects in trials and clinical practice.

Three modalities of treatment have been tested in this study. We first tried systemic administration through intranasal and intraperitoneal injections, but we failed in detecting the administered immunoglobulins in the brains and spinal cords of the treated mice. This observation could be explained by the fact that very few circulating antibodies enter the CNS in vivo, due to tight control of the blood-brain barrier (BBB)[22]. Although continuous intra-ventricular injections were too invasive to correctly assess the efficiency of our treatment, repeated lumbar intrathecal injections allowed a reliable, safe and reproducible diffusion of the antibody to the neurons and microglial cells of the CNS. However, this technique did not allow to reach the encephalon. In patients, intrathecal administration of monoclonal antibodies through both intra-ventricular and lumbar intrathecal injections are performed in clinical practice, with low risk and few side effects related to the technique[23–25]. Such techniques could thus be considered for E6 immunotherapy administration to ALS/FTLD patients, allowing a diffusion of the treatment to the entire CNS.

In our study, E6 interaction with TDP-43 RRM1 domain did not result in toxic effects both in vitro and in vivo. This observation is probably due to the specific ability of E6 to target misfolded cytosolic TDP-43 without

interfering with the nuclear activity of the protein. Repeated intrathecal injection of E6 resulted in a trend towards a decrease of TDP-43 levels in the spinal cord of the treated mice, and a ~25% increase of TDP-43 nucleocytoplasmic ratio in motor neurons, suggesting a clearance of TDP-43 cytosolic fraction in these cells. Interestingly, these results were associated with a microglial activation in the spinal cord of the E6 treated animals. This activation could be one plausible mechanism of the clearance of TDP-43 in motor neurons, as recently reported in another ALS mouse model[26]. Furthermore, in our study, E6 antibody was detected in the cytosol of microglial cells of treated mice, so the occurrence of a Fc-mediated phagocytosis of the protein could also be a possible pathway for TDP-43 degradation, as seen in Alzheimer disease models with anti-tau monoclonal antibodies[27]. Finally, this decrease could be due to a limitation of the extracellular spreading and transcellular transfer of misfolded TDP-43[28] through E6 activity.

E6 administration was also accompanied with downregulation of p65/NFκB pathway in motor neurons. In ALS/FTLD, TDP-43 RRM1 domain activates p65/NFκB pro-inflammatory pathway through direct interaction with p65 subunit[8]. E6 antibody was thus able to disrupt this interaction in the CNS of treated mice, conferring a complementary therapeutic property of the immunotherapy through neuroinflammation downregulation.

Despites the effects of E6 on decreasing TDP-43 proteinopathy and NFκB activation in the spinal cord of the treated mice, these observations were not accompanied with major clinical improvements compared with the two control groups. This could be explained by the absence of strong motor impairment in the TDP-43^{A315T} mice. Indeed, transgenic mice carrying mutation on TDP-43 C-terminal domain have proved to display a slow onset and heterogeneous phenotype, with mainly FTLD-like cognitive symptoms, including hyperphagia and executive dysfunction[10,29,30]. In particular, these mice do not become paralysed and die at standard age. Thus, as the site of diffusion of our treatment was mainly spinal, the effects of E6 treatment could not been assessed in optimal conditions regarding clinical parameters.

It will therefore be of particular interest to further study the effects of E6 immunotherapy on animal models exhibiting a stronger ALS/FTLD-like phenotype, as for example the recently reported rNLS8 or double-transgenic UBQLN2^{P497H}; TDP-43^{G348C} mice models[26,31]. Long-term treatment trials will also be of interest to ensure the absence of potential long-term side effects. Finally, we are currently working on humanizing E6 antibody to ensure the reproducibility of the obtained results and to consider E6 immunotherapy for future therapeutic trials.

The results obtained in this study provide encouraging prospects for a patient-specific therapy for ALS/FTLD, but also for the other neurological disorders in which TDP-43 pathology may be involved, such as Alzheimer's disease[32] or Stroke[33].

Acknowledgements

This work was supported by the Canadian Institutes of Health Research (CIHR) and by the Institut National de la Santé et de la Recherche Médicale (INSERM Research Fellow 2017–2019).

Authors contributions

J-P. Julien supervised this project.

S. Pozzi, P. Codron, and J-P. Julien conceived the project,

S. Pozzi, P. Codron and L. Renaud performed the experiments.

G. Soucy and C. Bareil genotyped and treated the mice, and helped with mice maintenance.

S. Pozzi, P. Codron, and J-P. Julien analysed the data and wrote the paper.

Competing interests

The authors declare no competing interests.

References

1. Neumann, M. et al. Ubiquitinated TDP-43 in Frontotemporal Lobar Degeneration and Amyotrophic Lateral Sclerosis. Science 314, 130–133 (2006).

2. Arai, T. et al. TDP-43 is a component of ubiquitin-positive tau-negative inclusions in frontotemporal lobar degeneration and amyotrophic lateral sclerosis. Biochemical and Biophysical Research Communications 351, 602–611 (2006).

3. Benajiba, L. et al. TARDBP mutations in motoneuron disease with frontotemporal lobar degeneration. Ann Neurol 65, 470–473 (2009).

4. Sreedharan, J. et al. TDP-43 Mutations in Familial and Sporadic Amyotrophic Lateral Sclerosis. Science 319, 1668–1672 (2008).

5. Mitsumoto, H., Brooks, B. R. & Silani, V. Clinical trials in amyotrophic lateral sclerosis: why so many negative trials and how can trials be improved? Lancet Neurol 13, 1127–1138 (2014).

6. Freskgard, P.-O. & Urich, E. Antibody therapies in CNS diseases. Neuropharmacology 120, 38–55 (2017).

7. Shodai, A. et al. Aberrant assembly of RNA recognition motif 1 links to pathogenic conversion of TAR DNA-binding protein of 43 kDa (TDP-43). J Biol Chem 288, 14886–14905 (2013).

8. Swarup, V. et al. Deregulation of TDP-43 in amyotrophic lateral sclerosis triggers nuclear factor kappaB-mediated pathogenic pathways. J Exp Med 208, 2429–2447 (2011).

9. Congdon, E. E., Gu, J., Sait, H. B. R. & Sigurdsson, E. M. Antibody uptake into neurons occurs primarily via clathrin-dependent Fcgamma receptor endocytosis and is a prerequisite for acute tau protein clearance. J Biol Chem 288, 35452–35465 (2013).

10. Swarup, V. et al. Pathological hallmarks of amyotrophic lateral sclerosis/frontotemporal lobar degeneration in transgenic mice produced with TDP-43 genomic fragments. Brain 134, 2610–2626 (2011).

11. Valera, E., Spencer, B. & Masliah, E. Immunotherapeutic Approaches Targeting Amyloid-beta, alpha-Synuclein, and Tau for the Treatment of Neurodegenerative Disorders. Neurotherapeutics 13, 179–189 (2016).

12. Gros-Louis, F., Soucy, G., Lariviere, R. & Julien, J.-P. Intracerebroventricular infusion of monoclonal antibody or its derived Fab fragment against misfolded forms of SOD1 mutant delays mortality in a mouse model of ALS. J Neurochem 113, 1188–1199 (2010).

13. Ghadge, G. D., Pavlovic, J. D., Koduvayur, S. P., Kay, B. K. & Roos, R. P. Single chain variable fragment antibodies block aggregation and toxicity induced by familial ALS-linked mutant forms of SOD1. Neurobiol Dis 56, 74–78 (2013).

14. Takeuchi, S. et al. Induction of protective immunity by vaccination with wild-type apo superoxide dismutase 1 in mutant SOD1 transgenic mice. J Neuropathol Exp Neurol 69, 1044–1056 (2010).

15. Urushitani, M., Ezzi, S. A. & Julien, J.-P. Therapeutic effects of immunization with mutant superoxide dismutase in mice models of amyotrophic lateral sclerosis. Proc Natl Acad Sci U S A 104, 2495–2500 (2007).

16. Liu, H.-N. et al. Targeting of monomer/misfolded SOD1 as a therapeutic strategy for amyotrophic lateral sclerosis. J Neurosci 32, 8791–8799 (2012).

17. Patel, P. et al. Adeno-associated virus-mediated delivery of a recombinant single-chain antibody against misfolded superoxide dismutase for treatment of amyotrophic lateral sclerosis. Mol Ther 22, 498–510 (2014).

18. Benkler, C. et al. Aggregated SOD1 causes selective death of cultured human motor neurons. Sci Rep 8, 16393 (2018).

19. Iguchi, Y. et al. Loss of TDP-43 causes age-dependent progressive motor neuron degeneration. Brain 136, 1371–1382 (2013).

20. Sephton, C. F. et al. TDP-43 is a developmentally regulated protein essential for early embryonic development. J Biol Chem 285, 6826–6834 (2010).

21. Wu, L.-S. et al. TDP-43, a neuro-pathosignature factor, is essential for early mouse embryogenesis. Genesis 48, 56–62 (2010).

22. Poduslo, J. F., Curran, G. L. & Berg, C. T. Macromolecular permeability across the blood-nerve and blood-brain barriers. Proc Natl Acad Sci U S A 91, 5705–5709 (1994).

23. Bergman, J. et al. Intrathecal treatment trial of rituximab in progressive MS: An open-label phase 1b study. Neurology 91, e1893–e1901 (2018).

24. Rubenstein, J. L. et al. Phase I study of intraventricular administration of rituximab in patients with recurrent CNS and intraocular lymphoma. J Clin Oncol 25, 1350–1356 (2007).

25. Perissinotti, A. J. & Reeves, D. J. Role of intrathecal rituximab and trastuzumab in the management of leptomeningeal carcinomatosis. Ann Pharmacother 44, 1633–1640 (2010).

26. Spiller, K. J. et al. Microglia-mediated recovery from ALS-relevant motor neuron degeneration in a mouse model of TDP-43 proteinopathy. Nat Neurosci 21, 329–340 (2018).

27. Luo, W. et al. Microglial internalization and degradation of pathological tau is enhanced by an anti-tau monoclonal antibody. Sci Rep 5, 11161 (2015).

28. Iguchi, Y. et al. Exosome secretion is a key pathway for clearance of pathological TDP-43. Brain 139, 3187–3201 (2016).

29. White, M. A. et al. TDP-43 gains function due to perturbed autoregulation in a Tardbp knock-in mouse model of ALS-FTD. Nat Neurosci 21, 552–563 (2018).

30. Arnold, E. S. et al. ALS-linked TDP-43 mutations produce aberrant RNA splicing and adult-onset motor neuron disease without aggregation or loss of nuclear TDP-43. Proc Natl Acad Sci U S A 110, E736-745 (2013).

31. Picher-Martel, V., Renaud, L., Bareil, C. & Julien, J.-P. Neuronal Expression of UBQLN2(P497H) Exacerbates TDP-43 Pathology in TDP-43G348C Mice through Interaction with Ubiquitin. Mol Neurobiol (2018). doi:10.1007/s12035-018-1411-3

32. Tremblay, C., St-Amour, I., Schneider, J., Bennett, D. A. & Calon, F. Accumulation of transactive response DNA binding protein 43 in mild cognitive impairment and Alzheimer disease. J Neuropathol Exp Neurol 70, 788–798 (2011).

33. Thammisetty, S. S. et al. Age-related deregulation of TDP-43 after stroke enhances NF-kappaB-mediated inflammation and neuronal damage. J Neuroinflammation 15, 312 (2018).

Methods

Antibodies production

The EcoR1-Not1 428 bp hTDP-43 cDNA fragment was PCR-amplified and cloned into the pGEX-6P-1 vector (GE Healthcare, Chicago, IL, USA). This recombinant plasmid was used on the Escherichia Coli host BL21 with the aim of producing the TDP-43 RRM1 domain. The 136 amino acids (15.68kDa) recombinant protein was then purified using the Glutathione S-transferase (GST) gene fusion system (GE Healthcare, Chicago, IL, USA). From the obtained purified recombinant protein, Medimabs (Mount Royal, QC, Canada) produced different hybridoma cell lines. The medium of those cell lines was analysed by western blot in order to select the one producing the most specific anti-RRM1 antibody. Control mIgG2A 807.3 antibody was provided commercially (CTRL-2290, ATCC, Manassas, VA, USA). For direct fluorescence detection, E6 and 807.3 antibodies were conjugated with Alexa fluorochrome (807.3-488 - E6-488) using an Alexa Fluor 488 Antibody Labelling Kit (Thermofisher, Waltham, MA, USA) following manufacturer's instructions. The obtained preparation was then dialysed during 6 hours in order to avoid sodium bicarbonate toxicity.

Dot blots and ELISA Assays

Dot blots were performed by loading different concentrations of bovine serum albumin (BSA) and human recombinant TDP-43 on a PVDF membrane by vacuum filtration using a Dot-Blot apparatus (Bio-Rad, Hercules, CA, USA). Membranes were exposed overnight at room temperature to 807.3, E6 or commercial mouse anti-hTDP-43 N-Terminal (Abnova, Taipei City, Taiwan, China) antibodies. After 4 washes in TBS, membranes were incubated 2h in blocking reagent, washed 4 times with TBS and incubated 2h with an anti-mouse HRP conjugated antibody (Abcam, Cambridge, UK). Densitometry was done by Image Lab (Bio-Rad, Hercules, CA, USA) or Image Studio Lite 4.0 (Li-Cor, Lincoln, NE, USA) software.

ELISA assays were performed using Elisa assay kit (Peprotech, Somerset, NJ, USA). Human recombinant TDP-43 or BSA were diluted in PBS, and 100uL of the obtained solutions were loaded on an Elisa assay plate and incubated overnight at room temperature. The day after, wells were washed 4 times with washing buffer and incubated for 2h with 0.5 ug/mL of E6 monoclonal antibody, 807.3 monoclonal antibody, commercial mouse anti-hTDP-43 antibody (Abnova, Taipei City, Taiwan, China), PBS or BSA. After 4 washes in TBS, wells were incubated 2h in blocking reagent, washed 4 times with TBS and incubated 2h with anti-mouse and anti-rabbit HRP conjugated antibodies (Abcam, Cambridge, UK). After 4 washes in TBS, wells were incubated with 100µL of substrate solution and chemiluminescence was read at 450nm using an EnSpire 2300 Multilabel reader (Perkin Elmer, Waltham, MA, USA).

Cells Culture, transfection and treatment

HEK293 (human embryonic kidney cells) and Neuro2A cells (mouse neuroblastoma cells) were grown in Dulbecco's Modified Eagle Medium (DMEM) with 10% foetal bovine serum (FBS), 1% penicillin-streptomycin and 1% glutamine in a humidified atmosphere (95% air,5% CO2) at 37°C. Monolayers of cells were routinely maintained in T75 flasks. To induce TDP-43 overexpression, cells were transfected for 48h when at 70% confluence with hTDP-43 or Flag-TDP-43 plasmids (home-made) using Jet Prime (Polyplus, Strasbourg, France) transfection reagents according to manufacturer's instructions. To treat the cells, a 10µM solution of either free Alexa 488, 807.3-488 antibody or E6-488 antibody was added to the medium for 24 hours. All experiments were conducted on cells with similar passage numbers, ranging from 6 to 20, in order to avoid artefacts due to senescence.

Protein extraction and Western blot (cells)

For Western blot analysis, cells were grown to 70% confluence in wells in a humidified atmosphere (95% air, 5% CO2) at 37°C. If applicable, cells transfections and/or treatments were performed as described before.

To obtain nuclear and cytoplasmic fractions, cells were collected in cold PBS and centrifuged at 2000 x rpm 5 min. Pellets were lysated in hypotonic buffer (Hepes pH 8 10mM, KCl 10mM, MgCl2 1.5mM, NaF 1mM, PMSF 0.5mM supplemented with protease, phosphatase inhibitors) and incubated on ice for 15min. NP-40 (0.5%) was added and lysates were vortexed and centrifuged 10 min at 3000 x rpm. Supernatant were collected as cytoplasmic fractions. Pellets were then solubilized in extraction buffer (Hepes pH 8 20mM, NaCl 420mM, MgCl2 1.5mM, NaF 1mM, EDTA 0.2mM, glycerol 25%, PMSF 0.5mM supplemented with protease, phosphatase inhibitors), incubated on ice 15min, sonicated and centrifuged at 12.000 rpm for 10min. Supernatants were collected as nuclear fractions.

Total proteins from cells were obtained by lysating cells pellets in extraction buffer supplemented with 0.5% of NP-40 if immunoprecipitation experiments were planned, or with SDS 1% followed by centrifugation at 12.000 rpm for 10min.

For soluble and insoluble protein extraction, cell pellets were solubilized in Ripa buffer (Tris 50mM, NaCl 150mM, SDS 0.1%, Na-Deoxycholate 0.5%, Triton X100 1%, PMSF 1mM supplemented of protease and phosphatase inhibitors), sonicated and centrifuged 20 min at 13.000 rpm. Supernatants were collected as soluble portion, whereas pellets were washed twice in Ripa buffer, sonicated, centrifuged again 20 min at 13.000 rpm., and finally resuspended in SDS 2%. For Western blots, equal amount of proteins was resuspended in loading buffer supplemented with Dithiothreitol (DTT) 1mM, boiled 5 min at 100°C and loaded on 12% acrylamide gels (home-made) or precast gels (Bio-Rad, Hercules, CA, USA), transferred on PVDF membranes (Millipore, Burlington, MA, USA) and incubated 1h with blocking solution (BSA 3% or Milk

5% in TBS-Tween 0.1%). Membranes were incubated overnight with primary antibodies (Supp Table 1) diluted in blocking solution, washed in TBS-Tween, incubated 2h in secondary antibodies, and finally washed in TBS-Tween. Goat anti-mouse HRP or goat anti-rabbit HRP were diluted 1:5000 in blocking, whereas IRDye (Li-Cor, Lincoln, NE, USA) were diluted 1:10.000 in TBS-Tween and incubated in dark. Signal was acquired by exposing membranes to X-ray film (Biomax, Rochester, NY, USA) or using the Li-Cor sistem (Li-Cor, Lincoln, NE, USA).

Immunofluorescence (cells)

For immunofixation, cells were grown to 70% confluence on 0.17 mm thick cover glasses (Fisher Scientific, Hampton, NH, USA) in a humidified atmosphere (95% air, 5% CO2) at 37°C. If applicable, cells transfection and/or treatment were performed as described before. Cells were then washed once in PBS and fixed with 4% paraformaldehyde for 15min at room temperature. After three washes in phosphate buffered saline (PBS), cells were blocked and permeabilized in 0.1% triton X-100 and 5% bovine serum albumin in PBS for 1 h at room temperature. Cells were then washed and incubated over night at 4°C with primary antibodies (Supp Table 1) diluted in blocking solution. Finally, cells were washed in PBS and incubated with appropriate Alexa Fluor conjugated secondary antibodies (Invitrogen, Carlsbad, CA, USA, 1:1000). DNA was counterstained with Hoechst 33342 (Thermo Fisher Scientific, Waltham, MA, USA, 1:1000) and cover glasses were mounted on 1.0 mm thick slides (Fisher Scientific, Hampton, NH, USA) using Fluoromount-G Buffer (Southern Biotech, Birmingham, AL, USA).

Cells survival assay

Cell viability was assessed using [3-(4,5-dimethylthiazol-2-yl)-5-(3-carboxymethoxyphenyl)-2-(4-sulfophenyl)-2H-tetrazolium] MTS assay, following manufacturer's instructions (Promega, Madison, WI, USA). After one-hour incubation with the reagent, absorbance was determined at 490 nm using an EnSpire 2300 Multilabel reader (Perkin Elmer, Waltham, MA, USA).

TDP-43A315T transgenic animals

Transgenic mice bearing the human genomic fragment encoding for TDP-43^{A315T} mutation [ref Swarup] were identified by PCR performed on tail biopsies. The animals were constantly maintained as colony at the CERVO Brain Institute animal facility under standard conditions. The Animal Care Ethics Committee of the University of Laval approved all in vivo experimental protocols. Experiments were carried out in accordance with the Guide to the Care and Use of Experimental Animals of the Canadian Council on Animal Care.

Treatments administration

Mice were anesthetized with 2% isoflurane during all the procedures, and post-treated with subcutaneous buprenorphine (0.05 mg/kg) to prevent postoperative pain. For intranasal administration, anesthetized mice were placed on their back, and droplets of 0.9% saline or 2mg/mL purified monoclonal antibody solution were dropped into the mouse's nostrils using a pipette. Fifty microliters of solution per mouse (25µL per nostril) was administered twice a week. For intraperitoneal administrations, mice were placed on their back and 500µL of 0.9% saline or 1mg/mL purified monoclonal antibody solution were injected intraperitoneally. For continuous intraventricular delivery, a sterile brain infusion cannula was stereotaxically implanted into the right ventricle of the mice (David Kopf Instruments, Tujunga, CA, USA). After insertion, the infusion cannula was fixed to the skull with dental cement and connected to an osmotic minipump implanted under the skin (Alzet, Cupertino, CA, USA) filled with 200µL of 0.9% saline or 0.6 mg/mL purified monoclonal antibody solution. Mice received continuous amount of antibody in ventricles with a pumping rate of 0.25µL/h. For intrathecal injections, anesthetized mice were placed on their stomach, and a total of 20µL volume of 0.9% saline or 1,25mg/mL purified monoclonal antibody solution was slowly injected into the dura (L4-L5 intervertebral space) using a 10µL sterile Hamilton syringe. The presence of a reflex contraction of the hind legs or the tail was considered indicative of a successful administration. The syringe was removed 1 minute after the end of the injection to minimize CSF and vector leakage.

Behavioural experiments

All of the behavioural experiments were blindly conducted as such the experimenter had no knowledge of the drug treatment of animals. Accelerating Rotarod was performed at 4 rpm speed with 0.1 rpm/s acceleration as described elsewhere[12]. Mice were subjected to three trials per session, the mean (performance was considered. The novel object recognition test was performed as a 3 days test: on day 1 (habituation), the mouse was positioned in an empty 15 x 30 cm opaque box and allowed to discover the environment for 5 min; on day 2 (training), the mouse was allowed to interact with 2 equal objects positioned in the box for 5 min, time of interaction with each object was recorded; on day 3 (test), one object was replaced with a new and completely different object (colour and shape) and time of interaction with each object was again recorded. For the Step-through passive avoidance test, a two-compartment apparatus (bright and dark compartments separated by a guillotine door) was used (Ugo Basile, Trappe, PA, USA). Mice were placed in the bright compartment and allowed to explore for 30 seconds, at which point the guillotine door was raised to allow the mice to enter the dark compartment. When the mice entered the dark compartment, the guillotine door was closed and an electrical foot shock (0.5 mA) was delivered for 2 seconds on the second day. On the third day, mice were placed in the bright compartment and the time to

enter the dark compartment was recorded (no shock given if entering the dark compartment, maximum latency in the bright compartment = 300 seconds).

Sacrifice

Mice were anesthetized by intraperitoneal injection of 4% chloral hydrate (sodium pentobarbital, 100mg/kg). For protein analyses, mice were perfused intracardially with 30mL of cold 0.1M phosphate buffer (+4°C, flow rate 20 mL/minute), and tissues were then quickly collected, frozen on dry ice, and stored at -80°C until used for protein extraction. For histological analyses, mice were first perfused intracardially with 30mL of cold 0.1M phosphate buffer, and subsequently perfused with 30mL of cold 4% paraformaldehyde (PFA). Tissues were then collected, post-fixed for 24h in 4% PFA and cryoprotected in sucrose 30%.

Protein extraction and Western blot (tissues)

To obtain nuclear and cytoplasmic fractions, frozen tissues were lysed in hypotonic buffer (Hepes-KOH pH 7.6 10mM, NaCl 10mM, KH2PO4 1mM, NaHCO3 5mM, EDTA pH8 5mM, CaCl2 1mM, MgCl2 0.5mM supplemented by protease and phosphatase inhibitors), homogenized, solubilized by rotation at 4°C for 10min, added of 10% sucrose 2.5M and centrifuged 10 min at 6.300 x g. Supernatants were collected as cytoplasmic fraction. Pellets were resuspended in extraction buffer (Tris pH7.4 10mM, Sucrose 300mM, EDTA 1mM, NP-40 0,1% supplemented by protease and phosphatase inhibitors), homogenized and centrifuged 5min at 4.000 x g. Pellets were washed 3 times with extraction buffer followed by centrifugations. After last centrifugation pellets were resuspended in Ripa buffer (Tris pH7.4 50mM, EDTA 1mM, NaCl 150mM NP-40 1% supplemented with SDS 2% and protease and phosphatase inhibitors) and sonicated. To obtain insoluble proteins from cytoplasm, triton X100 1% was added to the cytoplasmic fraction, sonicated and ultracentrifuged at 107.000 x g 30min. Supernatants were collected as cytoplasmic soluble portions whereas pellets were resuspended in Ripa buffer and sonicated as for nuclear pellets. Proteins were quantified using Lowry method (Bio-Rad, Hercules, CA, USA) or BCA method (Bio-Rad, Hercules, CA, USA) when SDS was present in the lysate. Western blot analyses were performed as described before for cells protein extracts.

Immunofluorescence (tissues)

Paraformaldehyde fixed lumbar spinal cords and brains were 25µm sectioned using a SM2000 R microtome (Leica Microsystems, Wetzlar, Germany) and stored at -20°C in a glycerol and glycine solution. After 3 washes in PBS, tissue sections were blocked and permeabilized in 0.1% Triton X-100 and 5% normal goat serum in PBS for 1h at room temperature. Sections were then washed and incubated over night with primary antibodies (Supp Table 1) in blocking solution. Sections were then washed in PBS and incubated with

appropriate Alexa Fluor conjugated secondary antibodies (Invitrogen, Carlsbad, CA, USA, 1:1000) for 2 hours at room temperature. DNA was counterstained using Hoechst 33342 (Invitrogen, Carlsbad, CA, USA, 1:10000, 1mn), and TrueBlack (Biotium, Fremont, CA, USA, 1:20, 2mn) was used to quench lipofuscin autofluorescence. Sections were finally mounted on 1.0 mm thick slides and covered with 0.17 mm thick cover glasses (Fisher Scientific, Hampton, NH, USA) using Fluoromount-G Buffer (Southern Biotech, Birmingham, AL, USA).

For low magnificence fluorescence imaging, slides were placed on the stage of a DM5000 B wide-field microscope (Leica Microsystems, Wetzlar, Germany) connected to a CTR5000 station and a Mi-150 Fiber Optic Illumination System (Dolan-Jenner, Boxborough, MA, USA) and equipped with 10X/0.30 Ph1 HC PL Fluotar, 20X/0.50 Ph2 HC PL Fluotar and 40X/0.75 Ph2 HCX PL Fluotar objectives. Images were acquired using a Digital FireWire Monochrome Camera (DFC350 FX) controlled by Leica Application Suite software version 4.8.0. For high magnificence fluorescence Imaging, slides were placed on the stage of a Axio Imager Z1 wide-field microscope (Zeiss, Oberkochen, Germany) equipped with 40X EC-plan Neofluar 40x/0.75 Ph2 M27, 63X Plan Apochromat 63x/1.40 Oil DIC M27, and 100X EC-plan Neofluar 100x/1.30 Oil Ph3 M2 oil immersion objectives. Images were acquired using an AxioCam MRm camera controlled by AxioVision software (Carl Zeiss Imaging Solutions GmbH) version 4.8.1.0.

More than 15,000 images were acquired and analysed in total. ImageJ software was used for images reconstruction and morphometric analysis {Johannes, 2015 #1878}. To assess the number of motor neurons in ventral horns, neurons stained with anti-ChaT antibody were counted on pictures acquired at low magnification (20X). The nucleocytoplasmic ratio of TDP-43 was determined for each cell at high magnification (63X) as described before {Codron, 2018 #1880}. For astrogliosis and microgliosis assessments, an automated intensity detection threshold (IJ_IsoData) was applied to images acquired at medium magnification (40X), and elements higher than 30 µm were selected and analysed for area distribution. To quantify NFκB activation in neurons, the mean intensity of acetylated NFκB signal was measured in the nucleus and corrected to the mean cytoplasmic signal of the same cell (considered as basal signal).

Statistical analysis

Statistical analyses were carried out using PRISM software version 6.0 for Windows (GraphPad, La Jolla, CA, USA). Comparisons of means were performed using Student's t-test for two groups analysis, and the one-way analysis of variance (ANOVA) for multiple groups analysis, after verifying the normal distribution and the homoscedasticity of data using Shapiro–Wilk's and Bartlett's tests. Comparisons of percentages were performed using Fischer's test. Differences were considered to be significant at $p<0.05$.

Supplementary Data

Supplementary Figures

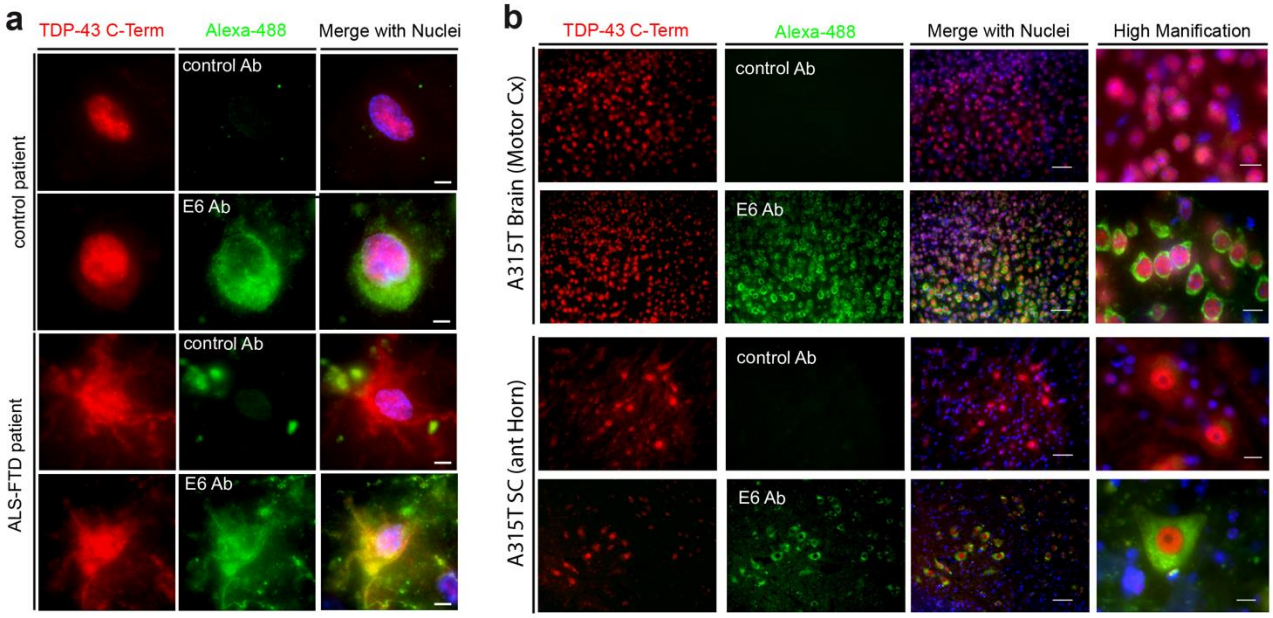

Supplementary Figure 1. Characterization of E6 monoclonal antibody directed against TDP-43 RRM1 domain. (a) Immunofluorescence performed on fixed brain sections from a control subject and a patient affected with ALS/FTD. Commercial anti-TDP-43 (Cterm) and 807.3-488 or E6-488 were used as primary antibodies. Scale bar 10µm. (b) Immunofluorescence performed on fixed brain and spinal cord sections from TDP-43^{A315T} transgenic mice. Commercial anti-TDP-43 (Cterm) and 807.3-488 or E6-488 were used as primary antibodies. Scale bar 50µm, (high magnification scale bar 10µm).

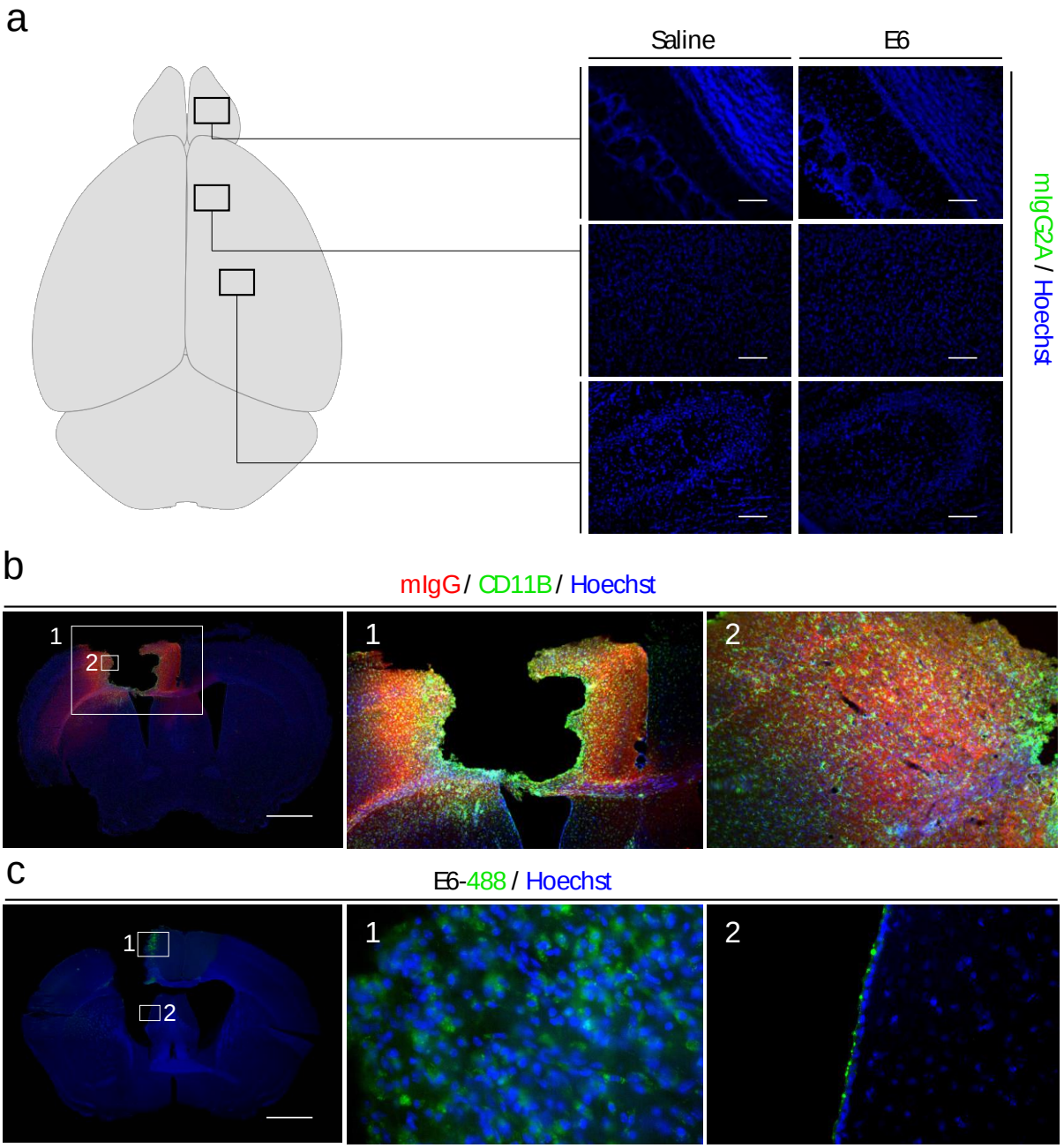

Supplementary Figure 2. (a) Representative images of mIgG2A immunofluorescence detection in brain (bulbs, prefrontal cortex and motor cortex) of mice 2 weeks after intranasal treatment with saline 0.9% or E6. Scalebar 100µm. (b) Representative immunofluorescence images of aseptic inflammation reactive to implanted device in brain of mice treated 28 days using osmotic minipump system (Alzet, Cupertino, CA, USA). Endogenous immunoglobulins ingress (red) and microglial activation (green) were observed both with saline 0.9% and E6 treatments. Scale bar 2mm. (c) Representative immunofluorescence images of E6 direct detection in brain of mice treated 28 days using osmotic minipump system filled with E6-488 antibody. Only a small amount of antibodies was detected in necrotic tissue around the injection point (1) and on the wall of the ipsilateral ventricle (2). Scale bar 2mm

Supplementary Tables

Supplementary Table 1: List of antibodies.

Antigen	Antibody	WB dilution	IF dilution	Company
Actin	mouse monoclonal	1:10000		Millipore (Temecula, CA, USA)
CD11B	rat monoclonal		1:1000	Bio-Rad (Hercules CA, USA)
Chat	goat polyclonal		1:500	Millipore (Temecula, CA, USA)
Iba-1	rabbit polyclonal	1:500	1:1000	Wako Chemicals (Richmond, VA, USA)
Glial fibrillary acidic protein	rabbit polyclonal		1:1000	Dako (Santa Clara, CA, USA)
Glyceraldehyde 3-phosphate dehydrogenase	mouse monoclonal	1:2000		Santa Cruz (Santa Cruz, CA, USA)
Mouse IgG2A	goat polyclonal (alexa-488 conjugated)		1:4000	Invitrogen (Carlsbad, CA, USA)
NeuN	rabbit monoclonal		1:1000	Cell Signaling Technologies (Danvers, MA, USA)
NF-kB p65 subunit	rabbit polyclonal	1:1000		Santa Cruz (Santa Cruz, CA, USA)
p65 (acetylated)	rabbit polyclonal		1:1000	Abcam (Cambridge, UK)
p65 (phospho Ser 536)	mouse monoclonal	1:1000		Cell Signaling Technologies (Danvers, MA, USA)
Oligodendrocyte Specific Protein	Rabbit polyclonal		1:1000	Abcam (Cambridge, UK)
p84 nuclear membrane	mouse monoclonal	1:500		Abcam (Cambridge, UK)
TDP-43 N-Term	rabbit polyclonal	1:5000	1:1000	Proteintech (Chicago, IL, USA)
TDP-43 C-Term	rabbit polyclonal	1:5000	1:1000	Proteintech (Chicago, IL, USA)
TDP-43 human specific	mouse monoclonal	1:1000	1:1000	Abnova (Taipei City, Taiwan)

3. DISCUSSION ET PERSPECTIVES

3.1. Principaux résultats de l'étude

Dans ce troisième projet réalisé au sein de l'équipe du Professeur Jean-Pierre Julien (institut CERVO, Qc, Canada), nous avons travaillé à la mise au point d'une immunothérapie directe par injection d'IgG dirigées contre le domaine RRM1 de la protéine TDP-43. En utilisant une approche immunohistologique, nous avons pu observer chez des souris transgéniques surexprimant la mutation TDP-43^{A315T} traitées par injections intrathécales répétées un adressage motoneuronal du traitement et une diminution de la charge lésionnelle médullaire. Il s'agit à notre connaissance du premier travail portant sur une telle approche.

3.1.1. Choix de l'immunoglobuline

Les protocoles d'injection d'immunothérapie directe chez l'animal et chez l'homme sont bien établis, et cette approche permet de contrôler les posologies administrées et d'arrêter le traitement en cas de survenue d'effet indésirable. Nous avons pour cette étude choisi de générer une immunoglobuline monoclonale de type G, plus adaptée aux immunothérapies directes de par une demi-vie longue et un fragment Fc assurant une endocytose neuronale et microgliale. Les analyses en immunofluorescence ont permis d'observer une endocytose neuronale spontanée des immunoglobulines administrées, tant in vitro que chez les souris traitées. Ces résultats soutiennent l'existence d'une internalisation neuronale des anticorps médiée par des récepteurs membranaires aux fragments Fc (Gros Louis et al., 2011, Congdon et al., 2013), et confortent le choix des IgG dans la mise au point des immunothérapies par injection directe dans la SLA.

L'endocytose de l'immunoglobuline E6 n'a pas été responsable d'une toxicité chez les cellules en culture ni chez les souris. En effet, une fois internalisé, l'anticorps restait localisé au sein du cytoplasme des neurones, ne pouvant ainsi interagir avec la fraction nucléaire physiologique de TDP-43. De plus, l'analyse en immunofluorescence du co-marquage TDP-43 / E6 chez les cellules N2A en culture a mis en évidence une interaction sélective de l'anticorps avec les agrégats pathologiques intracytoplasmiques de TDP-43 in vitro. Ces résultats, associés aux données obtenues par DotBlot et ELISA, démontrent une bonne spécificité de l'anticorps pour sa cible.

3.1.2. Stratégie d'administration

Plusieurs modalités d'administration de l'immunothérapie ont été testées dans cette étude. Bien que les anticorps injectés par abord systémique (injections intrapéritonéales et intranasales) aient pu être détectés au sein des vaisseaux du SNC des animaux traités, leur trop faible passage de la BHE (0.1%) et l'absence de rupture lésionnelle chez les souris transgéniques TDP-43^{A315T} n'a pas permis une diffusion suffisante du traitement à l'ensemble du parenchyme cérébral et médullaire. Toutefois, compte tenu des résultats positifs obtenus dans de précédents travaux portant sur des immunothérapies anti-SOD1 administrées par voie systémique (Dong et al., 2018 ; Maier et al., 2018), cette approche pourrait être envisagée sur des modèles animaux TDP-43 présentant une atteinte clinico-pathologique plus marquée responsable d'une rupture de la BHE.

Nous avons par la suite employé des techniques d'injection centrale pour administrer le traitement. La mise en place chirurgicale de minipompes osmotiques intra-cérébroventriculaires s'est révélée traumatisante et responsable d'une forte réaction inflammatoire réactionnelle empêchant toute analyse histologique. En revanche, l'administration par injections intrathécales répétées a permis une excellente diffusion du traitement à l'ensemble de la moelle épinière et au tronc cérébral tout en étant peu invasive et non vectrice de réaction inflammatoire locale. De plus, les anticorps une fois présents au sein du système nerveux central étaient naturellement captés par les deux types cellulaires cibles du traitement : les neurones et les cellules microgliales. A l'inverse, les analyses en immunofluorescence n'ont pas mis en évidence d'anticorps au sein du cytoplasme des astrocytes et des oligodendrocytes. Cette différence de biodisponibilité cellulaire peut être attribuée à l'expression par les premiers (neurones et microgliocytes) de récepteurs membranaires aux fragments Fc des immunoglobulines permettant leur endocytose, absents ou exprimés dans une moindre mesure chez les seconds (astrocytes et oligodendrocytes) (Fuller et al., 2014). L'administration par injections intrathécales n'a toutefois pas permis d'atteindre l'extrémité encéphalique du névraxe, limitant son action aux étages spinal et bulbaire.

3.1.3. Observations histopathologiques

Dans cette étude nous avons pu observer chez des souris transgéniques exprimant la mutation TDP-43^{A315T} traitées par immunothérapie une tendance à la diminution du taux de TDP-43 au niveau de la moelle épinière associée à une augmentation significative du rapport nucléocytoplasmique de TDP-43 au sein des motoneurones.

Ces résultats étaient accompagnés par une activation microgliale au niveau de la corne antérieure des souris traitées. Cette dernière pourrait être l'un des mécanismes d'élimination des inclusions de protéine TDP-43 présents au niveau de la matrice extra-cellulaire, mais également des agrégats intra-neuronaux. En effet les cellules microgliales activées « réparatrices » participent à la dégradation des agrégats protéiques intra- et extra-cellulaires présents dans le SNC dans le cadre des maladies neurodégénératives (Lee CY et al., 2010 ; Luo et al., 2015). Une récente étude utilisant un modèle murin rNLS8 dont la surexpression motoneuronale inductible de hTDP-43 aboutit à un phénotype clinico-histologique sévère mais réversible, a montré que l'élimination des inclusions motoneuronales de TDP-43 après arrêt de l'induction était précédée par une activation microgliale transitoire (Spiller et al., 2018). De plus, dans le cadre d'un traitement par immunothérapie, la dégradation des inclusions protéiques par les cellules microgliales semble être stimulée par la présence des anticorps ciblant ces agrégats, par internalisation des complexes immuns via les récepteurs membranaires aux fragments Fc (Luo et al., 2015). Cette hypothèse est renforcée par la détection dans notre travail d'anticorps E6 au sein des cellules microgliales en immunofluorescence.

Nous avons également pu constater dans notre étude une inhibition de la voie NFκB au sein des motoneurones des souris traitées par E6. L'anticorps bloquant l'interaction de P65 avec le domaine RRM1 de la protéine TDP-43, cette inhibition des voies de la neuroinflammation pourrait constituer un élément neuroprotecteur supplémentaire du traitement.

3.1.4. Performances cliniques

Si aucun effet secondaire n'est survenu durant le traitement, nous n'avons pas observé d'amélioration significative des performances motrices et cognitives des souris traitées par immunothérapie intrathécale, malgré les observations histopathologiques et contrairement aux résultats obtenus lors de notre précédente étude portant sur les scFv. Cette différence peut être expliquée par une durée de traitement plus courte et un âge moins avancé des souris. De plus, les modèles murins transgéniques surexprimant une mutation située sur l'extrémité C-terminale de TDP-43 présentent des phénotypes hétérogènes et majoritairement cognitifs, rendant difficile l'établissement de critères de jugement moteurs pour évaluer l'efficacité d'un traitement chez ces modèles (Arnold et al., 2013 ; White, et al., 2018). Ainsi, L'utilisation de souris transgéniques présentant un phénotype moteur plus marqué, tels que les récents modèles rNLS8 et double-transgénique UBQLN2^{P497H};TDP-43^{G348C} (Picher-Martel et al., 2019 ; Spiller et al., 2018) serait

particulièrement intéressante pour tester l'efficacité de notre traitement sur les symptômes déficitaires. Ce dernier modèle, en particulier, a été généré suite à l'observation in vitro d'une augmentation des agrégats TDP-43 intraneuronaux et de l'activation de la voie NFkB lors de la surexpression de la protéine UBQLN2 (sauvage ou mutée), conséquences d'une perturbation du système ubiquitine-protéasome (UPS) (Picher-Martel et al., 2015). La génération de souris transgéniques exprimant la protéine mutée UBQLN2^{P497H} sous contrôle du promoteur hNFH, puis le croisement de ces dernières avec des souris porteuses de la mutation TDP-43^{G348C} a permis l'obtention de souris double-transgéniques UBQLN2^{P497H};TDP-43^{G348C} dont le phénotype clinique et pathologique était exacerbé (Picher-Martel et al., 2019). La majoration de la perte motoneuronale et l'importance de la charge lésionnelle TDP-43 dès 5 mois pourrait permettre de mieux apprécier les effets d'une immunothérapie chez ces modèles. Toutefois, la configuration particulière d'une double pathogénicité, avec en particulier l'existence d'une altération du système UPS associée, doit être prise en compte dans l'interprétation des résultats et des conclusions portées lors de l'utilisation de ce modèle. Enfin, allonger la durée du traitement permettrait d'évaluer l'efficacité du traitement à plus long terme, et de s'assurer de l'absence de survenue d'effets indésirables tardifs.

3.2. Perspectives en recherche

Nous travaillons actuellement à compléter l'ensemble de ces résultats en utilisant des techniques d'analyse quantitatives par Western-Blot et Immunoprécipitation. Les concentrations d'IgG2A sont mesurées au sein de culots de cellules en cultures traitées et des prélèvements médullaires congelés des souris sacrifiées afin d'étudier la biodisponibilité du traitement. Nous étudions également dans ces échantillons les taux de protéine TDP-43, en distinguant les fractions solubles et insolubles, mais également nucléaires et cytoplasmiques. De même, l'analyse en Western Blot de l'expression des protéines GFAP, Iba1 et p65 permettra de mettre en perspective les résultats obtenus en immunofluorescence sur l'activation gliale et l'inhibition des voies de la neuroinflammation. Enfin l'étude de protéines dont l'expression est modulée par TDP-43 telles que FUS, NFL et POLDIP3, permettra d'évaluer l'impact de l'internalisation de E6 sur l'activité physiologique nucléaire de la protéine.

4. CONCLUSION ET OUVERTURE

Les résultats obtenus dans cette étude sont encourageants, montrant l'efficacité de l'adressage du traitement et une diminution de la charge lésionnelle chez les souris traitées. Plusieurs projets s'inscrivant dans la continuité de ce travail sont actuellement en développement au sein de l'unité de recherche du Pr Jean-Pierre Julien. Les modalités de vectorisation de l'anticorps E6 sont étudiées pour faciliter son passage de la BHE et permettre d'envisager une administration systémique du traitement. Un second projet porte sur l'injection d'ARNm codant pour des scFv ciblant le segment RRM1 de TDP-43. Enfin, une immunoglobuline E6 humanisée sera prochainement générée pour être testée sur modèle animal avant d'envisager son utilisation dans des protocoles d'études cliniques.

CONCLUSION

CONCLUSION GENERALE

Durant ces 3 années dédiées à la recherche en neurosciences sur la thématique de la SLA, nous avons cherché à contribuer à l'effort de recherche et tenté d'apporter des éléments de réponse aux enjeux actuels dans ce domaine en menant trois projets aux approches et objectifs distincts.

Nous avons tout d'abord travaillé à la mise au point d'une nouvelle technique de préparation et d'analyse de tissu par imagerie super-résolutive permettant l'étude d'échantillons cérébraux, médullaires et musculaires de patients atteints de maladies neurodégénératives à l'échelle nanométrique. Si cette approche a permis d'augmenter considérablement la résolution des images obtenues, pour des raisons administratives et chronologiques nous n'avons pas pu l'utiliser sur des prélèvements issus de patients atteints de SLA dans les délais impartis pour la finalisation de cette thèse.

Dans un second travail, nous nous sommes attachés à caractériser l'ultrastructure, le métabolisme et la réponse au stress de fibroblastes issus de patients atteints de SLA sporadique afin de tenter d'identifier de nouveaux marqueurs pathologiques de la maladie décelables du vivant des patients, et de préciser la place du fibroblaste en tant que modèle d'étude de la sSLA. Malgré l'absence d'altérations de l'ultrastructure cellulaire, nous avons pu identifier chez ces fibroblastes une altération de certaines voies métaboliques, ainsi qu'une augmentation de la synthèse du collagène.

Enfin, grâce à l'aimable invitation du Pr Jean-Pierre JULIEN, nous avons eu la chance de contribuer à la mise au point d'une immunothérapie par anticorps monoclonaux ciblant les agrégats de protéine TDP-43 niveau du système nerveux central. Si l'administration du traitement n'a pas permis d'amélioration clinique chez les souris testées, les résultats pathologiques, en particulier la diminution de la charge lésionnelle et de l'activation des voies de la neuroinflammation, sont encourageants.

PERSPECTIVES EN RECHERCHE

Sur la base des résultats obtenus mais également des limites rencontrées au cours des projets menés durant ces trois années de thèse, plusieurs pistes s'ouvrent pour les années à venir :

Un projet de deux ans financé à hauteur de 18.000€ par le CHU d'Angers débutera au mois de Novembre 2019 au sein de notre laboratoire Mitolab UMR CNRS 6015 INSERM 1083, avec pour objectif l'analyse en microscopie super-résolutive STORM de prélèvements cérébraux et médullaires de patients atteints de SLA sporadique et de sujets contrôles issus de la Biocollection du service de neuropathologie du CHU d'Angers. Un travail complémentaire portant sur des biopsies musculaires sera également effectué, afin de tenter d'identifier des anomalies ultrastructurelles au sein des myofibrilles des patients. Plusieurs partenariats ont été établis pour ce projet (Paris, Brest Limoges). Notre objectif est de tenter de caractériser la composition et l'architecture des lésions présentes au sein des neurones moteurs des patients afin de tenter d'identifier de nouveaux marqueurs pathologiques et de mieux comprendre les mécanismes de dégénérescence motoneuronale.

Un second projet débutera au sein de notre laboratoire dans le cadre d'un Master 2 à partir du mois de Janvier 2020, également financé par le CHU d'Angers, visant à étudier plus précisément la quantité et la structure des éléments de la matrice extracellulaire produits par les fibroblastes en culture issus de patients atteints de SLA. Des analyses complémentaires seront effectuées en parallèle sur des échantillons de moelle épinière de patients et de sujets contrôles de la biocollection du service de Neuropathologie du CHU d'Angers. Notre objectif est d'identifier un possible nouveau marqueur biologique de la maladie observable du vivant des patients, ainsi qu'une voie d'étude du métabolisme du collagène.

Un troisième projet initié sur la base de résultats complémentaires obtenus au cours de ces 3 ans (non présentés dans ce manuscrit), porte sur une possible nouvelle fonction de la protéine TDP-43. Ce projet d'un an, mené en partenariat avec plusieurs structures de recherche (Québec, Gif sur Yvette, et Lyon), pourra par la suite être poursuivi en fonction des premiers résultats obtenus.

Enfin, les travaux portant sur la mise au point d'une immunothérapie dans la SLA se poursuivent au sein de l'équipe de recherche Québécoise du Pr Jean-Pierre JULIEN, plusieurs cibles, vecteurs et modalités d'administrations sont actuellement à l'essai sur différents modèles cellulaires et animaux.

REFERENCES

REFERENCES

Abbe, E. "Beitrage zur Theorie des Mikroskops und der mikroskopischen Wahrmehmung". Archiv für Mikroskopische Anatomie. 1873. 9: 413–420.

Afroz T, Hock EM, Ernst P, Foglieni C, Jambeau M, Gilhespy LAB, Laferriere F, Maniecka Z, Plückthun A, Mittl P, Paganetti P, Allain FHT, Polymenidou M. Functional and dynamic polymerization of the ALS-linked protein TDP-43 antagonizes its pathologic aggregation. Nat Commun. 2017 Jun 29;8(1):45.

Al-Saif A, Al-Mohanna F, Bohlega S. A mutation in sigma-1 receptor causes juvenile amyotrophic lateral sclerosis. Ann Neurol. 2011 Dec;70(6):913-9.

Allen SP, Rajan S, Duffy L, Mortiboys H, Higginbottom A, Grierson AJ, Shaw PJ. Superoxide dismutase 1 mutation in a cellular model of amyotrophic lateral sclerosis shifts energy generation from oxidative phosphorylation to glycolysis. Neurobiol Aging. 2014 Jun;35(6):1499-509.

Allen SP, Duffy LM, Shaw PJ, Grierson AJ. Altered age-related changes in bioenergetic properties and mitochondrial morphology in fibroblastsfrom sporadic amyotrophic lateral sclerosis patients. Neurobiol Aging. 2015 Oct;36(10):2893-903.

Appel SH, Beers D, Siklos L, Engelhardt JI, Mosier DR. Calcium: the Darth Vader of ALS. Amyotroph Lateral Scler Other Motor Neuron Disord. 2001 Mar;2 Suppl 1:S47-54.

Arai T, Hasegawa M, Akiyama H, Ikeda K, Nonaka T, Mori H, Mann D, Tsuchiya K, Yoshida M, Hashizume Y, Oda T. TDP-43 is a component of ubiquitin-positive tau-negative inclusions in frontotemporal lobar degeneration and amyotrophic lateral sclerosis. Biochem Biophys Res Commun. 2006 Dec 22;351(3):602-11.

Arnold ES, Ling SC, Huelga SC, Lagier-Tourenne C, Polymenidou M, Ditsworth D, Kordasiewicz HB, McAlonis-Downes M, Platoshyn O, Parone PA, Da Cruz S, Clutario KM, Swing D, Tessarollo L, Marsala

M, Shaw CE, Yeo GW, Cleveland DW. ALS-linked TDP-43 mutations produce aberrant RNA splicing and adult-onset motor neuron disease without aggregation or loss of nuclear TDP-43. Proc Natl Acad Sci U S A. 2013 Feb 19;110(8):E736-45.

Auburger G, Klinkenberg M, Drost J, Marcus K, Morales-Gordo B, Kunz WS, Brandt U, Broccoli V, Reichmann H, Gispert S, Jendrach M. Primary skin fibroblasts as a model of Parkinson's disease. Mol Neurobiol. 2012 Aug;46(1):20-7.

Ayala YM, De Conti L, Avendaño-Vázquez SE, Dhir A, Romano M, D'Ambrogio A, Tollervey J, Ule J, Baralle M, Buratti E, Baralle FE. TDP-43 regulates its mRNA levels through a negative feedback loop. EMBO J. 2011 Jan 19;30(2):277-88.

Bannwarth S, Ait-El-Mkadem S, Chaussenot A, Genin EC, Lacas-Gervais S, Fragaki K, Berg-Alonso L, Kageyama Y, Serre V, Moore DG, Verschueren A, Rouzier C, Le Ber I, Augé G, Cochaud C, Lespinasse F, N'Guyen K, de Septenville A, Brice A, Yu-Wai-Man P, Sesaki H, Pouget J, Paquis-Flucklinger V. A mitochondrial origin for frontotemporal dementia and amyotrophic lateral sclerosis through CHCHD10 involvement. Brain. 2014 Aug;137(Pt 8):2329-45.

Bard F, Cannon C, Barbour R, Burke RL, Games D, Grajeda H, Guido T, Hu K, Huang J, Johnson-Wood K, Khan K, Kholodenko D, Lee M, Lieberburg I, Motter R, Nguyen M, Soriano F, Vasquez N, Weiss K, Welch B, Seubert P, Schenk D, Yednock T. Peripherally administered antibodies against amyloid beta-peptide enter the central nervous system and reduce pathology in a mouse model of Alzheimer disease. Nat Med. 2000 Aug;6(8):916-9.

Bartolome F, Wu HC, Burchell VS, Preza E, Wray S, Mahoney CJ, Fox NC, Calvo A, Canosa A, Moglia C, Mandrioli J, Chiò A, Orrell RW, Houlden H, Hardy J, Abramov AY, Plun-Favreau H. Pathogenic VCP mutations induce mitochondrial uncoupling and reduced ATP levels. Neuron. 2013 Apr 10;78(1):57-64.

Beach RL, Rao JS, Festoff BW, Reyes ET, Yanagihara R, Gajdusek DC. Collagenase activity in skin fibroblasts of patients with amyotrophic lateral sclerosis. J Neurol Sci. 1986 Jan;72(1):49-60.

Beal MF, Ferrante RJ, Browne SE, Matthews RT, Kowall NW, Brown RH Jr. Increased 3-nitrotyrosine in both sporadic and familial amyotrophic lateral sclerosis. Ann Neurol. 1997 Oct;42(4):644-54.

Benard G, Bellance N, James D, Parrone P, Fernandez H, Letellier T, Rossignol R. Mitochondrial bioenergetics and structural network organization. J Cell Sci. 2007 Mar 1;120(Pt 5):838-48.

Bensimon G, Lacomblez L, Meininger V. A controlled trial of riluzole in amyotrophic lateral sclerosis. ALS/Riluzole Study Group. N Engl J Med. 1994 Mar 3;330(9):585-91.

Bentmann E, Haass C, Dormann D. Stress granules in neurodegeneration--lessons learnt from TAR DNA binding protein of 43 kDa and fused in sarcoma. FEBS J. 2013 Sep;280(18):4348-70.

Borthwick GM, Johnson MA, Ince PG, Shaw PJ, Turnbull DM. Mitochondrial enzyme activity in amyotrophic lateral sclerosis: implications for the role of mitochondria in neuronal cell death. Ann Neurol. 1999 Nov;46(5):787-90.

Bosco DA, Morfini G, Karabacak NM, Song Y, Gros-Louis F, Pasinelli P, Goolsby H, Fontaine BA, Lemay N, McKenna-Yasek D, Frosch MP, Agar JN, Julien JP, Brady ST, Brown RH Jr. Wild-type and mutant SOD1 share an aberrant conformation and a common pathogenic pathway in ALS. Nat Neurosci. 2010 Nov;13(11):1396-403.

Boveris A, Chance B. The mitochondrial generation of hydrogen peroxide. General properties and effect of hyperbaric oxygen. Biochem J. 1973 Jul;134(3):707-16.

Bradley LJ, Taanman JW, Kallis C, Orrell RW. Increased sensitivity of myoblasts to oxidative stress in amyotrophic lateral sclerosis peripheral tissues. Exp Neurol. 2009 Jul;218(1):92-7

Burkhardt MF, Martinez FJ, Wright S, Ramos C, Volfson D, Mason M, Garnes J, Dang V, Lievers J, Shoukat-Mumtaz U, Martinez R, Gai H, Blake R, Vaisberg E, Grskovic M, Johnson C, Irion S, Bright J, Cooper B, Nguyen L, Griswold-Prenner I, Javaherian A. A cellular model for sporadic ALS using patient-derived induced pluripotent stem cells. Mol Cell Neurosci. 2013 Sep;56:355-64.

Buratti E, Baralle FE. Characterization and functional implications of the RNA binding properties of nuclear factor TDP-43, a novel splicing regulator of CFTR exon 9. J Biol Chem. 2001 Sep 28;276(39):36337-43.

Camu W, Tremblier B, Plassot C, Alphandery S, Salsac C, Pageot N, Juntas-Morales R, Scamps F, Daures JP, Raoul C. Vitamin D confers protection to motoneurons and is a prognostic factor of amyotrophic lateral sclerosis. Neurobiol Aging. 2014 May;35(5):1198-205.

Chang CK, Chiang MH, Toh EK, Chang CF, Huang TH. Molecular mechanism of oxidation-induced TDP-43 RRM1 aggregation and loss of function. FEBS Lett. 2013 Mar 18;587(6):575-82.

Chen JJ, Bertrand H, Yu BP. Inhibition of adenine nucleotide translocator by lipid peroxidation products. Free Radic Biol Med. 1995 Nov;19(5):583-90.

Chen YZ, Bennett CL, Huynh HM, Blair IP, Puls I, Irobi J, Dierick I, Abel A, Kennerson ML, Rabin BA, Nicholson GA, Auer-Grumbach M, Wagner K, De Jonghe P, Griffin JW, Fischbeck KH, Timmerman V, Cornblath DR, Chance PF. DNA/RNA helicase gene mutations in a form of juvenile amyotrophic lateral sclerosis (ALS4). Am J Hum Genet. 2004 Jun;74(6):1128-35.

Chiò A, Logroscino G, Hardiman O, Swingler R, Mitchell D, Beghi E, Traynor BG; Eurals Consortium. Prognostic factors in ALS: A critical review. Amyotroph Lateral Scler. 2009 Oct-Dec;10(5-6):310-23.

Chiò A, Logroscino G, Traynor BJ, Collins J, Simeone JC, Goldstein LA, White LA. Global epidemiology of amyotrophic lateral sclerosis: a systematic review of the publishedliterature. Neuroepidemiology. 2013;41(2):118-30.

Chow CY, Landers JE, Bergren SK, Sapp PC, Grant AE, Jones JM, Everett L, Lenk GM, McKenna-Yasek DM, Weisman LS, Figlewicz D, Brown RH, Meisler MH. Deleterious variants of FIG4, a phosphoinositide phosphatase, in patients with ALS. Am J Hum Genet. 2009 Jan;84(1):85-8.

Codron P, Cassereau J, Eyer J, Letournel F. Neuronal intermediate filaments in amyotrophic lateral sclerosis. In: Foyaca-Sibat H, ed. Update on amyotrophic lateral sclerosis. InTech; 2016.

Codron P, Chevrollier A, Kane MS, Echaniz-Laguna A, Latour P, Reynier P, Bonneau D, Verny C, Procaccio V, Lenaers G, Cassereau J. Increased mitochondrial fusion in a autosomal recessive CMT2A family with mitochondrial GTPase mitofusin 2 mutations. J Peripher Nerv Syst. 2016 Dec;21(4):365-369.

Codron P, Cassereau J, Vourc'h P, Veyrat-Durebex C, Blasco H, Kane S, Procaccio V, Letournel F, Verny C, Lenaers G, Reynier P, Chevrollier A. Primary fibroblasts derived from sporadic amyotrophic lateral sclerosis patients do not show ALS cytological lesions. Amyotroph Lateral Scler Frontotemporal Degener. 2018 Aug;19(5-6):446-456.

Congdon EE, Gu J, Sait HB, Sigurdsson EM. Antibody uptake into neurons occurs primarily via clathrin-dependent Fcγ receptor endocytosisand is a prerequisite for acute tau protein clearance. J Biol Chem. 2013 Dec 6;288(49):35452-65.

Corcia P, Blasco H, Camu W. Genetics of amyotrophic lateral sclerosis. Presse Med. 2014 May;43(5):555-62.

Da Cruz S, Bui A, Saberi S, Lee SK, Stauffer J, McAlonis-Downes M, Schulte D, Pizzo DP, Parone PA, Cleveland DW, Ravits J. Misfolded SOD1 is not a primary component of sporadic ALS. Acta Neuropathol. 2017 Jul;134(1):97-111.

Dani A, Huang B, Bergan J, Dulac C, Zhuang X. Superresolution imaging of chemical synapses in the brain. Neuron. 2010 Dec 9;68(5):843-56.

DeJesus-Hernandez M, Mackenzie IR, Boeve BF, Boxer AL, Baker M, Rutherford NJ, Nicholson AM, Finch NA, Flynn H, Adamson J, Kouri N, Wojtas A, Sengdy P, Hsiung GY, Karydas A, Seeley WW, Josephs KA, Coppola G, Geschwind DH, Wszolek ZK, Feldman H, Knopman DS, Petersen RC, Miller BL, Dickson DW, Boylan KB, Graff-Radford NR, Rademakers R. Expanded GGGGCC hexanucleotide repeat in noncoding region of C9ORF72 causes chromosome 9p-linked FTD and ALS. Neuron. 2011 Oct 20;72(2):245-56.

Deng HX, Chen W, Hong ST, Boycott KM, Gorrie GH, Siddique N, Yang Y, Fecto F, Shi Y, Zhai H, Jiang H, Hirano M, Rampersaud E, Jansen GH, Donkervoort S, Bigio EH, Brooks BR, Ajroud K, Sufit RL, Haines JL, Mugnaini E, Pericak-Vance MA, Siddique T. Mutations in UBQLN2 cause dominant X-linked juvenile and adult-onset ALS and ALS/dementia. Nature. 2011 Aug 21;477(7363):211-5.

Dong QX, Zhu J, Liu SY, Yu XL, Liu RT. An oligomer-specific antibody improved motor function and attenuated neuropathology in the SOD1-G93A transgenic mouse model of ALS. Int Immunopharmacol. 2018 Dec;65:413-421.

EFNS Task Force on Diagnosis and Management of Amyotrophic Lateral Sclerosis:, Andersen PM, Abrahams S, Borasio GD, de Carvalho M, Chio A, Van Damme P, Hardiman O, Kollewe K, Morrison KE, Petri S, Pradat PF, Silani V, Tomik B, Wasner M, Weber M. EFNS guidelines on the clinical management of amyotrophic lateral sclerosis (MALS)--revised report of an EFNS task force. Eur J Neurol. 2012 Mar;19(3):360-75.

Eggen BJ, Raj D, Hanisch UK, Boddeke HW. Microglial phenotype and adaptation. J Neuroimmune Pharmacol. 2013 Sep;8(4):807-23.

Elden AC, Kim HJ, Hart MP, Chen-Plotkin AS, Johnson BS, Fang X, Armakola M, Geser F, Greene R, Lu MM, Padmanabhan A, Clay-Falcone D, McCluskey L, Elman L, Juhr D, Gruber PJ, Rüb U, Auburger G, Trojanowski JQ, Lee VM, Van Deerlin VM, Bonini NM, Gitler AD. Ataxin-2 intermediate-length polyglutamine expansions are associated with increased risk for ALS. Nature. 2010 Aug 26;466(7310):1069-75.

Ellison D, Love S, Chimelli M, Harding B, Lowe J, Vinters H, Brandner S, Yong W. Neuropathology, A Reference Text of CNS Pathology, 3rd Edition. Kindle Edition, 2012; ISBN:9780702057687

Ezzi SA, Urushitani M, Julien JP. Wild-type superoxide dismutase acquires binding and toxic properties of ALS-linked mutant forms through oxidation. J Neurochem. 2007 Jul;102(1):170-8.

Fang YS, Tsai KJ, Chang YJ, Kao P, Woods R, Kuo PH, Wu CC, Liao JY, Chou SC, Lin V, Jin LW, Yuan HS, Cheng IH, Tu PH, Chen YR. Full-length TDP-43 forms toxic amyloid oligomers that are present in frontotemporal lobar dementia-TDP patients. Nat Commun. 2014 Sep 12;5:4824

Fang L, Huber-Abel F, Teuchert M, Hendrich C, Dorst J, Schattauer D, Zettlmeissel H, Wlaschek M, Scharffetter-Kochanek K, Tumani H, Ludolph AC, Brettschneider J. Linking neuron and skin: matrix metalloproteinases in amyotrophic lateral sclerosis (ALS). J Neurol Sci. 2009 Oct 15;285(1-2):62-6.

Fecto F, Yan J, Vemula SP, Liu E, Yang Y, Chen W, Zheng JG, Shi Y, Siddique N, Arrat H, Donkervoort S, Ajroud-Driss S, Sufit RL, Heller SL, Deng HX, Siddique T. SQSTM1 mutations in familial and sporadic amyotrophic lateral sclerosis. Arch Neurol. 2011 Nov;68(11):1440-6.

Feiler MS, Strobel B, Freischmidt A, Helferich AM, Kappel J, Brewer BM, Li D, Thal DR, Walther P, Ludolph AC, Danzer KM, Weishaupt JH. TDP-43 is intercellularly transmitted across axon terminals. J Cell Biol. 2015 Nov 23;211(4):897-911

Ferrante RJ, Browne SE, Shinobu LA, Bowling AC, Baik MJ, MacGarvey U, Kowall NW, Brown RH Jr, Beal MF. Evidence of increased oxidative damage in both sporadic and familial amyotrophic lateral sclerosis. J Neurochem. 1997 Nov;69(5):2064-74.

Forsberg K, Jonsson PA, Andersen PM, Bergemalm D, Graffmo KS, Hultdin M, Jacobsson J, Rosquist R, Marklund SL, Brännström T. Novel antibodies reveal inclusions containing non-native SOD1 in sporadic ALS patients. PLoS One. 2010 Jul 14;5(7):e11552.

Fridovich I. Superoxide anion radical (O2-.), superoxide dismutases, and related matters. J Biol Chem. 1997 Jul 25;272(30):18515-7.

Fujimori K, Ishikawa M, Otomo A, Atsuta N, Nakamura R, Akiyama T, Hadano S, Aoki M, Saya H, Sobue G, Okano H. Modeling sporadic ALS in iPSC-derived motor neurons identifies a potential therapeutic agent. Nat Med. 2018 Oct;24(10):1579-1589.

Fukazawa H, Tsukie T, Higashida K, Fujikura M, Ono S. An immunohistochemical study of increased tumor necrosis factor-α in the skin of patients with amyotrophic lateral sclerosis. J Clin Neurosci. 2013 Oct;20(10):1371-6.

Fuller JP, Stavenhagen JB, Teeling JL. New roles for Fc receptors in neurodegeneration - the impact on Immunotherapy for Alzheimer's Disease. Front Neurosci. 2014 Aug 21;8:235.

Fullmer, H. M., Gibson W. A., Lazarus G., Stam A.C., and Link C. Collagenolytic activity of the skin associated with neuromuscular diseases including amyotrophic lateral sclerosis. Lancet 1966, 1: 1007.

Furukawa Y, Kaneko K, Watanabe S, Yamanaka K, Nukina N. A seeding reaction recapitulates intracellular formation of Sarkosyl-insoluble transactivation response element (TAR) DNA-binding protein-43 inclusions. J Biol Chem. 2011 May 27;286(21):18664-72.

Gagliardi D, Meneri M, Saccomanno D, Bresolin N, Comi GP, Corti S. Diagnostic and Prognostic Role of Blood and Cerebrospinal Fluid and Blood Neurofilaments in Amyotrophic Lateral Sclerosis: A Review of the Literature. Int J Mol Sci. 2019 Aug 25;20(17).

Ghadge GD, Kay BK, Drigotas C, Roos RP. Single chain variable fragment antibodies directed against SOD1 ameliorate disease in mutant SOD1 transgenic mice. Neurobiol Dis. 2019 Jan;121:131-137.

Gilman S, Koller M, Black RS, Jenkins L, Griffith SG, Fox NC, Eisner L, Kirby L, Rovira MB, Forette F, Orgogozo JM; AN1792(QS-21)-201 Study Team. Clinical effects of Abeta immunization (AN1792) in patients with AD in an interrupted trial. Neurology. 2005 May 10;64(9):1553-62.

Gitcho MA, Baloh RH, Chakraverty S, Mayo K, Norton JB, Levitch D, Hatanpaa KJ, White CL 3rd, Bigio EH, Caselli R, Baker M, Al-Lozi MT, Morris JC, Pestronk A, Rademakers R, Goate AM, Cairns NJ. TDP-43 A315T mutation in familial motor neuron disease. Ann Neurol. 2008 Apr;63(4):535-8.

Gray F, Duyckaerts C, De Girolami U. Escourolle & Poirier's Manual of Basic Neuropathology, 3rd Edition. Oxford University Press; 2013; IBSN:9780199929054

Greenway MJ, Andersen PM, Russ C, Ennis S, Cashman S, Donaghy C, Patterson V, Swingler R, Kieran D, Prehn J, Morrison KE, Green A, Acharya KR, Brown RH Jr, Hardiman O. ANG mutations segregate with familial and 'sporadic' amyotrophic lateral sclerosis. Nat Genet. 2006 Apr;38(4):411-3.

Griparic L, van der Bliek AM. The many shapes of mitochondrial membranes. Traffic. 2001 Apr;2(4):235-44.

Gros-Louis F, Soucy G, Larivière R, Julien JP. Intracerebroventricular infusion of monoclonal antibody or its derived Fab fragment against misfolded forms of SOD1 mutant delays mortality in a mouse model of ALS. J Neurochem. 2010 Jun;113(5):1188-99.

Guo W, Chen Y, Zhou X, Kar A, Ray P, Chen X, Rao EJ, Yang M, Ye H, Zhu L, Liu J, Xu M, Yang Y, Wang C, Zhang D, Bigio EH, Mesulam M, Shen Y, Xu Q, Fushimi K, Wu JY. An ALS-associated mutation affecting TDP-43 enhances protein aggregation, fibril formationand neurotoxicity. Nat Struct Mol Biol. 2011 Jun 12;18(7):822-30.

Gurney ME, Pu H, Chiu AY, Dal Canto MC, Polchow CY, Alexander DD, Caliendo J, Hentati A, Kwon YW, Deng HX, et al. Motor neuron degeneration in mice that express a human Cu,Zn superoxide dismutasemutation. Science. 1994 Jun 17;264(5166):1772-5.

Hadano S, Hand CK, Osuga H, Yanagisawa Y, Otomo A, Devon RS, Miyamoto N, Showguchi-Miyata J, Okada Y, Singaraja R, Figlewicz DA, Kwiatkowski T, Hosler BA, Sagie T, Skaug J, Nasir J, Brown RH Jr, Scherer SW, Rouleau GA, Hayden MR, Ikeda JE. A gene encoding a putative GTPase regulator is mutated in familial amyotrophic lateralsclerosis 2. Nat Genet. 2001 Oct;29(2):166-73.

Hardiman O, Al-Chalabi A, Chio A, Corr EM, Logroscino G, Robberecht W, Shaw PJ, Simmons Z, van den Berg LH. Amyotrophic lateral sclerosis. Nat Rev Dis Primers. 2017 Oct 5;3:17071.

Hergesheimer RC, Chami AA, de Assis DR, Vourc'h P, Andres CR, Corcia P, Lanznaster D, Blasco H. The debated toxic role of aggregated TDP-43 in amyotrophic lateral sclerosis: a resolution in sight? Brain. 2019 May 1;142(5):1176-1194.

del Hoyo, P., García-Redondo, A., de Bustos, F., Molina, J.A., Sayed, Y., Alonso-Navarro, H., Caballero, L., Arenas, J., Jiménez-Jiménez, F.J., Oxidative stress in skin fibroblasts cultures of patients with Huntington's disease. Neurochem. Res. 2006. 31, 1103–1109.

Iguchi Y, Katsuno M, Takagi S, Ishigaki S, Niwa J, Hasegawa M, Tanaka F, Sobue G. Oxidative stress induced by glutathione depletion reproduces pathological modifications of TDP-43 linked to TDP-43 proteinopathies. Neurobiol Dis. 2012 Mar;45(3):862-70.

Iguchi Y, Katsuno M, Niwa J, Takagi S, Ishigaki S, Ikenaka K, Kawai K, Watanabe H, Yamanaka K, Takahashi R, Misawa H, Sasaki S, Tanaka F, Sobue G. Loss of TDP-43 causes age-dependent progressive motor neuron degeneration. Brain. 2013 May;136(Pt 5):1371-82.

Iguchi Y, Eid L, Parent M, Soucy G, Bareil C, Riku Y, Kawai K, Takagi S, Yoshida M, Katsuno M, Sobue G, Julien JP. Exosome secretion is a key pathway for clearance of pathological TDP-43. Brain. 2016 Dec;139(Pt 12):3187-3201

Ishikawa H, Yasui K, Oketa Y, Suzuki M, Ono S. Increased expression of valosin-containing protein in the skin of patients with amyotrophic lateral sclerosis. J Clin Neurosci. 2012 Apr;19(4):522-6.

Janmaat CJ, de Rooij KE, Locher H, de Groot SC, de Groot JC, Frijns JH, Huisman MA. Human Dermal Fibroblasts Demonstrate Positive Immunostaining for Neuron- and Glia- Specific Proteins. PLoS One. 2015 Dec 17;10(12):e0145235.

Jésus P, Fayemendy P, Nicol M, Lautrette G, Sourisseau H, Preux PM, Desport JC, Marin B, Couratier P. Hypermetabolism is a deleterious prognostic factor in patients with amyotrophic lateral sclerosis. Eur J Neurol. 2018 Jan;25(1):97-104.

Johnson JO, Mandrioli J, Benatar M, Abramzon Y, Van Deerlin VM, Trojanowski JQ, Gibbs JR, Brunetti M, Gronka S, Wuu J, Ding J, McCluskey L, Martinez-Lage M, Falcone D, Hernandez DG, Arepalli S, Chong S, Schymick JC, Rothstein J, Landi F, Wang YD, Calvo A, Mora G, Sabatelli M, Monsurrò MR, Battistini S, Salvi F, Spataro R, Sola P, Borghero G; ITALSGEN Consortium, Galassi G, Scholz SW, Taylor

JP, Restagno G, Chiò A, Traynor BJ. Exome sequencing reveals VCP mutations as a cause of familial ALS. Neuron. 2010 Dec 9;68(5):857-64.

Johnson JO, Pioro EP, Boehringer A, Chia R, Feit H, Renton AE, Pliner HA, Abramzon Y, Marangi G, Winborn BJ, Gibbs JR, Nalls MA, Morgan S, Shoai M, Hardy J, Pittman A, Orrell RW, Malaspina A, Sidle KC, Fratta P, Harms MB, Baloh RH, Pestronk A, Weihl CC, Rogaeva E, Zinman L, Drory VE, Borghero G, Mora G, Calvo A, Rothstein JD; ITALSGEN, Drepper C, Sendtner M, Singleton AB, Taylor JP, Cookson MR, Restagno G, Sabatelli M, Bowser R, Chiò A, Traynor BJ. Mutations in the Matrin 3 gene cause familial amyotrophic lateral sclerosis. Nat Neurosci. 2014 May;17(5):664-666.

Kabashi E, Valdmanis PN, Dion P, Spiegelman D, McConkey BJ, Vande Velde C, Bouchard JP, Lacomblez L, Pochigaeva K, Salachas F, Pradat PF, Camu W, Meininger V, Dupre N, Rouleau GA. TARDBP mutations in individuals with sporadic and familial amyotrophic lateral sclerosis. Nat Genet. 2008 May;40(5):572-4.

Karbowski M, Youle RJ. Dynamics of mitochondrial morphology in healthy cells and during apoptosis. Cell Death Differ. 2003 Aug;10(8):870-80.

Kerman A, Liu HN, Croul S, Bilbao J, Rogaeva E, Zinman L, Robertson J, Chakrabartty A. Amyotrophic lateral sclerosis is a non-amyloid disease in which extensive misfolding of SOD1 is unique to the familial form. Acta Neuropathol. 2010 Mar;119(3):335-44.

Khalil M, Teunissen CE, Otto M, Piehl F, Sormani MP, Gattringer T, Barro C, Kappos L, Comabella M, Fazekas F, Petzold A, Blennow K, Zetterberg H, Kuhle J. Neurofilaments as biomarkers in neurological disorders. Nat Rev Neurol. 2018 Oct;14(10):577-589.

Khan TK, Sen A, Hongpaisan J, Lim CS, Nelson TJ, Alkon DL. PKCε deficits in Alzheimer's disease brains and skin fibroblasts. J Alzheimers Dis. 2015;43(2):491-509.

Kiernan MC, Vucic S, Cheah BC, Turner MR, Eisen A, Hardiman O, Burrell JR, Zoing MC. Amyotrophic lateral sclerosis. Lancet. 2011 Mar 12;377(9769):942-55.

Kim SH, Shanware NP, Bowler MJ, Tibbetts RS. Amyotrophic lateral sclerosis-associated proteins TDP-43 and FUS/TLS function in a common biochemical complex to co-regulate HDAC6 mRNA. J Biol Chem. 2010 Oct 29;285(44):34097-105.

Kim HJ, Kim NC, Wang YD, Scarborough EA, Moore J, Diaz Z, MacLea KS, Freibaum B, Li S, Molliex A, Kanagaraj AP, Carter R, Boylan KB, Wojtas AM, Rademakers R, Pinkus JL, Greenberg SA, Trojanowski JQ, Traynor BJ, Smith BN, Topp S, Gkazi AS, Miller J, Shaw CE, Kottlors M, Kirschner J, Pestronk A, Li YR, Ford AF, Gitler AD, Benatar M, King OD, Kimonis VE, Ross ED, Weihl CC, Shorter J, Taylor JP. Mutations in prion-like domains in hnRNPA2B1 and hnRNPA1 cause multisystem proteinopathyand ALS. Nature. 2013 Mar 28;495(7442):467-73.

Kirk K, Gennings C, Hupf JC, Tadesse S, D'Aurelio M, Kawamata H, Valsecchi F, Mitsumoto H; ALS/PLS COSMOS Study Groups, Manfredi G. Bioenergetic markers in skin fibroblasts of sporadic amyotrophic lateral sclerosis and progressive lateral sclerosis patients. Ann Neurol. 2014 Oct;76(4):620-4.

Kolde G, Bachus R, Ludolph AC. Skin involvement in amyotrophic lateral sclerosis. Lancet. 1996 May 4;347(9010):1226-7.

Komatsu M, Ueno T, Waguri S, Uchiyama Y, Kominami E, Tanaka K. Constitutive autophagy: vital role in clearance of unfavorable proteins in neurons. Cell Death Differ. 2007 May;14(5):887-94.

Konrad C, Kawamata H, Bredvik KG, Arreguin AJ, Cajamarca SA, Hupf JC, Ravits JM, Miller TM, Maragakis NJ, Hales CM, Glass JD, Gross S, Mitsumoto H, Manfredi G. Fibroblast bioenergetics to classify amyotrophic lateral sclerosis patients. Mol Neurodegener. 2017 Oct 24;12(1):76.

Koopman WJ, Visch HJ, Verkaart S, van den Heuvel LW, Smeitink JA, Willems PH. Mitochondrial network complexity and pathological decrease in complex I activity are tightly correlated in isolated human complex I deficiency. Am J Physiol Cell Physiol. 2005 Oct;289(4):C881-90.

Kraemer BC, Schuck T, Wheeler JM, Robinson LC, Trojanowski JQ, Lee VM, Schellenberg GD. Loss of murine TDP-43 disrupts motor function and plays an essential role in embryogenesis. Acta Neuropathol. 2010 Apr;119(4):409-19.

Kuhle J, Lindberg RL, Regeniter A, Mehling M, Steck AJ, Kappos L, Czaplinski A. Increased levels of inflammatory chemokines in amyotrophic lateral sclerosis. Eur J Neurol. 2009 Jun;16(6):771-4.

Kwiatkowski TJ Jr, Bosco DA, Leclerc AL, Tamrazian E, Vanderburg CR, Russ C, Davis A, Gilchrist J, Kasarskis EJ, Munsat T, Valdmanis P, Rouleau GA, Hosler BA, Cortelli P, de Jong PJ, Yoshinaga Y, Haines JL, Pericak-Vance MA, Yan J, Ticozzi N, Siddique T, McKenna-Yasek D, Sapp PC, Horvitz HR, Landers JE, Brown RH Jr. Mutations in the FUS/TLS gene on chromosome 16 cause familial amyotrophic lateral sclerosis. Science. 2009 Feb 27;323(5918):1205-8.

Lacomblez L, Bensimon G, Leigh PN, Guillet P, Meininger V. Dose-ranging study of riluzole in amyotrophic lateral sclerosis. Amyotrophic Lateral Sclerosis/Riluzole Study Group II. Lancet. 1996 May 25;347(9013):1425-31.

Lee CY, Landreth GE. The role of microglia in amyloid clearance from the AD brain. J Neural Transm (Vienna). 2010 Aug;117(8):949-60.

Lee H, Lee S, Cho IH, Lee SJ. Toll-like receptors: sensor molecules for detecting damage to the nervous system. Curr Protein Pept Sci. 2013 Feb;14(1):33-42

Lee S, Lee TA, Song SJ, Park T, Park B. Hyperproduction of IL-6 caused by aberrant TDP-43 overexpression in high-fat diet-induced obese mice. FEBS Lett. 2015 Jul 8;589(15):1825-31.

Leigh PN, Meldrum BS. Excitotoxicity in ALS. Neurology. 1996 Dec;47(6 Suppl 4):S221-7.

Lim GP, Backstrom JR, Cullen MJ, Miller CA, Atkinson RD, Tokes ZA. Matrix metalloproteinases in the neocortex and spinal cord of amyotrophic lateral sclerosis patients. J Neurochem 1996;67(1):251–9.

Liu HN, Sanelli T, Horne P, Pioro EP, Strong MJ, Rogaeva E, Bilbao J, Zinman L, Robertson J. Lack of evidence of monomer/misfolded superoxide dismutase-1 in sporadic amyotrophic lateral sclerosis. Ann Neurol. 2009 Jul;66(1):75-80.

Liu HN, Tjostheim S, Dasilva K, Taylor D, Zhao B, Rakhit R, Brown M, Chakrabartty A, McLaurin J, Robertson J. Targeting of monomer/misfolded SOD1 as a therapeutic strategy for amyotrophic lateral sclerosis. J Neurosci. 2012 Jun 27;32(26):8791-9.

Luo W, Liu W, Hu X, Hanna M, Caravaca A, Paul SM. Microglial internalization and degradation of pathological tau is enhanced by an anti-taumonoclonal antibody. Sci Rep. 2015 Jun 9;5:11161.

Luty AA, Kwok JB, Dobson-Stone C, Loy CT, Coupland KG, Karlström H, Sobow T, Tchorzewska J, Maruszak A, Barcikowska M, Panegyres PK, Zekanowski C, Brooks WS, Williams KL, Blair IP, Mather KA, Sachdev PS, Halliday GM, Schofield PR. Sigma nonopioid intracellular receptor 1 mutations cause frontotemporal lobar degeneration-motor neuron disease. Ann Neurol. 2010 Nov;68(5):639-49.

Mackenzie IR, Bigio EH, Ince PG, Geser F, Neumann M, Cairns NJ, Kwong LK, Forman MS, Ravits J, Stewart H, Eisen A, McClusky L, Kretzschmar HA, Monoranu CM, Highley JR, Kirby J, Siddique T, Shaw PJ, Lee VM, Trojanowski JQ. Pathological TDP-43 distinguishes sporadic amyotrophic lateral sclerosis from amyotrophic lateral sclerosis with SOD1 mutations. Ann Neurol. 2007 May;61(5):427-34.

Mackenzie IR, Rademakers R, Neumann M. TDP-43 and FUS in amyotrophic lateral sclerosis and frontotemporal dementia. Lancet Neurol. 2010 Oct;9(10):995-1007

Maier M, Welt T, Wirth F, Montrasio F, Preisig D, McAfoose J, Vieira FG, Kulic L, Späni C, Stehle T, Perrin S, Weber M, Hock C, Nitsch RM, Grimm J. A human-derived antibody targets misfolded SOD1 and ameliorates motor symptoms in mouse models of amyotrophic lateral sclerosis. Sci Transl Med. 2018 Dec 5;10(470).

Marin B, Hamidou B, Couratier P, Nicol M, Delzor A, Raymondeau M, Druet-Cabanac M, Lautrette G, Boumediene F, Preux PM; French register of ALS in Limousin. Population-based epidemiology of amyotrophic lateral sclerosis (ALS) in an ageing Europe--the French register of ALS in Limousin (FRALim register). Eur J Neurol. 2014 Oct;21(10):1292-300

Maruyama H, Morino H, Ito H, Izumi Y, Kato H, Watanabe Y, Kinoshita Y, Kamada M, Nodera H, Suzuki H, Komure O, Matsuura S, Kobatake K, Morimoto N, Abe K, Suzuki N, Aoki M, Kawata A, Hirai T, Kato T, Ogasawara K, Hirano A, Takumi T, Kusaka H, Hagiwara K, Kaji R, Kawakami H. Mutations of optineurin in amyotrophic lateral sclerosis. Nature. 2010 May 13;465(7295):223-6.

Matsumoto G, Shimogori T, Hattori N, Nukina N. TBK1 controls autophagosomal engulfment of polyubiquitinated mitochondria through p62/SQSTM1 phosphorylation. Hum Mol Genet. 2015 Aug 1;24(15):4429-42.

Meyer K, Ferraiuolo L, Miranda CJ, Likhite S, McElroy S, Renusch S, Ditsworth D, Lagier-Tourenne C, Smith RA, Ravits J, Burghes AH, Shaw PJ, Cleveland DW, Kolb SJ, Kaspar BK. Direct conversion of patient fibroblasts demonstrates non-cell autonomous toxicity of astrocytes to motor neurons in familial and sporadic ALS. Proc Natl Acad Sci U S A. 2014 Jan 14;111(2):829-32.

Miller KE, Sheetz MP. Axonal mitochondrial transport and potential are correlated. J Cell Sci. 2004 Jun 1;117(Pt 13):2791-804.

Mitsumoto H, Brooks BR, Silani V. Clinical trials in amyotrophic lateral sclerosis: why so many negative trials and how can trials be improved? Lancet Neurol. 2014;13:1127–38.

Mocali A, Della Malva N, Abete C, Mitidieri Costanza VA, Bavazzano A, Boddi V, Sanchez L, Dessì S, Pani A, Paoletti F. Altered proteolysis in fibroblasts of Alzheimer patients with predictive implications for subjects at risk of disease. Int J Alzheimers Dis. 2014;2014:520152.

Morgan D, Diamond DM, Gottschall PE, Ugen KE, Dickey C, Hardy J, Duff K, Jantzen P, DiCarlo G, Wilcock D, Connor K, Hatcher J, Hope C, Gordon M, Arendash GW. A beta peptide vaccination prevents memory loss in an animal model of Alzheimer's disease. Nature. 2000 Dec 21-28;408(6815):982-5.

Munoz DG, Greene C, Perl DP, Selkoe DJ. Accumulation of phosphorylated neurofilaments in anterior horn motoneurons of amyotrophic lateral sclerosis patients. J Neuropathol Exp Neurol. 1988 Jan;47(1):9-18.

Neumann M, Sampathu DM, Kwong LK, Truax AC, Micsenyi MC, Chou TT, Bruce J, Schuck T, Grossman M, Clark CM, McCluskey LF, Miller BL, Masliah E, Mackenzie IR, Feldman H, Feiden W, Kretzschmar HA, Trojanowski JQ, Lee VM. Ubiquitinated TDP-43 in frontotemporal lobar degeneration and amyotrophic lateral sclerosis. Science. 2006 Oct 6;314(5796):130-3.

Nicoll JA, Wilkinson D, Holmes C, Steart P, Markham H, Weller RO. Neuropathology of human Alzheimer disease after immunization with amyloid-beta peptide: a case report. Nat Med. 2003 Apr;9(4):448-52

Nishimura AL, Mitne-Neto M, Silva HC, Richieri-Costa A, Middleton S, Cascio D, Kok F, Oliveira JR, Gillingwater T, Webb J, Skehel P, Zatz M. A mutation in the vesicle-trafficking protein VAPB causes late-onset spinal muscular atrophy and amyotrophic lateral sclerosis. Am J Hum Genet. 2004 Nov;75(5):822-31.

Nonaka T, Masuda-Suzukake M, Arai T, Hasegawa Y, Akatsu H, Obi T, Yoshida M, Murayama S, Mann DM, Akiyama H, Hasegawa M. Prion-like properties of pathological TDP-43 aggregates from diseased brains. Cell Rep. 2013 Jul 11;4(1):124-34.

Onesto E, Colombrita C, Gumina V, Borghi MO, Dusi S, Doretti A, Fagiolari G, Invernizzi F, Moggio M, Tiranti V, Silani V, Ratti A. Gene-specific mitochondria dysfunctions in human TARDBP and C9ORF72 fibroblasts. Acta Neuropathol Commun. 2016 May 5;4(1):47.

Ono S, Toyokura Y, Mannen T, Ishibashi Y. Increased dermal collagen density in amyotrophic lateral sclerosis. J Neurol Sci. 1988 Jan;83(1):81-92.

Ono S, Imai T, Munakata S, Takahashi K, Kanda F, Hashimoto K, Yamano T, Shimizu N, Nagao K, Yamauchi M. Collagen abnormalities in the spinal cord from patients with amyotrophic lateral sclerosis. J Neurol Sci. 1998 Oct 8;160(2):140-7.

Ono S, Hu J, Shimizu N, Imai T, Nakagawa H. Increased interleukin-6 of skin and serum in amyotrophic lateral sclerosis. J Neurol Sci. 2001 Jun 15;187(1-2):27-34.

Orgogozo JM, Gilman S, Dartigues JF, Laurent B, Puel M, Kirby LC, Jouanny P, Dubois B, Eisner L, Flitman S, Michel BF, Boada M, Frank A, Hock C. Subacute meningoencephalitis in a subset of patients with AD after Abeta42 immunization. Neurology. 2003 Jul 8;61(1):46-54

Orrù S, Coni P, Floris A, Littera R, Carcassi C, Sogos V, Brancia C. Reduced stress granule formation and cell death in fibroblasts with the A382T mutation of TARDBP gene: evidence for loss of TDP-43 nuclear function. Hum Mol Genet. 2016 Oct 15;25(20):4473-4483.

Paré B, Lehmann M, Beaudin M, Nordström U, Saikali S, Julien JP, Gilthorpe JD, Marklund SL, Cashman NR, Andersen PM, Forsberg K, Dupré N, Gould P, Brännström T, Gros-Louis F. Misfolded SOD1 pathology in sporadic Amyotrophic Lateral Sclerosis. Sci Rep. 2018 Sep 21;8(1):14223.

Paré B, Touzel-Deschênes L, Lamontagne R, Lamarre MS, Scott FD, Khuong HT, Dion PA, Bouchard JP, Gould P, Rouleau GA, Dupré N, Berthod F, Gros-Louis F. Early detection of structural abnormalities and cytoplasmic accumulation of TDP-43 in tissue-engineered skins derived from ALS patients. Acta Neuropathol Commun. 2015 Jan 31;3:5.

Parkinson N, Ince PG, Smith MO, Highley R, Skibinski G, Andersen PM, Morrison KE, Pall HS, Hardiman O, Collinge J, Shaw PJ, Fisher EM; MRC Proteomics in ALS Study; FReJA Consortium. ALS phenotypes with mutations in CHMP2B (charged multivesicular body protein 2B). Neurology. 2006 Sep 26;67(6):1074-7.

Patel P, Kriz J, Gravel M, Soucy G, Bareil C, Gravel C, Julien JP. Adeno-associated virus-mediated delivery of a recombinant single-chain antibody against misfolded superoxide dismutase for treatment of amyotrophic lateral sclerosis. Mol Ther. 2014 Mar;22(3):498-510.

Phukan J, Elamin M, Bede P, Jordan N, Gallagher L, Byrne S, Lynch C, Pender N, Hardiman O.The syndrome of cognitive impairment in amyotrophic lateral sclerosis: a population-based study. J Neurol Neurosurg Psychiatry. 2012 Jan;83(1):102-8.

Pich S, Bach D, Briones P, Liesa M, Camps M, Testar X, Palacín M, Zorzano A. The Charcot-Marie-Tooth type 2A gene product, Mfn2, up-regulates fuel oxidation through expression of OXPHOS system. Hum Mol Genet. 2005 Jun 1;14(11):1405-15.

Picher-Martel V, Dutta K, Phaneuf D, Sobue G, Julien JP. Ubiquilin-2 drives NF-κB activity and cytosolic TDP-43 aggregation in neuronal cells. Mol Brain. 2015 Oct 31;8(1):71.

Picher-Martel V, Renaud L, Bareil C, Julien JP. Neuronal Expression of UBQLN2P497H Exacerbates TDP-43 Pathology in TDP-43G348C Mice through Interaction with Ubiquitin. Mol Neurobiol. 2019 Jul;56(7):4680-4696.

Poduslo JF, Curran GL, Berg CT. Macromolecular permeability across the blood-nerve and blood-brain barriers. Proc Natl Acad Sci U S A. 1994 Jun 7;91(12):5705-9.

Polymenidou M, Lagier-Tourenne C, Hutt KR, Huelga SC, Moran J, Liang TY, Ling SC, Sun E, Wancewicz E, Mazur C, Kordasiewicz H, Sedaghat Y, Donohue JP, Shiue L, Bennett CF, Yeo GW, Cleveland DW. Long pre-mRNA depletion and RNA missplicing contribute to neuronal vulnerability from loss of TDP-43. Nat Neurosci. 2011 Apr;14(4):459-68.

Pozzi S, Thammisetty SS, Codron P, Rahimian R, Plourde KV, Soucy G, Bareil C, Phaneuf D, Kriz J, Gravel C, Julien JP. Virus-mediated delivery of antibody targeting TAR DNA-binding protein-43 mitigates associated neuropathology. J Clin Invest. 2019 Feb 25;129(4):1581-1595.

Radunović A, Mitsumoto H, Leigh PN. Clinical care of patients with amyotrophic lateral sclerosis. Lancet Neurol. 2007 Oct;6(10):913-25.

Rakhit R, Crow JP, Lepock JR, Kondejewski LH, Cashman NR, Chakrabartty A. Monomeric Cu,Zn-superoxide dismutase is a common misfolding intermediate in the oxidation models of sporadic and familial amyotrophic lateral sclerosis. J Biol Chem. 2004 Apr 9;279(15):15499-504.

Ratti A, Buratti E. Physiological functions and pathobiology of TDP-43 and FUS/TLS proteins. J Neurochem. 2016 Aug;138 Suppl 1:95-111.

Renaud J, Thérien HM, Plouffe M, Martinoli MG. Neuroinflammation: Dr Jekyll or Mr Hyde?. Med Sci (Paris). 2015 Nov;31(11):979-88.

Renaud L, Picher-Martel V, Codron P, Julien JP. Key role of UBQLN2 in pathogenesis of amyotrophic lateral sclerosis and frontotemporal dementia. Acta Neuropathol Commun. 2019 Jul 18;7(1):103.

Renton AE, Majounie E, Waite A, Simón-Sánchez J, Rollinson S, Gibbs JR, Schymick JC, Laaksovirta H, van Swieten JC, Myllykangas L, Kalimo H, Paetau A, Abramzon Y, Remes AM, Kaganovich A, Scholz SW, Duckworth J, Ding J, Harmer DW, Hernandez DG, Johnson JO, Mok K, Ryten M, Trabzuni D, Guerreiro RJ, Orrell RW, Neal J, Murray A, Pearson J, Jansen IE, Sondervan D, Seelaar H, Blake D, Young K, Halliwell N, Callister JB, Toulson G, Richardson A, Gerhard A, Snowden J, Mann D, Neary D, Nalls MA, Peuralinna T, Jansson L, Isoviita VM, Kaivorinne AL, Hölttä-Vuori M, Ikonen E, Sulkava R, Benatar M, Wuu J, Chiò A, Restagno G, Borghero G, Sabatelli M; ITALSGEN Consortium, Heckerman D, Rogaeva E, Zinman L, Rothstein JD, Sendtner M, Drepper C, Eichler EE, Alkan C, Abdullaev Z, Pack SD, Dutra A, Pak E, Hardy J, Singleton A, Williams NM, Heutink P, Pickering-Brown S, Morris HR, Tienari PJ, Traynor BJ. A hexanucleotide repeat expansion in C9ORF72 is the cause of chromosome 9p21-linked ALS-FTD. Neuron. 2011 Oct 20;72(2):257-68.

Rodríguez GE, González DM, Monachelli GM, Costa JJ, Nicola AF, Sica RE. Morphological abnormalities in mitochondria of the skin of patients with sporadic amyotrophic lateral sclerosis. Arq Neuropsiquiatr. 2012 Jan;70(1):40-4.

Rosen DR, Siddique T, Patterson D, Figlewicz DA, Sapp P, Hentati A, Donaldson D, Goto J, O'Regan JP, Deng HX, et al. Mutations in Cu/Zn superoxide dismutase gene are associated with familial amyotrophic lateral sclerosis. Nature. 1993 Mar 4;362(6415):59-62

Rosenmann H, Grigoriadis N, Karussis D, Boimel M, Touloumi O, Ovadia H, Abramsky O. Tauopathy-like abnormalities and neurologic deficits in mice immunized with neuronal tau protein. Arch Neurol. 2006 Oct;63(10):1459-67.

Rotunno MS, Bosco DA. An emerging role for misfolded wild-type SOD1 in sporadic ALS pathogenesis. Front Cell Neurosci. 2013 Dec 16;7:253

Sabatelli M, Zollino M, Conte A, Del Grande A, Marangi G, Lucchini M, Mirabella M, Romano A, Piacentini R, Bisogni G, Lattante S, Luigetti M, Rossini PM, Moncada A. Primary fibroblasts cultures reveal TDP-43 abnormalities in amyotrophic lateral sclerosis patients with and without SOD1 mutations. Neurobiol Aging. 2015 May;36(5):2005.e5-2005.e13.

Sábado J, Casanovas A, Rodrigo H, Arqué G, Esquerda JE. Adverse effects of a SOD1-peptide immunotherapy on SOD1 G93A mouse slow model of amyotrophic lateral sclerosis. Neuroscience. 2015 Dec 3;310:38-50.

Sala G, Trombin F, Mattavelli L, Beretta S, Tremolizzo L, Andreoni S, Calabrese E, Sanvito L, Ferrarese C. Lack of evidence for oxidative stress in sporadic amyotrophic lateral sclerosis fibroblasts. Neurodegener Dis. 2009;6(1-2):9-15.

Sama RR, Ward CL, Bosco DA. Functions of FUS/TLS from DNA repair to stress response: implications for ALS. ASN Neuro. 2014 Jun 1;6(4).

Sasaki S, Iwata M. Mitochondrial alterations in the spinal cord of patients with sporadic amyotrophic lateral sclerosis. J Neuropathol Exp Neurol. 2007;66:10–6.

Schenk D, Barbour R, Dunn W, Gordon G, Grajeda H, Guido T, Hu K, Huang J, Johnson-Wood K, Khan K, Kholodenko D, Lee M, Liao Z, Lieberburg I, Motter R, Mutter L, Soriano F, Shopp G, Vasquez N, Vandevert C, Walker S, Wogulis M, Yednock T, Games D, Seubert P. Immunization with amyloid-beta attenuates Alzheimer-disease-like pathology in the PDAPP mouse. Nature. 1999 Jul 8;400(6740):173-7.

Schermelleh L, Ferrand A, Huser T, Eggeling C, Sauer M, Biehlmaier O, Drummen GPC. Super-resolution microscopy demystified. Nat Cell Biol. 2019 Jan;21(1):72-84.

Schwartz JC, Podell ER, Han SS, Berry JD, Eggan KC, Cech TR. FUS is sequestered in nuclear aggregates in ALS patient fibroblasts. Mol Biol Cell. 2014 Sep 1;25(17):2571-8.

Scotter EL, Vance C, Nishimura AL, Lee YB, Chen HJ, Urwin H, Sardone V, Mitchell JC, Rogelj B, Rubinsztein DC, Shaw CE. Differential roles of the ubiquitin proteasome system and autophagy in the clearance of solubleand aggregated TDP-43 species. J Cell Sci. 2014 Mar 15;127(Pt 6):1263-78.

Shiina Y, Arima K, Tabunoki H, Satoh J. TDP-43 dimerizes in human cells in culture. Cell Mol Neurobiol. 2010 May;30(4):641-52.

Shodai A, Morimura T, Ido A, Uchida T, Ayaki T, Takahashi R, Kitazawa S, Suzuki S, Shirouzu M, Kigawa T, Muto Y, Yokoyama S, Takahashi R, Kitahara R, Ito H, Fujiwara N, Urushitani M. Aberrant assembly of RNA recognition motif 1 links to pathogenic conversion of TAR DNA-binding protein of 43 kDa (TDP-43). J Biol Chem. 2013 May 24;288(21):14886-905.

Siddique T, Figlewicz DA, Pericak-Vance MA, Haines JL, Rouleau G, Jeffers AJ, Sapp P, Hung WY, Bebout J, McKenna-Yasek D, et al. Linkage of a gene causing familial amyotrophic lateral sclerosis to chromosome 21 and evidence of genetic-locus heterogeneity. N Engl J Med. 1991 May 16;324(20):1381-4.

Sigal YM, Zhou R, Zhuang X. Visualizing and discovering cellular structures with super-resolution microscopy. Science. 2018 Aug 31;361(6405):880-887.

Siklos L, Engelhardt J, Harati Y, et al. Ultrastructural evidence for altered calcium in motor nerve terminals in amyotropic lateral sclerosis. Ann Neurol, 1996;39 (2): 203-16.

Spiller KJ, Restrepo CR, Khan T, Dominique MA, Fang TC, Canter RG, Roberts CJ, Miller KR, Ransohoff RM, Trojanowski JQ, Lee VM. Microglia-mediated recovery from ALS-relevant motor neuron degeneration in a mouse model of TDP-43 proteinopathy. Nat Neurosci. 2018 Mar;21(3):329-340.

Sreedharan J, Blair IP, Tripathi VB, Hu X, Vance C, Rogelj B, Ackerley S, Durnall JC, Williams KL, Buratti E, Baralle F, de Belleroche J, Mitchell JD, Leigh PN, Al-Chalabi A, Miller CC, Nicholson G, Shaw CE. TDP-43 mutations in familial and sporadic amyotrophic lateral sclerosis. Science. 2008 Mar 21;319(5870):1668-72.

Steyn FJ, Ioannides ZA, van Eijk RPA, Heggie S, Thorpe KA, Ceslis A, Heshmat S, Henders AK, Wray NR, van den Berg LH, Henderson RD, McCombe PA, Ngo ST. Hypermetabolism in ALS is associated with greater functional decline and shorter survival. J Neurol Neurosurg Psychiatry. 2018 Oct;89(10):1016-1023.

Stoica R, De Vos KJ, Paillusson S, Mueller S, Sancho RM, Lau KF, Vizcay-Barrena G, Lin WL, Xu YF, Lewis J, Dickson DW, Petrucelli L, Mitchell JC, Shaw CE, Miller CC. ER-mitochondria associations are regulated by the VAPB-PTPIP51 interaction and are disrupted by ALS/FTD-associated TDP-43. Nat Commun. 2014 Jun 3;5:3996.

Strong MJ, Volkening K, Hammond R, Yang W, Strong W, Leystra-Lantz C, Shoesmith C. TDP-43 is a human low molecular weight neurofilament (hNFL) mRNA-binding protein. Mol Cell Neurosci. 2007 Jun;35(2):320-7.

Sun X, Song J, Huang H, Chen H, Qian K. Modeling hallmark pathology using motor neurons derived from the family and sporadic amyotrophic lateral sclerosis patient-specific iPS cells. Stem Cell Res Ther. 2018 Nov 15;9(1):315.

Suzuki M, Watanabe T, Mikami H, Nomura M, Yamazaki T, Irie T, Ishikawa H, Yasui K, Ono S. Immunohistochemical studies of vascular endothelial growth factor in skin of patients with amyotrophic lateral sclerosis. J Neurol Sci. 2009 Oct 15;285(1-2):125-9.

Suzuki M, Mikami H, Watanabe T, Yamano T, Yamazaki T, Nomura M, Yasui K, Ishikawa H, Ono S. Increased expression of TDP-43 in the skin of amyotrophic lateral sclerosis. Acta Neurol Scand. 2010 Nov;122(5):367-72.

Swarup V, Phaneuf D, Bareil C, Robertson J, Rouleau GA, Kriz J, Julien JP. Pathological hallmarks of amyotrophic lateral sclerosis/frontotemporal lobar degeneration in transgenic mice produced with TDP-43 genomic fragments. Brain. 2011 Sep;134(Pt 9):2610-26.

Swarup V, Phaneuf D, Dupré N, Petri S, Strong M, Kriz J, Julien JP. Deregulation of TDP-43 in amyotrophic lateral sclerosis triggers nuclear factor κB-mediated pathogenic pathways. J Exp Med. 2011 Nov 21;208(12):2429-47.

Swinnen B, Robberecht W. The phenotypic variability of amyotrophic lateral sclerosis. Nat Rev Neurol. 2014 Nov;10(11):661-70.

Tanaka K, Matsuda N. Proteostasis and neurodegeneration: the roles of proteasomal degradation and autophagy. Biochim Biophys Acta. 2014 Jan;1843(1):197-204.

Takahashi Y, Fukuda Y, Yoshimura J, Toyoda A, Kurppa K, Moritoyo H, Belzil VV, Dion PA, Higasa K, Doi K, Ishiura H, Mitsui J, Date H, Ahsan B, Matsukawa T, Ichikawa Y, Moritoyo T, Ikoma M, Hashimoto T, Kimura F, Murayama S, Onodera O, Nishizawa M, Yoshida M, Atsuta N, Sobue G; JaCALS, Fifita JA, Williams KL, Blair IP, Nicholson GA, Gonzalez-Perez P, Brown RH Jr, Nomoto M, Elenius K, Rouleau GA, Fujiyama A, Morishita S, Goto J, Tsuji S. ERBB4 mutations that disrupt the neuregulin-ErbB4 pathway cause amyotrophic lateralsclerosis type 19. Am J Hum Genet. 2013 Nov 7;93(5):900-5

Takeuchi S, Fujiwara N, Ido A, Oono M, Takeuchi Y, Tateno M, Suzuki K, Takahashi R, Tooyama I, Taniguchi N, Julien JP, Urushitani M. Induction of protective immunity by vaccination with wild-type apo superoxide dismutase 1 in mutant SOD1 transgenic mice. J Neuropathol Exp Neurol. 2010 Oct;69(10):1044-56.

Tang D, Kang R, Coyne CB, Zeh HJ, Lotze MT. PAMPs and DAMPs: signal 0s that spur autophagy and immunity. Immunol Rev. 2012 Sep;249(1):158-75.

Thouvenot E, Demattei C, Lehmann S, Maceski-Maleska A, Hirtz C, Juntas-Morales R, Pageot N, Esselin F, Alphandéry S, Vincent T, Camu W. Serum neurofilament light chain at time of diagnosis is an independent prognostic factor of survival in amyotrophic lateral sclerosis. Eur J Neurol. 2019 Aug 22.

Tollervey JR, Curk T, Rogelj B, Briese M, Cereda M, Kayikci M, König J, Hortobágyi T, Nishimura AL, Zupunski V, Patani R, Chandran S, Rot G, Zupan B, Shaw CE, Ule J. Characterizing the RNA targets and position-dependent splicing regulation by TDP-43. Nat Neurosci. 2011 Apr;14(4):452-8.

Troost D, Sillevis Smitt PA, de Jong JM, Swaab DF. Neurofilament and glial alterations in the cerebral cortex in amyotrophic lateral sclerosis. Acta Neuropathol. 1992;84(6):664-73.

Tyzack GE, Luisier R, Taha DM, Neeves J, Modic M, Mitchell JS, Meyer I, Greensmith L, Newcombe J, Ule J, Luscombe NM, Patani R. Widespread FUS mislocalization is a molecular hallmark of amyotrophic lateral sclerosis. Brain. 2019 Sep 1;142(9):2572-2580.

Urushitani M, Ezzi SA, Julien JP. Therapeutic effects of immunization with mutant superoxide dismutase in mice models of amyotrophic lateral sclerosis. Proc Natl Acad Sci U S A. 2007 Feb 13;104(7):2495-500.

Vance C, Rogelj B, Hortobágyi T, De Vos KJ, Nishimura AL, Sreedharan J, Hu X, Smith B, Ruddy D, Wright P, Ganesalingam J, Williams KL, Tripathi V, Al-Saraj S, Al-Chalabi A, Leigh PN, Blair IP, Nicholson G, de Belleroche J, Gallo JM, Miller CC, Shaw CE. Mutations in FUS, an RNA processing protein, cause familial amyotrophic lateral sclerosis type6. Science. 2009 Feb 27;323(5918):1208-1211.

Veyrat-Durebex C, Bris C, Codron P, Bocca C, Chupin S, Corcia P, Vourc'h P, Hergesheimer R, Cassereau J, Funalot B, Andres CR, Lenaers G, Couratier P, Reynier P, Blasco H. Metabo-lipidomics of Fibroblasts and Mitochondrial-Endoplasmic Reticulum Extracts from ALS Patients Shows Alterations in Purine, Pyrimidine, Energetic, and Phospholipid Metabolisms. Mol Neurobiol. 2019 Aug;56(8):5780-5791.

Wang MD, Little J, Gomes J, Cashman NR, Krewski D. Identification of risk factors associated with onset and progression of amyotrophic lateral sclerosis using systematic review and meta-analysis. Neurotoxicology. 2017 Jul;61:101-130.

Wang W, Li L, Lin WL, Dickson DW, Petrucelli L, Zhang T, Wang X. The ALS disease-associated mutant TDP-43 impairs mitochondrial dynamics and function in motor neurons. Hum Mol Genet. 2013 Dec 1;22(23):4706-19.

Wang W, Wang L, Lu J, Siedlak SL, Fujioka H, Liang J, Jiang S, Ma X, Jiang Z, da Rocha EL, Sheng M, Choi H, Lerou PH, Li H, Wang X. The inhibition of TDP-43 mitochondrial localization blocks its neuronal toxicity. Nat Med. 2016 Aug;22(8):869-78.

Watanabe T, Okeda Y, Yamano T, Ono S. An immunohistochemical study of ubiquitin in the skin of sporadic amyotrophic lateral sclerosis. J Neurol Sci. 2010 Nov 15;298(1-2):52-6.

Weidberg H, Elazar Z. TBK1 mediates crosstalk between the innate immune response and autophagy. Sci Signal. 2011 Aug 9;4(187):pe39.

White MA, Kim E, Duffy A, Adalbert R, Phillips BU, Peters OM, Stephenson J, Yang S, Massenzio F, Lin Z, Andrews S, Segonds-Pichon A, Metterville J, Saksida LM, Mead R, Ribchester RR, Barhomi Y, Serre T, Coleman MP, Fallon JR, Bussey TJ, Brown RH Jr, Sreedharan J. TDP-43 gains function due to perturbed autoregulation in a Tardbp knock-in mouse model of ALS-FTD. Nat Neurosci. 2018 Apr;21(4):552-563.

Wiedemann FR, Manfredi G, Mawrin C, Beal MF, Schon EA. Mitochondrial DNA and respiratory chain function in spinal cords of ALS patients. J Neurochem. 2002 Feb;80(4):616-25.

Writing Group; Edaravone (MCI-186) ALS 19 Study Group. Safety and efficacy of edaravone in well defined patients with amyotrophic lateral sclerosis: a randomised, double-blind, placebo-controlled trial. Lancet Neurol. 2017 Jul;16(7):505-512.

Wu CH, Fallini C, Ticozzi N, Keagle PJ, Sapp PC, Piotrowska K, Lowe P, Koppers M, McKenna-Yasek D, Baron DM, Kost JE, Gonzalez-Perez P, Fox AD, Adams J, Taroni F, Tiloca C, Leclerc AL, Chafe SC, Mangroo D, Moore MJ, Zitzewitz JA, Xu ZS, van den Berg LH, Glass JD, Siciliano G, Cirulli ET, Goldstein DB, Salachas F, Meininger V, Rossoll W, Ratti A, Gellera C, Bosco DA, Bassell GJ, Silani V, Drory VE, Brown RH Jr, Landers JE. Mutations in the profilin 1 gene cause familial amyotrophic lateral sclerosis. Nature. 2012 Aug 23;488(7412):499-503.

Wu LS, Cheng WC, Shen CK. Targeted depletion of TDP-43 expression in the spinal cord motor neurons leads to the development of amyotrophic lateral sclerosis-like phenotypes in mice. J Biol Chem. 2012 Aug 10;287(33):27335-44

Xiao S, Sanelli T, Dib S, Sheps D, Findlater J, Bilbao J, Keith J, Zinman L, Rogaeva E, Robertson J. RNA targets of TDP-43 identified by UV-CLIP are deregulated in ALS. Mol Cell Neurosci. 2011 Jul;47(3):167-80.

Xu K, Zhong G, Zhuang X. Actin, spectrin, and associated proteins form a periodic cytoskeletal structure in axons. Science. 2013 Jan 25;339(6118):452-6.

Yang C, Wang H, Qiao T, Yang B, Aliaga L, Qiu L, Tan W, Salameh J, McKenna-Yasek DM, Smith T, Peng L, Moore MJ, Brown RH Jr, Cai H, Xu Z. Partial loss of TDP-43 function causes phenotypes of amyotrophic lateral sclerosis. Proc Natl Acad Sci U S A. 2014 Mar 25;111(12):E1121-9.

Yang S, Zhang KY, Kariawasam R, Bax M, Fifita JA, Ooi L, Yerbury JJ, Nicholson GA, Blair IP. Evaluation of Skin Fibroblasts from Amyotrophic Lateral Sclerosis Patients for the Rapid Study of Pathological Features. Neurotox Res. 2015 Aug;28(2):138-46.

Yang Y, Hentati A, Deng HX, Dabbagh O, Sasaki T, Hirano M, Hung WY, Ouahchi K, Yan J, Azim AC, Cole N, Gascon G, Yagmour A, Ben-Hamida M, Pericak-Vance M, Hentati F, Siddique T. The gene encoding alsin, a protein with three guanine-nucleotide exchange factor domains, is mutated in a form of recessive amyotrophic lateral sclerosis. Nat Genet. 2001 Oct;29(2):160-5.

Yu Y, Chi B, Xia W, Gangopadhyay J, Yamazaki T, Winkelbauer-Hurt ME, Yin S, Eliasse Y, Adams E, Shaw CE, Reed R. U1 snRNP is mislocalized in ALS patient fibroblasts bearing NLS mutations in FUS and is required for motor neuron outgrowth in zebrafish. Nucleic Acids Res. 2015 Mar 31;43(6):3208-18.

Zhang YJ, Xu YF, Cook C, Gendron TF, Roettges P, Link CD, Lin WL, Tong J, Castanedes-Casey M, Ash P, Gass J, Rangachari V, Buratti E, Baralle F, Golde TE, Dickson DW, Petrucelli L. Aberrant cleavage of TDP-43 enhances aggregation and cellular toxicity. Proc Natl Acad Sci U S A. 2009 May 5;106(18):7607-12.

ANNEXES

LISTE DES ANNEXES

Article Scientifique Complémentaire N°1

Published in

Molecular Neurobiology

August 2019, Volume 56, Issue 8, pp 5780–5791

Metabo-lipidomics of Fibroblasts and Mitochondrial-Endoplasmic Reticulum Extracts from ALS Patients Shows Alterations in Purine, Pyrimidine, Energetic, and Phospholipid Metabolisms

C. Veyrat-Durebex[1,2,3], C. Bris[1,2], P. Codron[2,4], C. Bocca[2], S. Chupin[1], P. Corcia[5,6,7], P. Vourc'h[3,5], R. Hergesheimer[5], J. Cassereau[2,4], B. Funalot[7], C. R Andres[3,5], G. Lenaers[2], P. Couratier[7], P.Reynier[1,2], H. Blasco[2,3,5]

1. Département de Biochimie et Génétique, CHU d'Angers, Angers, France
2. Unité Mixte de Recherche MITOVASC, CNRS 6015-INSERM 1083, Université d'Angers, Angers, France
3. Laboratoire de Biochimie et Biologie Moléculaire, CHRU Hôpital Bretonneau, 2 Bd Tonnellé, 37044 Tours, France
4. Centre de Ressources et de Compétences SLA, Service de Neurologie, CHU Angers, Angers, France
5. Université de Tours, Inserm U1253, Tours, France
6. Centre de Référence SLA, Service de Neurologie, CHRU Bretonneau, Tours, France
7. Fédération des CRCSLA Tours et Limoges, LITORALS, Tours, France

Molecular Neurobiology
https://doi.org/10.1007/s12035-019-1484-7

Metabo-lipidomics of Fibroblasts and Mitochondrial-Endoplasmic Reticulum Extracts from ALS Patients Shows Alterations in Purine, Pyrimidine, Energetic, and Phospholipid Metabolisms

Charlotte Veyrat-Durebex[1,2,3] &Céline Bris[1,2] &Philippe Codron[2,4] &Cinzia Bocca[2] &Stéphanie Chupin[1] & Philippe Corcia[5,6,7] &Patrick Vourc'h[3,5] &Rudolf Hergesheimer[5] &Julien Cassereau[2,4] &Benoit Funalot[7] & Christian R Andres[3,5] &Guy Lenaers[2] &Philippe Couratier[7] &Pascal Reynier[1,2] &Hélène Blasco[2,3,5]

Received: 29 October 2018 / Accepted: 10 January 2019

Abstract

Amyotrophic lateral sclerosis (ALS) is characterized by a wide metabolic remodeling, as shown by recent metabolomics and lipidomics studies performed in samples from patient cohorts and experimental animal models. Here, we explored the metabolome and lipidome of fibroblasts from sporadic ALS patients (n = 13) comparatively to age- and sex-matched controls (n = 11), and the subcellular fraction containing the mitochondria and endoplasmic reticulum (mito-ER), given that mitochondrial dysfunctions and ER stress are important features of ALS patho-mechanisms. We also assessed the mitochondrial oxidative respiration and the mitochondrial genomic (mtDNA) sequence, although without yielding significant differences. Compared to controls, ALS fibroblasts did not exhibit a mitochondrial respiration defect nor an increased proportion of mitochondrial DNA mutations. In addition, non-targeted metabolomics and lipidomics analyses identified 124 and 127 metabolites, and 328 and 220 lipids in whole cells and the mito-ER fractions, respectively, along with partial least-squares–discriminant analysis (PLS-DA) models being systematically highly predictive of the disease. The most discriminant metabolomic features were the alteration of purine, pyrimidine, and energetic metabolisms, suggestive of oxidative stress and of pro-inflammatory status. The most important lipidomic feature in the mito-ER fraction was the disturbance of phosphatidylcholine PC (36:4p) levels, which we had previously reported in the cerebrospinal fluid of ALS patients and in the brain from an ALS mouse model. Thus, our results reveal that fibroblasts from sporadic ALS patients share common metabolic remodeling, consistent with other metabolic studies performed in ALS, opening perspectives for further exploration in this cellular model in ALS.

Keywords Amyotrophic lateral sclerosis · Metabolomics · Lipidomics · Fibroblasts · Mitochondria · Oxidative stress

Electronic supplementary material The online version of this article (https://doi.org/10.1007/s12035-019-1484-7) contains supplementary material, which is available to authorized users.

* Charlotte Veyrat-Durebex
charlotte.veyrat@live.fr

* Hélène Blasco
helene.blasco@univ-tours.fr

1 Département de Biochimie et Génétique, CHU d'Angers, Angers, France

2 Unité Mixte de Recherche MITOVASC, CNRS 6015-INSERM 1083, Université d'Angers, Angers, France

3 Laboratoire de Biochimie et Biologie Moléculaire, CHRU Hôpital Bretonneau, 2, Bd Tonnellé, 37044 Tours, France

4 Centre de Ressources et de Compétences SLA, Service de Neurologie, CHU Angers, Angers, France

5 Université de Tours, Inserm U1253, Tours, France

6 Centre de Référence SLA, Service de Neurologie, CHRU Bretonneau, Tours, France

7 Fédération des CRCSLA Tours et Limoges, LITORALS, Tours, France

Published online: 24 January 2019

Introduction

Amyotrophic lateral sclerosis (ALS) is a fatal, neurodegenerative disease causing the progressive loss of motor neurons, and death only 3 to 5 years after diagnosis [1]. There is no cure for ALS, and the only two drugs available to date are riluzole and, more recently, edaravone that present limited efficacy. The pathophysiology of ALS includes glutamatergic excitotoxicity, oxidative stress, mitochondrial dysfunctions, abnormal protein aggregations, and neuroinflammation [2–5]. Nevertheless, these mechanisms and their interconnectedness are still only partially understood. Thus, new "omics" strategies further integrating these patho-mechanisms and revealing undescribed targets remain of utmost importance for the development of ALS treatments. Metabolic alterations have been largely described in ALS through targeted and untargeted approaches in the body fluids and tissues of patients, as well as in animal and cellular models [6].

Patient fibroblasts, often used in the exploration of mitochondrial diseases, have proven to be of use to understand ALS etiology, but so far they have not been analyzed by metabolomics. In ALS, skin fibroblasts have shown to display numerous abnormalities found in motor neurons [7] suggesting that these apparently unaffected cells may share common pathogenic pathways with motor neurons. Moreover, human fibroblast cultures have demonstrated that they are an accessible model to study the function of mitochondrial metabolism in ALS [8]. Fibroblasts of sporadic ALS (sALS) patients display an increased, uncoupled mitochondrial respiration and glycolytic rate compared to same-age control fibroblasts [9]. Similar defects in mitochondrial respiration with increased glycolytic flux were observed in fibroblasts from patients carrying *SOD1* pathogenic variants [10]. A higher mitochondrial membrane potential associated to decreased mitochondrial content was observed in ALS fibroblasts, and the correlation with age at diagnosis offers hope in discovering potential ALS biomarkers [11]. A recent study showed that fibroblasts from patients affected with sALS, primary lateral sclerosis, or familial ALS related to *C9ORF72* expansion repeats, were hyper-metabolic in order to counteract the energetic impairment [7]. This highlights the relevance of mitochondrial membrane potential, respiration, glycolysis, and ATP content to the classification of patients. Mitochondrial function also depends on its structure, including membrane composition, and the cellular environment. According to the link of polyunsaturated fatty acids with inflammatory mediators, and with the breakdown of cell membranes during neuronal degeneration [12, 13], we hypothesize that specific lipid and metabolic profiles may characterize the ALS pathologic condition. Mitochondria and ER are physically closely related by the mitochondria-associated membranes (MAM) that constitute the sites of lipids, calcium, and proteins transferred from the ER towards mitochondria, with a crucial regulatory role in cell homeostasis. MAM display a key role in the mitochondrial fission, apoptosis, and ROS generation. Defects in lipid metabolism observed at the MAM contact sites might be involved in pathophysiology of various conditions such as neurodegenerative or metabolic diseases [14], especially in ALS [15]. Since endoplasmic reticulum (ER) stress has been observed in familial and sporadic ALS [16, 17], the association between mitochondrial and ER defects in ALS led us to specifically explore this subcellular fraction, using a quick extraction protocol for metabolomics and lipidomics analyses [18]. Indeed, recent studies reported mitochondrial lipidome [19–22], but the long procedures used to isolate mitochondria are incompatible with metabolomics analyses due to the risk of metabolite degradation.

Here, we report metabolomic and lipidomic explorations of fibroblasts from ALS patients, both on whole cells and their mitochondrial-endoplasmic reticulum (mito-ER) fraction, and correlate these data to the functional assessment of oxidative phosphorylation (OXPHOS) and complete mitochondrial DNA sequencing, in order to unravel the metabolic disturbances through a multi-omics approach and to specify the alterations of the mitochondria-ER fraction.

Materials and Methods

Patients

Skin fibroblasts were obtained from 13 sporadic ALS patients diagnosed and followed in two French ALS reference centers: Angers and Limoges University Hospitals. ALS patients satisfied the diagnostic criteria of "probable" or "definite" symptoms as defined by the El Escorial workshop [23]. Information on diagnosis, gender, current age, site of onset, diagnostic delay, and age at onset were obtained for each patient. We also collected the parameters of disease progression, such as the revised ALS functional rating scale (ALSFRS-r), the forced vital capacity (FVC), and the body mass index (BMI) at the time of diagnosis.

Control fibroblasts from 11 gender- and age-matched healthy subjects were selected in the Biological Resource Center (Centre de Ressource Biologique CRB) from the hospital of Angers. All the participants in this current study provided their informed consent for the use of their fibroblasts for research. The ethic committees of the Centre for Human Research of Angers and Limoges Hospitals approved the study and the consent process (no 2016/36, 2016-A01425-46).

Fibroblast Culture

Human fibroblasts were cultured in a medium consisting of two-third Dulbecco's modified Eagle medium with nutrient mixture F12 (DMEM-F12, PAN Biotech), one-third AmnioMAX™

(Gibco, Invitrogen) supplemented with 10% fetal bovine serum (PAN Biotech) at 37 °C and 5% CO_2. To avoid artifacts due to senescence, all experiments were conducted on fibroblast cultures between the 6th and the 15th passages [24].

A schematic flowchart of experiments is presented in Fig. 1.

OXPHOS Exploration

The mitochondrial respiration rates were measured using a two-channel, high-resolution oxygraph respirometer (Oroboros, Innsbruck, Austria) in a minimum of three replicates. Cells were grown to 70–90% confluency and approximatively three million cells in DMEM-F12 were used for analysis. Firstly, the basal respiration was measured (i.e., routine oxygen consumption rate (OCR)). Secondly, the non-phosphorylating respiration (proton leak) was evaluated by adding an ATP synthase inhibitor, oligomycin (4 μg/mL) (Oligomycin OCR). Then, maximal capacity of cellular respiration was assessed by adding successive doses of FCCP (p-trifluoromethoxy-carbonyl-cyanide-phenyl hydrazine). Finally, we used an inhibitor of mitochondrial complex III, antimycin (2 μg/mL) to evaluate the non-mitochondrial oxygen consumption. The respiration capacity rate (RCR) was calculated as the ratio between the maximal capacity of respiration and the non-phosphorylating respiration. The phosphorylating RCR was obtained by the subtraction of non-phosphorylating respiration to basal respiration divided by the maximal capacity of respiration. We measured the concentration of proteins of each sample to normalize oxygen uptake between samples.

Metabolomic and Lipidomic Analyses

Whole Cell Extraction

Samples were extracted as previously described [25]. After medium removal, the cellular monolayer was rinsed twice with an aqueous solution containing 0.22% NaCl before being quenched with cold methanol for metabolomic analysis and with a cold mixture of ammonium bicarbonate at 155 mM and methanol (67.7/32.3) for lipidomics. The cell suspension (4 million cells) obtained after mechanical scraping was then collected in aliquots of one million cells and stored at −80 °C until analysis.

Mitochondria and Endoplasmic Reticulum (Mito-ER) Extraction

The mitochondria plus endoplasmic reticulum (mito-ER) fraction was extracted as previously described [18]. Briefly, cell lysis of pellets containing 10 million cells was achieved in a Precellys24® homogenizer (Bertin Instruments) using 1 cycle of grinding 5 s at 2500 rpm at 4 °C. Then differential centrifugations were performed for mito-ER purification.

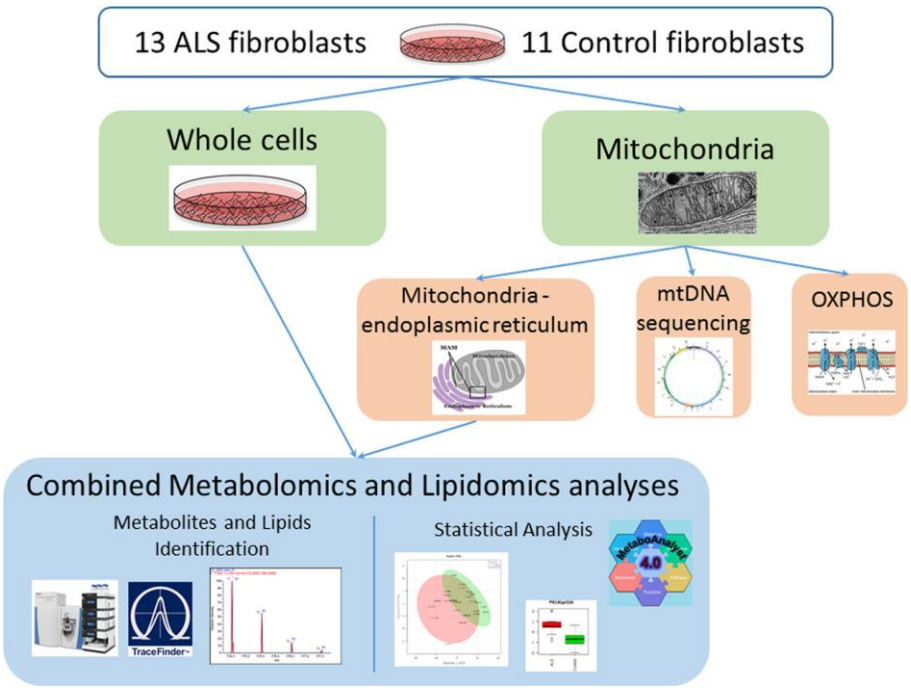

Fig. 1 Flowchart summarizing the global methodology

Metabolomics and Lipidomics

Metabolomics and lipidomics protocols and analytical systems have been detailed and recently published [18, 25]. HRMS system was based on UPLC Ultimate 3000 system (Dionex) coupled to a Q-Exactive Mass Spectrometer (ThermoFisher Scientific, Bremen, Germany) using electrospray ionization (positive and negative Electrospray Ionization (ESI+ and ESI-)). Quality controls (QC) were analyzed regularly on the plate (every 8 samples) to ensure the stability of the mass system over time. Accordingly, peaks that had high variability (coefficient of variation > 30%) were excluded from further analysis. Metabolites were identified at level 1 and lipids at level 2 according to the level of compound identification process [26].

Mitochondrial DNA Sequencing

Total DNA was extracted from patient fibroblasts using the Nucleospin® tissue Kit (Macherey-Nagel®) and the EZ1 DNA extraction automate (Qiagen) according to the manufacturer's recommendations. Whole mitochondrial genome (mtDNA) was sequenced using Ion Proton high-throughput sequencing platform and analyzed as previously described [27]. Variants were filtered using the following criteria: at least three callers predicting the variant, strand bias between 0.25–0.75, and a minimum mtDNA heteroplasmy level of 2%. Putative variants were visualized on Integrative Genome Viewer [28] to avoid artifacts. Variant prioritization relies on databases, i.e., Mitomap [29], HmtDB [30], Mamit [31], and prediction tools, i.e., MitImpact [32] and MitoTip [33]. Variant heteroplasmy was considered as low under 30%, medium between 30% and 70% and high between 70% and 95%, and above 95% variants were considered as homoplasmic. Mitochondrial haplogroups were determined using Phy-Mer [34]. Structural mtDNA rearrangements were analyzed trough a home-made tool based on soft-clipping.

Statistical Analysis

We performed both multivariate and univariate analyses using Metaboanalyst, version 3.0 (http://www.metaboanalyst.ca) for metabolomics and lipidomics data. Classification method was based on Partial Least-Squares Discriminant Analysis (PLS-DA). Values of variable importance in projection (VIP) represent the importance of the compound (metabolite/lipid) for the PLS-DA models. The score plots show the classified samples and the loadings characterize the relation between the Y and X variables (metabolites, lipids). Metaboanalyst modeling includes leave-one-out cross-validation (LOOCV). We retained the 15 most discriminant compounds based on the VIP to explore pathways. To attest the relevance of these selected compounds, the quality of the model built with these selected discriminant metabolites was assessed by prediction accuracy and permutation test (set permutation $n = 100$). The performance measures of the permutated data usually form a normal distribution and if the performance score of the original data lies outside the distribution, then the results are considered significant.

The univariate analysis of metabolites and lipids levels was based on the fold-change values and the threshold of significance after non-parametric Wilcoxon test, using Benjamini and Hochberg correction for multiple tests.

Non-parametric Wilcoxon test was used to compare clinical data, oxygen consumption rate, and mtDNA sequencing data between ALS and controls.

Pathway Analysis

We used KEGG pathway database (http://www.genome.jp/kegg/pathway.html) on Metaboanalyst tool to discuss the highlighted metabolic pathways. To focus on the most relevant data, we highlighted only the pathways that had significant Holm p and a pathway impact > 0.05. The pathway impact value is the cumulative percentage from the matched metabolite nodes.

Results

Patients

No statistical difference was found regarding age and gender between the 13 ALS and 11 control subjects. The mean age at onset of ALS was 60.5 ± 9.9 years, and percentage of females was 38.5% (Table 1). About 77% of ALS patients had a spinal onset. None of these patients carried mutations or expansions in *SOD1*, *TARDBP*, *FUS*, or *C9ORF72* genes. Characteristics of ALS patients at diagnosis defined by BMI, FVC, and ALSFRS-r score were as follows: 22.8 ± 3.2 kg/m^2, 81.6 ± 18.9%, and 38.2 ± 4.5, respectively. There was no significant difference in mean passage number between ALS and control fibroblast cultures used for analyses (data not shown).

Mitochondrial Exploration

OXPHOS Analysis

The OXPHOS analysis revealed no differences in basal and maximal respiration between ALS and control fibroblasts. We did not detect any difference in respiratory capacity rate (RCR) or in phosphorylating RCR (Table 2).

Table 1 Clinical characteristics of ALS patients and controls. SD = standard deviation

	ALS patients mean ± SD	Controls mean ± SD	*p* value
Age (mean ± SD)	60.5 ± 9.9	54.3 ± 11.4	0.12
Gender (% of female)	38.5	33.3	1
Age of onset (years)	59.4 ± 9.1		
BMI (kg/m^2)	22.8 ± 3.2		
FVC (%)	81.6 ± 18.9		
ALSFRS-R	38.2 ± 4.5		

mtDNA Sequencing

mtDNA from 12 ALS and 11 control fibroblasts was sequenced, while one ALS sample could not be processed. We did not identify any large-scale rearrangement in patients or controls. Considering all samples together, 505 punctual variants were found, among which 124 were unrelated to the mitochondrial haplogroups (combinations of polymorphisms retracing human evolution), including 66 heteroplasmic variants. Among the non-haplogroup variants, 32 (25.8%) occurred in the D-Loop, the non-coding region controlling replication and transcription of mtDNA, 69 (55.6%) were located in polypeptide-coding regions, 10 (8.1%) in tRNA genes, and 13 (10.5%) in rRNA genes. Figure 2 shows the repartitioning of these variants in ALS and control fibroblasts. Twenty-eight (42.4%) of the heteroplasmic variants were recognized as non-pathogenic variants, nine (13.6%) were associated with clinical phenotypes, and 29 (44%) were not reported in all mitochondrial databases. The level of heteroplasmy was considered to be low for 61 (63.5%) variants and medium for five of them (15.4%).

Statistical comparison between the ALS and control groups did not disclose difference between the total number of variants, the number of non-haplogroup variants, or the number of variants in the different mtDNA genes (Table 2). Of note, the mean level of heteroplasmic variants per ALS patient was 3.4, while it was 2.3 per control, but this difference was not significant. Interestingly, only ALS patients had mtDNA variants with medium levels of heteroplasmy among the non-haplogroup variants ($p = 0.0179$) (Table 3). We did not observe any difference in the number of pathogenic variants between ALS and controls. Reported pathogenic variants found in the ALS and control fibroblasts are reported in supplementary Table S1.

Metabolomic and Lipidomic Signatures of ALS Fibroblasts

We detected and identified 124 and 127 metabolites and 328 and 220 complex lipids in fibroblasts and mito-ER extracts, respectively (Supplementary Tables S2 and S3).

The PLS-DA model from metabolomic data on total fibroblasts revealed an excellent discrimination between ALS patients and controls (75% accuracy, *p* value of permutation test: 0.01) (Fig. 3a). The 15 most discriminant metabolites were attributed with VIP scores higher than 1 and are presented in Fig. 3b. Mito-ER metabolomics correctly distinguished ALS patients and controls (accuracy: 62.5%, *p* value of permutation test: 0.1) (Fig. 3d). VIP scores of the 15 most discriminant metabolites were higher than 1.5, and 3 of them were significant after univariate analysis: inosine, guanosine, and guanine ($p < 0.03$ and FC > 1.5) (Fig. 3e).

Whole cell and mito-ER lipidomics also displayed correct discriminations between ALS and control subjects (64% and 50% accuracies, *p* values of permutation tests 0.17 and 0.75, respectively). In these two non-optimized models, the 15 most discriminant lipids had VIP scores higher than two (Fig. 4b and d). Optimized PLS-DA models using only the 15 top VIP metabolites improved the discriminations between ALS and controls in both whole cells and mito-ER lipidomic data, with

Table 2 Exploration of oxidative phosphorylation of ALS and control fibroblasts. SD = standard deviation

Oxygen consumption rate (OCR) (pmol O_2/min)	ALS patients mean ± SD	Controls mean ± SD	*p* value
Routine OCR	152.7 ± 27.6	160.9 ± 31.1	0.5
Oligomycin OCR	46.1 ± 7.7	48.9 ± 7.5	0.5
Maximal capacity of respiration	399.3 ± 82.4	406.5 ± 97.2	0.88
Respiration capacity rate (RCR)	3.5 ± 0.8	3.4 ± 0.5	0.5
Phosphorylating RCR	0.009 ± 0.002	0.009 ± 0.001	0.93

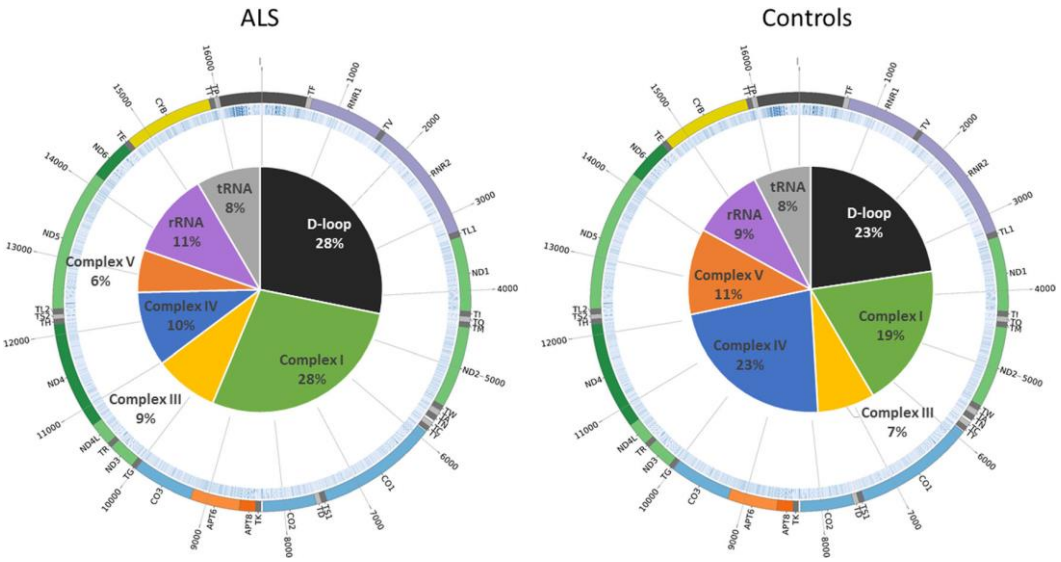

Fig. 2 Circos representing mtDNA sequence (black: D-loop; gray: tRNA genes; purple: rRNA genes; green: complex I genes; yellow: complex III genes; blue: complex IV genes; orange: complex V genes). The pie chart in the center of each circos (ALS and controls) shows the repartition of heteroplasmic variants on the mtDNA

80% and 83% accuracy, and 0.03 and 0.08 for *p* values of permutation tests in whole cells and mito-ER extracts, respectively (Fig. 4a and c). Univariate analysis did not reveal significant variation in lipid concentrations.

Metabolomic Findings

Using the "pathway analysis" module of the MetaboAnalyst software, we explored the pathways involved in the

Table 3 Summary of mtDNA variants found in ALS and control fibroblasts. *p value < 0.05 was considered as significant

	mtDNA	ALS		Control		*p* value
	Total sites	Total	Per individual ($n = 12$)	total	Per individual ($n = 11$)	
Total variants	16,569	264	22.0	241	21.9	0.9508
Total non-haplogroup (HP) variants	16,569	71	5.9	53	4.8	0.5536
Total homoplasmic variants non HP	16,569	30	2.5	28	2.5	0.9000
Total heteroplamic variants non HP	16,569	41	3.4	25	2.3	0.4330
Variants non HP location						
D-loop	1121	20	1.7	12	1.1	0.2624
All coding	15,409	51	4.3	41	3.7	0.9255
Complex I	6349	20	1.7	10	0.9	0.1829
Complex III	1141	6	0.5	4	0.4	0.3886
Complex IV	3010	7	0.6	12	1.1	0.2018
Complex V	888	4	0.3	6	0.5	0.4724
rRNA	2513	8	0.7	5	0.5	0.8558
tRNA	1508	6	0.5	4	0.4	0.8835
Type of variants						
Reported pathogenic variants	16,569	6	0.5	3	0.3	0.2358
Non reported in DB variants	16,569	17	1.4	12	1.1	0.5524
Heteroplasmy						
Low (1–30%)	16,569	36	3.0	25	2.3	0.7018
Medium (30–70%)	16,569	5	0.4	0	0.0	0.0179 *
High (70–95%)	16,569	0	0.0	0	0.0	

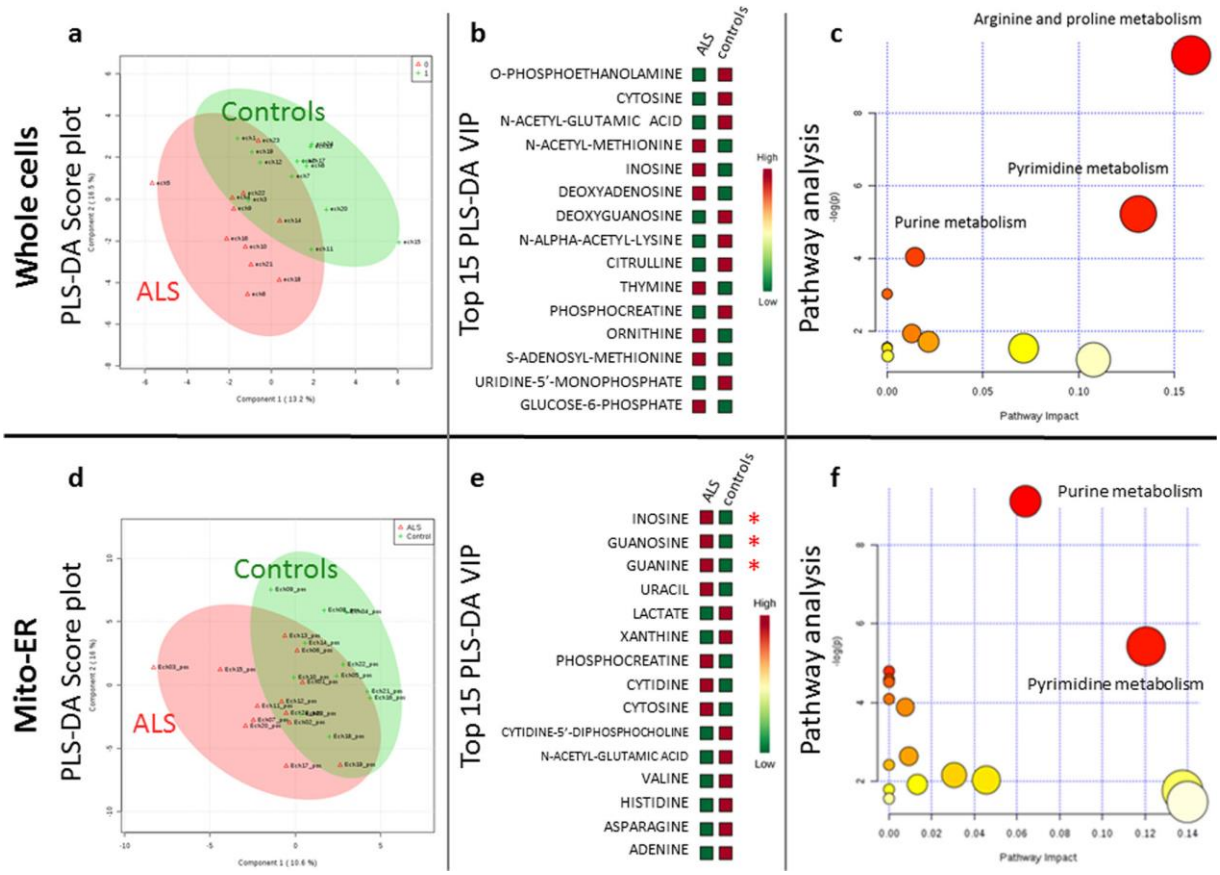

Fig. 3 Metabolomic data analyses of whole cells and mito-ER fraction. A. Optimized PLS-DA 2D-score plot from metabolomic whole cells data (red triangle: ALS samples; green cross: control samples) showing discrimination between the two groups. B. List of the top 15 VIP (variable importance in projection) from non-optimized PLS-DA model from metabolomic whole cells data. C. Results of pathway analysis including the top 15 VIP metabolites of whole cells PLS-DA model (using MetaboAnalyst module). D. Optimized PLS-DA 2D-score plot from metabolomic mito-ER data (red triangle: ALS samples; green cross: control samples) showing the discrimination between the two groups. E. List of the top 15 VIP (variable importance in projection) from non-optimized PLS-DA model from metabolomic mito-ER data (red stars show metabolites significant in univariate analysis with $p < 0.05$ and fold change > 1.2). F. Results of pathway analysis including top 15 VIP metabolites of mito-ER PLS-DA model (using MetaboAnalyst module)

metabolomic signatures of ALS whole fibroblasts and mito-ER extracts. The main pathways involving the 15 most discriminant metabolites identified with robustness in ALS fibroblasts were arginine and proline metabolism, pyrimidine, and purine metabolism (Fig. 3c). The pathway analysis of the metabolomic signature of ALS mito-ER notably underscored the involvement of purine and pyrimidine metabolism, as well (Fig. 3f).

The global analysis of metabolic disturbances based on fibroblasts and their mito-ER fraction disclosed modifications of purine (adenine and guanine) and pyrimidine bases (cytosine, uracil, and thymine), and various nucleosides and their derivatives (inosine, guanosine, cytidine, deoxyadenosine, deoxyguanosine, uridine-5′-monophosphate, and cytidine-5′-diphosphocholine). We also observed a decrease in xanthine in the mito-ER fraction.

Metabolomic signatures also highlighted several compounds involved in energy metabolism. Indeed, we noticed variations in glucose-6-phosphate levels in ALS whole fibroblasts and in lactate levels in the mito-ER fraction. This was associated with a modification of the phosphocreatine levels in both ALS fibroblasts and mito-ER fractions.

Lipidomic Findings

We found a reduction in several ceramide concentrations in the ALS mito-ER fraction and a gain in sphingolipid (SM) levels in ALS whole cells (Fig. 4). Lipidomic profiles of ALS fibroblasts highlighted modifications in phosphatidylcholine (PC) and phosphatidylethanolamine (PE) levels, both in whole cell and mito-ER extracts (Fig. 4). Interestingly, we observed several plasmalogen species among the VIP

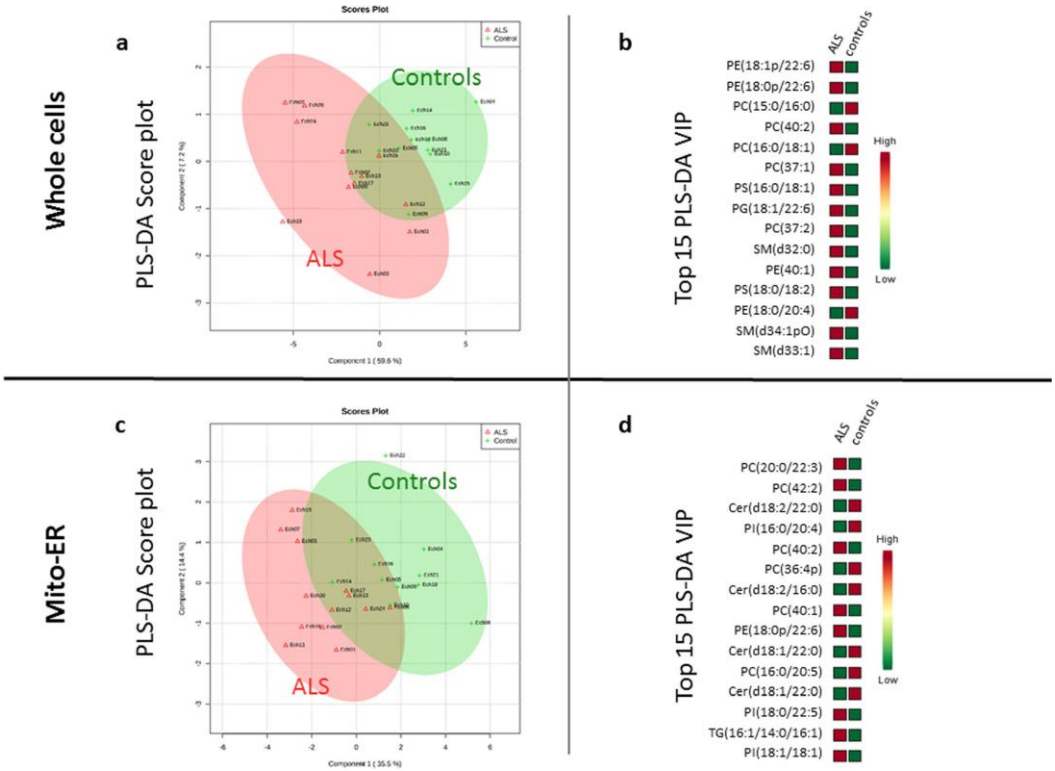

Fig. 4 Lipidomic data analyses of whole cells and mito-ER fraction. A. Optimized PLS-DA 2D-score plot from lipidomic whole cells data (red triangle: ALS samples; green cross: control samples) showing discrimination between the two groups. B. List of the top 15 VIP (variable importance in projection) from non-optimized PLS-DA model from lipidomic whole cells data. C. Optimized PLS-DA 2D-score plot from lipidomic mito-ER data (red triangle: ALS samples; green cross: control samples) showing discrimination between the two groups. D. List of the top 15 VIP (variable importance in projection) from non-optimized PLS-DA model from lipidomic mito-ER data

metabolites of both models—PE plasmalogen (PEp) in the whole cells with PE(18:1p/22:6) and PE(18:0p/22:6); and PE(18:0p/22:6) and PC(36:4p) in the mito-ER extract.

Discussion

This study provides the first report of a multi-omics profiling on sporadic ALS fibroblasts, both at the whole cell and mito-ER subcellular levels, complemented by OXPHOS measurement and mtDNA complete sequencing.

Multiple Implications of the Purine and Pyrimidine Metabolisms in Oxidative Stress and Inflammation in ALS

The alterations of purine and pyrimidine metabolisms recognized in this study are convergent with data from a previous study that we performed on rodent motor neurons and astrocytes [35], placing these pathways at the core of oxidative stress and inflammatory mechanisms observed in ALS [36]. Purine catabolism leads to the production of xanthine, which is converted to uric acid by xanthine oxidase, finally producing reactive oxygen species (ROS) [37]. This is consistent with the increase in uric acid and ROS production found in ALS patients; we also found that xanthine levels were lower in the mito-ER samples compared to the controls, possibly signifying an augmented depletion due to uric acid production. We did not highlight significant differences in uric acid levels in our study ($p = 0.6635$), but we had a small cohort reducing statistical power. Uric acid has numerous roles in cell homeostasis, and its function in oxidative stress, especially increased in ALS, may explain this finding. Indeed, uric acid concentrations increase in response to oxidative stress and act as a scavenger of singlet oxygen and hydroxyl radicals [38]. Therefore, uric acid acts as either an antioxidant (especially in plasma) or a pro-oxidant in cells [39], suggesting a role in oxidative stress as a primary phenomenon or as a neuroprotective effect [40]. Interestingly, multiple studies have displayed support for the latter. It has been shown that uric acid modulates neuroinflammation by decreasing the serum levels of IL-1β, IL-6, and TNF-α in Parkinson's disease murine models [41]. Furthermore, primary astrocyte-conditioned medium provides a neuroprotective effect against both H_2O_2-

induced and SOD1^{G93A} astrocyte-induced oxidative stress in NSC-34 cells, when the normal or mutant astrocytes are first treated with uric acid [42].

Disturbances in Energy Metabolism in ALS

An imbalance in ATP production and consumption could explain an increased rate of purine catabolism with consequent modifications in purine end-product levels, as xanthine and inosine observed here. A recent study showed that multiple sclerosis is characterized by perturbations in energy metabolism, leading to significant changes in the serum profiles of compounds directly (purines) or indirectly (creatinine, lactate, and pyrimidines) connected to ATP homeostasis [43]. Our findings are consistent with the results of this study, since ALS also involves metabolic imbalances. In this respect, we also noticed modified amounts of phosphocreatine, which mediates ADP phosphorylation and could be a response to energetic impairment. It is also known to stabilize mitochondrial membranes by binding phospholipids [44]. In addition, phosphocreatine has neuroprotective effects against oxidative stress and mitochondrial dysfunction [45]. As in cancer cells, significant levels of aerobic glycolysis, the so-called Warburg Effect, have been documented in ALS due to the overactivation of the WNT/β-catenin pathway [46]. This is supported by the observation of modifications in the concentration of glucose-6-phosphate, a glycolytic intermediate, related with variations in lactate levels. All these findings support the alteration of the energy metabolism in ALS, associated with oxidative imbalance and inflammation. As explained by Lu et al., the reported concentrations of cellular ATP are notoriously inconsistent because of incomplete quenching and incomplete extraction for mass spectrometry method. Enzyme assays reveal that ATP concentration is more reflective of overall purine abundance than cellular energetics [47]. Thus, these results also lead us to program further explorations of energy metabolism through the measurement of glycolytic and mitochondrial production of ATP.

Involvement of Phospholipids and Sphingomyelins in Neuroprotective Mechanisms

Lipidomic results further suggest perturbations in the oxidative mechanism and inflammation. Indeed, higher concentrations of PCs observed in ALS fibroblasts may stimulate the metabolic activity of phospholipase A2 (PLA2), resulting in an increased production of lipid mediators, such as eicosanoids that promote inflammation and are considered to play a role in ALS pathophysiology [48, 49].

Three plasmalogen species, corresponding to phospholipids (PL) having an ether bond between fatty acids and glycerol, were discriminants between ALS and control fibroblasts: (PE(18:1p/22:6), PE(18:0p/22:6), PC(36:4p)). Plasmalogens are important components of myelin, subcellular membranes as the mitochondrial membranes, and the membranes of secretory granules. The main functions of plasmalogens are the generation of lipid second messengers and the conservation of membrane integrity. Plasmalogens, which terminate lipid oxidation and protect ROS-vulnerable myelin, are considered to act as endogenous antioxidants [50, 51], which, in the context of ALS, can prevent the oxidation of polyunsaturated fatty acids and other lipids.

Our results further disclosed higher levels of sphingomyelins (SM) in ALS fibroblasts, associated with lower ceramide (Cer) levels in mito-ER fractions. Classically, ceramides are synthesized using serine in the ER then are converted to SM. These results are consistent with the lipidomic signature of the cerebrospinal fluid (CSF) from ALS patients [52], with the higher levels of ceramides and glucosylceramides found in the spinal cord of ALS patients and in ALS mouse model [53], and with the fact that ceramides have been associated with apoptosis in response to cytotoxic humoral factors [54]. Indeed, the accumulation of ceramide-derived agents may be protective by reducing ceramide synthesis and increasing the entry of ceramides into the CerG1 pathway, thus limiting the direct toxic effect on motor neurons [53]. Higher ceramide and downstream glycosphingolipid levels have also been reported in the muscle of an ALS mouse model, as well as in other mice after muscle injury [55]. Taken together, these findings clearly show a perturbation of the glycosphingolipid metabolism in ALS fibroblasts. These results open perspectives of deeply studying ER function in ALS.

The identification of the fatty acid chain 22:6 in the discriminant phospholipids, i.e., (PE(18:0p/22:6), PE(18:1p/22:6), PG(18:1/22:6)), corresponds to docosahexaenoic acid (DHA), an omega-3 polyunsaturated fatty acid (n-3 PUFA) that is involved in the maintenance of neuronal membranes, signal transduction, neuronal differentiation, neurogenesis, and protection against synaptic loss and spinal cord injury [56]. Moreover, some authors have highlighted the significant increase in DHA in the frontal cortex of ALS patients [17]. This phenomenon may be considered as a potentially defensive response of the nervous tissue to brain ischemia and Alzheimer's disease [57], or as an inflammatory process via the production of n-3-derived anti-inflammatory resolvins and docosatrienes by the brain cortex [58]. We also recently reported discriminant phospholipids containing DHA in the lipidomic signature of ALS cerebrospinal fluids [52].

Mitochondrial Instability as a Protective Mechanism?

The assessment of OXPHOS capacities revealed that there was no difference in cellular respiration between ALS and control fibroblasts. MtDNA sequences of ALS fibroblasts were similar to those of controls in terms of total number of

variants per sample, frequency of mtDNA variants, type of mtDNA variants, and patterns of distribution. Nevertheless, we found that ALS cells exhibited higher levels of heteroplasmy, which may attest to a higher mtDNA instability. We could note that reported pathogenic variants found in ALS fibroblasts are associated with Parkinson's disease, dystonia and myopathy, hypertrophic cardiomyopathy, and Leber Hereditary Optic Neuropathy (LHON) mitochondrial diseases. Despite the absence of obvious mtDNA alteration in ALS fibroblasts, mitochondrial dysfunction observed so far in ALS could be related to epigenetic mtDNA modifications, as already suggested in Alzheimer's disease [59]. Intriguingly, it was demonstrated that mitochondrial heteroplasmy alters mtDNA methylation [60]. Moreover, a recent study in blood mtDNA of ALS patients, especially from *SOD1* mutation carriers, showed a significant decrease in D-loop methylation accompanied by an increase in mtDNA copy number, the latter representing a mitochondrial compensation for metabolic deregulation caused by oxidative stress in ALS [61]. However, we did not evidence difference in the mtDNA copy number in ALS fibroblasts compared to controls (data not shown). It neither seems likely that the inverse relationship between mtDNA copy number and D-loop methylation in the blood specifically points to ALS; rather, it could point generally to a metabolic imbalance.

Conclusion

Provided that the discriminant metabolites found in this study are also available in the blood and/or CSF, a collective reading of purine, pyrimidine, arginine, proline metabolites, and DHA-containing lipids could reflects a specific ALS signature. These results in agreement with the ALS research literature, in different affected tissues and body fluids (motor neurons, CSF, blood etc.…), reinforce the interest of fibroblast cultures in the study of ALS. These findings reveal a robust methodology to apply omics, even in subcellular organelles, with data integration with promise to deeply understand ALS pathophysiology. Thus, this approach may be applied to other complex and multifactorial neurological diseases with high confidence.

Acknowledgements We thank University Hospitals of Angers and Limoges for patients' recruitment and fibroblasts' sampling.

Authors' Contributions C.V-D and H.B designed and supervised the study, performed statistical analysis and wrote the manuscript; C. Br performed mtDNA experiments and analyzed mtDNA sequence; C.V-D and C.Bo performed metabolomic and lipidomic assays, S.C performed cell cultures and mitochondrial function assessment; P.Cod and B.F recruited ALS patients and performed fibroblast sampling; J.C and P. Cou supervised patients' recruitment; P.V supervised genetic determination of genes involved in ALS; R.H gave technical and intellectual support and critical advice for English writing; P.Cor, P.V, and C.R.A gave technical and intellectual support; G.L and P.R gave intellectual support and conceptual advice for manuscript writing. All authors offered conceptual advice and comments on the manuscript. All authors read and approved the final manuscript.

Compliance with Ethical Standards

Ethical Approval and Consent to Participate All the participants in this current study provided their informed consent for the use of their fibroblasts for research. The ethic committees of the Centre for Human Research of Angers and Limoges Hospitals approved the study and the consent process.

Conflict of Interest All authors declare that they have no conflict of interest.

Abbreviations ALS, amyotrophic lateral sclerosis; sALS, sporadic ALS; ER, endoplasmic reticulum; mtDNA, mitochondrial DNA; PCA, principal component analysis; PLS-DA, partial least square discriminant analysis; OXPHOS, oxidative phosphorylation; FVC, forced vital capacity; BMI, body mass index; HRMS, high-resolution mass spectrometry; UPLC, ultra-performance liquid chromatography; ESI, electrospray ionization; QC, quality control; VIP, variable importance in projection; OCR, oxygen consumption rate; RCR, respiration capacity rate; SM, sphingomyelins; PC, phosphatidylcholines; PE, phosphatidylethanolamines; ROS, reactive oxygen species; CSF, cerebrospinal fluid; Cer, ceramides; DHA, docosahexaenoic acid

References

1. Korner S, Kollewe K, Ilsemann J, Muller-Heine A, Dengler R, Krampfl K, Petri S (2013) Prevalence and prognostic impact of comorbidities in amyotrophic lateral sclerosis. Eur J Neurol 20(4): 647–654. https://doi.org/10.1111/ene.12015
2. Barber SC, Shaw PJ (2010) Oxidative stress in ALS: key role in motor neuron injury and therapeutic target. Free Radic Biol Med 48(5):629–641. https://doi.org/10.1016/j.freeradbiomed.2009.11.018
3. Guegan C, Vila M, Rosoklija G, Hays AP, Przedborski S (2001) Recruitment of the mitochondrial-dependent apoptotic pathway in amyotrophic lateral sclerosis. J Neurosci 21(17):6569–6576
4. Watanabe M, Dykes-Hoberg M, Culotta VC, Price DL, Wong PC, Rothstein JD (2001) Histological evidence of protein aggregation in mutant SOD1 transgenic mice and in amyotrophic lateral sclerosis neural tissues. Neurobiol Dis 8(6):933–941. https://doi.org/10.1006/nbdi.2001.0443
5. Ferraiuolo L, Kirby J, Grierson AJ, Sendtner M, Shaw PJ (2011) Molecular pathways of motor neuron injury in amyotrophic lateral sclerosis. Nat Rev Neurol 7(11):616–630. https://doi.org/10.1038/nrneurol.2011.152
6. Vandoorne T, De Bock K, Van Den Bosch L (2018) Energy metabolism in ALS: an underappreciated opportunity? Acta Neuropathol 135(4):489–509. https://doi.org/10.1007/s00401-018-1835-x
7. Konrad C, Kawamata H, Bredvik KG, Arreguin AJ, Cajamarca SA, Hupf JC, Ravits JM, Miller TM et al (2017) Fibroblast bioenergetics to classify amyotrophic lateral sclerosis patients. Mol Neurodegener 12(1):76. https://doi.org/10.1186/s13024-017-0217-5

8. Walczak J, Debska-Vielhaber G, Vielhaber S, Szymanski J, Charzynska A, Duszynski J, Szczepanowska J (2018) Distinction of sporadic and familial forms of ALS based on mitochondrial characteristics. Faseb j:fj201801843R. doi:https://doi.org/10.1096/fj.201801843R
9. Allen SP, Duffy LM, Shaw PJ, Grierson AJ (2015) Altered age-related changes in bioenergetic properties and mitochondrial morphology in fibroblasts from sporadic amyotrophic lateral sclerosis patients. Neurobiol Aging 36(10):2893–2903. https://doi.org/10.1016/j.neurobiolaging.2015.07.013
10. Allen SP, Rajan S, Duffy L, Mortiboys H, Higginbottom A, Grierson AJ, Shaw PJ (2014) Superoxide dismutase 1 mutation in a cellular model of amyotrophic lateral sclerosis shifts energy generation from oxidative phosphorylation to glycolysis. Neurobiol Aging 35(6):1499–1509. https://doi.org/10.1016/j.neurobiolaging.2013.11.025
11. Kirk K, Gennings C, Hupf JC, Tadesse S, D'Aurelio M, Kawamata H, Valsecchi F, Mitsumoto H et al (2014) Bioenergetic markers in skin fibroblasts of sporadic amyotrophic lateral sclerosis and progressive lateral sclerosis patients. Ann Neurol 76(4):620–624. https://doi.org/10.1002/ana.24244
12. Fonteh AN, Fisher RD (2009) Combining lipidomics and proteomics of human cerebrospinal fluids. Methods Mol Biol 579:71–86. https://doi.org/10.1007/978-1-60761-322-0_4
13. Puentes F, Malaspina A, van Noort JM, Amor S (2016) Non-neuronal cells in ALS: Role of glial, immune cells and blood-CNS barriers. Brain Pathol 26(2):248–257. https://doi.org/10.1111/bpa.12352
14. Szymanski J, Janikiewicz J, Michalska B, Patalas-Krawczyk P, Perrone M, Ziolkowski W, Duszynski J, Pinton P et al (2017) Interaction of mitochondria with the endoplasmic reticulum and plasma membrane in calcium homeostasis, lipid trafficking and mitochondrial structure. Int J Mol Sci 18(7). https://doi.org/10.3390/ijms18071576
15. Kaus A, Sareen D (2015) ALS patient stem cells for unveiling disease signatures of motoneuron susceptibility: perspectives on the deadly mitochondria, ER stress and calcium triad. Front Cell Neurosci 9:448. https://doi.org/10.3389/fncel.2015.00448
16. Turner BJ, Atkin JD (2006) ER stress and UPR in familial amyotrophic lateral sclerosis. Curr Mol Med 6(1):79–86
17. Ilieva EV, Ayala V, Jove M, Dalfo E, Cacabelos D, Povedano M, Bellmunt MJ, Ferrer I et al (2007) Oxidative and endoplasmic reticulum stress interplay in sporadic amyotrophic lateral sclerosis. Brain 130(Pt 12):3111–3123. https://doi.org/10.1093/brain/awm190
18. Veyrat-Durebex C, Bocca C, Chupin S, Kouassi Nzoughet J, Simard G, Lenaers G, Reynier P, Blasco H (2018) Metabolomics and lipidomics profiling of a combined mitochondrial plus endoplasmic reticulum fraction of human fibroblasts: a robust tool for clinical studies. J Proteome Res 17(1):745–750. https://doi.org/10.1021/acs.jproteome.7b00637
19. Aviram R, Manella G, Kopelman N, Neufeld-Cohen A, Zwighaft Z, Elimelech M, Adamovich Y, Golik M et al (2016) Lipidomics analyses reveal temporal and spatial lipid organization and uncover daily oscillations in intracellular organelles. Mol Cell 62(4):636–648. https://doi.org/10.1016/j.molcel.2016.04.002
20. Kappler L, Li J, Haring HU, Weigert C, Lehmann R, Xu G, Hoene M (2016) Purity matters: a workflow for the valid high-resolution lipid profiling of mitochondria from cell culture samples. Sci Rep 6:21107. doi:https://doi.org/10.1038/srep21107
21. Bird SS, Stavrovskaya IG, Gathungu RM, Tousi F, Kristal BS (2015) Qualitative characterization of the rat liver mitochondrial lipidome using all ion fragmentation on an Exactive benchtop Orbitrap MS. Methods Mol Biol 1264:441–452. https://doi.org/10.1007/978-1-4939-2257-4_36
22. Angelini R, Vitale R, Patil VA, Cocco T, Ludwig B, Greenberg ML, Corcelli A (2012) Lipidomics of intact mitochondria by MALDI-TOF/MS. J Lipid Res 53(7):1417–1425. https://doi.org/10.1194/jlr.D026203
23. Brooks BR, Miller RG, Swash M, Munsat TL (2000) El Escorial revisited: revised criteria for the diagnosis of amyotrophic lateral sclerosis. Amyotroph Lateral Scler Other Motor Neuron Disord 1(5):293–299
24. Hutter E, Renner K, Pfister G, Stockl P, Jansen-Durr P, Gnaiger E (2004) Senescence-associated changes in respiration and oxidative phosphorylation in primary human fibroblasts. The Biochem J 380 (Pt 3):919–928. doi:https://doi.org/10.1042/bj20040095
25. Bocca C, Kane MS, Veyrat-Durebex C, Chupin S, Alban J, Kouassi Nzoughet J, Le Mao M, Chao de la Barca JM et al (2018) The metabolomic bioenergetic signature of Opa1-disrupted mouse embryonic fibroblasts highlights aspartate deficiency. Sci Rep 8(1):11528. https://doi.org/10.1038/s41598-018-29972-9
26. Sumner LW, Amberg A, Barrett D, Beale MH, Beger R, Daykin CA, Fan TW, Fiehn O et al (2007) Proposed minimum reporting standards for chemical analysis chemical analysis working group (CAWG) metabolomics standards initiative (MSI). Metabolomics 3(3):211–221. https://doi.org/10.1007/s11306-007-0082-2
27. Boucret L, Bris C, Seegers V, Goudenege D, Desquiret-Dumas V, Domin-Bernhard M, Ferre-L'Hotellier V, Bouet PE et al (2017) Deep sequencing shows that oocytes are not prone to accumulate mtDNA heteroplasmic mutations during ovarian ageing. Hum Reprod 32(10):2101–2109. https://doi.org/10.1093/humrep/dex268
28. Robinson JT, Thorvaldsdottir H, Winckler W, Guttman M, Lander ES, Getz G, Mesirov JP (2011) Integrative genomics viewer. In: Nat Biotechnol, vol 29. vol 1. United States, pp 24–26. doi:https://doi.org/10.1038/nbt.1754
29. Lott MT, Leipzig JN, Derbeneva O, Xie HM, Chalkia D, Sarmady M, Procaccio V, Wallace DC (2013) mtDNA variation and analysis using Mitomap and Mitomaster. Curr Protoc Bioinformatics 44:1.23.21–1.23.26. https://doi.org/10.1002/0471250953.bi0123s44
30. Clima R, Preste R, Calabrese C, Diroma MA, Santorsola M, Scioscia G, Simone D, Shen L et al (2017) HmtDB 2016: data update, a better performing query system and human mitochondrial DNA haplogroup predictor. Nucleic Acids Res 45(D1):D698–d706. https://doi.org/10.1093/nar/gkw1066
31. Putz J, Dupuis B, Sissler M, Florentz C (2007) Mamit-tRNA, a database of mammalian mitochondrial tRNA primary and secondary structures. RNA (New York, NY) 13(8):1184–1190. https://doi.org/10.1261/rna.588407
32. Castellana S, Ronai J, Mazza T (2015) MitImpact: an exhaustive collection of pre-computed pathogenicity predictions of human mitochondrial non-synonymous variants. Hum Mutat 36(2):E2413–E2422. https://doi.org/10.1002/humu.22720
33. Sonney S, Leipzig J, Lott MT, Zhang S, Procaccio V, Wallace DC, Sondheimer N (2017) Predicting the pathogenicity of novel variants in mitochondrial tRNA with MitoTIP. PLoS Comput Biol 13(12):e1005867. https://doi.org/10.1371/journal.pcbi.1005867
34. Navarro-Gomez D, Leipzig J, Shen L, Lott M, Stassen AP, Wallace DC, Wiggs JL, Falk MJ, van Oven M, Gai X (2015) Phy-Mer: a novel alignment-free and reference-independent mitochondrial haplogroup classifier. Bioinformatics 31(8):1310–1312. https://doi.org/10.1093/bioinformatics/btu825
35. Madji Hounoum B, Mavel S, Coque E, Patin F, Vourc'h P, Marouillat S, Nadal-Desbarats L, Emond P et al (2017) Wildtype motoneurons, ALS-linked SOD1 mutation and glutamate profoundly modify astrocyte metabolism and lactate shuttling. Glia 65(4):592–605. https://doi.org/10.1002/glia.23114
36. Volonte C, Apolloni S, Parisi C, Amadio S (2016) Purinergic contribution to amyotrophic lateral sclerosis. Neuropharmacology 104:180–193. https://doi.org/10.1016/j.neuropharm.2015.10.026

37. Angermuller S, Islinger M, Volkl A (2009) Peroxisomes and reactive oxygen species, a lasting challenge. Histochem Cell Biol 131(4):459–463. https://doi.org/10.1007/s00418-009-0563-7
38. Ames BN, Cathcart R, Schwiers E, Hochstein P (1981) Uric acid provides an antioxidant defense in humans against oxidant- and radical-caused aging and cancer: a hypothesis. Proc Natl Acad Sci U S A 78(11):6858–6862
39. Sautin YY, Johnson RJ (2008) Uric acid: the oxidant-antioxidant paradox. Nucleosides, Nucleotides Nucleic Acids 27(6):608–619. https://doi.org/10.1080/15257770802138558
40. Fang P, Li X, Luo JJ, Wang H, Yang XF (2013) A double-edged sword: uric acid and neurological disorders. Brain Disord Ther 2(2): 109. https://doi.org/10.4172/2168-975x.1000109
41. Huang TT, Hao DL, Wu BN, Mao LL, Zhang J (2017) Uric acid demonstrates neuroprotective effect on Parkinson's disease mice through Nrf2-ARE signaling pathway. Biochem Biophys Res Commun 493(4):1443–1449. https://doi.org/10.1016/j.bbrc.2017.10.004
42. Bakshi R, Xu Y, Mueller KA, Chen X, Granucci E, Paganoni S, Sadri-Vakili G, Schwarzschild MA (2018) Urate mitigates oxidative stress and motor neuron toxicity of astrocytes derived from ALS-linked SOD1(G93A) mutant mice. Mol Cell Neurosci 92: 12–16. https://doi.org/10.1016/j.mcn.2018.06.002
43. Lazzarino G, Amorini AM, Petzold A, Gasperini C, Ruggieri S, Quartuccio ME, Di Stasio E, Tavazzi B (2017) Serum compounds of energy metabolism impairment are related to disability, disease course and neuroimaging in multiple sclerosis. Mol Neurobiol 54(9):7520–7533. https://doi.org/10.1007/s12035-016-0257-9
44. Persky AM, Brazeau GA (2001) Clinical pharmacology of the dietary supplement creatine monohydrate. Pharmacol Rev 53(2): 161–176
45. Li H, Tang Z, Chu P, Song Y, Yang Y, Sun B, Niu M, Qaed E et al (2018) Neuroprotective effect of phosphocreatine on oxidative stress and mitochondrial dysfunction induced apoptosis in vitro and in vivo: Involvement of dual PI3K/Akt and Nrf2/HO-1 pathways. Free Radic Biol Med 120:228–238. https://doi.org/10.1016/j.freeradbiomed.2018.03.014
46. Vallee A, Lecarpentier Y, Guillevin R, Vallee JN (2018) Aerobic glycolysis in amyotrophic lateral sclerosis and Huntington's disease. Rev Neurosci 29(5):547–555. https://doi.org/10.1515/revneuro-2017-0075
47. Lu W, Su X, Klein MS, Lewis IA, Fiehn O, Rabinowitz JD (2017) Metabolite measurement: pitfalls to avoid and practices to follow. Annu Rev Biochem 86:277–304. https://doi.org/10.1146/annurev-biochem-061516-044952
48. Farooqui AA, Horrocks LA (2001) Plasmalogens, phospholipase A2, and docosahexaenoic acid turnover in brain tissue. J Mol Neurosci 16(2–3):263–272 discussion 279–284
49. Peters OM, Ghasemi M, Brown RH Jr (2015) Emerging mechanisms of molecular pathology in ALS. J Clin Invest 125(6):2548. https://doi.org/10.1172/jci82693
50. Luoma AM, Kuo F, Cakici O, Crowther MN, Denninger AR, Avila RL, Brites P, Kirschner DA (2015) Plasmalogen phospholipids protect internodal myelin from oxidative damage. Free Radic Biol Med 84:296–310. https://doi.org/10.1016/j.freeradbiomed.2015.03.012
51. Sindelar PJ, Guan Z, Dallner G, Ernster L (1999) The protective role of plasmalogens in iron-induced lipid peroxidation. Free Radic Biol Med 26(3–4):318–324
52. Blasco H, Veyrat-Durebex C, Bocca C, Patin F, Vourc'h P, Kouassi Nzoughet J, Lenaers G, Andres CR et al (2017) Lipidomics reveals cerebrospinal-fluid signatures of ALS. Sci Rep 7(1):17652. https://doi.org/10.1038/s41598-017-17389-9
53. Dodge JC, Treleaven CM, Pacheco J, Cooper S, Bao C, Abraham M, Cromwell M, Sardi SP et al (2015) Glycosphingolipids are modulators of disease pathogenesis in amyotrophic lateral sclerosis. Proc Natl Acad Sci U S A 112(26):8100–8105. https://doi.org/10.1073/pnas.1508767112
54. Ariga T, Jarvis WD, Yu RK (1998) Role of sphingolipid-mediated cell death in neurodegenerative diseases. J Lipid Res 39(1):1–16
55. Henriques A, Croixmarie V, Priestman DA, Rosenbohm A, Dirrig-Grosch S, D'Ambra E, Huebecker M, Hussain G et al (2015) Amyotrophic lateral sclerosis and denervation alter sphingolipids and up-regulate glucosylceramide synthase. Hum Mol Genet 24(25):7390–7405. https://doi.org/10.1093/hmg/ddv439
56. Arima H, Hanada M, Hayasaka T, Masaki N, Omura T, Xu D, Hasegawa T, Togawa D et al (2014) Blockade of IL-6 signaling by MR16-1 inhibits reduction of docosahexaenoic acid-containing phosphatidylcholine levels in a mouse model of spinal cord injury. Neuroscience 269:1–10. https://doi.org/10.1016/j.neuroscience.2014.03.012
57. Akbar M, Calderon F, Wen Z, Kim HY (2005) Docosahexaenoic acid: a positive modulator of Akt signaling in neuronal survival. Proc Natl Acad Sci U S A 102(31):10858–10863. https://doi.org/10.1073/pnas.0502903102
58. Hong S, Gronert K, Devchand PR, Moussignac RL, Serhan CN (2003) Novel docosatrienes and 17S-resolvins generated from docosahexaenoic acid in murine brain, human blood, and glial cells. Autacoids in anti-inflammation. J Biol Chem 278(17):14677–14687. https://doi.org/10.1074/jbc.M300218200
59. Devall M, Mill J, Lunnon K (2014) The mitochondrial epigenome: a role in Alzheimer's disease? Epigenomics 6(6):665–675. https://doi.org/10.2217/epi.14.50
60. Hua S, Lu C, Song Y, Li R, Liu X, Quan F, Wang Y, Liu J et al (2012) High levels of mitochondrial heteroplasmy modify the development of ovine-bovine interspecies nuclear transferred embryos. Reprod Fertil Dev 24(3):501–509. https://doi.org/10.1071/rd11091
61. Stoccoro A, Mosca L, Carnicelli V, Cavallari U, Lunetta C, Marocchi A, Migliore L, Coppede F (2018) Mitochondrial DNA copy number and D-loop region methylation in carriers of amyotrophic lateral sclerosis gene mutations. Epigenomics 10:1431–1443. https://doi.org/10.2217/epi-2018-0072

Article Scientifique Complémentaire N°2

Published in

Journal of Clinical Investigation

Volume 129, Issue 4 on April 1, 2019

Virus-mediated delivery of antibody targeting TAR DNA-binding protein-43 mitigates associated neuropathology

S. Pozzi[1], S. Thammisetty[1], P. Codron[1,2], R. Rahimian[1], K. Plourde[1], G. Soucy[1], C. Bareil[1], D. Phaneuf[1], J. Kriz[1,3], C. Gravel[1,3], J.-P. Julien[1,3]

1. CERVO Brain Research Institute, Québec City G1J 2G3, Canada.

2. UMR CNRS 6015, INSERM U1083, University of Angers, Angers Cedex 9, France.

3. Department of Psychiatry and Neuroscience, University of Laval, Québec City G1V 0A6, Canada.

Virus-mediated delivery of antibody targeting TAR DNA-binding protein-43 mitigates associated neuropathology

Silvia Pozzi,[1] Sai Sampath Thammisetty,[1] Philippe Codron,[1,2] Reza Rahimian,[1] Karine Valérie Plourde,[1] Geneviève Soucy,[1] Christine Bareil,[1] Daniel Phaneuf,[1] Jasna Kriz,[1,3] Claude Gravel,[1,3] and Jean-Pierre Julien[1,3]

[1]CERVO Brain Research Centre, Québec, Québec, Canada. [2]MITOVASC Institute, Centre National de la Recherche Scientifique (CNRS) 6015, INSERM U1083, University of Angers, Angers, France. [3]Department of Psychiatry and Neuroscience, Université Laval, Québec City, Québec, Canada.

The cytoplasmic aggregation of TAR DNA-binding protein-43 (TDP-43) is a hallmark of degenerating neurons in amyotrophic lateral sclerosis (ALS) and subsets of frontotemporal dementia (FTD). In order to reduce TDP-43 pathology, we generated single-chain (scFv) antibodies against the RNA recognition motif 1 (RRM1) of TDP-43, which is involved in abnormal protein self-aggregation and interaction with p65 NF-κB. Virus-mediated delivery into the nervous system of a scFv antibody, named VH7Vk9, reduced microgliosis in a mouse model of acute neuroinflammation and mitigated cognitive impairment, motor defects, TDP-43 proteinopathy, and neuroinflammation in transgenic mice expressing ALS-linked TDP-43 mutations. These results suggest that antibodies targeting the RRM1 domain of TDP-43 might provide new therapeutic avenues for the treatment of ALS and FTD.

Introduction

Amyotrophic lateral sclerosis (ALS) is a fatal neurodegenerative disease characterized by the selective degeneration of both upper and lower motor neurons. Middle-aged patients (average age of 55 years) present to the clinician with main muscle–related symptomatology. The disease then progresses to muscle atrophy followed by complete paralysis, and death generally occurs by respiratory failure 3 to 5 years after symptom onset. Diagnosis, which is still based on clinical evaluations, aims to exclude other disorders that resemble ALS and is thus often delayed by about 1 year from the first appearance of symptoms (1, 2). Ninety percent of patients with ALS have sporadic-origin ALS (sALS), while ten percent have familial inherited mutations (fALS) (1, 3).

TAR DNA-binding protein 43 (TDP-43) is a DNA/RNA-binding protein that is highly and ubiquitously expressed, with main localization in the cell nucleus (4). Thanks to its 2 RNA recognition domains (RRM1 and RRM2), the protein is a multifunctional factor involved in different aspects of RNA metabolism such as transcription, splicing, stabilization, and transport (4). Although mutations in TDP-43 are very rare, occurring in 3% of patients with fALS and 1.5% of those with sALS, more than 90% of ALS cases (fALS and sALS) show a pathological behavior of this protein called TDP-43 proteinopathy (4, 5). This event was first described in 2006 (6) as a consistent mislocalization and aggregation of the protein in the cytoplasm where TDP-43 can form hyperphosphorylated, fragmented, and ubiquitinated inclusions that impair the physiological function of the protein (6–8). TDP-43 proteinopathy is not exclusive to ALS disease. It is in fact present in 50% of patients with frontotemporal lobar dementia (FTLD) (5, 9). FTLD, also referred to as frontotemporal dementia (FTD), is a midlife-onset disease that is clinically heterogeneous and characterized by changes in behavior, personality, and/or language (9). Because of TDP-43 proteinopathy, ALS and FTD are now considered a disease continuum, with 50% of ALS patients presenting with cognitive impairment (15%–20% recognized as FTD) and 15% of FTD patients having motor impairments (3, 5). Interestingly, TDP-43 proteinopathy has also been observed in other neurodegenerative disorders such as Alzheimer's disease (AD), Parkinson's disease (PD), and Huntington's disease (HD) (4, 10).

Different studies have highlighted the sensitivity of the RRM1 domain in inducing TDP-43 proteinopathy. Oxidation or misfolding of this domain results in cytosolic mislocalization with irreversible protein aggregation (11, 12). Apart from RNA metabolism, the RRM1 domain is also responsible for the interaction between TDP-43 and the p65 subunit of NF-κB (13). This interaction mediates overactivation of the NF-κB pathway, which induces an increased vulnerability of neurons to toxic injuries and a hyperactive inflammatory response of glial cells (13). Both TDP-43 and p65 proteins are overexpressed in patients with sALS (13, 14), and the downregulation of TDP-43 can reduce NF-κB activation (13).

Here, we describe the generation of single-chain (scFv) antibodies specifically against the RRM1 domain of TDP-43, with the dual aim to (a) block TDP-43–p65 interaction and thereby reduce NF-κB activation, and (b) interfere with protein aggregation. Single-chain antibodies are small molecules made by the linking of

Conflict of interest: JPJ, CG, and SP are owners of US patent application no. 15/532,909 titled "TDP-43-binding polypeptides useful for the treatment of neurodegenerative diseases." JPJ is chief scientific officer of ImStar Therapeutics.

Submitted: July 31, 2018; **Accepted:** January 15, 2019.
Reference information: *J Clin Invest.* https://doi.org/10.1172/JCI123931.

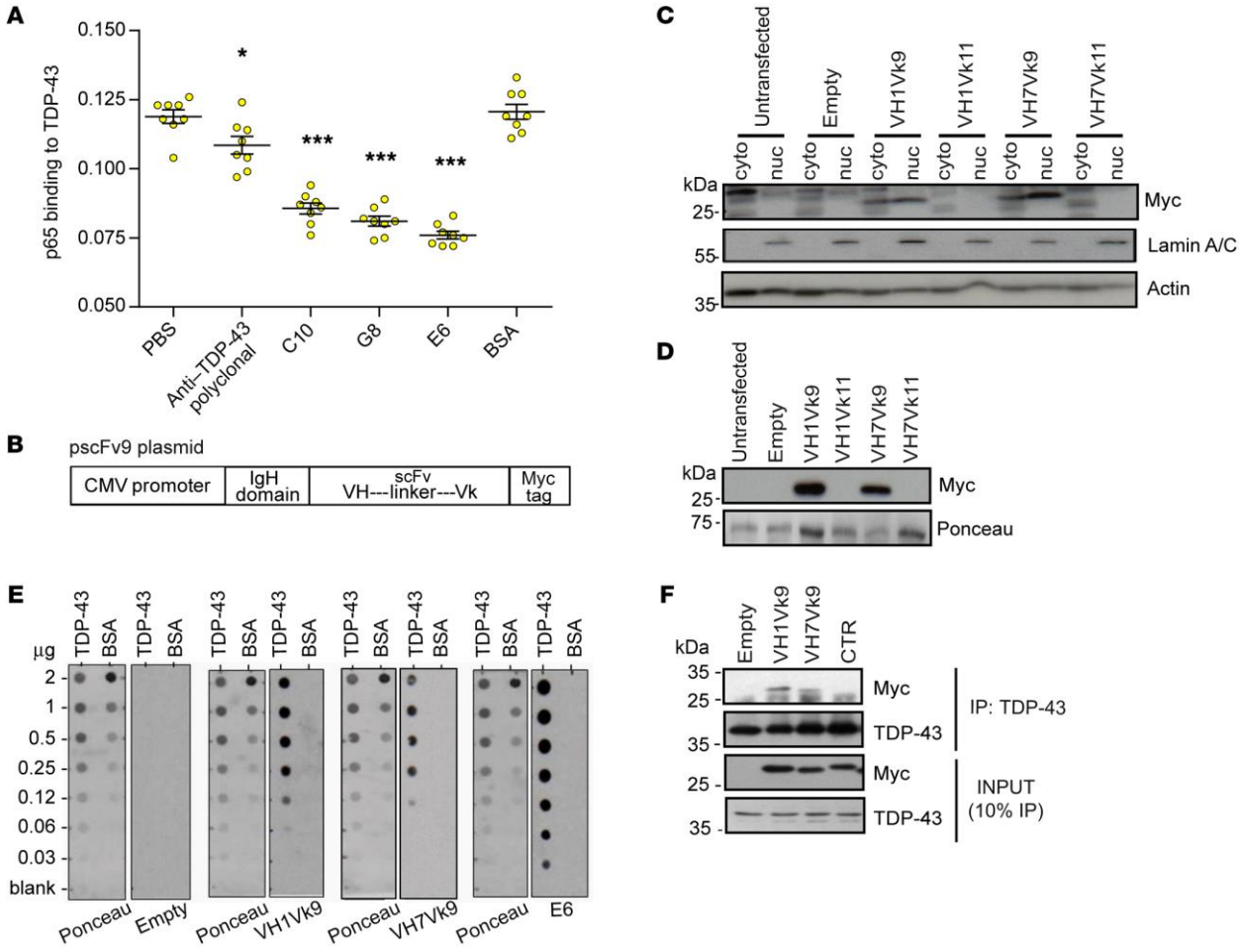

Figure 1. E6-derived scFv antibodies are able to recognize TDP-43. (**A**) Binding of p65 to TDP-43 was measured in the presence of PBS or anti–TDP-43 N-terminal antibody (Proteintech), monoclonal antibodies against RRM1 TDP-43 (named C10, G8, and E6), or BSA. *n* = 8 wells per condition (dots). One-way ANOVA $P < 0.0001$; $^{*}P < 0.05$ and $^{***}P < 0.001$ versus PBS, by Tukey's multiple comparisons test. Data represent the mean ± SEM. (**B**) Schematic representation of the pscFv9 plasmid used for scFv production and expression. (**C**) Representative Western blot of cytoplasmic and nuclear fractions of Hek293 cells. Anti-Myc antibody revealed scFv and laminin A/C or actin in the different fractions. (**D**) Representative image of media from transfected Hek293 cells probed with anti-Myc antibody. Ponceau staining was used as a reference. (**E**) Different concentrations of TDP-43 (1–206 aa, Proteintech) or BSA were loaded onto a dot blot membrane. Immunoblots were performed with media containing pscFv9-transfected Hek293 cells and E6 monoclonal antibody. Signals were revealed with anti–Myc-HRP antibody for scFv conditions or anti–mouse HRP for E6. Ponceau staining was used as a reference. (**F**) Representative blot of TDP-43 immunoprecipitation in pscFv9-transfected Hek293 cells. Experiments in **C**, **D**, and **F** were conducted more than 3 times. Empty, no scFv; CTR, control D1.3 scFv.

variable heavy and light chains of the antigen-binding domain of an antibody (15). Given their small size, good tissue penetration, and low immunogenicity (16), scFv antibodies have been produced for different neurodegenerative disorders such as AD (17–20), Lewy body disease, PD (21, 22), HD (23, 24), and ALS (25–27). We report for the first time to our knowledge the in vivo therapeutic effects of a scFv antibody against TDP-43 in transgenic mouse models of ALS/FTD.

Results

Selection of monoclonal antibodies against the RRM1 domain of TDP-43. We generated monoclonal antibodies against the RRM1 domain of TDP-43, because this domain contributes to protein aggregation (11, 12) and to the interaction with p65 NF-κB (13). Among 8 hybridoma clones produced, only 3 of them, named C10, G8, and E6, were able to clearly detect TDP-43 on immunoblots after SDS-PAGE (Supplemental Figure 1A; supplemental material available online with this article; https://doi.org/10.1172/JCI123931DS1). We then examined the ability of these 3 antibodies to disrupt the interaction between TDP-43 and p65 NF-κB. We performed an ELISA with human recombinant TDP-43 and human recombinant p65 protein (Supplemental Figure 1B). The results revealed that the 2 proteins have a direct interaction that is TDP-43 dose dependent. Using the same ELISA system, we incubated p65 recombinant protein together with a fixed amount of monoclonal antibodies against the RRM1 domain of TDP-43 (Fig-

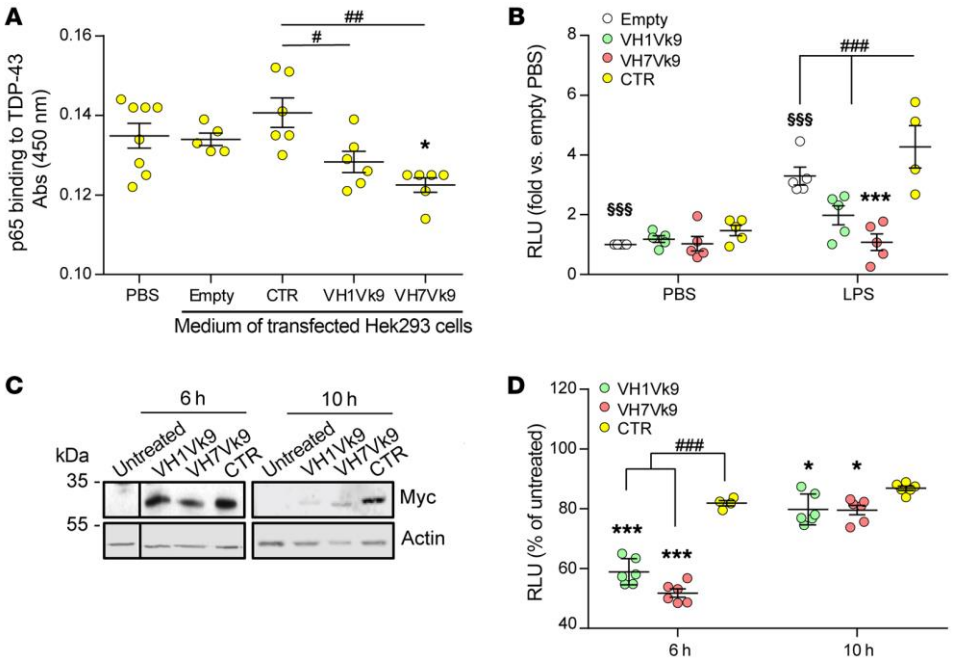

Figure 2. ScFv antibodies disrupt the interaction between TDP-43 and p65 and reduce NF-κB activity. (**A**) Binding of p65 to TDP-43 was measured in the presence of equal volumes of PBS or media from pscFv9-transfected Hek293cells. n = 5–8 wells per condition (dots). One-way ANOVA P = 0.002; $^{*}P < 0.05$ versus PBS; $^{\#}P < 0.05$ or $^{\#\#}P < 0.001$ versus control scFv by Tukey's multiple comparisons test. (**B**) BV2 cells were transfected with pscFv9, stimulated with LPS or PBS, and lysated for the luciferase assay. n = 4–5 individual experiments (dots). Two-way ANOVA P = 0.0002; $^{§§§}P < 0.001$ versus LPS; $^{***}P < 0.001$ versus empty; and $^{\#\#\#}P < 0.001$ versus control scFv, by Tukey's multiple comparisons test. (**C** and **D**) BV2 p65-luc cells were treated or not for 6 hours or 10 hours with scFv antibodies, together with 4 hours of LPS treatment. (**C**) Representative Western blots of total lysates of Myc-tag scFv inside the cells and actin (n = 3 pooled experiments). The blot of the untreated cells at 6 hours was run on the same gel but was noncontiguous. (**D**) NF-κB activity assessed by luciferase assay. n = 4–6 replicates (dots) from 2 independent experiments (2–3 wells each). Two-way ANOVA $P < 0.0001$; $^{*}P < 0.05$ and $^{***}P < 0.001$ versus untreated cells; $^{\#\#\#}P < 0.001$ versus control scFv, by Tukey's multiple comparisons test. Data represent the mean ± SEM. RLU, relative luminescence units; CTR, control D1.3 scFv.

ure 1A). All 3 of the selected monoclonal antibodies against RRM1 were able to disrupt TDP-43/p65 interaction more efficiently than the polyclonal antibody against the TDP-43 N-terminal. Among our monoclonal antibodies, the E6 clone was the most effective at interfering with the binding. Therefore, we derived scFv antibodies from this monoclonal antibody.

Production and characterization of E6-derived single-chain antibodies. Reverse transcription PCR (RT-PCR) of cDNA from E6 hybridoma cells using degenerative primers led to production of 2 different heavy chains, named VH1 and VH7, and 2 different light chains, named Vk9 and Vk11. Four different plasmids were therefore produced encoding all different combinations of heavy and light chains purified from the E6 clone. Figure 1B shows a schematic representation of the plasmid (pscFv9) (26) used for the production of scFv antibodies. The plasmid contains a CMV promoter, an IgH domain for proper folding and secretion, a single-chain antibody made of variable heavy and light chains, and a human c-Myc tag for immunodetection. As shown in Figure 1C, two plasmids encoding for VH1Vk9 and VH7Vk9 fusion proteins were able to yield the expression of scFv antibodies in transfected human embryonic kidney 293 (Hek293) cells. The scFv antibody was detected in both nuclear and cytoplasmic fractions. The recombinant scFv antibodies were also secreted into the medium (Figure 1D). From the same clone, we therefore produced 2 different scFv antibodies against the TDP-43 RRM1 domain. Both antibodies shared the same variable light chain VK9 but had 1-aa difference in the heavy chain, with VH1 owning a glutamic acid (E) after the cloning site and VH7 having a glutamine (Q) in the same position (Supplemental Figure 1C) (GenBank accession numbers MK210239 and MK210240).

To test the ability of the scFv antibodies to bind TDP-43, we used the medium of vector-transfected cells as a source of scFv antibodies. Different concentrations of TDP-43 peptide (1–206 aa containing RRM1) or BSA were applied on a dot blot membrane and probed with the medium of transfected cells. Figure 1E shows that the media containing VH1Vk9 or VH7Vk9 were able to detect TDP-43 specifically, whereas no cross-reaction was observed on spots loaded with BSA, confirming the specificity of the scFv antibody in recognizing only TDP-43. Full-length E6 antibody was used as a positive control, confirming the ability of the monoclonal antibody to recognize TDP-43. The specific interaction between scFv and TDP-43 was also confirmed by immunoprecipitation of TDP-43 from Hek293-transfected cells expressing scFv antibodies (Figure 1F). A clear band for the scFv (c-Myc–tagged) at 28 kDa was indeed detectable when cells were transfected with E6-derived scFv VH1Vk9 and VH7Vk9. This band was absent in cells transfected with the empty plasmid or in cells transfected with a control scFv (D1.3) encoding for a scFv antibody against

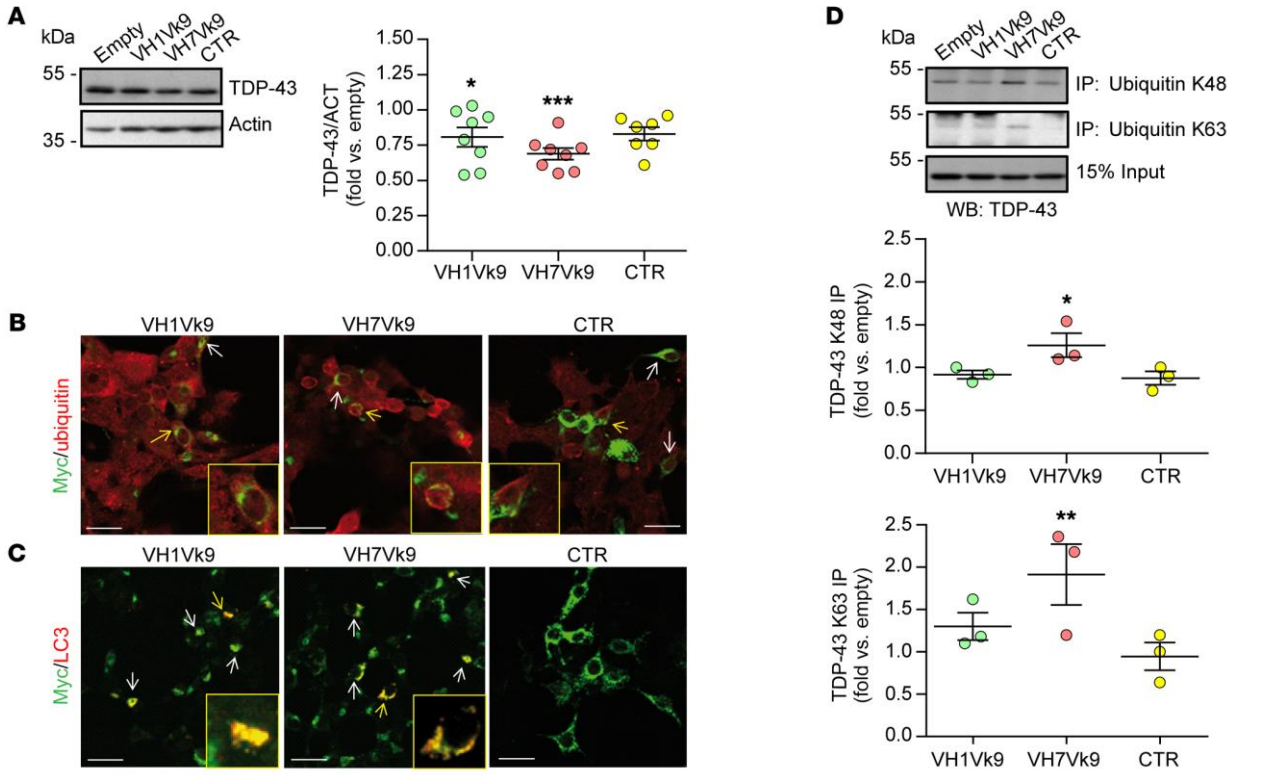

Figure 3. ScFv antibodies mediate TDP-43 degradation. (**A**) Representative blot and quantification of TDP-43 levels in Hek293 cells transfected with pscFv9 plasmid. Graph shows quantification of TDP-43 normalized to actin and expressed as the fold change versus empty vector. n = 7–9 independent experiments (dots). One-way ANOVA $P = 0.0003$; $^{*}P < 0.05$ and $^{***}P < 0.0001$ versus empty transfected, by Tukey's multiple comparisons test. (**B** and **C**) Representative merged images of colocalization between scFv (Myc, green) and ubiquitin or LC3 (red). Arrows show cells with colocalization; yellow arrows indicate cells enlarged 2.5 times in the insets. Scale bars: 20 μm. The experiment was performed twice. (**D**) Representative blots and quantification of immunoprecipitation for all K48-polyubiquitinated (proteasome) or K63-polyubiquitinated (autophagy) proteins and Western blot for TDP-43. Graphs indicate the quantification of TDP-43 signal in immunoprecipitation experiments, expressed as the fold change versus empty vector. n = 3 independent experiment (dots). K63-ubiquitinated TDP-43: $P = 0.0082$, by 1-way ANOVA; $^{**}P < 0.01$ versus empty vector–transfected cells, by Dunnett's multiple comparisons test. K48-ubiquitinated TDP-43: $P = 0.0128$, by 1-way ANOVA; $^{*}P < 0.05$ versus empty vector–transfected cells, by Dunnett's multiple comparisons test. Data represent the mean ± SEM. Empty, no scFv (**A** and **D**); CTR, D1.3 scFv (**B** and **C**) or 8H11 anti-GFP scFv (**A** and **D**).

chicken lysozyme. Immunoprecipitation of TDP-43 from nuclear and cytoplasmic fractions of transfected cells revealed that the binding of VH1Vk9 or VH7Vk9 to TDP-43 occurred predominantly in the cytoplasm (Supplemental Figure 1D).

Since the scFv antibodies were generated against the RRM1 domain of TDP-43, we examined whether the binding of scFv antibodies altered the ability of TDP-43 to bind RNAs. Thus, we performed UV cross-linking immunoprecipitation (UV-CLIP) experiments in pscFv9-transfected Hek293 cells and verified the ability of TDP-43 protein to bind its own RNA (28) in the presence of the scFv antibodies. As shown in Supplemental Figure 1E, only the presence of VH1Vk9 antibody was able to reduce the binding between the protein and the RNA, whereas no alterations were observed in the presence of VH7Vk9 antibody.

Single-chain antibodies reduced p65 NF-κB activation. To determine whether E6-derived scFv antibodies against TDP-43 were able to disrupt the interaction between p65 NF-κB and TDP-43, we performed an ELISA, in which human recombinant p65 was incubated with media of transfected cells containing scFv antibodies (Supplemental Figure 2A). Figure 2A shows that both VH1Vk9 and VH7Vk9 were able to disrupt the protein-protein interaction between TDP-43 and p65. We then examined the effect on NF-κB activity of scFv antibodies against TDP-43 in BV2 cells harboring a NF-κB–luciferase reporter gene (29). BV2 cells were transfected with scFv vectors or controls and stimulated for 4 hours with LPS or PBS (Figure 2B). We observed that NF-κB activity was strongly increased after LPS treatment in empty and control scFv vector–transfected cells, whereas activation was reduced in the presence of VH1Vk9 and VH7Vk9 antibodies. It is well established that microglia-induced toxicity toward neurons is strongly dependent on microglial NF-κB activation (13, 30). Therefore, we tested the effect of these scFv antibodies in such a paradigm. As shown in Supplemental Figure 2B, expression of VH7Vk9 scFv in LPS-treated BV2 cells rescued the toxicity of microglial medium toward N2A neuronal cells.

Since the scFv antibodies can be secreted from transfected cells, we examined whether VH1Vk9 or VH7Vk9 scFv antibodies were able to penetrate cells and inhibit NF-κB activity. We first purified these scFv antibodies from media of Hek293-transfected cells. The preparation yielded a single 28-kDa protein detectable by Coomassie

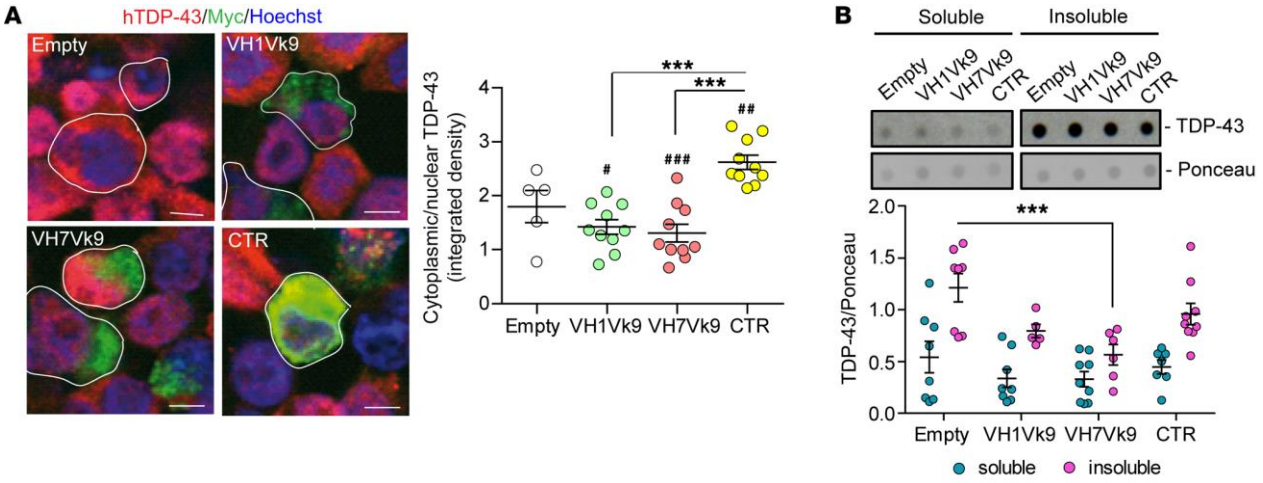

Figure 4. ScFv antibodies reduce TDP-43 mislocalization and aggregation. (**A**) Representative enlarged images and TDP-43 mislocalization determined by quantification of the integrated density of TDP-43 immunoreactivity in nuclear and cytoplasmic compartments. Images show merged scFv (Myc, green), hTDP-43 (red), and Hoechst (nuclei, blue) channels, and lines circumscribe the perimeter of the representative cells. Scale bars: 5 μm. Data in the graph represent the cytoplasmic to nuclear ratio quantified in at least 200 cells per frame. n = 5–10 different frames (dots) analyzed from 2 independent experiments. One-way ANOVA $P < 0.0001$; $^{***}P < 0.001$ versus control-transfected cells; $^{\#}P < 0.05$ and $^{\#\#\#}P < 0.001$ versus empty vector–transfected cells, by Tukey's multiple comparisons test. (**B**) Representative image and quantification of dot blot analysis for soluble or insoluble TDP-43 in transfected Hek293 cells treated with 50 μM EA. Data represent TDP-43 immunoreactivity normalized to Ponceau from 5 to 9 replicates (dots) from 3 independent experiments. Two-way ANOVA interaction $P = 0.249$, scFv $P = 0.0014$, and soluble/insoluble $P < 0.0001$; $^{***}P < 0.001$ versus empty vector–transfected cells, by Tukey's multiple comparisons test. Data represent the mean ± SEM. Empty, no scFv, CTR, control D1.3 scFv.

blue after SDS-PAGE and anti-Myc antibody (Supplemental Figure 2, C and D). The purified scFv antibodies were added to the medium (5 μg/ml) of BV2 p65-luciferase cells for 6 or 10 hours, together with 4 hours of LPS treatment, and NF-κB activity was then measured (Supplemental Figure 2E). In extracts of cells treated with scFv antibodies, we were able to detect a band corresponding to the intracellular scFv antibody at 6 hours and, to a lesser extent, after 10 hours of treatment (Figure 2C). The levels of intracellular VH1Vk9 or VH7Vk9 scFv antibodies were associated with a reduction of NF-κB activity (Figure 2D). These results indicate that scFv antibodies are able to penetrate cells and exert functional effects.

Single-chain antibodies drove TDP-43 to proteasome- and autophagy-mediated degradation. Transfection of E6-derived vectors encoding scFv antibodies in Hek293 cells led to a decrease in total cellular levels of TDP-43 compared with empty vector–transfected cells (Figure 3A). This reduction was not sufficient to affect cell viability (Supplemental Figure 3A). We then questioned the mechanism underlying the reduction of TDP-43 levels mediated by single-chain antibodies. First, we considered the possibility that secreted scFv could facilitate the release of TDP-43 into the medium. As expected, we found that scFv antibodies localized mainly in the cytoplasm with the *trans*-Golgi network where proteins are processed for secretion (Supplemental Figure 3B). However, our results revealed no changes in the levels of TDP-43 in the media due to expression of VH1Vk9 or VH7Vk9 scFv antibodies (data not shown). As an alternative mechanism, we investigated whether intracellular scFv antibodies, binding to TDP-43, might promote its degradation via proteasomal or autophagic pathways (31, 32). This idea was supported by our finding that scFv antibodies partially colocalized with ubiquitin and LC3 in Hek293 cells (Figure 3, B and C, and Supplemental 3, C and D). Moreover, VH1Vk9 and VH7Vk9 scFv antibodies were coimmunoprecipitated with K48 or K63 polyubiquitinated proteins, which are destined for proteasomal and autophagic degradation, respectively (Supplemental Figure 4A). Using the same immunoprecipitation method, we found that expression of VH7Vk9 scFv stimulated the K63 and K48 polyubiquitination of TDP-43 (Figure 3D). We confirmed the degradative pathways by treating cells with an autophagy inhibitor (bafilomycin) or a proteasome inhibitor (MG-132) (Supplemental Figure 4, B and C). Interestingly, we found that the levels of TDP-43 were increased in the presence of VH1Vk9 and VH7Vk9 scFv antibodies in the cells treated with bafilomycin (Supplemental Figure 4B), and the proteasome-mediated degradation of TDP-43 via VH7Vk9 scFv was confirmed by the accumulation of TDP-43 in the presence of MG-132 (Supplemental Figure 4C). Thus, these results suggest that intracellular scFv antibodies drive TDP-43 to degradation pathways, leading to a decrease in cytoplasmic TDP-43 levels.

Single-chain antibodies reduced TDP-43 mislocalization and aggregation. To assess the ability of scFv antibodies to reduce TDP-43 mislocalization and aggregation, we used a cell model system of TDP-43 proteinopathy that is based on oxidative stress caused by treatment with 50 μM ethacrynic acid (EA) in Hek293 cells (33). As shown in Supplemental Figure 5, A–C, treatment of Hek293 cells with EA increased oxidative stress and induced TDP-43 cytoplasmic mislocalization and aggregation. Remarkably, the presence of VH1Vk9 and VH7Vk9 scFv antibodies in transfected cells led to a reduction in cytoplasmic levels of TDP-43 detected by immunofluorescence microscopy (Figure 4A and Supplemental Figure 5D). Moreover, in the insoluble fractions prepared from cells treated with EA, TDP-43 levels were reduced by up to 50% in cells expressing VH7Vk9 scFv antibody (Figure 4B and Supplemental Figure 5E).

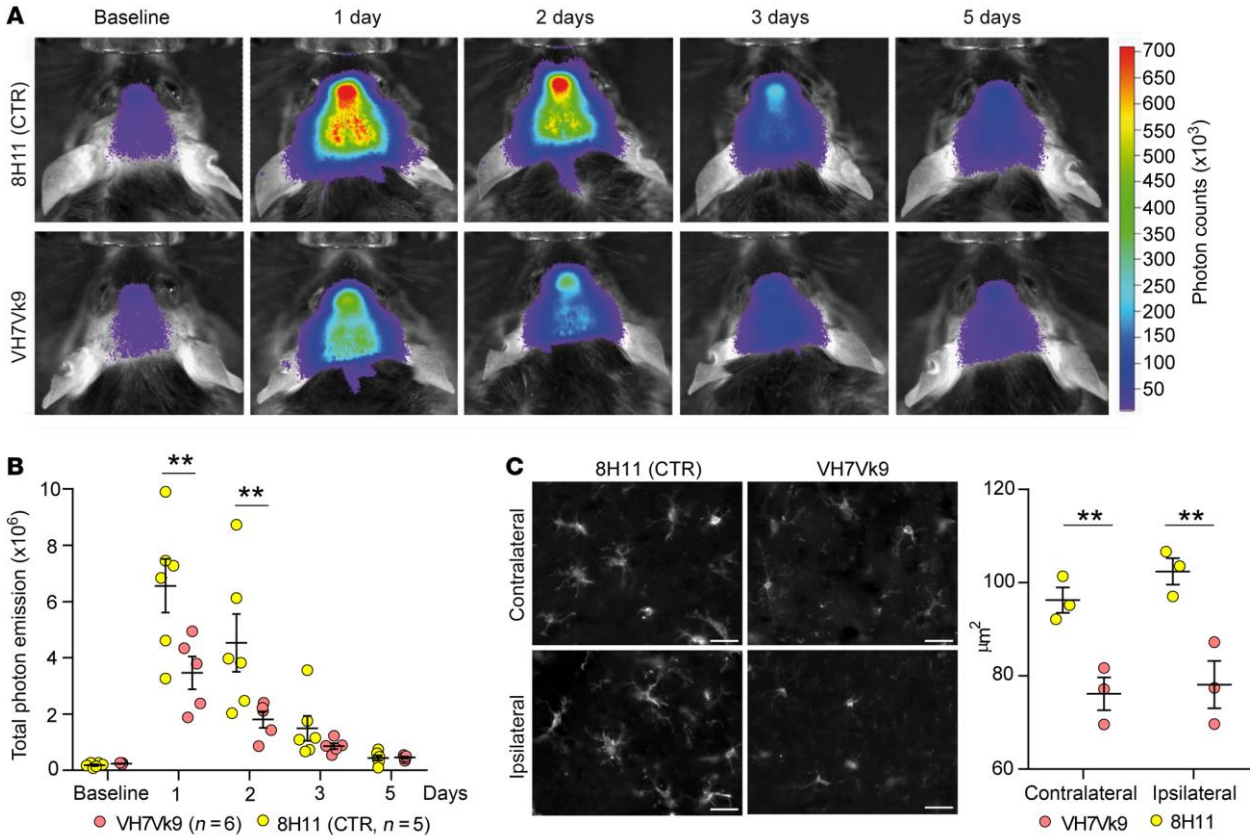

Figure 5. ScFv antibody reduces NF-κB activation in LPS-induced inflammation in vivo. (**A**) Real-time imaging of *TLR2*-luciferase response before (baseline) and 1 to 5 days after LPS injection and (**B**) relative quantification. Images of representative mouse brains previously injected with scAAV2/9 expressing control or VH7Vk9 scFv. Color scale calibration in photon counts (minimum 10,000, maximum 7.08×10^5). Graph shows quantification of photon emission. n = 5–6 individual mice. Two-way, repeated-measures ANOVA $P = 0.0004$; $^{**}P < 0.01$ versus VH7Vk9, by Sidak's multiple comparisons test. (**C**) Representative enlarged images of Iba1 staining and quantification of cell body size in contralateral and ipsilateral cortices of mice injected with scAAV2/9 and challenged with LPS. Graph shows quantification of Iba1$^+$ cells. n = 3 individual mice (dots). Two-way ANOVA interaction $P = 0.582$, hemisphere $P = 0.300$, and scFv $P = 0.0003$; $^{**}P < 0.01$, by Bonferroni's multiple comparisons test. Data represent the mean ± SEM. Scale bars: 25 μm. CTR, 8H11 scFv.

Virus-mediated expression of VH7Vk9 scFv antibody reduced microglial activation and NF-κB activity in an acute model of inflammation. Among the 2 single-chain antibodies, VH7Vk9 was more efficient at reducing NF-κB activity and TDP-43 proteinopathy in vitro. We therefore generated a scAAV2/9 viral vector encoding VH7Vk9 scFv (CMV promoter, IgH region and Myc tag included) to further investigate the effect of the antibody in vivo. As a control, we used a scAAV2/9 vector (named 8H11) encoding scFv against GFP.

Virus (1.5×10^{10} vg) was injected unilaterally into the cortex of mice (n = 5 control mice and n = 6 VH7Vk9-treated mice; 4 months of age) bearing the *TLR2*-luciferase transgene, a reporter of microglial activation (34). One month after virus delivery, mice were intraperitoneally injected with LPS, and *TLR2*-luciferase activity was monitored for 5 days (Supplemental Figure 6A). As shown in Figure 5, A and B, LPS injection induced strong luciferase activity in the brain after 1 and 2 days in control scAAV-treated mice. Remarkably, expression of VH7Vk9 scFv reduced *TLR2*-luciferase activity by almost 50% compared with activity induced by control scFv antibody. We repeated the experiment with age-matched nontransgenic mice (n = 3 per group) (Supplemental Figure 6B) and analyzed brain samples 24 hours after LPS injection. Quantification of ionized calcium–binding adaptor molecule 1 (Iba1) staining revealed a consistent reduction in microglial body size (Figure 5C) in the brains of mice treated with VH7Vk9 scFv when compared with control 8H11 scFv and a concomitant reduction in total staining (Supplemental Figure 6C). Interestingly, the effect on microglial cells was the same in ipsilateral and contralateral brain hemispheres, suggesting an effect of secreted scFv antibodies at a long distance from the site of viral injection. We performed a cytokine array on the ipsilateral cerebral cortex of the injected mice. All inflammatory factors significantly different from the control condition were found to be reduced by VH7Vk9 expression (Supplemental Figure 6D).

Virus-mediated expression of VH7Vk9 scFv antibody ameliorated cognitive deficits and TDP-43 pathology in TDP-43^{G348C} mice. We injected scAAV2/9 virus encoding VH7Vk9 or 8H11 (anti-GFP) scFv antibodies into transgenic mice expressing genomic fragments encoding human *TDP-43^{G348C}*, a mouse model that exhibits cytoplasmic accumulations of TDP-43 in neurons during aging

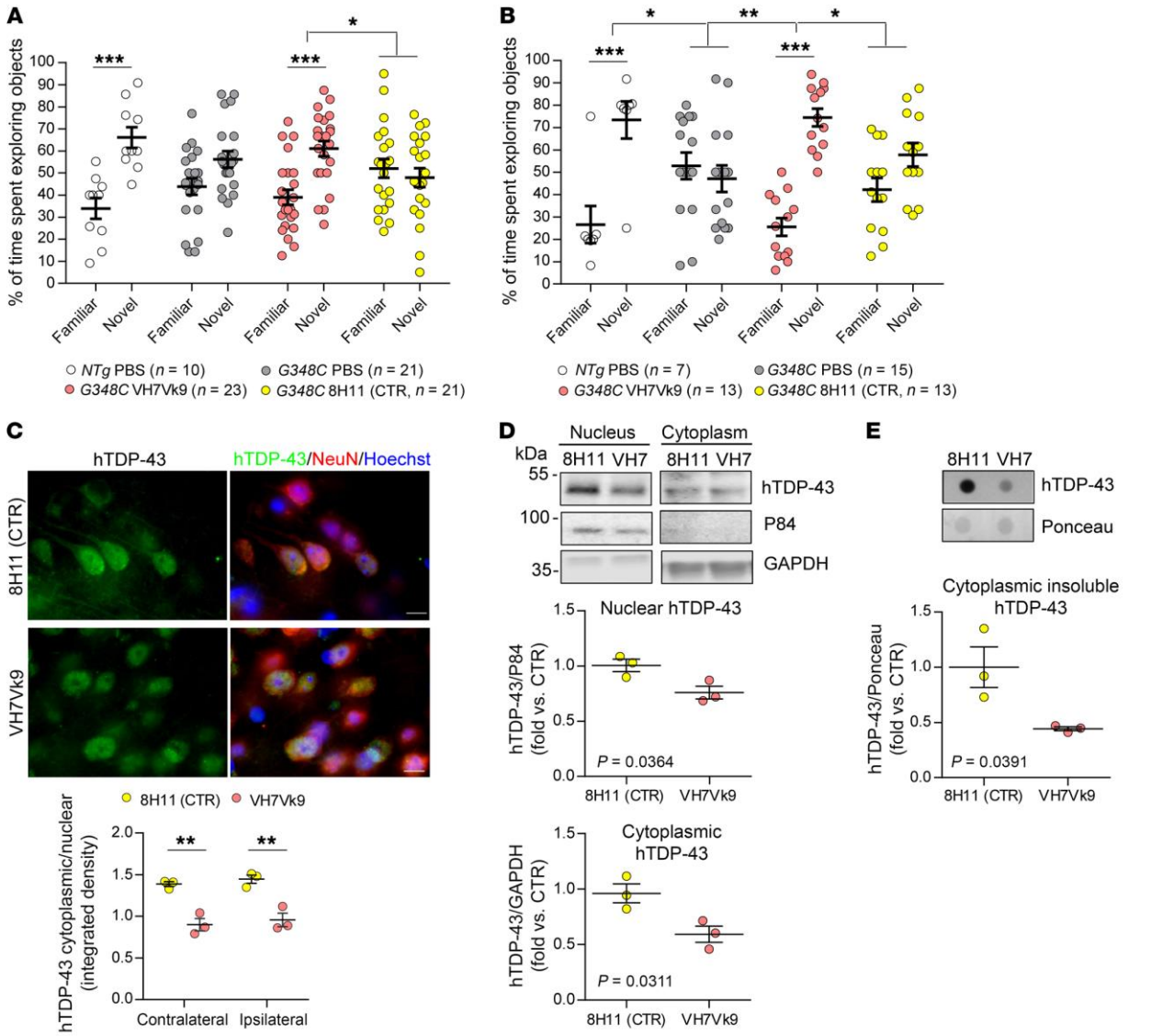

Figure 6. Intracortical injection of scAAV2/9 encoding for scFv antibody improves cognitive deficits and restores TDP-43 mislocalization in *TDP-43^{G348C}* mice. NOR test 2 months (**A**) and 4 months (**B**) after injection. Graphs in **A** and **B** show the percentage of time spent with objects and the number of individual mice tested (dots). (**A**) Two-way ANOVA $P = 0.0004$; ***$P < 0.001$ and *$P < 0.05$, by Sidak's multiple comparisons test. (**B**) Two-way ANOVA $P < 0.0001$; ***$P < 0.001$ for familiar versus novel object, by Sidak's multiple comparisons test; *$P < 0.05$ and **$P < 0.01$ among groups, by uncorrected Fisher's least significant difference (LSD) test. (**C**) Quantification of hTDP-43 mislocalization in cortical neurons and representative images. Data represent the cytoplasmic to nuclear ratio of TDP-43 integrated density. $n = 3$ individual mice (dots). Two-way ANOVA interaction $P = 0.979$, hemisphere $P = 0.3747$, scFv $P < 0.0001$; **$P < 0.01$ versus control scFv, by Sidak's multiple comparisons test. Shown are hTDP-43 (green) and merged images of hTDP-43, NeuN (red), and Hoechst (nuclei, blue). Scale bars: 20 μm. Representative blots and quantification of nuclear and cytoplasmic (**D**) and insoluble (**E**) hTDP-43 in ipsilateral cortices. $n = 3$ individual mice (dots). hTDP-43 was normalized to p84 or GAPDH fraction markers (**D**) and to Ponceau (**E**). Values are expressed as the fold change versus control scFv. Statistical analysis was done by unpaired *t* test. Data represent the mean ± SEM. CTR, 8H11 scFv.

(35). Eight-month-old *TDP-43^{G348C}* symptomatic mice were injected intracortically and unilaterally with scAAV2/9 viral vectors (9.2×10^9 vg) carrying virus coding for VH7Vk9 ($n = 23$ mice: 11 males and 12 females); virus bearing the control 8H11 scFv antibody ($n = 23$ mice: 11 males and 12 females); or PBS ($n = 24$ mice: 11 males and 13 females). We also injected nontransgenic (*NTg*) mice ($n = 6$ male and 4 females) with PBS as healthy controls for the behavioral tests. The mice were analyzed for cognitive changes at 2 and 4 months after virus injection. Immunohistochemical microscopy with anti-Myc antibody confirmed the expression of VH7Vk9 scFv antibody in brain cortex in neurons and microglial cells (data not shown).

Two and four months after injection, the novel object recognition (NOR) test was performed (Figure 6, A and B). The *TDP-43^{G348C}* mice (10 or 12 months of age) injected with PBS or control 8H11 scFv showed memory impairments, as they were unable to discriminate between novel and familiar objects. In contrast, *NTg* mice and

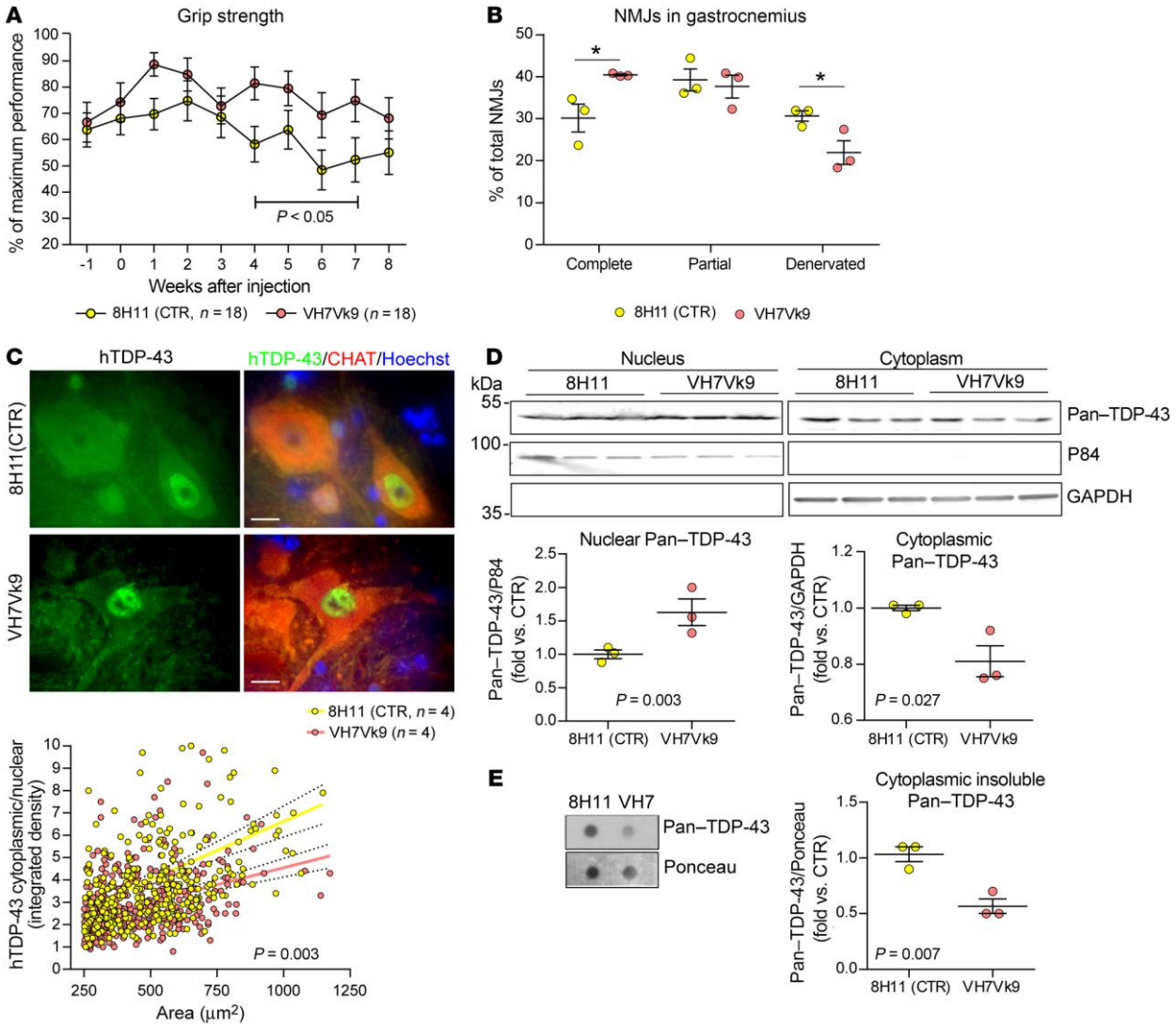

Figure 7. scAAV2/9-mediated delivery of scFv ameliorates motor performance and pathological defects in *TDP-43^{A315T}* mice. (**A**) Grip strength analysis showing the percentage of maximum performance of each single mouse and the number of individual mice (dots) analyzed. Two-way ANOVA corrected for repeated-measures interaction $P = 0.823$, time $P = 0.0512$, scFv $P < 0.0001$; $^*P < 0.05$ versus control scFv, by uncorrected Fisher's LSD. (**B**) Percentage of total NMJs. $n = 3$ individual mice (dots). Two-way ANOVA $P = 0.0063$; $^*P < 0.05$ versus control scFv, by uncorrected Fisher's LSD test. (**C**) Representative image and quantification of hTDP-43 (green) in motor neurons (CHAT, red) of lumbar spinal cord. The cytoplasmic to nuclear ratio of the TDP-43 integrated density of each cell was plotted according to the area of the cell. Data represent single-cell ratios (dots) analyzed from 4 individual mice. Solid line indicates the linear regression and dotted lines the 95% CIs. Slope diversity $P = 0.0033$. Scale bars: 10 µm. Representative blots and quantification of nuclear and cytoplasmic (**D**) and insoluble (**E**) pan–TDP-43 in lumbar spinal cord from 3 individual mice (dots). TDP-43 was normalized to p84 or GAPDH fraction markers (**D**) or to Ponceau (**E**), and values are expressed as the fold change versus control scFv. (**B**–**E**) Statistical significance was determined by unpaired *t* test. Data represent the mean ± SEM. CTR, 8H11 scFv.

TDP-43^{G348C} mice expressing VH7Vk9 scFv spent significantly more time with the novel object both 2 months (Figure 6A) and 4 months (Figure 6B) after virus injection, almost matching the results obtained with healthy nontransgenic mice intracortically injected with PBS. We analyzed brain tissue samples ($n = 3$ mice per group) by immunofluorescence microscopy to determine the distribution of human TDP-43 (hTDP-43) in cortical neurons. Neurons were visualized by NeuN staining, and cytoplasmic and nuclear TDP-43 was measured in each cell. The data revealed a reduction in cytoplasmic staining of hTDP-43 in VH7Vk9-expressing *TDP-43^{G348C}* mice, with an approximately 40% reduction of the cytoplasmic to nuclear ratio of hTDP-43 in both ipsilateral and contralateral cortical neurons (Figure 6C and Supplemental Figure 7A).

We performed Western blotting on nuclear and cytoplasmic fractions from ipsilateral cortices. As shown in Figure 6D, the analyses confirmed decreased levels of hTDP-43 in the cytoplasmic and nuclear fractions of VH7Vk9-expressing *TDP-43^{G348C}* mice. We also detected a reduction of insoluble cytoplasmic hTDP-

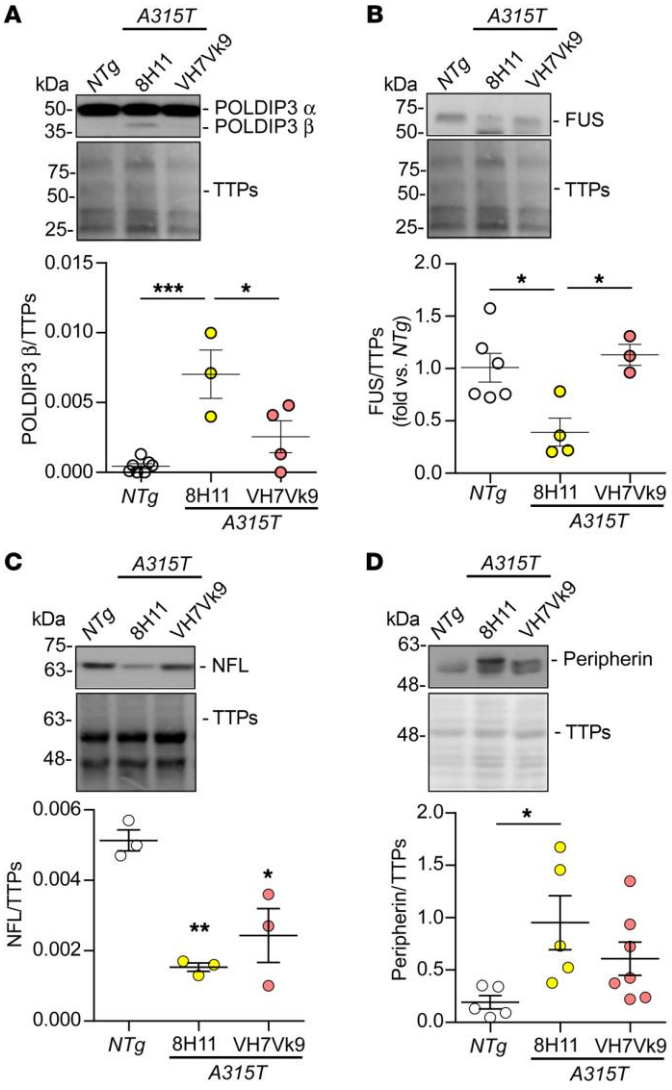

Figure 8. scAAV2/9-mediated delivery of scFv restores TDP-43 functions in the lumbar spinal cord of *TDP-43^{A315T}* mice. (**A**) Representative Western blot and quantification of nuclear POLDIP3 splicing in *NTg* (n = 7), *A315T* scAAV control–treated (n = 4), and *A315T* scAAV-VH7Vk9–treated (n = 4) individual mice (dots). One-way ANOVA P = 0.0008; ***P < 0.001 and *P < 0.05, by Tukey's multiple comparisons test. (**B**) Representative Western blot and quantification of nuclear FUS in *NTg* (n = 6), *A315T* scAAV control–treated (n = 4), and *A315T* scAAV-VH7Vk9–treated (n = 3) individual mice (dots). One-way ANOVA P = 0.0112; *P < 0.05, by Tukey's multiple comparisons test. Values are expressed as the fold change versus *NTg*. (**C**) Representative Western blot and quantification of cytoplasmic NFL in *NTg* (n = 3), *A315T* scAAV control–treated (n = 3), and *A315T* scAAV-VH7Vk9–treated (n = 3) individual mice (dots). One-way ANOVA P = 0.0042; **P < 0.01 and *P < 0.05, by Tukey's multiple comparisons test. (**D**) Representative Western blot and quantification of cytoplasmic peripherin in *NTg* (n = 5), *A315T* scAAV control–treated (n = 6), and *A315T* scAAV-VH7Vk9–treated (n = 7) individual mice (dots). One-way ANOVA P = 0.0392; *P < 0.05, by Tukey's multiple comparisons test. Protein levels were normalized to total transferred proteins (TTPs). Data represent the mean ± SEM. CTR, 8H11 scFv.

43 (Figure 6E). In addition to neuronal changes in the hTDP-43 pathology, we detected a reduction of microgliosis, observed by Iba1 staining, in both the ipsilateral and contralateral cortices of VH7Vk9 scFv–injected mice (Supplemental Figure 7B).

Finally, 4 months after injection, the open field test (OFT) showed that the VH7Vk9-injected TDP-43^{G34C} mice had less anxiety (Supplemental Figure 8A). Mice injected with VH7Vk9 were indeed able to remain in the center of the box for a longer period of time than the control scFv *TDP-43^{G348C}*–injected mice and for a duration nearly equivalent to that of nontransgenic mice that were intracortically injected with PBS. The cognitive improvements observed 4 months after injection correlated with reduced levels of insoluble hTDP-43 in the cerebral cortex of VH7Vk9-injected mice (Supplemental Figure 8B).

Virus-mediated expression of VH7Vk9 scFv antibody improved motor performance and reduced TDP-43 pathology in TDP-43^{A315T} mice. We also tested the effect of VH7Vk9 scFv in mice expressing a human genomic transgene encoding the *TDP-43^{A315T}* mutant (35). We injected 8-month-old *TDP-43^{A315T}* mice intrathecally with scAAV2/9 virus (5×10^{10} vg) expressing VH7Vk9 (n = 18 mice: 11 females and 7 males) or 8H11 anti-GFP control scFv (n = 18 mice: 11 females and 7 males). An inverted grid test was carried out to measure muscle strength over a period of 2 months after virus injection and revealed improved performance for VH7Vk9-treated *TDP-43^{A315T}* mice when compared with scAAV-8H11–injected mice (Figure 7A). No changes were observed in body weight (data not shown). In agreement with the improved motor strength observed, the VH7Vk9-expressing *TDP-43^{A315T}* mice exhibited better preservation of neuromuscular junctions (NMJs) (Figure 7B), with an increase of completely innervated junctions and a decrease of denervated junctions in the muscles analyzed. We then analyzed the lumbar spinal cords of the injected mice (n = 4 mice per group). Our analysis of choline acetyltransferase–positive (CHAT$^+$) cells, i.e., motor neurons, revealed no difference in the number of cells (Supplemental Figure 9A), nevertheless, immunofluorescence quantification revealed a significant reduction of cytoplasmic hTDP-43 (Figure 7C and Supplemental Figure 9, B and C). A correlation between TDP-43 mislocalization and cell body size revealed that larger cells were more sensitive to TDP-43 proteinopathy (Figure 7C), however, the slope of the linear regression of TDP-43 mislocalization in motor neurons of scAAV-VH7Vk9–injected mice was significantly reduced compared with that of scAAV-8H11–injected mice ($Y = 0.0052 \times X + 1.409$ for control motor neurons and $Y = 0.0030 \times X + 1.505$ for VH7Vk9 motor neurons), confirming a reduction of TDP-43 mislocalization mediated by VH7Vk9.

Western blots of cytoplasmic and nuclear TDP-43 fractions showed a significant decrease of cytoplasmic TDP-43 in lumbar spinal cords of mice injected intrathecally with scAAV-VH7Vk9 (Figure 7D). Moreover, dot blot analyses of cytoplasmic insoluble TDP-43 revealed a significant decrease of aggregated/insoluble pan–TDP-43 in VH7Vk9-treated mice (Figure 7E).

We then analyzed the activation of NF-κB and inflammation in the lumbar spinal cords. Western blot analysis of cytoplasmic total p65 showed no differences, whereas a significant decrease of

the activated and phosphorylated subunit of NF-κB was observed in VH7Vk9-treated mice (Supplemental Figure 10A). We observed a concomitant reduction of the glial fibrillary acidic protein (GFAP) and Iba1 markers, suggesting decreased neuroinflammation (Supplemental Figure 10A), which was further confirmed by immunofluorescence analyses. Iba1 and GFAP staining was indeed reduced in VH7Vk9-treated mice, in which both microglia and astrocytes had smaller body sizes (Supplemental Figure 10, B and C). Next, we performed a cytokine array on spinal cord and detected a general downregulation of inflammatory cytokines in the scAAV-VH7Vk9–injected mice (Supplemental Figure 10D).

Finally, we examined whether treatment with scFv VH7Vk9 antibody in the spinal cord of *TDP-43^{A315T}* mice was able to restore proper functionality of the protein (Figure 8). We performed Western blotting to analyze the splicing of DNA polymerase delta–interacting protein 3 (POLDIP3) (36) as well as the regulation of RNA-binding protein FUS (37) and light-chain neurofilament protein (NFL) (38), three proteins whose RNAs are regulated by TDP-43 in the nucleus or cytoplasm (Figure 8, A–C). We found that, in *TDP-43^{A315T}* mice, POLDIP3 was aberrantly spliced, whereas FUS and NFL levels were downregulated compared with levels in *NTg* mice, confirming the alteration of TDP-43 functions. In spinal cord samples from *TDP-43^{A315T}* mice injected with VH7Vk9, we observed a partial restoration of normal levels of these 3 different proteins, close to the levels detected in the nontransgenic mice. We also examined the levels of peripherin, another pathological marker of ALS, which is abnormally upregulated in *TDP-43^{A315T}* mice (35). Expression of VH7Vk9 antibodies produced a downregulation of peripherin levels in the spinal cords of *TDP-43^{A315T}* mice (Figure 8D). Thus, the combined results show that expression of VH7Vk9 antibodies reestablished the normal functions of TDP-43 in the *TDP-43^{A315T}*–transgenic mouse model.

Discussion

Single-chain antibodies, a new tool in nanomedicine, have been recently introduced to the field of neurodegenerative diseases through the generation of a variety of recombinant antibodies that bind to various epitopes of pathological proteins implicated in AD, PD, HD, and prion disease (39) and through the preclinical demonstration of their efficacy in ameliorating pathological symptoms. Some single-chain antibodies are now available for ALS (25–27), but only the scFv targeting misfolded superoxide dismutase 1 (SOD1) proved to be effective in vivo in ameliorating pathological changes and slowing disease progression in a mouse model with an ALS-linked SOD1 mutation (26, 40, 41).

Here, we report for the first time to our knowledge the generation of a novel scFv antibody against TDP-43, named VH7Vk9, and its therapeutic effect when delivered in mouse models of ALS/FTD with TDP-43 pathology. The VH7Vk9 scFv antibody specifically targeted the RRM1 domain of TDP-43, a region implicated in the cytosolic mislocalization and aggregation of the protein (11, 12) and in the interaction with the p65 NF-κB subunit (13). The VH7Vk9 antibody was designed with a secretion signal peptide to allow the antibody to also be effective on distant cells. We demonstrated that virus-mediated delivery of VH7Vk9 in the CNS of transgenic mice expressing mutant hDP-43 succeeded in ameliorating cognitive and motor deficits as well as in reducing TDP-43 proteinopathy and neuroinflammatory changes.

It is now well established that the cytoplasmic accumulation of TDP-43 can be cytotoxic (8, 42). Both mRNA and protein levels of TDP-43 were found to be increased in CNS tissues (13) and peripheral cells (14) of patients with sALS. The factors triggering the initial mislocalization of TDP-43 in pathologies are largely unknown. Yet a reduction of cytoplasmic TDP-43 levels can rescue neurons from death (42–45). TDP-43 can be degraded through proteasomal and autophagic pathways (32). There is evidence that both of these pathways can act on the soluble TDP-43 present in the cytoplasm, with the proteasome contributing to the degradation of monomers and autophagy promoting the degradation of early oligomers, microaggregates, or late macroaggregates (32). Previous studies have established the therapeutic potential of autophagy enhancers in clearing TDP-43 from the cytoplasm (46, 47). Here, we showed that the scFv VH7Vk9 antibody against the RRM1 domain of TDP-43 can enhance the Lys-48 and Lys-63 polyubiquitin chains bound to TDP-43, thereby enhancing protein degradation toward the proteasomal and autophagic pathways (Figure3).

There are previous reports of scFv antibodies able to decrease the levels of target proteins in other neurodegenerative disorders. This can be achieved by inserting a specific signal peptide for degradation in the scFv constructs (21, 24, 27). In contrast, we show here that a scFv without signal peptide for degradation can help to drive target proteins to degradation pathways by enhancing their polyubiquitination. We can speculate that the scFv antibody against the RRM1 domain may interfere with TDP-43 aggregation and increase the soluble TDP-43 forms that might be more suitable for polyubiquitination. Alternatively, the scFv antibody may form complexes with TDP-43, which in turn may become more prone to polyubiquitination. In any case, the observed reduction of TDP-43 levels mediated by the VH7Vk9 scFv antibody appeared to occur at the protein degradation level. As shown in Supplemental Figure 1E, the VH7Vk9 scFv antibody did not interfere with the binding of TDP-43 to its own RNA in Hek293 cells, and therefore it does not affect TDP-43 autoregulation via mRNA binding (28). Our cell culture studies also revealed that the scFv antibodies can alleviate mislocalization and aggregation of TDP-43 under conditions of oxidative stress (Figure4). Therefore, it is possible that the scFv antibody also protects the TDP-43 RRM1 domain from oxidative damage and misfolding, which can trigger protein aggregation (11, 12). Interestingly, the reduction of TDP-43 levels mediated by VH7Vk9 was found to be safe for cultured cells in vitro (Supplemental Figure 3A) as well as for motor neurons in *TDP-43^{A315T}* mice (Supplemental Figure 9A). Our studies with TDP-43–transgenic mouse models revealed an antibody-mediated reduction of cytoplasmic and aggregated TDP-43 levels in neurons (Figure 6, C–E, and Figure 7, C–E) that was associated with a concomitant restoration of cognitive (Figure 6, A and B, and Supplemental Figure 8A) and motor functions (Figure 7A), together with an alleviation of NMJ loss (Figure 7B). We also observed that the presence of VH7Vk9 restored normal levels of proteins such as POLDIP3, FUS, NFL, and peripherin that are aberrantly deregulated in the context of cytoplasmic TDP-43 pathology (Figure 8).

Another therapeutic effect observed with the anti–RRM1 scFv antibody was the reduction of NF-κB–mediated inflammation. By blocking the interaction of TDP-43 with p65 (Figure 2A), the scFv antibody was able to reduce NF-κB activation in microglial

cells (Figure 2B). In mouse models with LPS-induced inflammation (Figure 5) or TDP-43 mutations (Supplemental Figure 7B and Supplemental Figure 10B), viral delivery of VH7Vk9 resulted in reduced microgliosis and levels of phosphorylated p65. As a further confirmation of VH7Vk9-mediated NF-κB inhibition, we observed a downregulation of different inflammatory factors in tissues treated with the virus encoding for the scFv antibody (Supplemental Figure 6D and Supplemental Figure 10D). Most of these factors are relevant to ALS. Indeed, studies on cerebrospinal fluid (CSF), plasma, or serum from patients with ALS revealed an upregulation of granulocyte CSF (GCSF) and granulocyte-macrophage CSF (GM-CSF) (48), IFN-γ (48), IL-12 (49), IL-17 (48, 50), TNF-α and receptors (51), Rantes (52), monocyte chemoattractant protein 1 (MCP1) (48), and macrophage inflammatory protein 1 (MIP1) (48, 53).

It should be noted that the inhibition of NF-κB signaling by VH7Vk9 antibodies is partial and occurs in the context of TDP-43 pathology in neurons or in the context of innate immune activation (such as with LPS) in microglial cells. A previous study (13) showed that TDP-43 can act as a coactivator of p65 and that overexpression of TDP-43 can enhance NF-κB activation. The blocking of TDP-43 interaction with p65 NF-κB is beneficial rather than toxic. First, the results presented in Supplemental Figure 2B revealed that attenuation of NF-κB activity by scFv antibodies in microglial cells (BV2 cells) challenged by LPS confers protection to N2A neuronal cells exposed to media from LPS-treated BV2 cells. Second, *TLR2*-luciferase mice injected in the brain with an adeno-associated virus (AAV) vector encoding VH7Vk9 scFv antibody remained healthy, and the presence of VH7Vk9 scFv antibodies attenuated microglial activation induced by LPS treatment (Figure 5). Third, expression of scFv antibodies in transfected Hek293 cells did not affect cell survival (Supplemental Figure 3A), nor did it reduce the number of motor neurons in *TDP-43*^{A315T} mice (Supplemental Figure 9A). So far, we have obtained no evidence that VH7Vk9 scFv antibodies cause cellular toxicity. On the contrary, the VH7Vk9 antibody can alleviate mislocalization and aggregation of TDP-43 (Figure 6 and Figure 7), and it can restore normal levels of proteins that are aberrantly regulated in TDP-43 pathology (Figure 8).

It is worth highlighting the fact that our scFv was designed with a secretion signal, which allowed the antibody to act not only on virus-infected cells but also on distal cells from the injection site. It is indeed remarkable that a reduction of microgliosis in *TDP-43*^{G348C} and LPS-challenged mice was observed not only in the injected ipsilateral hemisphere but also in the contralateral one. Similarly, the reduction in TDP-43 mislocalization was detected in the ipsilateral and contralateral cortical neurons of mice injected with *TDP-43*^{G348C}. The diffusion of scFv antibodies in the CNS may explain the improved cognitive performance in VH7Vk9-injected mice after a focal intracortical injection of viral vectors.

In conclusion, we demonstrate for the first time to our knowledge that a single-chain antibody against the RRM1 domain of TDP-43 is an efficient therapeutic approach to target TDP-43 proteinopathy and ameliorate cognitive and motor deficits in transgenic mouse models. The target specificity and therapeutic effects of the scFv antibody support the feasibility of developing immunotherapeutic approaches to target intracellular TDP-43 aggregates and neuroinflammation, two hallmarks of ALS and FTD.

Methods

Anti–TDP-43 antibody, scFv plasmid, and virus production. The BamH1-Not1 411-bp fragment was PCR amplified from a previously produced vector containing the full-length hTDP-43 cDNA (13) using the primers *TDP-43 BamH1* (5′-GGGGGATCC ACCATGCGCTA-CAGGAATCCAGT-3′) and *TDP-43 Not1* (5′-GGGGCGGCCGCT-CATTTGCAGTCACACCAT C-3′) and subcloned into the pGEX-6P-1 vector (GE Healthcare). This recombinant plasmid was used to transform BL21-competent (DE3-competent) *E. coli* cells for expression of the 136-aa protein encoding a portion of the N-Terminal region, the nuclear localization signal (NLS), and the entire RRM1 domain of hTDP-43. The 15.68-kDa recombinant protein was subsequently purified using the glutathione S-transferase (GST) gene fusion system (GE Healthcare). From the recombinant protein, MediMabs produced different hybridoma cell lines.

Single-chain antibodies were produced as previously described (26). The pscFv9 plasmid generated contained a CMV promoter, a murine Ig H-secretory signal for efficient folding and secretion, and a human c-Myc epitope to facilitate detection. The control single-chain antibodies D1.3 anti–chicken lysozyme (26) or 8H11 anti-GFP (produced in-house) were produced in the same way. To produce scAAV2/9 (AAV2 terminal repeats and AAV9 capsid) encoding scFv, we followed a previously described protocol (26). Briefly, the fragment encoding for the secreted scFv was first HindIII and EcoRV excised, subcloned into the plasmid BluescriptII KS(+) (Stratagene) and then the excised SalI/NotI, and subcloned into the XhoI/NotI-digested plasmid AAV-CMV-GFP (54) replacing the EGFP-encoding sequence. scAAV recombinant viruses were produced in the Hek293T cells cultured in DMEM (Gibco, Thermo Fisher Scientific) supplemented with 10% normal bovine serum, 100 U/ml penicillin G, and 100 μg/ml streptomycin. Cotransfection was done with scAAV-scFv, pXR1, and pxx-6 as packaging and helper plasmids, respectively (54, 55).

Animal injections, imaging, and tissues collection. For intracortical injections of scAAV2/9, the mice were anesthetized with 2% isoflurane during the entire procedure and received a unilateral intracortical injection of scAAV2/9 (9.2×10^9 vg for *TDP-43*^{G348C} and 1.5×10^{10} vg for *TLR2*-luciferase) or PBS solution. Mice were placed in a stereotaxic apparatus (David Kopf Instruments), and the primary frontal cortex was then reached (−1.75 mm lateral, +1.0 mm anteroposterior and −1.25 mm dorsoventral to the bregma) with a 33-gauge stainless steel cannula (Plastics One) that was connected to a 25-μl Hamilton syringe with intramedic polyethylene tubing (PE-50, Clay Adams). A maximum volume of 2μl was infused over a 2-minute period by means of a microinjection pump (Razel Scientific Instruments, model A-99). Intrathecal injection of scAAV2/9 into *TDP-43*^{A315T} mice was performed as previously described (26). A maximum volume of 10 μl (5×10^{10} vg) was injected with a Hamilton syringe.

Bioluminescence imaging was performed in *TLR2*-luciferase mice over a period of 5 days after intraperitoneal injection of 5 mg/kg LPS as previously described (34).

Tissue collection was done after deep anesthesia of the mice with 10 μl/g pentobarbital 12 mg/ml. Mice were perfused transcardially with PBS followed by 4% paraformaldehyde (PFA) solution in PBS. Brain, spinal cord, and gastrocnemius muscle were rapidly removed, post-fixed overnight in 4% PFA, and transferred into 30% sucrose in PBS until they sank. Tissues for protein analyses were rapidly removed from the anesthetized mice and frozen on dry ice before storage at −80°C.

Behavioral analyses. Starting 1 week before the virus injection and throughout the treatment period, mutant *TDP-43*^{A315T} mice were subjected once a week to an inverted grid test to monitor their grip strength (56). Briefly, during the test, the mice were allowed to hang on an upside-down grid for a maximum of 90 seconds, and the latency to fall from the grid was considered for analyses. The body weight of the mice was also measured in each session. *TDP-43*^{G348C} mice were subjected to novel object recognition (NOR) to test their memory and to an OFT for anxiety at established time points. NOR was done as a 3-day test, as previously described (57), in a 20 × 50 × 30 cm Plexiglas box for 5 minutes per session. The OFT was performed in a single session. Mice were allowed to discover and move freely in a computer-monitored box (58), and the time spent in the center of the box over a total period of 30 minutes was considered for analyses.

Cell transfection and treatments. Mouse microglia (BV2), Hek293, Hek293T, and mouse brain neuroblastoma Neuro-2a (N2A) cell lines were purchased from the American Type Culture Collection (ATCC). All cell lines were maintained in DMEM supplemented with 1% sodium pyruvate (Gibco, Thermo Fisher Scientific) and 1% penicillin G and streptomycin (Gibco, Thermo Fisher Scientific) with 10% FBS (Gibco, Thermo Fisher Scientific). The murine microglial cell line BV2 p65-luc (29) was continuously selected and maintained with 100 μg/ml hygromycin (MilliporeSigma).

When 60% to 70% confluence was attained, the cells were transfected for 48 hours with Lipofectamine (Invitrogen, Thermo Fisher Scientific) or Jet Prime (Polyplus) transfection reagents according to the manufacturer's instructions.

After 32 hours of transfection, Hek293 cells were treated overnight with 50 μM ethacrynic acid (MilliporeSigma) or the same volume of DMSO (MilliporeSigma) . Forty-four hours after transfection, BV2 cells were treated for 4 hours with 500 ng/ml LPS (MilliporeSigma) or PBS (Gibco, Thermo Fisher Scientific).

Media of transfected BV2 cells were collected after 4 hours of LPS/PBS treatment, centrifuged at 400 *g* for 5 minutes to eliminate dead cells and debris, and added to N2A cells seeded the day before.

Untransfected BV2 cells were treated with 5 μg/ml purified scFv for 2 or 6 hours and then treated for 4 hours with 500 ng/ml LPS for a total of 6 or 10 hours of treatment with scFv. Before the experiments, cells were washed 3 times with PBS to avoid detection of scFv bound to the cell membrane.

For pulse-chase experiments, after 48 hours of transfection with scFv antibodies, Hek293 cell medium was replaced with OptiMEM (Gibco, Thermo Fisher Scientific) containing 10 μg/ml cycloheximide (MilliporeSigma) and 300 nM bafilomycin (MilliporeSigma) or 0.5 μM MG-132 (MilliporeSigma) and treated for 3 or 6 hours.

For immunofluorescence, cells were seeded on coverslips. After transfection or treatment, cells were washed in PBS and fixed for 30 minutes with 4% PFA.

The UV-CLIP procedure, as well as cell survival, luciferase, and DCHFDA assays are described in the Supplemental Methods.

scFv purification. scFv antibodies were purified from the medium of Hek293 cells transfected for 48 hours in Opti-MEM (Gibco, Thermo Fisher Scientific). The medium was collected and centrifuged at 400 *g* for 5 minutes to eliminate dead cells and debris and then stored at –80°C. scFv was immunoprecipitated from 10 ml medium overnight with 400 μl Myc-tagged agarose beads (25% slurry, Thermo Fisher Scientific). The next day, the beads were spun down by centrifugation at 2500 *g* for 5 minutes, moved to columns provided with the kit, and washed twice with TBS and 10-second spins. A double elution was performed by competition with 500 μl c-Myc peptide (Gene Script) at 0.5 mg/ml concentration for 2 hours of rotation at room temperature. Unbound c-Myc peptide was removed by a 5-kDa cutoff spin column (Bio-Rad) and centrifugation (5 min at 15,000 *g*). Purified scFv antibodies were quantified using an Eon Plate Reader (BioTek).

Human recombinant TDP-43 protein production. The recombinant plasmid expressing the hTDP-43 cDNA (13) was used to transform competent cells of the *E. coli* host BL21 (DE3) for the expression of total hTDP-43. After cell lysis, the 43-kDa recombinant protein was purified using the GST gene fusion system (GE Healthcare).

ELISA. ELISA assays were performed with an ELISA kit (Peprotech). Different concentrations of TDP-43-GST-tag (made in-house) or BSA (BioBasic) as a control were diluted in PBS, and 100 μl was loaded onto an ELISA plate and incubated overnight at room temperature. The following day, the wells were washed 4 times with washing buffer and incubated for 2 hours with 0.2 μg/ml p65-His-tag (Enzo Life Sciences, ALX-201-284) in PBS, 0.4 μg/ml monoclonal antibodies (MédiMabs), 0.4 μg/ml polyclonal anti–TDP-43 (Proteintech), and BSA — all diluted in PBS or directly diluted in medium of transfected cells. The wells were then incubated for 2 hours with rabbit polyclonal anti–His-tag 6X-HRP–conjugated antibody (rabbit polyclonal, Abcam ab1187; 1:10,000). Chemiluminescence was read at 450 nm using an EnSpire 2300 Multilabel Reader (PerkinElmer).

Cell protein extraction methods. To obtain nuclear and cytoplasmic fractions, cells were collected in cold PBS and centrifuged at 400 *g* for 5 minutes. Pellets were lysated in hypotonic buffer (10 mM HEPES, pH 8, 10 mM KCl, 1.5 mM $MgCl_2$, 1 mM NaF, 0.5 mM PMSF supplemented with protease and phosphatase inhibitors) and incubated on ice for 15 minutes. NP-40 (0.5%) was added, and lysates were vortexed and centrifuged for 10 minutes at 900 *g*. Supernatant was collected as the cytoplasmic fraction. Pellets were then solubilized in extraction buffer (20 mM HEPES, pH 8, 420 mM NaCl, 1.5 mM $MgCl_2$, 1 mM NaF, 0.2 mM EDTA, 25% glycerol, 0.5 mM PMSF supplemented with protease and phosphatase inhibitors), incubated on ice for 15 minutes, sonicated, and centrifuged at 15,000 *g* for 10 minutes. Supernatant was collected as the nuclear fraction. Total proteins from cells were obtained by lysis in extraction buffer supplemented with 0.5% NP-40 if immunoprecipitation experiments were planned, or in boiled 1% SDS followed by centrifugation at 15,000 *g* for 10 minutes. RIPA soluble and insoluble proteins were obtained as previously described (57).

For Western blot analysis of cellular media, proteins were precipitated with 4 volumes of cold acetone at –80°C overnight and pelleted by centrifugation at 15,000 *g* for 20 minutes. Pellets were resuspended directly in loading buffer.

Proteins were extracted from animal tissues. To obtain the nuclear and cytoplasmic fractions, tissues were lysated in hypotonic buffer (10 mM HEPES-KOH, pH 7.6, 10 mM NaCl, 1 mM KH_2PO_4, 5 mM $NaHCO_3$, 5 mM EDTA, pH 8, 1 mM $CaCl_2$, 0.5 mM $MgCl_2$ supplemented by protease and phosphatase inhibitors), homogenized, and solubilized by rotation at 4°C for 10 minutes, followed by addition of 2.5 M 10% sucrose and centrifugation for 10 minutes at 6300 *g*. Supernatant was collected as the cytoplasmic fraction. Pellets were resuspended in extraction buffer (10 mM Tris, pH 7.4, 300 mM sucrose, 1 mM EDTA, 0.1% NP-40 supplemented by protease and

phosphatase inhibitors), homogenized, and centrifuged for 5 minutes at 4000 *g*. The pellets were washed 3 times with extraction buffer followed by centrifugations. After the last centrifugation, the pellets were resuspended in RIPA buffer (50 mM Tris, pH 7.4, 1 mM EDTA, 150 mM NaCl, 1% NP-40 supplemented with 2 % SDS and protease and phosphatase inhibitors) and sonicated. To obtain insoluble proteins from the cytoplasm, 1% Triton X-100 was added to the cytoplasmic fraction, sonicated, and ultracentrifuged at 107,000 *g* for 30 minutes. Supernatant was collected as the cytoplasmic soluble portion, whereas pellets were resuspended in RIPA buffer and sonicated, as with nuclear pellets.

Proteins were quantified using the Lowry method (Bio-Rad) or the bicinchoninic acid (BCA) method (Bio-Rad) when SDS was present in the lysate. Western blotting and dot blot methods and cytokine array procedures are described in the Supplemental Methods.

Immunoprecipitation. Immunoprecipitation of TDP-43 was done by coating 40 μl Dynabeads (Invitrogen, Thermo Fisher Scientific) with 2 μg rabbit polyclonal anti–TDP-43 antibody (Proteintech) for 2 hours at room temperature on rotation. The antibody was cross-linked to the beads by a 30-minute incubation, rotating with 20 mM dimethyl pimelimiolate dihydroxichloride (MilliporeSigma) in 0.2 M triethanolamine (pH 8.2, MilliporeSigma) (59). The beads were incubated with 300 μg proteins overnight at 4°C. The following day, output was collected, and beads were washed in PBST (PBS, pH 5, Tween 0.02%) before elution of bound proteins. Immunoprecipitation of scFv was performed in the same way, but the beads were coated with 2 μg mouse monoclonal anti–c-Myc antibody (Santa Cruz Biotechnology).

Immunoprecipitation of ubiquitinated proteins was performed as previously described (60). Briefly, pellets of transfected cells collected from 10-cm dishes were lysated in 200 μl lysis buffer (2% SDS, 150 mM NaCl, 10 mM Tris-HCl pH8, 2 mM sodium orthovanadate, 50 mM sodium fluoride supplemented with protease inhibitors). Proteins were then diluted in 800 μl dilution buffer (10 mM Tris-HCl pH8, 150 mM NaCl, 2 mM EDTA and 1% Triton-X), resuspended for 1 hour with rotation at 4°C, and centrifuged for 30 minutes at 20,000 *g*. Supernatant was collected, quantified, and used for the immunoprecipitation experiments. Magnetic beads (30 μl) were coated with 10 μg rabbit monoclonal anti–ubiquitin Lys48 (MilliporeSigma, rabbit monoclonal, clone Apu2, 05-1307) or Lys63-specific (MilliporeSigma, rabbit monoclonal, clone Apu3, 05-1308) antibodies for 2 hours at room temperature with rotation. Immunoprecipitation was then performed as previously described, except for the washes done in washing buffer (10 mM Tris-HCl, 1 M NaCl, 1 mM EDTA, 1% NP-40).

Immunoprecipitated proteins were eluted from beads by boiling for 5 minutes at 100°C in loading buffer supplemented with 100 mM DTT (MilliporeSigma).

All Western blotting was performed with antibodies with Igs different from those used for immunoprecipitation to avoid cross-reactions.

Immunofluorescence and image analysis. Fixed cells or 30-μm tissue sections cut with a microtome (Leica) were washed 3 times in PBS and incubated for 1 hour with blocking solution (NGS 10%, Triton X-100 0.2% in PBS) and then overnight with primary antibodies diluted in blocking solution (Supplemental Table 1). After washes in PBS, the samples were incubated for 2 hours with goat-anti mouse or goat anti–rabbit Alexa Fluor (Invitrogen, Thermo Fisher Scientific) secondary antibodies diluted at 1:500 in blocking solution and washed again in PBS. Nuclei were visualized with a 5-minute incubation with Hoechst 33342 (Invitrogen, Thermo Fisher Scientific) diluted 1:1000 in PBS. Slides were mounted with Fluoromount-G Buffer (Southern Biotech). Images were acquired using a BX-61 Virtual Stage confocal microscope (Olympus), an Apotome microscope (Carl Zeiss), or a DM5000 B wide-field microscope (Leica Microsystems).

For lumbar spinal cord sections, images were acquired focusing on the ventral horns for TDP-43 location and astrogliosis and microgliosis assessments. For TDP-43 localization analysis in brain sections, images were acquired focusing on the neurons located in the fifth layer of the primary motor cortex (Betz cells). Global microgliosis assessment was performed in all 6 layers of the primary motor cortex. All acquired brain images distinguished injected and noninjected hemispheres by making a lateral incision in the contralateral hemisphere.

For nuclear and cytoplasmic localization of TDP-43, images were analyzed with ImageJ software (NIH) as previously described (61). Briefly, for each cell analyzed, total or nuclear TDP-43 integrated density was obtained by selecting the compartment according to the neuronal (NeuN, CHAT) or nuclear (Hoechst) markers. Cytoplasmic TDP-43 was obtained by substraction of the integrated nuclear density from the total. The cytoplasm to nuclear ratio was considered for analyses. For Iba1 and GFAP quantification, images were analyzed with ImageJ software. The adequate threshold was determined for all the images, and an average of them was used for the final analysis. The parameters analyzed included area fraction, number of events, and size of cells. Motoneurons, microglia and astrocytes sizes were obtained by setting the scale according to the enlargement. CHAT+ve cells larger than 250 μm^2 and Iba1+ve or GFAP+ve cells larger than 20 to 35 μm^2 were included in the analysis as previously reported (62). Neuromuscular junction (NMJ) staining was performed as previously described (29, 61) on mouse gastrocnemius muscle sections (25-μm thick) obtained by cryostat sectioning (Thermo Fisher Scientific).

Mice overexpressing the human *TDP-43^{A315T}* or *TDP-43^{G348C}* transgene were generated in the laboratory of JPJ (35) and maintained, after more than 20 backcrosses, on a C57/BL6 background (Charles River Laboratories). *hTDP-43^{G348C}* mice (n = 37 females, n = 33 males), *hTDP-43^{A315T}* mice (n = 22 females, n = 14 males), or nontransgenic (*NTg*, from the *hTDP-43^{G348C}* line) mice (n = 4 females, n = 6 males) were injected with PBS or virus at 8 months of age. Mice expressing the *TLR2*-luciferase transgene were generated in the laboratory of JK (34) and maintained, after more than 20 backcrosses, on a C57/BL6 Albino background (Charles River Laboratories), and nontransgenic (*NTg*) mice were obtained from the same colony. Mice were injected with virus at 4 months of age (n = 11 *TLR2*-luciferase males, n = 6 *NTg* males). Transgenic mice were identified by PCR of DNA tail biopsies and constantly maintained as a colony at the CERVO Brain Centre animal facility under standard conditions.

Experimental design. Mice were randomly assigned to the experimental groups, although sex was taken into consideration. Technical randomization was applied for the in vitro experiments when possible.

Data collection was performed in a blinded manner for all in vivo experiments. One researcher determined the treatment for each mouse. Virus injections were performed by experimenters blinded to the type of scFv produced by the virus; behavioral tests and biochemistry and immunofluorescence experiments on mice were performed only with the knowledge of their identification number and treatment group but not the type of treatment received. Data collection was not done in a blinded manner for the in vitro experiments.

Statistics. GraphPad Prism 5.0 (GraphPad Software) was used for all statistical analyses. Data distribution was assumed to be normal but was not formally tested. Unpaired, 2-tailed *t* tests and 1- or 2-way ANOVA followed by post hoc test for multiple comparisons correction or repeated-measures correction were performed depending on the experimental design. A *P* value of less than 0.05 was considered statistically significant.

For quantitative analyses, the numbers of biological replicates are stated in the text. Sample size for the in vivo analyses was not determined by statistical methods but was consistent with other studies in the field (61), and biochemical and histological experiments were always performed using at least 3 individual mice for each experiment.

Data exclusion was carried out in several instances. For in vitro analyses in Figure 2B, data from 1 experiment involving control scFv+LPS were excluded because of a technical mistake. For in vivo analyses, several mice were not evaluated because of technical problems during the evaluation. Data exclusion for *TDP-43*^{G348C}–injected mice involved the following: PBS-injected mice (n = 3) and 8H11-injected mice (n = 2) in the NOR test at 2 months; VH7Vk9-injected mice (n = 1) in the NOR test at 4 months; VH7Vk9-injected mice (n = 3), 8H11-injected mice (n = 4), and *NTg* PBS-injected mice (n = 2) in the OFT at 4 months. For *TDP-43*^{A315T}–injected mice, several individual time data points were excluded: n = 4 excluded for VH7Vk9 and n = 3 excluded for 8H11 among 180 data points for each group. Some values were excluded from the cytokine array analysis because they were undetectable by the assay.

Study approval. The Animal Care Ethics Committee of the Université Laval approved all in vivo experimental protocols. All experiments were performed in accordance with the *Guide to the Care and Use of Experimental Animals* (Canadian Council on Animal Care, 1993, 2nd edition, revised March 2017).

Author contributions

SP and JPJ designed the study. SP performed the majority of the experiments; SST helped with behavioral tests, tissue preparation, and immunofluorescence; PC helped with immunofluorescence and image analysis, RR performed in vivo bioimaging; KVP performed UV-CLIP experiments; GS performed mouse injections; CB produced the recombinant hTDP-43 protein; DP produced the hTDP-43 plasmids; CG produced the original pscFv9 empty plasmid, the pscFv9-8H11 scFv plasmid, and the scAAV2/9 virus; and JK provided the *TLR2*-luciferase mice. SP analyzed the data and wrote the manuscript. JPJ revised the manuscript. All authors read and approved the final manuscript.

Acknowledgments

SP would like to thank Kallol Dutta and Hejer Boutej for useful discussions, Louis-Charles Béland for the production of the graphical abstract, and Marie-Eve Crochetière for help during her summer training (all from CERVO Brain Research Centre). This work was funded by the Canadian Institutes of Health Research and the Packard Center for ALS Research at Johns Hopkins. JPJ holds a Canada Research Chair in Neurodegeneration.

Address correspondence to: Jean-Pierre Julien, Department of Psychiatry and Neuroscience, Faculty of Medicine, Laval University, CERVO Brain Research Centre, 2601 Chemin de la Canardière, Québec, Québec G1J 2G3, Canada. Phone: 418.663.5000 ext 4785; Email: jean-pierre.julien@fmed.ulaval.ca.

1. Morgan J. Ammar Al-Chalabi: from complex genetics to acoustic rock. *Lancet Neurol*. 2017;16(5):347.
2. Hardiman O, et al. Amyotrophic lateral sclerosis. *Nat Rev Dis Primers*. 2017;3:17071.
3. Taylor JP, Brown RH, Cleveland DW. Decoding ALS: from genes to mechanism. *Nature*. 2016;539(7628):197–206.
4. Buratti E. Functional Significance of TDP-43 Mutations in Disease. *Adv Genet*. 2015;91:1–53.
5. Burrell JR, et al. The frontotemporal dementia-motor neuron disease continuum. *Lancet*. 2016;388(10047):919–931.
6. Neumann M, et al. Ubiquitinated TDP-43 in frontotemporal lobar degeneration and amyotrophic lateral sclerosis. *Science*. 2006;314(5796):130–133.
7. Arai T, et al. TDP-43 is a component of ubiquitin-positive tau-negative inclusions in frontotemporal lobar degeneration and amyotrophic lateral sclerosis. *Biochem Biophys Res Commun*. 2006;351(3):602–611.
8. Barmada SJ, Skibinski G, Korb E, Rao EJ, Wu JY, Finkbeiner S. Cytoplasmic mislocalization of TDP-43 is toxic to neurons and enhanced by a mutation associated with familial amyotrophic lateral sclerosis. *J Neurosci*. 2010;30(2):639–649.
9. Mackenzie IR, Neumann M. Molecular neuropathology of frontotemporal dementia: insights into disease mechanisms from postmortem studies. *J Neurochem*. 2016;138 Suppl 1:54–70.
10. Arai T. Significance and limitation of the pathological classification of TDP-43 proteinopathy. *Neuropathology*. 2014;34(6):578–588.
11. Chang CK, Chiang MH, Toh EK, Chang CF, Huang TH. Molecular mechanism of oxidation-induced TDP-43 RRM1 aggregation and loss of function. *FEBS Lett*. 2013;587(6):575–582.
12. Shodai A, et al. Aberrant assembly of RNA recognition motif 1 links to pathogenic conversion of TAR DNA-binding protein of 43 kDa (TDP-43). *J Biol Chem*. 2013;288(21):14886–14905.
13. Swarup V, et al. Deregulation of TDP-43 in amyotrophic lateral sclerosis triggers nuclear factor κB-mediated pathogenic pathways. *J Exp Med*. 2011;208(12):2429–2447.
14. Nardo G, et al. Amyotrophic lateral sclerosis multiprotein biomarkers in peripheral blood mononuclear cells. *PLoS ONE*. 2011;6(10):e25545.
15. Messer A, Joshi SN. Intrabodies as neuroprotective therapeutics. *Neurotherapeutics*. 2013;10(3):447–458.
16. Ahmad ZA, Yeap SK, Ali AM, Ho WY, Alitheen NB, Hamid M. scFv antibody: principles and clinical application. *Clin Dev Immunol*. 2012;2012:980250.
17. Esquerda-Canals G, Marti J, Rivera-Hernández G, Giménez-Llort L, Villegas S. Loss of deep cerebellar nuclei neurons in the 3xTg-AD mice and protection by an anti-amyloid β antibody fragment. *MAbs*. 2013;5(5):660–664.
18. Giménez-Llort L, Rivera-Hernández G, Marin-Argany M, Sánchez-Quesada JL, Villegas S. Early intervention in the 3xTg-AD mice with an amyloid β-antibody fragment ameliorates first hallmarks of Alzheimer disease. *MAbs*. 2013;5(5):665–677.
19. Meli G, et al. Conformational targeting of intracellular Aβ oligomers demonstrates their pathological oligomerization inside the endoplasmic reticulum. *Nat Commun*. 2014;5:3867.
20. Sebollela A, et al. A human scFv antibody that targets neutralizes high molecular weight pathogenic amyloid-beta oligomers [published online ahead of print July 3, 2017]. *J Neurochem*. https://doi.org/10.1111/jnc.14118.
21. Spencer B, et al. ESCRT-mediated uptake and degradation of brain-targeted α-synuclein single chain antibody attenuates neuronal degeneration in vivo. *Mol Ther*. 2014;22(10):1753–1767.
22. Spencer B, et al. α-synuclein conformational antibodies fused to penetratin are effective in models of Lewy body disease. *Ann Clin Transl Neurol*. 2016;3(8):588–606.
23. Snyder-Keller A, McLear JA, Hathorn T, Messer A. Early or late-stage anti-N-terminal Huntingtin intrabody gene therapy reduces pathological features in B6.HDR6/1 mice. *J Neuropathol Exp Neurol*. 2010;69(10):1078–1085.
24. Butler DC, Messer A. Bifunctional anti-huntingtin proteasome-directed intrabodies mediate

efficient degradation of mutant huntingtin exon 1 protein fragments. *PLoS One*. 2011;6(12):e29199.
25. Ghadge GD, Pavlovic JD, Koduvayur SP, Kay BK, Roos RP. Single chain variable fragment antibodies block aggregation and toxicity induced by familial ALS-linked mutant forms of SOD1. *Neurobiol Dis*. 2013;56:74–78.
26. Patel P, et al. Adeno-associated virus-mediated delivery of a recombinant single-chain antibody against misfolded superoxide dismutase for treatment of amyotrophic lateral sclerosis. *Mol Ther*. 2014;22(3):498–510.
27. Tamaki Y, et al. Elimination of TDP-43 inclusions linked to amyotrophic lateral sclerosis by a misfolding-specific intrabody with dual proteolytic signals. *Sci Rep*. 2018;8(1):6030.
28. Ayala YM, et al. TDP-43 regulates its mRNA levels through a negative feedback loop. *EMBO J*. 2011;30(2):277–288.
29. Dutta K, Patel P, Rahimian R, Phaneuf D, Julien JP. Withania somnifera reverses transactive response DNA binding protein 43 proteinopathy in a mouse model of amyotrophic lateral sclerosis/frontotemporal lobar degeneration. *Neurotherapeutics*. 2017;14(2):447–462.
30. Frakes AE, et al. Microglia induce motor neuron death via the classical NF-κB pathway in amyotrophic lateral sclerosis. *Neuron*. 2014;81(5):1009–1023.
31. Urushitani M, Sato T, Bamba H, Hisa Y, Tooyama I. Synergistic effect between proteasome and autophagosome in the clearance of polyubiquitinated TDP-43. *J Neurosci Res*. 2010;88(4):784–797.
32. Scotter EL, et al. Differential roles of the ubiquitin proteasome system and autophagy in the clearance of soluble and aggregated TDP-43 species. *J Cell Sci*. 2014;127(Pt 6):1263–1278.
33. Iguchi Y, et al. Oxidative stress induced by glutathione depletion reproduces pathological modifications of TDP-43 linked to TDP-43 proteinopathies. *Neurobiol Dis*. 2012;45(3):862–870.
34. Lalancette-Hébert M, Phaneuf D, Soucy G, Weng YC, Kriz J. Live imaging of Toll-like receptor 2 response in cerebral ischaemia reveals a role of olfactory bulb microglia as modulators of inflammation. *Brain*. 2009;132(Pt 4):940–954.
35. Swarup V, et al. Pathological hallmarks of amyotrophic lateral sclerosis/frontotemporal lobar degeneration in transgenic mice produced with TDP-43 genomic fragments. *Brain*. 2011;134(Pt 9):2610–2626.
36. Fiesel FC, Weber SS, Supper J, Zell A, Kahle PJ. TDP-43 regulates global translational yield by splicing of exon junction complex component SKAR. *Nucleic Acids Res*. 2012;40(6):2668–2682.
37. Sephton CF, et al. Identification of neuronal RNA targets of TDP-43-containing ribonucleoprotein complexes. *J Biol Chem*. 2011;286(2):1204–1215.
38. Strong MJ, et al. TDP43 is a human low molecular weight neurofilament (hNFL) mRNA-binding protein. *Mol Cell Neurosci*. 2007;35(2):320–327.
39. Manoutcharian K, Perez-Garmendia R, Gevorkian G. Recombinant antibody fragments for neurodegenerative diseases. *Curr Neuropharmacol*. 2017;15(5):779–788.
40. Ghadge GD, Kay BK, Drigotas C, Roos RP. Single chain variable fragment antibodies directed against SOD1 ameliorate disease in mutant SOD1 transgenic mice. *Neurobiol Dis*. 2019;121:131–137.
41. Dong QX, Zhu J, Liu SY, Yu XL, Liu RT. An oligomer-specific antibody improved motor function and attenuated neuropathology in the SOD1-G93A transgenic mouse model of ALS. *Int Immunopharmacol*. 2018;65:413–421.
42. Walker AK, et al. Functional recovery in new mouse models of ALS/FTLD after clearance of pathological cytoplasmic TDP-43. *Acta Neuropathol*. 2015;130(5):643–660.
43. Thomas M, Alegre-Abarrategui J, Wade-Martins R. RNA dysfunction and aggrephagy at the centre of an amyotrophic lateral sclerosis/frontotemporal dementia disease continuum. *Brain*. 2013;136(Pt 5):1345–1360.
44. Budini M, Baralle FE, Buratti E. Targeting TDP-43 in neurodegenerative diseases. *Expert Opin Ther Targets*. 2014;18(6):617–632.
45. Scotter EL, Chen HJ, Shaw CE. TDP-43 proteinopathy and ALS: insights into disease mechanisms and therapeutic targets. *Neurotherapeutics*. 2015;12(2):352–363.
46. Wang IF, et al. Autophagy activators rescue and alleviate pathogenesis of a mouse model with proteinopathies of the TAR DNA-binding protein 43. *Proc Natl Acad Sci U S A*. 2012;109(37):15024–15029.
47. Barmada SJ, et al. Autophagy induction enhances TDP43 turnover and survival in neuronal ALS models. *Nat Chem Biol*. 2014;10(8):677–685.
48. Guo J, Yang X, Gao L, Zang D. Evaluating the levels of CSF and serum factors in ALS. *Brain Behav*. 2017;7(3):e00637.
49. Rentzos M, et al. Interleukin-15 and interleukin-12 are elevated in serum and cerebrospinal fluid of patients with amyotrophic lateral sclerosis. *Eur Neurol*. 2010;63(5):285–290.
50. Rentzos M, et al. Interleukin-17 and interleukin-23 are elevated in serum and cerebrospinal fluid of patients with ALS: a reflection of Th17 cells activation? *Acta Neurol Scand*. 2010;122(6):425–429.
51. Cereda C, et al. TNF and sTNFR1/2 plasma levels in ALS patients. *J Neuroimmunol*. 2008;194(1-2):123–131.
52. Rentzos M, et al. RANTES levels are elevated in serum and cerebrospinal fluid in patients with amyotrophic lateral sclerosis. *Amyotroph Lateral Scler*. 2007;8(5):283–287.
53. Yang X, Gao L, Wu X, Zhang Y, Zang D. Increased levels of MIP-1α in CSF and serum of ALS. *Acta Neurol Scand*. 2016;134(2):94–100.
54. McCarty DM, Monahan PE, Samulski RJ. Self-complementary recombinant adeno-associated virus (scAAV) vectors promote efficient transduction independently of DNA synthesis. *Gene Ther*. 2001;8(16):1248–1254.
55. Rabinowitz JE, et al. Cross-packaging of a single adeno-associated virus (AAV) type 2 vector genome into multiple AAV serotypes enables transduction with broad specificity. *J Virol*. 2002;76(2):791–801.
56. Lucchetti J, et al. A mouse model of familial ALS has increased CNS levels of endogenous ubiquinol9/10 and does not benefit from exogenous administration of ubiquinol10. *PLoS One*. 2013;8(7):e69540.
57. Iguchi Y, et al. Exosome secretion is a key pathway for clearance of pathological TDP-43. *Brain*. 2016;139(Pt 12):3187–3201.
58. Gainetdinov RR, Wetsel WC, Jones SR, Levin ED, Jaber M, Caron MG. Role of serotonin in the paradoxical calming effect of psychostimulants on hyperactivity. *Science*. 1999;283(5400):397–401.
59. Lauranzano E, et al. Peptidylprolyl isomerase A governs TARDBP function and assembly in heterogeneous nuclear ribonucleoprotein complexes. *Brain*. 2015;138(Pt 4):974–991.
60. Choo YS, Zhang Z. Detection of protein ubiquitination. *J Vis Exp*. 2009;(30):1293.
61. Pozzi S, Thammisetty SS, Julien JP. Chronic administration of pimozide fails to attenuate motor and pathological deficits in two mouse models of amyotrophic lateral sclerosis. *Neurotherapeutics*. 2018;15(3):715–727.
62. Pasetto L, et al. Targeting extracellular cyclophilin A reduces neuroinflammation and extends survival in a mouse model of amyotrophic lateral sclerosis. *J Neurosci*. 2017;37(6):1413–1427.

Travail Complémentaire N°1

Participation à l'écriture d'un travail de review

Published in

Acta Neuropathologica Communications

volume 7 Article number: 103, 18 July 2019

Key role of UBQLN2 in pathogenesis of amyotrophic lateral sclerosis and frontotemporal dementia

L. Renaud[1,2], V. Picher-Martel[1,2], P. Codron3, J.-P. Julien[1,2]

1. Department of Psychiatry and Neuroscience, Laval University, Quebec, Canada

2. CERVO Brain Research Center, 2601 Chemin de la Canardière, Québec, QC, G1J 2G3, Canada.

3. UMR CNRS 6015, INSERM U1083, University of Angers, Angers Cedex 9, France.

Renaud *et al. Acta Neuropathologica Communications* (2019) 7:103
https://doi.org/10.1186/s40478-019-0758-7

Acta Neuropathologica Communications

REVIEW Open Access

Key role of UBQLN2 in pathogenesis of amyotrophic lateral sclerosis and frontotemporal dementia

Laurence Renaud[1,2], Vincent Picher-Martel[1,2*], Philippe Codron[3] and Jean-Pierre Julien[1,2]

Abstract

Ubiquilin-2 (UBQLN2) is a member of the ubiquilin family, actively implicated in the degradation of misfolded and redundant proteins through the ubiquitin-proteasome system and macroautophagy. UBQLN2 received much attention after the discovery of gene mutations in amyotrophic lateral sclerosis and frontotemporal dementia (ALS/FTD). The abnormal presence of positive UBQLN2 inclusion in the cytosol of degenerating motor neurons of familial and sporadic forms of ALS patients has been newly related to neurodegeneration. Only recently, data have emerged on its role in liquid-liquid phase separation, in stress granule development and in the formation of secondary amyloid structures. Furthermore, several animal models are available to investigate its involvement in TDP-43 pathology and neuroinflammation in ALS. This review addresses the molecular pathogenetic pathways involving UBQLN2 abnormalities which are converging toward defects in clearance mechanisms. UBQLN2.

Keywords: Amyotrophic lateral sclerosis (ALS), Ubiquilin-2 (UBQLN2), TAR DNA-binding protein 43 (TDP-43), Ubiquitin-proteasome system (UPS), Autophagy, Animal models

Introduction

Amyotrophic lateral sclerosis (ALS) is a progressive and fatal disorder associated with degeneration of upper and lower motor neurons [55]. The disease is characterized by progressive and diffuse paralysis leading to death from respiratory failure within 2 to 5 years of symptoms onset. Approximately 90% of ALS cases are sporadic (sALS), occurring without any familial history of the disease. The remaining 5–10% of cases constitute the familial form of ALS (fALS). Several genes have been implicated in fALS, notably the hexanucleotide repeat expansion in *C9ORF72* (Chromosome 9 open reading frame 72), *SOD1* (Superoxide dismutase 1), *TDP-43* (TAR DNA-binding protein 43) and *FUS* (Fused in Sarcoma) [28, 53, 61]. In 2011, Deng et al. first identified missense mutations in the Ubiquilin-2 (UBQLN2) gene in large ALS and ALS/FTD families, which has placed this protein as a new central actor in the physiopathology of ALS.

UBQLN2 is a shuttle protein implicated in the ubiquitin-proteasome system (UPS). One of the most actively studied mechanism in UBQLN2-related pathology is the mutant-related dysfunction of the UPS. However, its implication in the cytoplasmic mislocalization of TDP-43 into insoluble aggregates is also well described in ALS. More recently, ALS-linked mutations in *UBQLN2* gene were found to be associated with dysfunction of autophagy [24], neuroinflammation [49, 50] and formation of stress granules (SGs) [9]. These recent data surely placed UBQLN2 as an essential player in noxious protein accumulation and clearance pathways in ALS and FTD pathogenesis.

In this review we will describe the structure and the function of UBQLN2, and we will propose an integrative mechanism for the pathogenesis of UBQLN2 in ALS and FTD.

UBQLN2

Structure

The *UBQLN2* gene, also called *Chap1*/*Dsk2* or *PLIC*, is located on the Xp11.21 chromosome. UBQLN2 is a single-exon coded, 66 kDa protein member of the

* Correspondence: vincent.picher-martel.1@ulaval.ca
[1]Department of Psychiatry and Neuroscience, Laval University, Quebec, Canada
[2]CERVO Brain Research Center, 2601 Chemin de la Canardière, Québec, QC G1J 2G3, Canada
Full list of author information is available at the end of the article

ubiquilin family [12, 29]. UBQLN2 has a ubiquitin-like domain (UBL) in its N-terminal that can interact with the proteasome, and a ubiquitin-associated domain (UBA) on the C-terminal which recognizes the polyubiquitin chains on marked proteins [63]. UBQLN2 contains four stress-induced protein 1-like domains (STI-1 like), located between the residues 178–247 and 379–462, which are involved in the interaction with heat-shock proteins and autophagy mediators. UBQLN2 has also a unique PXX domain containing 12 tandem repeats implicated in protein-protein interactions [1, 12] (Fig. 1). This domain differentiates UBQLN2 from other members of the ubiquilin family. Interestingly, most of the mutations identified in the *UBQLN2* gene are located in the PXX domain. Yet, it is unclear how the mutations impact the secondary structure and functions of the PXX domain. The 3-dimensional structure of UBQLN2 is formed by five β-strands, an α-helix of 3.5 turns and an additional 3_{10}-helix [63].

Biological functions

UBQLN2 and the ubiquitin-proteasome system

UBQLN2 is located in the cytosol and has been reported to be mainly expressed in the brain, spleen, heart, liver, pancreas and other tissues [69]. The other members of the ubiquilin family have different tissue expression. UBQLN1 is expressed ubiquitously whereas UBQLN3 is expressed only in testis. UBQLN4 has the same expression profile than UBQLN2. UBQLN2 is mainly involved in protein homeostasis, directing misfolded or redundant proteins towards the proteasome. Proteins marked by ubiquitin, a highly conserved 76-residue polypeptide, are destined to get degraded in a three-step enzymatic cascade [63]. First, the ubiquitin activating enzyme E1 is binding ubiquitin to the protein by building a high-energy thiol ester intermediate. Then, the activated ubiquitin is shuttled from E1 to E2, building another high-energy thiol ester intermediate. A third-class enzyme, the ubiquitin ligase E3, mediates the covalent conjugation of polyubiquitin chains to a lysine residue of the specific UPS substrates. Polyubiquitinated proteins are then recognized by the UBL domain of UBQLN2 and brought to the S5a proteasomal cap of the 26S proteasome for degradation [39] (Fig. 2a). Likewise, UBQLN2 can be activated by heat shock protein 70 (HSP70) [24]. UBQLN2 is inactive under resting conditions but it becomes activated when HSP70 binds to proteins, generating an exposure of a UBQLN2-binding site. The activation of UBQLN2 promotes its binding to the 26S proteasome to form a degradation-competent complex.

Furthermore, UBQLN2 has been implicated in the degradation of endoplasmic reticulum (ER) proteins. UBQLN2 can interact with the ubiquitin regulatory X domain-containing protein 8 protein (Ubxd8), which is localized in the ER membrane and it facilitates the transport of endoplasmic-reticulum-associated protein degradation (ERAD) substrates to the cytosol [66]. UBQLN2 can also interact with Herp (homocysteine-induced ER protein) an ER membrane protein activated in stress conditions which induce the cellular protection by stabilizing ER Ca^{2+} homeostasis and maintaining mitochondrial function (Fig. 2a) [32].

UBQLN2 and autophagy

The implication of UBQLN2 in autophagy is now well established. Autophagy, specifically macroautophagy, is

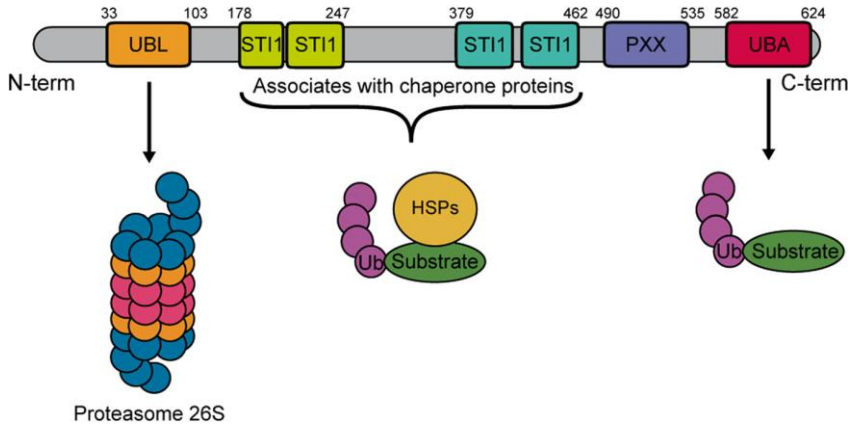

Fig. 1 Schematic representation of the domain architecture of the human *Ubiquilin-2* gene. *UBQLN2* gene is in the chromosome Xp11.21 and have only one coding exon. UBQLN2 possess a ubiquitin-like domain (UBL) domain on the N-terminal that interacts with the proteasome and a ubiquitin-associated domain (UBA) on the C-terminal required for the UPS activity. *UBQLN2* gene also arbors four stress-induced protein 1 (STI-1)-like motif and a proline-rich repeat domain containing 12 PXX repeats. UBL: Ubiquitin-like domain; STI-1: Stress-induced protein 1; UBA: Ubiquitin-associated domain; HSP70: Heat-shock protein 70; Ub: Ubiquitin

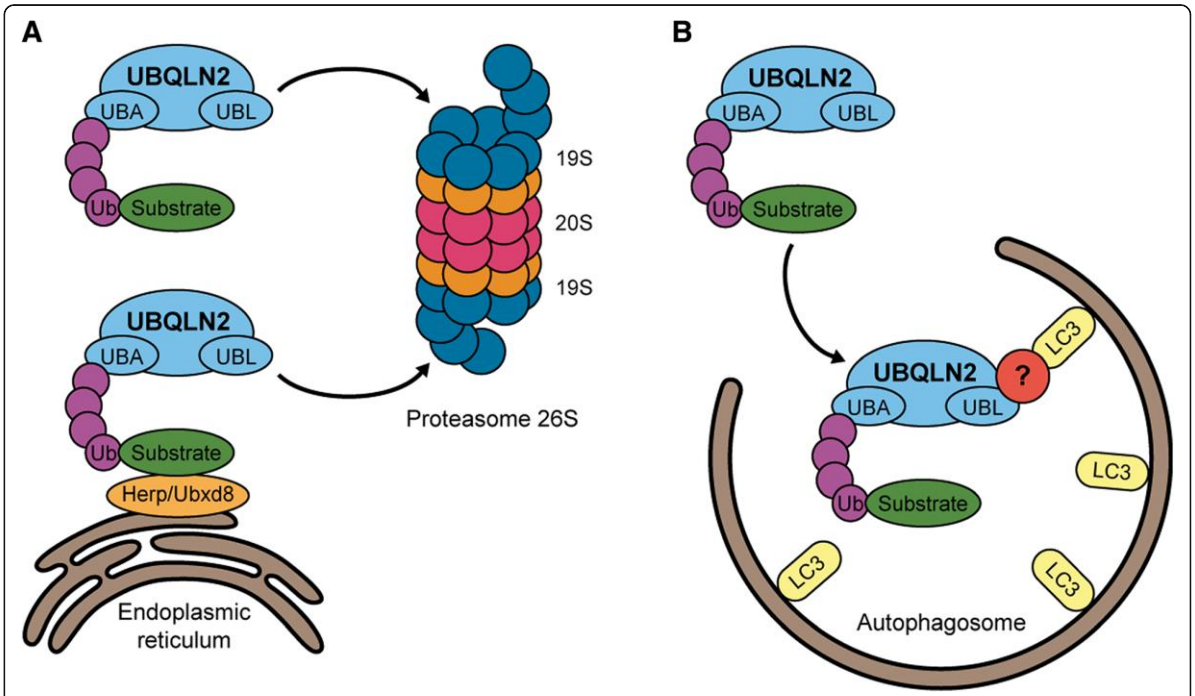

Fig. 2 Roles of UBQLN2 in protein degradation in both the UPS and the autophagy systems. **a** UBQLN2 targets ubiquitinated substrates and interacts with ER proteins involved in endoplasmic-reticulum-associated protein degradation (ERAD), such as Herp and Ubxd8, to drive substrates degradation by the 26S proteasome. **b** UBQLN2 is also implicated in the macroautophagy and interacts with LC3 indirectly through an unknown mechanism and can deliver ubiquitinated proteins bound to the ubiquitin-associated domain (UBA). UBQLN2: Ubiquilin-2; Ub: Ubiquitin; LC3: Microtubule-associated protein 1 light chain 3, Herp: Homocysteine-induced endoplasmic reticulum protein, isoform A. Ubxd8: ubiquitin regulatory X domain-containing protein 8

crucial for the bulk turnover of redundant cellular components, including protein aggregates and damaged organelles. A specific region of the cytosol is isolated in an intracellular double membrane stretch called autophagosome, secondarily fusing with lysosomes for degradation [23, 42, 43, 68]. UBQLN2 can indirectly interact with the membrane protein LC3, a marker for starvation-induced autophagy, of autophagosomes through its UBA domain to promote autophagosome formation and lysosomal fusion (Fig. 2b) [42, 54]. Interestingly, UBQLN2 was found to be recruited to Optineurin (OPTN)-containing vesicles in Neuro2a and HeLa cells co-transfected with wild-type myc-UBQLN2 and wild-type or E50K HA-OPTN [45]. Those vesicles are positives for autophagy markers, such as p62, LC3, autophagy-related protein 9a (APG9A) and autophagy-related 16 (ATG16). Likewise, a study with ChAttTA-9 transgenic rats crossed with TRE-UBQLN2^{P497H} measured the autophagic flux with an LC3 turnover assay [7]. LC3-II is one of the isoforms of LC3 and is broadly used to measure autophagic flux since its reduced levels is related to impaired autophagy. Transgenic rats used in the study showed significant decreased levels of LC3-II from 6 months of age. The same result was observed for ATG7, another autophagy component essential for autophagosome formation [7]. Thus, those results suggested that mutant UBQLN2^{P497H} compromised autophagy-lysosomal pathways in an age-related manner.

Ubiquilin-2 in amyotrophic lateral sclerosis

UBQLN2 mutations in familial ALS

UBQLN2 mutations were first identified in five unrelated families, suffering of ALS/FTD [12]. From this analysis, five mutations were found in the PXX domain and all consisted of substituted proline residues (P497H, P497S, P506T, P509S and P525S). Subsequently, more than 10 other mutations have been reported [11, 13, 16, 18, 20, 26, 41, 46, 59, 60, 64] (Table 1). Albeit most of mutations have been detected in the PXX domain, some of them were also found in the STI1 domains or between domains [62]. The authors examined 47 post-mortem spinal cord samples of a wide variety of ALS cases, such as sALS ($n = 23$), fALS without mutations in SOD1, TDP-43 and FUS ($n = 5$), ALS with dementia ($n = 5$) and fALS with G298S mutation in TDP-43 ($n = 21$) [12]. Also, brain autopsy samples of cases harboring UBQLN2^{P506T} mutation were analysed. All fALS cases exhibited co-localization of UBQLN2 and TDP-43 cytoplasmic inclusions in the brain and the spinal

Table 1 UBQLN2 mutations in ALS patients

Forms of ALS	Age at onset (years)	Mutations	Domain	Clinical features	Neuropathology	Ref.
Familial	16 to 71	P497H P497S P506T P509S P525S	PXX	Earlier onset in male (33.9 ± 14.0) than female (47.3 ± 10.8), ALS, ALS/FTD and pure FTD	TDP-43/UBQLN2 NCI in spinal cord and hippocampus	[12]
Familial	30 to 76	T487I	PXX	Earlier onset in male (39.5 ± 10.4) than female (51.2 ± 14.3), pure ALS, bulbar and spinal onset	FUS/UBQLN2/TDP-43/ubiquitin NCI in the spinal cord	[64]
Sporadic	51 to 73	Q425R A282V A283T	Outside domains	ALS and pure FTD, spinal onset	n/a	[59]
Familial	30 to 57	P506S P533L M446R V538 L N439I	PXX	ALS and ALS/FTD, spinal and bulbar onset	n/a	[18]
Sporadic	46 to 59	S155 N P189T	S155 N: outside P189T: STI-1	Pure ALS, bulbar and spinal onset	n/a	[11]
Familial	4 to 63	P497L	PXX	Phenotype diversity: Choreoathetoid movements, dysarthria, spastic paralysis, ALS, FTD	UBQLN2/TDP-43 NCI in brain stem and hippocampus, striatal atrophy, cerebral atrophy	[16]
Familial and sporadic[a]	27–62	P494L P500S P506A A488T	PXX A488T: outside	ALS and spastic paraplegia	n/a	[60]
Sporadic	62	M392 V	STI1	Pure ALS	n/a	[26]
Sporadic	14–16	M392I	STI1	Madras-type MND	n/a	[46]
Familial	52	p.Gly502_Ile504del	PXX	Bulbar ALS	n/a	[41]
Sporadic	30–77	S346C S400G P440L	Outside STI1	Pure FTD (S346C) and pure ALS	n/a	[13]

n/a not applicable, *NCI* neuronal cytoplasmic inclusions
[a] A488T was found in a sporadic case

cord neurons [12]. Interestingly, UBQLN2 was also found to be colocalizing with TDP-43 in the spinal cord of sALS patients, making it a component of the neuronal inclusions in patients affected with the sporadic form of the disease, suggesting a central role for this protein in ALS pathology [12, 17].

Proteasome and autophagy impairment

The degradation of misfolded or redundant proteins is critical for the maintenance of cellular health, specifically in neurons which are not proliferating cells. There is evidence that UBQLN2 mutations can provoke proteasome as well as autophagy impairments. First, an accumulation of the proteasome efficacy reporter Ubiquitin^{G76V}–GFP was detected in Neuro2a cells expressing mutant UBQLN2^{P497H} [12]. They further analyzed the dynamic of this reporter after blocking new protein synthesis with cycloheximide for 0, 2, 4 and 6 h in cells. The rates of Ubiquitin^{G76V}–GFP degradation were significantly slower in UBQLN2 mutations (P497H and P506T) when compared to the WT, suggesting the impairment of the protein degradation pathway by UBQLN2 mutations. Another group took advantage of the endogenous Myc as a proteasome efficiency reporter, as it is quickly degraded by the proteasome when its synthesis is blocked by cycloheximide [6]. In HeLa cells expressing mutant UBQLN2 (P497H, P497S, P506T, P509S or P525S) and treated with cycloheximide, a delay in the degradation of Myc was observed as compared to untransfected cells. However, when a chymotrypsin-like test was used to measure efficiency of the proteasome, no dysfunction of the proteasome was detected, which is contradictory with the previous study. Other studies suggested that mutant IVm-UBQLN2 could impede the UPS by reducing the delivery of ubiquitinated proteins to the proteasome [6, 44]. Indeed, ALS-linked mutation in UBQLN2 led to accumulation of ubiquitinated high-molecular-weight complexes (HMWCs). Deletion of the UBL domain of mutant UBQLN2 sequestered ubiquitinated substrates from both the UPS and autophagy (mATG9 and ATG16L1), resulting in an enhanced HMWCs accumulation [44]. Those results suggest that mutant UBQLN2 potentially interferes with the degradation of the polyubiquitinated substrates. Likewise, deletion of UBQLN2 UBL domain impaired the clearance of unfolded nascent polypeptide chains while UBQLN2 levels remained unaffected [24]. Recently, our group highlighted that overexpression of mutant UBQLN2^{P497H}

in Neuro2A cells sequestered lys^{48}– bound ubiquitin and resulted in a reduction in the efficiency of the proteasome [50]. This also supports the evidences that mutant UBQLN2 is actively impairing the UPS pathway.

Another study reported, with a knocked-in hUBQLN2^{P506T} mouse, that UBQLN2 works with the HSP70 system for proteasomal degradation of insoluble ubiquitylated protein aggregates [24]. Under non-stressed conditions nor mutations, UBQLN2 is inactive in homo- or heterodimers. In presence of HSP70 clients, UBQLN2 binds itself to HSP70 and associated ubiquitinated aggregated/misfolded proteins. HSP70-HSP110-dependent disaggregase activities can pull aggregated proteins apart, allowing UBQLN2 to form a HSP70-client-UBQLN2-proteasome degradation complex. UBQLN2 can then act as a proteasomal shuttle by connecting ubiquitylated proteins to the proteasome for degradation, leading to the proteolysis of the client. However, mutant UBQLN2 no longer recognized client-bound HSP70 and remained in its inactive phase, leading to accumulation of misfolded/aggregated proteins [24]. Defect in HSP70 binding was later confirmed in ALS patients' lymphoblasts with P494L, P497H or P506A mutations in UBQLN2 [60]. They also confirmed the role of UBQLN2 as a shuttle factor for HSP70-bound substrates which was previously shown [24]. Thus, activation of UBQLN2 in order to bind to HSP70 seems to represent an important step to accomplish its normal degradation function.

Lastly, optineurin (OPTN) is a ubiquitin-binding multifunctional adaptor protein and is mainly implicated in the autophagy processes. It has also been proposed to be an important factor implicated in regulation of inflammation [38]. UBQLN2 and OPTN can be localized to the same cellular compartment, the Rab11-positive endosomal vesicles [45]. This observation led to propose that these proteins are involved in the same pathological processes in motor neurons diseases. Indeed, OPTN+/UBQLN2+ vesicles showed features of recycling endosomes and were positives for the key autophagy-regulating molecules p62, LC3, mAPG9L1, ATG16, and the autophagy initiator ULK1, suggesting that these vesicles are involved in protein homeostasis [45]. Thus, OPTN and UBQLN2 are implicated in protein homeostasis of the endosomal system via autophagy. Disrupting the function of these vesicles may contribute to development of ALS.

Direct interaction with TDP-43 promoting aggregation

It has been reported that cytoplasmic inclusions of mutant C-terminal TDP-43 colocalized with either WT or mutant UBQLN2 in co-transfected Neuro2a cells [12]. UBQLN2 directly interacts with the C-terminal fragments of TDP-43 [4]. Moreover, results from our laboratory suggested that the overexpression of either hUBQLN2^{WT} or mutated hUBQLN2^{P497H} in Neuro2A cells can promote the formation of TDP-43 cytoplasmic inclusions [49]. Yet, the mutated form of UBQLN2 induced a stronger cytoplasmic mis-localization of TDP-43 as compared to the WT form. Those results were consistent with other studies that reported the high affinity of TDP-43 and UBQLN2 to form inclusions in the cytosol [4, 12, 16, 27, 34]. The formation of these inclusions has also been reported to be dose dependent. Cells with low expression of WT or mutant UBQLN2 did not exhibit cytoplasmic inclusions of UBQLN2 in TDP-43 aggregates [12, 49].

Strategies to increase ubiquitination have been proposed to boost UPS function [8]. In this regard, our group hypothesised that mutated UBQLN2 may sequester ubiquitin proteins, thereby reducing the degradation of mutated TDP-43 by the UPS and exacerbating the formation of cytoplasmic aggregates [50]. The co-expression, in Neuro2A cells, of hUBQLN2^{P497H} and hTDP-43^{G348C} vectors led to the accumulation of cytoplasmic TDP-43. However, ubiquitin overexpression reduced the cytoplasmic aggregation of TDP-43 [50]. A chymotrypsin-like assay was completed to measure the proteasome efficacy in hUBQLN2^{P497H} and hTDP-43^{G348C} transfected cells. This assay revealed a significant reduction in proteasome efficacy in all transfected cells as compared to control cells. The presence of up-regulated ubiquitin levels corrected the proteasome dysfunction in cells transfected with hUBQLN2^{P497H} and in cells co-transfected with both hUBQLN2^{P497H} and hTDP-43^{G348C}. These results suggested that the proteasome impairment caused by hUBQLN2^{P497H} up-regulation may participate to cytoplasmic TDP-43 accumulation. In summary, UBQLN2 overexpression or mutation exacerbated TDP-43 pathology in vitro (Fig. 3). A reduction of UBQLN2 expression or an up-regulation of ubiquitin may constitute potential therapeutic avenues for ALS pathology.

UBQLN2 in neuroinflammation

The implication of UBQLN2 in inflammation has emerged in the last two to 3 years. The overexpression of hUBQLN2^{WT} and hUBQLN2^{P497H} in Neuro2A cells was found to increase the phosphorylation of p38 MAPK and the nuclear levels of the phosphorylated form of the Nuclear Factor kappa-B (NF-κB), a potent inflammatory mediator [49]. However, it remains unclear if the activation of NF-κB is directly caused by the accumulation of UBQLN2 or comes from the UBQLN2-drived mislocalization of TDP-43 or other mechanisms [58]. Nevertheless, the down-regulation of UBQLN2 with siRNA reversed the increased NF-κB activation. NF-κB is a transcription factor involved in inflammation and probably has a noxious role in ALS and other neurological diseases. Indeed, the RNA levels of NF-κB as well as the

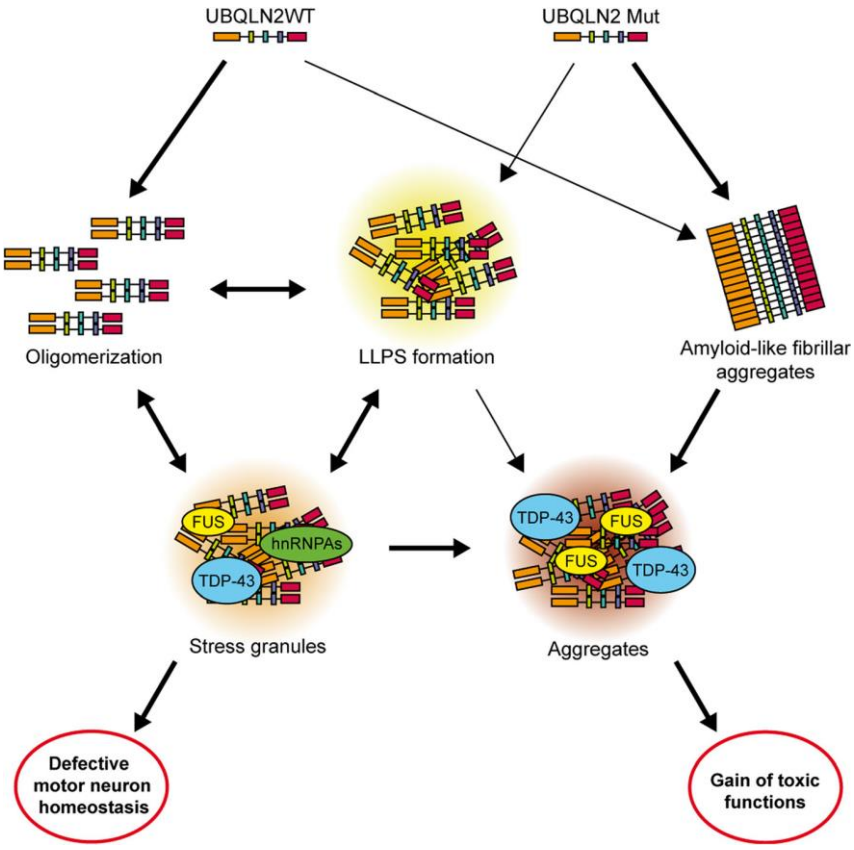

Fig. 3 The integrative model for WT and mutant UBQLN2 pathology in ALS. WT UBQLN2 is prone to form oligomers with itself and associates with ubiquitinated substrates, chaperones and other molecules. WT UBQLN2 oligomers can assemble into membraneless organelles and form liquid-liquid phase separation droplets. The mechanism is UBQLN2 levels-dependant. Ubiquitin-binding can prevent this self-assembly and oligomerization of UBQLN2 and an increase of ubiquitin can remove the UBQLN2 LLPS formation. LLPS formations as well as oligomers of UBQLN2 can also become stress granules (SGs). The persistence of SGs can become aggregates or can lead to defect in RNA processing, leading to motor neurons death. Mutant UBQLN2 forms amyloid-like fibrillar aggregates, even in the absence of ubiquitin and chaperones. UBQLN2 mutation increase its insolubility and ubiquitin-binding. A reduced HSP70 binding and autophagy degradation can lead to the formation of aggregates. Aggregation is suspected to be driven by the UBA domain, while the UBL domain seems to inhibit aggregations. UBQLN2WT: Ubiquilin-2 wild-type; UBQLN2 Mut: Ubiquilin-2 mutants; LLPS: Liquid-liquid phase separation; FUS: Fused in sarcoma RNA-binding protein; TDP-43: TAR DNA-binding protein-encoding TDP-43; hnRNPAs: Heterogeneous nuclear ribonucleoprotein A

levels of TDP-43 were abnormally up-regulated in the spinal cord of ALS patients [58]. TDP-43 was found to interact with p65 NF-κB in spinal cord of ALS but not in control. NF-κB inhibition by withaferin A treatment attenuated disease phenotype in mice expressing mutant TDP-43 and it increased survival in mutant SOD1 mice [14, 15, 48, 58]. Mice harboring UBQLN2^{P497H};TDP-43^{G348C} mutations also exhibited increased levels of NF-κB in spinal cord as compared to TDP-43^{G348C} mice [50]. The double transgenic mice also expressed higher levels of pro-inflammatory cytokines CCL1, CCL5 and CXCL1 and higher stages of activated microglia in the spinal cord as compared to single TDP-43 transgenic mice. Noteworthy, the UBQLN2^{P497H} transgene was only expressed in neurons. The increased inflammation markers could suggest that microglia were hyperactivated in reaction to UBQLN2/TDP-43 neuronal pathology. These results also suggested that UBQLN2 pathology may favorize neuroinflammation and the reduction of UBQLN2 cytoplasmic accumulation may be a potential treatment approach to reduce glial cells activation observed in ALS.

Stress granules

Stress granules (SGs) are cytoplasmic inclusions of proteins and maintenance mRNAs with the aim of promoting stress response proteins translation in stressful situations, such as oxidative stress, osmotic stress, infection, ER stress and inhibition of the proteasome [3]. Under stress conditions, rather than engaging with the

protein degradation system via its UBA and UBL domains, UBQLN2 associates with SGs components through its STI1-like region. UBQLN2 influences the early processes of molecular complex dynamics in phase separation that drives SGs formation. A group recently suggested that UBQLN2 modulates the state of the components to be recruited to SGs rather than regulating the levels of core SGs components [2]. One of the main components identified as UBQLN2-interacting SGs were heterogeneous nuclear ribonucleoproteins A (hnRNPAs) [2, 19]. UBQLN2 has been shown to colocalize with SGs in vitro under different cellular stressor. Indeed, UBQLN2 undergoes liquid-liquid phase separation (LLPS) which correlates with UBQLN2 ability to form stress-induced puncta inside cells [9]. LLPS consist of phase-separation of proteins composed of low-complexity or prion-like domains into membrane-less and spherical compartments. Persistent stress, mutations and aging are suspected to induce liquid-solid phase separation (LSPS) and might become irreversible aggregation, such as amyloid-like aggregates [52, 57]. Also, UBQLN2 puncta formation and stress granules (SGs) colocalization are highly sensitive to levels of UBQLN2 expression.

Stress granules contain various proteins, including fALS related proteins, TDP-43, FUS, hnRNPA1 and 2. A disturbance in stress granules homeostasis can lead to disruption of RNA processing [37] (Fig. 3). It has been recently reported that overexpression of mutated UBQLN2 (P497H and P506T) in HeLa cells directly impaired the binding of UBQLN2 to FUS which resulted in a loss of the ability of UBQLN2 to regulate FUS-RNA complexes and SGs formation [2]. Mutations in FUS and hnRNPA1 have been reported to increase their propensity to accumulate in SGs, disrupting SGs primary function to act as a stress response modulator [30, 36, 47]. Other studies reported that UBQLN2 upregulation can cause a cellular stress leading to MAPK activation, which have been recently shown to have a critical role in TDP-43 accumulation in stress granules following a chronic stress [40, 49].

Ubiquitin is also a common component of SGs [12, 33]. The specific binding between ubiquitin and UBQNL2 could prevent the self-assembly and oligomerization of UBQLN2 [9]. Spectrophotometric assays of ubiquitin and UBQLN2 at different molar ratios, revealed that LLPS formation decreased with the enhancement of ubiquitin. Those results might provide an insight by which UBQLN2 could traffic ubiquitinated substrates from SGs to the proteasome (Fig. 3) [9]. Another group reported that the UBA domain of UBQLN2 drove amyloid-like aggregation of UBQLN2 in vitro and without the help of ubiquitin or chaperones [56]. The UBA domain responsible for binding ubiquitinated substrates was also implicated in the promotion of aggregation because of the propensity of UBQLN2 to self-assemble and then aggregate. That process was modulated by ubiquitin binding to UBQLN2. Indeed, the behavior of the ubiquitin-binding-deficient form $UBQLN2^{L619A}$ in neurons could prevent UBQLN2 self-assembly and could inhibit LLPS of UBQLN2 [56]. Also, expression of $UBQLN2^{L619A}$ induced a 50% increase in neuronal death compared to WT. Collectively, those results suggest that the UBA domain promotes self-assembly of the protein leading to an increase in UBQLN2 aggregation with toxic consequences for neurons.

The LLPS capacity of a protein is based on its multivalent interactions in "sticker" regions which are separated by "spacers" [22]. Recently, a group exposed that ALS-linked mutations, depending of amino acid and sequence position, differently affect the implication of UBQLN2 in LLPS [10]. PXX domain mutations favorize UBQLN2 oligomerization and LLPS formation, creating reversible aggregates which can be cleared by binding to ubiquitin. Mutations to hydrophobic amino acid (P497L, P506A, T487I) increased the interaction between stickers and increased oligomerization of UBQLN2. Inversely, mutations to hydrophile residues (A488T, P500S, P506S, P509S, P525S) have small impact on oligomerization [10]. Increasing the hydrophobicity within "stickers", but not "spacers", favorized the oligomerization tendency of UBQLN2 [67]. The sequence position also greatly impacts UBQLN2 capacity for oligomerization. Oligomerization was high with mutation in 497 position and appeared to be little with mutation 500, 509 or 525 positions [10].

ALS animal models of Ubiquilin-2

Animal models are essential to study in vivo pathological mechanisms as well as to test experimental therapeutic avenues, and numerous animal models were generated for ALS research (recently reviewed in [51]). Several models expressing UBQLN2 mutations have been reported in the past years (Table 2). The first transgenic mouse model was expressing $hUBQLN2^{P497H}$ under the control of the hUBQLN2 promoter [21]. The animals developed cognitive deficits, a dendritic spinopathy as well as UBQLN2 inclusions in the hippocampus. However, no TDP-43 pathology nor loss of motor neurons were reported in this study. This may be explained by the low level of transgene expression. Indeed, in this model, the levels of $hUBQLN2^{P497H}$ was comparable to the levels of endogenous $UBQLN2^{WT}$. Another group used a transgenic $hUBQLN2^{P497H}$ rat model with TRE-doxycycline system [65]. Their model displayed cognitive deficits associated with UBQLN2 aggregates in hippocampus and evidence of neuronal death in cortex at the age of 130 days. Using knocked-in technique, $hUBQLN2^{P506T}$ mice were generated and showed cognitive impairment but no motor deficits [24]. The

Table 2 UBQLN2 animal models

Species	Mutations	Age at onset (days)	Motor neuron loss	Cognitive deficits	Neuropathological particularities	Ref.
Mice	P497H	30	N	Y	Dendritic spinopathy. Hippocampal NCI (no TDP-43 but with proteasome component, VCP and OPTN)	[21]
Rats	KO P497H	130	N	Y	Hippocampal and cortical neuronal loss, UBQLN2/P62 NCI (no TDP-43), KO rats exhibit no phenotype	[65]
Mice	WT P497H P497S P506T	90	N	Y	UBQLN2 AAV expression, hippocampal and cortical NCI (with UBQLN2, TDP-43, p62, ubiquitin and OPTN), motor phenotype	[5]
Mice	WT P497S P506T	90	Y	Y	Hippocampal and MN NCI (with UBQLN2, TDP-43 and Ubiquitin), motor phenotype, muscle atrophy, NMJ loss, axonal degeneration, gliosis some MN loss and axonal degeneration in WT	[34]
Mice	mP520T (KI)	270	N	Y	Hippocampal, cortical and brainstem NCI (with UBQLN2 and p62) no motor phenotype	[24]
Rats	WT P497H	40	N	Y	Similar phenotype in WT and P497H hippocampal and cortical neuronal loss, NCI (UBQLN2, p62, ubiquitin and RPT1), no motor phenotype	[25]
DM	WT P497H P525S P4X	28 7 14 0	Y	N	NMJ loss in P497H, eye degeneration in mutant, NCI (UBQLN2, ubiquitin and p62) motor phenotype	[31]
Rats	P497H	90	Y	N	Muscle atrophy, axonal degeneration, NMJ loss, MN NCI (UBQLN2, p62, p-TDP-43), motor phenotype no phenotype when expressed in astrocytes	[7]
DM	KO	3	N	N	NCI (UBQLN2, TDP-43 and ubiquitin) motor phenotype	[27]
Mice	UB^{P497H}/$TDP\text{-}43^{G348C}$	150	Y	Y	Hippocampal and MN NCI (UBQLN2, TDP-43, pTDP-43, ubiquitin and p62), muscle atrophy, axonal degeneration, gliosis, motor phenotype	[50]

WT wild-type, *Y* yes, *N* no, *n/a* not applicable, *HTT* huntington disease protein, *NCI* neuronal cytoplasmic inclusions, *MN* motor neurons, *NMJ* neuromuscular junction, *KI* knock-in, *DM Drosophila melanogaster*

knocked-in approach resulted in low levels of UBQLN2, which may explain the results.

Transgenic mice bearing Thy1.2-driven $hUBQLN2^{P497S}$ or $hUBQLN2^{P506T}$ mutations exhibited motor neurons loss and cognitive impairments [34]. The levels of mutated UBQLN2 expression in those mice were 70–80% of the endogenous mouse UBQLN2 but the phenotypes were not consistent within all the animal cohorts. Indeed, only 10% of the transgenic $hUBQLN2^{P497S}$ mice and 40% of $hUBQLN2^{P506T}$ mice developed hindlimb paralysis. Interestingly, TDP-43 mislocalization could be noted in neurons. Transgenic mice overexpressing $hUBQLN2^{WT}$ also showed loss of upper motor neurons as well as hippocampal neurons. Nevertheless, the effects were less important than those observed in the mutant transgenic mice. Knockout models were also generated, but phenotypes were highly divergent between species (Table 2). While knockout rats did not exhibit any phenotype [65], UBQLN2 knockout in *Drosophila melanogaster* (DM) created a severe motor phenotype with TDP-43/Ubiquitin/UBQLN2 aggregation [27]. The cause for this discrepancy is unknown, but could potentially be explained by the fact that DM carry only one human UBQLN2 orthologue (dUbqn), as compared to rats and human, which possesses four members of the UBQLN family [35]. Consequently, other members of the UBQLN family could possibly compensate for UBQLN2 functions in rats.

Lastly, our team generated the first double transgenic mouse model harboring both $hUBQLN2^{P497H}$ and $hTDP\text{-}43^{G348C}$ mutations using a NFH promoter with low levels of expression [50]. The simple transgenic mice $hUBQLN2^{P497}$animal models are summarized in Table 2.

Conclusion and future directions

Collectively, these multiple reports suggest that UBQLN2 is acting on various ALS pathological mechanisms and is not only causing an UPS dysfunction as previously recognized. It is now documented that UBQLN2 is acting on

stress granules formation, on TDP-43 mislocalization into cytoplasmic inclusions, on cellular clearance pathways and neuroinflammation. Thus far, the pathological role of mutated UBQLN2 is more defined, but many questions remain on the exact role of the WT UBQLN2 in sporadic cases of ALS. Nevertheless, the tight control in the levels of UBQLN2 appears to be a primary factor for its role in the clearance pathway and stress granules formation. A small disturbance in its levels could promote oligomerization and trigger dysfunction in LLPS formation, inducing aggregates formation and causing toxicity in neurons. To our knowledge, the levels of UBQLN2 in tissues from sporadic ALS cases without UBQLN2 mutation have never been evaluated nor neuropathological studied and this question should be addressed. Indeed, the WT UBQLN2 form also appears to have a toxic role when overexpressed [12, 49]. It would be of interest to study the relationship between levels of UBQLN2 and the proteasome dysfunction in sporadic ALS. The down regulation of UBQLN2 using antisense oligonucleotide (ASO) or other gene therapy approaches could be a potential strategy for cases with genetic UBQLN2 mutations. This could have an impact on the efficacy of the proteasomal and autophagy clearance pathways to reduce toxic protein accumulation in motor neurons. While, UBQLN2 may provide a promising target for the development of new therapeutics, more work is needed to analyze the potential impact of reducing UBQLN2 levels with therapies in familial and sporadic diseases.

Abbreviations

ALS: Amyotrophic lateral sclerosis; APG9A: Autophagy-related protein 9a; ATG16: Autophagy-related 16; C9ORF72: Chromosome 9 open reading frame 72; CCL1: C-c motif chemokine ligand 1; CCL5: C-c motif chemokine ligand 5; CXCL1: C-x-c motif chemokine ligand 1; ER: Endoplasmic reticulum; ERAD: Endoplasmic-reticulum-associated protein degradation; fALS: Familial amyotrophic lateral sclerosis; FTD: Frontotemporal dementia; FUS: Fused in Sarcoma; HMWCs: High-molecular-weight complexes; hnRNPA1: Heterogeneous nuclear ribonucleoprotein A1; HSP70: Heat shock protein 70; LLPS: Liquid-liquid phase separation; LSPS: Liquid-solid phase separation; MAPK: Mitogen-activated protein kinases; NF-κB: Nuclear Factor kappa-B; OPTN: Optineurin; RNA: Ribonucleic acid; sALS: Sporadic amyotrophic lateral sclerosis; SGs: Stress granules; SH3: Src homologue 3 protein; SOD1: Super-oxide dismutase 1; STI-I: Stress induced protein 1-like; TDP-43: TAR DNA-binding protein 43; UBA: Ubiquitin-associated domain; UBL: Ubiquitin-like domain; UBQLN2: Ubiquilin-2; Ubxd8: Ubiquitin regulatory X domain-containing protein 8 protein; UPS: Ubiquitin-proteasome system; WT: Wild-type

Acknowledgements

We want to thank Philippe Codron for his resourceful advices and Louis-Charles Béland for his grateful help with figures production.

Authors' contributions

L.R. performed the review of the literature, made the tables and figures and wrote the manuscript. P.C. reviewed the paper. V.P-M. and J-P.J. corrected the manuscript and provided income about the data. VP-M and J-P.J corrected the manuscript and provided income about the data. All authors read and approved the final manuscript.

Funding

This work was supported by the Canadian Institutes of Health Research (CIHR). J.-P. J. holds a Canada Research Chair in neurodegeneration and V.P-M. detained a Frederick Banting and Charles Best scholarship from CIHR.

Availability of data and materials

Not applicable.

Ethics approval and consent to participate

Not applicable.

Consent for publication

Not applicable.

Competing interests

The authors declare that they have no competing interests.

Author details

[1]Department of Psychiatry and Neuroscience, Laval University, Quebec, Canada. [2]CERVO Brain Research Center, 2601 Chemin de la Canardière, Québec, QC G1J 2G3, Canada. [3]UMR CNRS 6015, INSERM U1083, University of Angers, Angers, France.

Received: 18 May 2019 Accepted: 22 June 2019
Published online: 18 July 2019

References

1. Aitio O, Hellman M, Kazlauskas A, Vingadassalom DF, Leong JM, Saksela K et al (2010) Recognition of tandem PxxP motifs as a unique Src homology 3-binding mode triggers pathogen-driven actin assembly. Proc Natl Acad Sci U S A 107(50):21743–21748
2. Alexander EJ, Ghanbari Niaki A, Zhang T, Sarkar J, Liu Y, Nirujogi RS et al (2018) Ubiquilin 2 modulates ALS/FTD-linked FUS-RNA complex dynamics and stress granule formation. Proc Natl Acad Sci U S A 115(49):E11485–E11e94
3. Aulas A, Vande Velde C (2015) Alterations in stress granule dynamics driven by TDP-43 and FUS: a link to pathological inclusions in ALS? Front Cell Neurosci 9:423
4. Cassel JA, Reitz AB (2013) Ubiquilin-2 (UBQLN2) binds with high affinity to the C-terminal region of TDP-43 and modulates TDP-43 levels in H4 cells: characterization of inhibition by nucleic acids and 4-aminoquinolines. Biochim Biophys Acta 1834(6):964–971
5. Ceballos-Diaz C, Rosario AM, Park HJ, Chakrabarty P, Sacino A, Cruz PE et al (2015) Viral expression of ALS-linked ubiquilin-2 mutants causes inclusion pathology and behavioral deficits in mice. Mol Neurodegener 10(1):25
6. Chang L, Monteiro MJ (2015) Defective proteasome delivery of Polyubiquitinated proteins by Ubiquilin-2 proteins containing ALS mutations. PLoS One 10(6):e0130162
7. Chen T, Huang B, Shi X, Gao L, Huang C (2018) Mutant UBQLN2(P497H) in motor neurons leads to ALS-like phenotypes and defective autophagy in rats. Acta Neuropathol Commun. 6(1):122
8. Cozzolino M, Pesaresi MG, Gerbino V, Grosskreutz J, Carri MT (2012) Amyotrophic lateral sclerosis: new insights into underlying molecular mechanisms and opportunities for therapeutic intervention. Antioxid Redox Signal 17(9):1277–1330
9. Dao TP, Kolaitis RM, Kim HJ, O'Donovan K, Martyniak B, Colicino E et al (2018) Ubiquitin modulates liquid-liquid phase separation of UBQLN2 via disruption of multivalent interactions. Mol Cell 69(6):965–78.e6
10. Dao TP, Martyniak B, Canning AJ, Lei Y, Colicino EG, Cosgrove MS et al (2019) ALS-linked mutations affect UBQLN2 oligomerization and phase separation in a position- and amino acid-dependent manner. Structure. 27(6):937–51.e5
11. Daoud H, Suhail H, Szuto A, Camu W, Salachas F, Meininger V et al (2012) UBQLN2 mutations are rare in French and French-Canadian amyotrophic lateral sclerosis. Neurobiol Aging 33(9):2230.e1–2230.e5
12. Deng HX, Chen W, Hong ST, Boycott KM, Gorrie GH, Siddique N et al (2011) Mutations in UBQLN2 cause dominant X-linked juvenile and adult-onset ALS and ALS/dementia. Nature. 477(7363):211–215
13. Dillen L, Van Langenhove T, Engelborghs S, Vandenbulcke M, Sarafov S, Tournev I et al (2013) Explorative genetic study of UBQLN2 and PFN1 in an

extended Flanders-Belgian cohort of frontotemporal lobar degeneration patients. Neurobiol Aging 34(6):1711.e1–1711.e5
14. Dutta K, Patel P, Julien JP (2018) Protective effects of Withania somnifera extract in SOD1(G93A) mouse model of amyotrophic lateral sclerosis. Exp Neurol 309:193–204
15. Dutta K, Patel P, Rahimian R, Phaneuf D, Julien JP (2017) Withania somnifera reverses Transactive response DNA binding protein 43 Proteinopathy in a mouse model of amyotrophic lateral sclerosis/frontotemporal lobar degeneration. Neurotherapeutics. 14(2):447–462
16. Fahed AC, McDonough B, Gouvion CM, Newell KL, Dure LS, Bebin M et al (2014) UBQLN2 mutation causing heterogeneous X-linked dominant neurodegeneration. Ann Neurol 75(5):793–798
17. Fecto F, Siddique T (2011) Making connections: pathology and genetics link amyotrophic lateral sclerosis with frontotemporal lobe dementia. J Mol Neurosci 45(3):663–675
18. Gellera C, Tiloca C, Del Bo R, Corrado L, Pensato V, Agostini J et al (2013) Ubiquilin 2 mutations in Italian patients with amyotrophic lateral sclerosis and frontotemporal dementia. J Neurol Neurosurg Psychiatry 84(2):183–187
19. Gilpin KM, Chang L, Monteiro MJ (2015) ALS-linked mutations in ubiquilin-2 or hnRNPA1 reduce interaction between ubiquilin-2 and hnRNPA1. Hum Mol Genet 24:2565–2577
20. Gkazi SA, Troakes C, Topp S, Miller JW, Vance CA, Sreedharan J et al (2019) Striking phenotypic variation in a family with the P506S UBQLN2 mutation including amyotrophic lateral sclerosis, spastic paraplegia, and frontotemporal dementia. Neurobiol Aging 73(229):e5–e9
21. Gorrie GH, Fecto F, Radzicki D, Weiss C, Shi Y, Dong H et al (2014) Dendritic spinopathy in transgenic mice expressing ALS/dementia-linked mutant UBQLN2. Proc Natl Acad Sci U S A 111(40):14524–14529
22. Harmon TS, Holehouse AS, Rosen MK, Pappu RV (2017) Intrinsically disordered linkers determine the interplay between phase separation and gelation in multivalent proteins. Elife 6:e30294
23. Hayashi-Nishino M, Fujita N, Noda T, Yamaguchi A, Yoshimori T, Yamamoto A (2009) A subdomain of the endoplasmic reticulum forms a cradle for autophagosome formation. Nat Cell Biol 11(12):1433–1437
24. Hjerpe R, Bett JS, Keuss MJ, Solovyova A, McWilliams TG, Johnson C et al (2016) UBQLN2 mediates autophagy-independent protein aggregate clearance by the proteasome. Cell. 166(4):935–949
25. Huang B, Wu Q, Zhou H, Huang C, Xia XG (2016) Increased Ubqln2 expression causes neuron death in transgenic rats. J Neurochem 139(2): 285–293
26. Huang X, Shen S, Fan D (2017) No evidence for pathogenic role of UBQLN2 mutations in sporadic amyotrophic lateral sclerosis in the mainland Chinese population. PLoS One 12(1):e0170943
27. Jantrapirom S, Lo Piccolo L, Yoshida H, Yamaguchi M (2018) Depletion of Ubiquilin induces an augmentation in soluble ubiquitinated Drosophila TDP-43 to drive neurotoxicity in the fly. Biochim Biophys Acta Mol basis Dis 1864(9 Pt B):3038–3049
28. Kabashi E, Valdmanis PN, Dion P, Spiegelman D, McConkey BJ, Vande Velde C et al (2008) TARDBP mutations in individuals with sporadic and familial amyotrophic lateral sclerosis. Nat Genet 40(5):572–574
29. Kaye FJ, Shows TB (2000) Assignment of ubiquilin2 (UBQLN2) to human chromosome xp11. 23–>p11.1 by GeneBridge radiation hybrids. Cytogenet Cell Genet 89(1–2):116–117
30. Kim HJ, Kim NC, Wang YD, Scarborough EA, Moore J, Diaz Z et al (2013) Mutations in prion-like domains in hnRNPA2B1 and hnRNPA1 cause multisystem proteinopathy and ALS. Nature. 495(7442):467–473
31. Kim SH, Stiles SG, Feichtmeier JM, Ramesh N, Zhan L, Scalf MA et al (2018) Mutation-dependent aggregation and toxicity in a Drosophila model for UBQLN2-associated ALS. Hum Mol Genet 27(2):322–337
32. Kim TY, Kim E, Yoon SK, Yoon JB (2008) Herp enhances ER-associated protein degradation by recruiting ubiquilins. Biochem Biophys Res Commun 369(2):741–746
33. Kwong LK, Neumann M, Sampathu DM, Lee VM, Trojanowski JQ (2007) TDP-43 proteinopathy: the neuropathology underlying major forms of sporadic and familial frontotemporal lobar degeneration and motor neuron disease. Acta Neuropathol 114(1):63–70
34. Le NT, Chang L, Kovlyagina I, Georgiou P, Safren N, Braunstein KE et al (2016) Motor neuron disease, TDP-43 pathology, and memory deficits in mice expressing ALS-FTD-linked UBQLN2 mutations. Proc Natl Acad Sci U S A 113:E7580–E7589
35. Li A, Xie Z, Dong Y, McKay KM, McKee ML, Tanzi RE (2007) Isolation and characterization of the Drosophila ubiquilin ortholog dUbqln: in vivo interaction with early-onset Alzheimer disease genes. Hum Mol Genet 16(21):2626–2639
36. Lin Y, Protter DS, Rosen MK, Parker R (2015) Formation and maturation of phase-separated liquid droplets by RNA-binding proteins. Mol Cell 60(2): 208–219
37. Majcher V, Goode A, James V, Layfield R (2015) Autophagy receptor defects and ALS-FTLD. Mol Cell Neurosci 66(Pt A):43–52
38. Markovinovic A, Cimbro R, Ljutic T, Kriz J, Rogelj B, Munitic I (2017) Optineurin in amyotrophic lateral sclerosis: multifunctional adaptor protein at the crossroads of different neuroprotective mechanisms. Prog Neurobiol 154:1–20
39. McKinnon C, Tabrizi SJ (2014) The ubiquitin-proteasome system in neurodegeneration. Antioxid Redox Signal 21(17):2302–2321
40. Meyerowitz J, Parker SJ, Vella LJ, Ng D, Price KA, Liddell JR et al (2011) C-Jun N-terminal kinase controls TDP-43 accumulation in stress granules induced by oxidative stress. Mol Neurodegener 6:57
41. Millecamps S, Corcia P, Cazeneuve C, Boillee S, Seilhean D, Danel-Brunaud V et al (2012) Mutations in UBQLN2 are rare in French amyotrophic lateral sclerosis. Neurobiol Aging 33(4):839.e1–839.e3
42. N'Diaye EN, Kajihara KK, Hsieh I, Morisaki H, Debnath J, Brown EJ (2009) PLIC proteins or ubiquilins regulate autophagy-dependent cell survival during nutrient starvation. EMBO Rep 10(2):173–179
43. N'Diaye M, Le Ferrec E, Kronenberg F, Dieplinger H, Le Vee M, Fardel O (2009) TNFalpha- and NF-kappaB-dependent induction of the chemokine CCL1 in human macrophages exposed to the atherogenic lipoprotein(a). Life Sci 84(13–14):451–457
44. Osaka M, Ito D, Suzuki N (2016) Disturbance of proteasomal and autophagic protein degradation pathways by amyotrophic lateral sclerosis-linked mutations in ubiquilin 2. Biochem Biophys Res Commun 472(2):324–331
45. Osaka M, Ito D, Yagi T, Nihei Y, Suzuki N (2015) Evidence of a link between ubiquilin 2 and optineurin in amyotrophic lateral sclerosis. Hum Mol Genet 24(6):1617–1629
46. Ozoguz A, Uyan O, Birdal G, Iskender C, Kartal E, Lahut S et al (2015) The distinct genetic pattern of ALS in Turkey and novel mutations. Neurobiol Aging 36(4):1764.e9–1764e18
47. Patel A, Lee HO, Jawerth L, Maharana S, Jahnel M, Hein MY et al (2015) A liquid-to-solid phase transition of the ALS protein FUS accelerated by disease mutation. Cell. 162(5):1066–1077
48. Patel P, Julien JP, Kriz J (2014) Early-stage treatment with Withaferin a reduces levels of misfolded superoxide dismutase 1 and extends lifespan in a mouse model of amyotrophic lateral sclerosis. Neurotherapeutics 12(1):217-33
49. Picher-Martel V, Dutta K, Phaneuf D, Sobue G, Julien JP (2015) Ubiquilin-2 drives NF-kappaB activity and cytosolic TDP-43 aggregation in neuronal cells. Mol Brain 8(1):71
50. Picher-Martel V, Renaud L, Bareil C, Julien JP (2018) Neuronal expression of UBQLN2(P497H) exacerbates TDP-43 pathology in TDP-43(G348C) mice through interaction with ubiquitin. Mol Neurobiol. Epub ahead of print
51. Picher-Martel V, Valdmanis PN, Gould PV, Julien JP, Dupre N (2016) From animal models to human disease: a genetic approach for personalized medicine in ALS. Acta Neuropathol Commun 4(1):70
52. Prasad A, Bharathi V, Sivalingam V, Girdhar A, Patel BK (2019) Molecular mechanisms of TDP-43 Misfolding and pathology in amyotrophic lateral sclerosis. Front Mol Neurosci 12:25
53. Rosen DR, Siddique T, Patterson D, Figlewicz DA, Sapp P, Hentati A et al (1993) Mutations in cu/Zn superoxide dismutase gene are associated with familial amyotrophic lateral sclerosis. Nature. 362(6415):59–62
54. Rothenberg C, Srinivasan D, Mah L, Kaushik S, Peterhoff CM, Ugolino J et al (2010) Ubiquilin functions in autophagy and is degraded by chaperone-mediated autophagy. Hum Mol Genet 19(16):3219–3232
55. Rowland LP, Shneider NA (2001) Amyotrophic lateral sclerosis. N Engl J Med 344(22):1688–1700
56. Sharkey LM, Safren N, Pithadia AS, Gerson JE, Dulchavsky M, Fischer S et al (2018) Mutant UBQLN2 promotes toxicity by modulating intrinsic self-assembly. Proc Natl Acad Sci U S A 115(44):E10495–E1e504
57. Shin Y, Brangwynne CP (2017) Liquid phase condensation in cell physiology and disease. Science. 357(6357):eaaf4382
58. Swarup V, Phaneuf D, Dupre N, Petri S, Strong M, Kriz J et al (2011) Deregulation of TDP-43 in amyotrophic lateral sclerosis triggers nuclear factor kappaB-mediated pathogenic pathways. J Exp Med 208(12):2429–2447

59. Synofzik M, Maetzler W, Grehl T, Prudlo J, Vom Hagen JM, Haack T et al (2012) Screening in ALS and FTD patients reveals 3 novel UBQLN2 mutations outside the PXX domain and a pure FTD phenotype. Neurobiol Aging Elsevier Inc 33(12):2949.e13-7
60. Teyssou E, Chartier L, Amador MD, Lam R, Lautrette G, Nicol M et al (2017) Novel UBQLN2 mutations linked to amyotrophic lateral sclerosis and atypical hereditary spastic paraplegia phenotype through defective HSP70-mediated proteolysis. Neurobiol Aging 58:239.e11–239.e20
61. Vance C, Rogelj B, Hortobagyi T, De Vos KJ, Nishimura AL, Sreedharan J et al (2009) Mutations in FUS, an RNA processing protein, cause familial amyotrophic lateral sclerosis type 6. Science. 323(5918):1208–1211
62. Vengoechea J, David MP, Yaghi SR, Carpenter L, Rudnicki SA (2013) Clinical variability and female penetrance in X-linked familial FTD/ALS caused by a P506S mutation in UBQLN2. Amyotroph Lateral Scler Frontotemporal Degener 14(7–8):615–619
63. Walters KJ, Kleijnen MF, Goh AM, Wagner G, Howley PM (2002) Structural studies of the interaction between ubiquitin family proteins and proteasome subunit S5a. Biochemistry. 41(6):1767–1777
64. Williams KL, Warraich ST, Yang S, Solski JA, Fernando R, Rouleau GA et al (2012) UBQLN2/ubiquilin 2 mutation and pathology in familial amyotrophic lateral sclerosis. Neurobiol Aging 33(10):2527.e3–2527.10
65. Wu Q, Liu M, Huang C, Liu X, Huang B, Li N et al (2015) Pathogenic Ubqln2 gains toxic properties to induce neuron death. Acta Neuropathol 129(3):417–428
66. Xia Y, Yan LH, Huang B, Liu M, Liu X, Huang C (2014) Pathogenic mutation of UBQLN2 impairs its interaction with UBXD8 and disrupts endoplasmic reticulum-associated protein degradation. J Neurochem 129(1):99–106
67. Yang Y, Jones HB, Dao TP, Castaneda CA (2019) Single amino acid substitutions in stickers, but not spacers, substantially Alter UBQLN2 phase transitions and dense phase material properties. J Phys Chem B 123(17): 3618–3629
68. Yla-Anttila P, Vihinen H, Jokitalo E, Eskelinen EL (2009) 3D tomography reveals connections between the phagophore and endoplasmic reticulum. Autophagy. 5(8):1180–1185
69. Zhang C, Saunders AJ (2009) An emerging role for Ubiquilin 1 in regulating protein quality control system and in disease pathogenesis. Discov Med 8(40):18–22

Publisher's Note

Travail Complémentaire N°2

Rédaction d'un chapitre d'ouvrage scientifique

Update on Amyotrophic Lateral Sclerosis, Edited by Humberto Foyaca Sibat,

September 14th 2016, ISBN: 978-953-51-2601-0

Neuronal Intermediate Filaments in Amyotrophic Lateral Sclerosis

P. Codron[1,2,3], Julien Cassereau[1,2], Joël Eyer[4] and Franck Letournel[3,4]

1. UMR CNRS 6015, INSERM U1083, Université d'Angers, Angers, France.

2. Service de Neurologie, CHU d'Angers, Angers, France.

3. Service de Neuropathologie et de Neurobiologie, CHU d'Angers, Angers, France.

4. UPRES EA 3143 Laboratoire de neurobiologie et transgenèse, Université d'Angers, Angers, France.

Chapter 10

Neuronal Intermediate Filaments in Amyotrophic Lateral Sclerosis

Philippe Codron, Julien Cassereau, Joël Eyer and Franck Letournel

Additional information is available at the end of the chapter

http://dx.doi.org/10.5772/63161

Abstract

Neuronal intermediate filaments (NIFs) are the most abundant cytoskeletal element in mature neurons. They are composed of different protein subunits encoded by separate genes such as neurofilament light chain (NFL), neurofilament medium chain (NFM), neurofilament heavy chain (NFH), α-internexin and peripherin. NIFs are dynamic structures playing important functions in cell architecture and differentiation, interactions between proteins or subcellular organelles, and in axonal calibre determination and myelination. Consequently, their presence modulates electrophysiological properties of axons. NIFs have long been assigned a role in the pathogenesis of amyotrophic lateral sclerosis (ALS). Indeed, accumulation and abnormal phosphorylation of NIF subunits in motor neuron are one of the major pathological features in both sporadic and familial forms of the disease. Moreover, mutations in the NFH and peripherin genes and elevated cerebrospinal fluid NIF levels reported in ALS cases, associated with studies in transgenic mice, provided the evidence that primary defects in NIFs could be causative for motor neuron disease. However, the processes leading to the NIF abnormalities and the links to the pathogenesis of ALS remain unclear, leaving a challenging open field for further investigations in this highly disabilitating disease. Here, we review the main characteristics of these NIFs and their involvement in the pathomechanisms of ALS.

Keywords: Intermediate filaments, Neurofilaments, cytoskeleton, amyotrophic lateral sclerosis, tubulin, microtubules, axonal transport

1. Neuronal intermediate filaments

1.1. Characteristics

Intermediate filaments (IFs) are components of the cytoskeleton, together with microtubules (MTs) and microfilaments. IFs are defined by their diameter when examined by transmission electronic microscopy (10 nm), which is intermediate between microtubules (15 nm) and microfilaments (6 nm). They also differ from these two structures by the various sizes and primary organisation of their constitutive proteins, their non-polar architecture and their relative insolubility. Intermediate filaments form a large family of proteins; they are classified into five types according to their gene organisation, size, structure and cell-type expression (**Table 1**). IFs expressed in neurons of the central and peripheral nervous systems are called neuronal intermediate filaments (NIFs) and include nestin, synemin, vimentin, α-internexin, peripherin and neurofilaments (NFs) that are composed of three subunits, neurofilament light chain (NFL), neurofilament medium chain (NFM) and neurofilament heavy chain (NFH) (for low-, medium-, and high-molecular-weight NFs) [1–5].

Neurons express differentially IF proteins depending on their developing stage and their localisation in the nervous system. While nestin, synemin and vimentin are mainly expressed during the neuronal development, NFs, peripherin and α-internexin are the main intermediate filament subunits in mature neurons from the central and peripheral nervous system [6]. In this chapter, we focus on those three subtypes of NIFs.

Type	Name	Cell/tissue
I	Acid keratins	Epithelia
II	Basic keratins	Epithelia
III	Desmin	Muscle
	GFAP	Astroglia
	Peripherin	PNS neurons
	Vimentin	Mesenchyme
IV	Neurofilaments (NFL, NFM, NFH)	PNS and CNS neurons
	α-Internexin	CNS neurons
	Nestin	CNS stem cells
V	Nuclear lamins	Nucleus

IFs found in mature neurons are NFL, NFM, NFH, peripherin and α-internexin. Abbreviations: GFAP, glial fibrillary acidic protein; CNS, central nervous system; PNS, peripheral nervous system [7].

Table 1. Classification of intermediate filaments.

1.2. Expression and post-translational modifications

Genes coding for NFL and NFM (*NEFL* and *NEFM*) are closely linked on chromosome 8 (8p21), while NFH gene (*NEFH*) is located on chromosome 22 (22q12.2) [8–10]. Peripherin is encoded

by *PRPH* located on chromosome 12 (q12–q13) [11], and α-internexin is encoded by *INA* located on chromosome 10 (10q24.33) [3]. As for other IFs, NFs, peripherin and α-internexin share a common tripartite structure, with non-helical amino- and carboxy-terminal regions (head and tail domains) flanking a 46-nm-long central α-helical rod domain composed of approximately 310 highly conserved amino acids [9, 10, 12] (**Figure 1**). These segments are joined by short non-helical linker sequences, aligning the individual IF subunits prior to filament assembly. While peripherin and NFL have a short-tail domain, those of NFM and NFH are longer and contain numerous KSP (Lys-Ser-Pro) repeats that can be phosphorylated on serine (S) residues. These sites are frequently modified by phosphorylation, glycosylation, nitration, oxidation and ubiquitination, which can impact NIF interactions and dynamics [6].

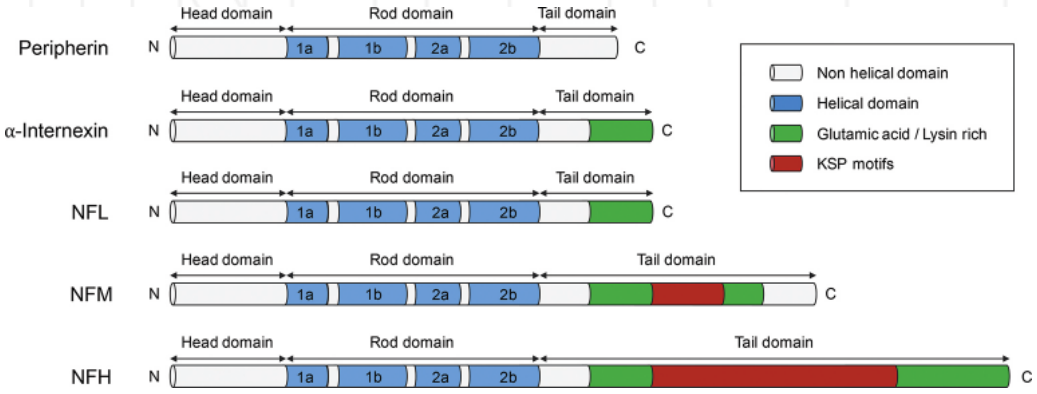

Figure 1. Schematic representation of adult neuronal IF subunits. All NIF subunits share a highly conserved central helical domain of 310 amino acid residues involved in the formation of coiled-coil structures. Flanking this central rod domain are the amino- and the carboxy-terminal domains conferring functional specificity to the different types of NIF proteins. The NFM and NFH carboxy-terminal regions contain Lys-Ser-Pro (KSP) repeats, which can be phosphorylated. Abbreviations: NF, neurofilament; NFL, NF-light; NFM, NF-medium; NFH, NF-heavy; C, carboxy-terminal; N, amino-terminal.

Multiple aspects of IF biology are regulated by their post-translational modifications. The phosphorylation state of NIF proteins depends on a dynamic balance between the activities of kinases and phosphatases. Phosphorylation of the head domain by secondary-messenger-dependent protein kinase A (PKA) and protein kinase C (PKC) prevents NIF subunits assembly or leads to the disassembly of pre-existing filaments [13, 14]. Phosphorylation of the KSP motifs on NFM and NFH tail domains by cyclin-kinase Cdk5 and microtubule-associated protein (MAP) kinase promotes the formation of cross-bridges with MTs and slows NF axonal transport [15, 16]. Phosphorylation of the head and tail domains is closely related; indeed, phosphorylation of NFM head domain by PKA reduces the phosphorylation of tail domain by MAP kinases [17]. This mechanism could be a way to protect neurons from abnormal accumulation of phosphorylated NIFs in perikarya. NIF dephosphorylation is mainly catalysed by phosphatase 2A; dephosphorylation of the head domain is necessary to allow NIF polymerization and transport into the axon, while dephosphorylation of the tail domain facilitates their interaction with other cytoskeletal proteins and their degradation [18, 19].

NIFs are also post-translationally modified by glycosylation and nitration. Glycosylation resides on attachment of *O*-linked *N*-acetyl glucosamine (O-GlcNAc) to S and threonine (T) residues; the precise function of glycosylation is still unknown, but several clues suggest a role in the NIF assembly [20]. NIF nitration is catalysed by superoxide dismutase 1 (SOD1) on tyrosine residues; the nitration of NIFs changes hydrophobic residues into negatively charged hydrophilic residues, thereby disrupting their assembly and stability.

1.3. Transport, assembly and degradation

Following their synthesis in the cell body, NIF proteins are assembled into filamentous structures and transported into the axons. They are transported bidirectionally in the axon along microtubules using kinesin (anterograde) or dynein (retrograde) motor proteins [21, 22]. Studies analysing the transport of green-fluorescent protein (GFP)-tagged NIF subunits have shown that NIFs are transported intermittently in axons, their movements being interrupted by prolonged pauses. Only a small fraction of NIFs moves at any given time and direction, and approximately 97% of NIFs spent their time pausing [23–25]. The direction of NIF transport is modulated by their phosphorylation status, since phosphorylation promotes their release from kinesin and increases their affinity for dynein [22, 26].

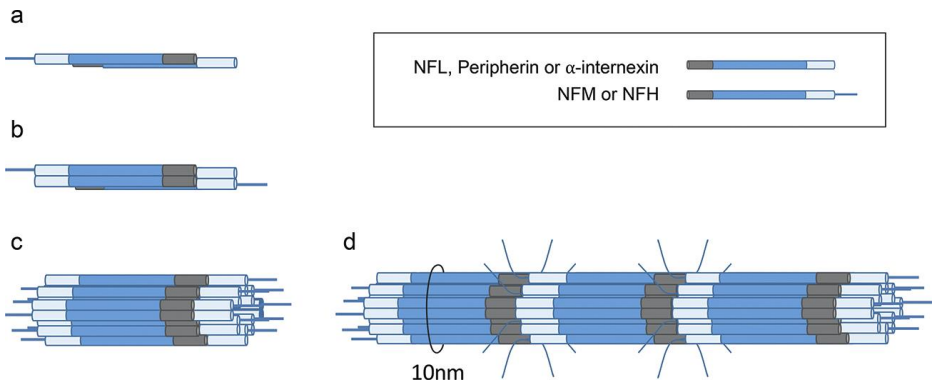

Figure 2. Schematic model of IF assembly in mature neurons. Two NIF subunits (NFL and either NFH or NFM) form head-to-tail coiled-coil dimers (a), anti-parallel half-staggered tetramers (b), protofilaments (c) and 10-nm NF (d). C-terminal domains of NFM and NFH form lateral projections and participate in the stabilisation of the filament network [33].

NIF subunits can assemble into filaments as soon as they are expressed in neurons, depending on their post-translational modifications. Subunits can also disassemble and reassemble during their transport. NIF assembly does not require nucleotide binding or hydrolysis. The first step of the filament formation is the dimerisation of an NFL subunit with either an NFM or an NFH subunit, via the association of their rod domains to form parallel side-to-side coiled-coil dimers. Two coiled-coil dimers line up in a half-staggered manner, forming an anti-parallel tetramer. Tetramers combine to form protofilaments, which finally assemble to constitute the final 10-nm filament [27, 28] (**Figure 2**). The C-terminal domains of NFM and NFH form lateral projections extending from the filament core [29]. Those projections participate to the stabili-

sation of the filament network and interact with other filament structures and subcellular organelles. Peripherin and α-internexin can co-assemble with NFL, NFM and NFH to form NIFs in mature neurons, respectively, in the peripheral and in the central nervous system [30–32]. Thus, NIFs are heteropolymers composed of different subunits, with a ratio changing during neuronal development and activity. This stoichiometry is particularly important and can lead to severe NF disorganisation when unbalanced.

In normal neurons, non-phosphorylated NIFs are found primarily in the soma and proximal axons, while phosphorylated NIFs are located more distal in axons and in terminals [34]. Inside the axon, NIFs are organised into a three-dimensional array interconnected with the other components of the cytoskeleton by several cross-bridges. NIFs, microtubules and actin filaments are interlinked by proteins of the plakin family including, among others, plectin, bullous pemphigoid antigen-1 protein (BPAG1), actin cross-linking factor 7 (ACF7), desmoplakin, envoplakin and periplakin [35–38]. Lateral projections of NFH and NFM tails also fasten adjacent structures (**Figure 3**).

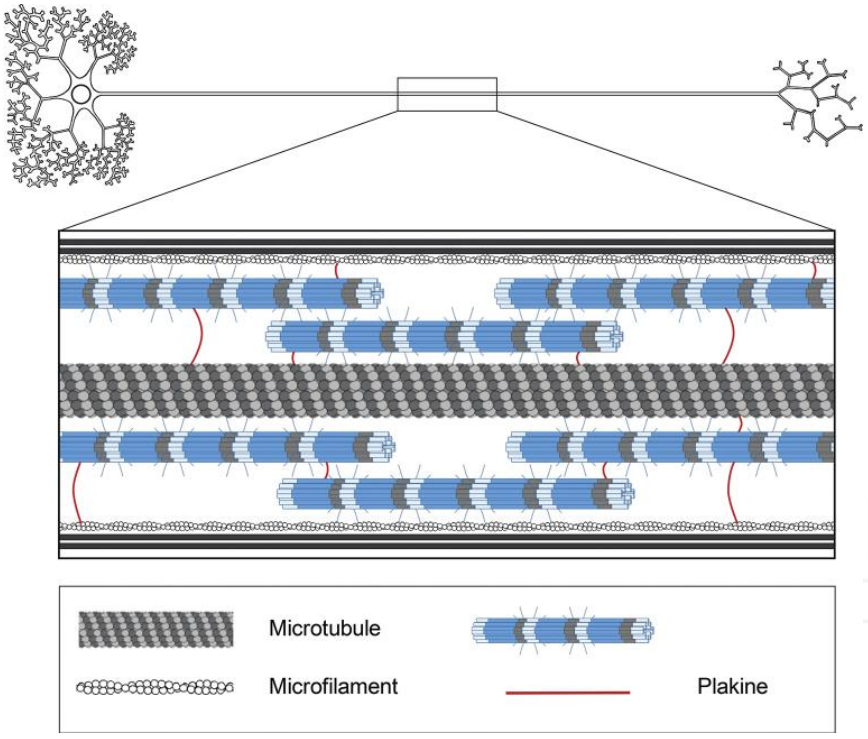

Figure 3. Schematic representation of the cytoskeleton organisation in axons. The components of the axoplasm are organised into a three-dimensional array interconnected by NFM and NFH tails and plakin-family proteins [39].

Following their synthesis, assembly and disassembly, NIFs are slowly transported towards the nerve terminal where they are degraded by specific calcium-activated proteases, such as calpain I, and neutral proteases. NIFs are also degraded by non-specific proteases like

cathepsin D, trypsin and α-chymotrypsin. As mentioned above, post-translational modifications regulate NIF degradation: for example, phosphorylation protects NIFs from proteolysis, while ubiquitination facilitates their degradation [40, 41].

1.4. Roles

As members of the cytoskeletal system, NIFs work together with microtubules and microfilaments to enhance structural integrity and cell shape [42]. In the last decades, it has become increasingly apparent that IFs, instead of being inert, are in fact highly dynamic structures [43] relaying signals from the plasma membrane to the nucleus [44], orchestrating the position and function of cellular organelles [45] and regulating protein synthesis [46]. These interactions are principally mediated through NIF-associated proteins that can modulate NIF structure and function. Linker proteins such as Fodrin, Hamartin or MAP2 are responsible for NIF interactions with filaments and organelles [29, 47, 48], whereas enzymes (principally kinases and phosphatases) modulate their architecture, assembly and spacing.

Another major role recognised for NIFs is to modulate the calibre of axons, with a direct repercussion on the axonal conduction velocity, myelin thickness and inter-nodal length. Indeed, NIF density is correlated with axonal calibre in sciatic nerve fibres of rats and mice [49]. Moreover, the axonal radial growth during axonal development or regeneration coincides with the entry of NFs into axons [50]. In the same way, triple heterozygous knockout mice (NFL±, NFM± and NFH±), with a reduction of NF content but with a normal structure and stoichiometry of the NIF network, exhibit a 50% decrease of the axonal diameter in L5 ventral root [51]. Finally, the disruption of the NFM gene expression or the deletion of its carboxy-terminal domain in mice reduces the inter-filament spacing and axonal calibre, illustrating the preponderant role of NFM in determining axonal diameter [52, 53]. The phosphorylation state of NFM and NFH carboxy-terminal domains might be linked to axon calibre control by regulating NF transport and inter-filament spacing, but the exact mechanisms remain unknown.

Thus, NIFs have a central role in cell architecture, dynamics of the organelles, axon structure and calibre. Therefore, defects in their metabolism could lead to neurodegenerative processes.

2. Implication in amyotrophic lateral sclerosis

2.1. Clinical features

Amyotrophic lateral sclerosis (ALS) is a progressive neurodegenerative disease characterised by the loss of motor neurons of the spinal cord, brain stem and motor cortex. Common clinical symptoms of the disease are progressive paralysis, muscle atrophy and death within 2–5 years usually from respiratory failure [54]. Although most cases are sporadic (sALS), approximately 10% of ALS patients have a positive family history (fALS). To date, there is no curative treatment of the disease.

Primary evidence for a contribution of NIFs in ALS pathogenesis came from neuropathological observations. Most of all, ALS is characterised by the loss and degeneration of upper motor

neurons in the motor cortex (Betz cells), and lower motor neurons in the brainstem (cranial motor nuclei) and spinal cord (anterior horn) [55]. One of the hallmarks of both sporadic and familial ALS is the presence of inclusion bodies in the perikarya of degenerating motor neurons, described as Lewy body-like inclusions (LBLIs), Skein-like inclusions (SLIs) or hyaline conglomerate inclusions (HCIs). Other typical images observed in the disease are motor neurons with swollen argyrophilic perikarya, and large swellings of the proximal part of the axons called spheroids. In immunocytochemical studies, these abnormalities have been shown to contain several proteins, such as ubiquitin or stable tubule-only polypeptide (STOP) [56], but they are particularly reactive for neurofilament subunits [57, 58] and peripherin [59, 60] (**Figure 4**). Interestingly, NIF inclusions in the cell body and the proximal axon are hyperphosphorylated, while as mentioned above in normal neurons NIFs are dephosphorylated in those sites and only phosphorylated in more distal part of the axon.

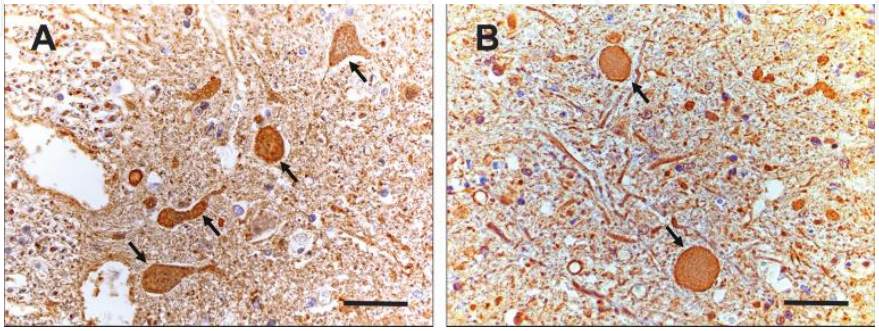

Figure 4. Neuropathological features in ALS. Immunohistochemistry for neurofilaments subunit (phosphorylated form): diffuse labelling in neuronal swelling perikarya (a) and axonal spheroids (b) in ventral horn of cervical spine. Scale bars, 20 μm.

Evidence for the involvement of NIFs in the pathogenesis of ALS has been reinforced in the last 20 years by the discovery of NIF gene mutations linked to the disease. Indeed, codon deletions and insertions in *PRPH* and *NEFH* genes have been identified in several sporadic ALS patients [61–64]. Although these mutations are not considered as a cause of familial ALS, they could be a risk factor for sporadic ALS occurrence.

Other evidences came from several studies showing that cerebrospinal fluid NIF levels are significantly higher in ALS patients than in patients with other neurodegenerative diseases, especially for those with rapidly progressive disease [65, 66]. Although their contributions to ALS pathogenesis remain unclear, all these clinical and neuropathological features suggest that NIFs represent a component of the pathological mechanisms of the disease.

2.2. Animal model contributions

On the basis of these findings, several animal models have been developed, including mice knockout for NIF genes, and mice expressing mouse, human and modified NIF subunits. While deletions of NIF genes have limited phenotype and thus are not extensively used to study ALS

pathogenesis, the axonal calibre reduction seen in knockout mice for NFL, NFM and NFH genes demonstrated that neurofilaments play an important role in the radial growth of axons (**Table 2**). Interestingly, transgenic mice overexpressing either NFL, NFM, NFH, human NFH, peripherin or a mutated NFL show clinical and/or neuropathological alterations similar to those found in ALS (**Table 3**). Finally, in order to investigate NF dynamics, NFH-LacZ and NFH-GFP mice have been generated; while NFs are retained in cell bodies and deficient in axons in NFH-LacZ mice, the fluorescent fusion protein is normally transported along axons in NFH-GFP mice, suggesting that β-galactosidase reporter alters the fusion protein dynamics whereas GFP does not [67, 68]. All these animal models are therefore very useful to study the processes underlying NIF accumulation and their role in motor neuron death.

Mice	Motor dysfunction	Axonal calibre reduction	References
NFL -/-	No	>50%	[69]
NFM -/-	No	>50%	[70]
NFH -/-	No	10%	[71]
α-Internexin -/-	No	No	[72]
Peripherin -/-	No	No	[73]

Table 2. Knockout mice for NIF genes.

Mice	Motor dysfunction	NF inclusions	References
Mouse NFL	Yes	Spinal motor neurons and DRG	[74]
Mouse NFM	No	Spinal motor neurons and DRG	[75]
Mouse NFH	No	Spinal motor neurons and DRG	[76]
Human NFL	No	Thalamus and cortex	[77]
Human NFM	No	Cortex and forebrain	[78]
Human NFH	Yes	Spinal motor neurons and DRG	[79]
Mutated NFL (tail)	Yes	Spinal motor neurons and DRG	[80]
α-Internexin	No	Purkinje cells	[81]
Peripherin	Yes	Spinal motor neurons	[82]

Table 3. Mice overexpressing neuronal IF genes or expressing mutated neuronal IF proteins.

2.3. Pathophysiological hypotheses

Accumulation of neurofilaments in motor neurons undeniably participates in the pathogenesis of ALS, breaking perikarya and axonal structures, disrupting organelles dynamics and interactions, and affecting axonal transport. However, it is still difficult to determine whether

http://dx.doi.org/10.5772/63161

NIF aggregations are the cause or consequence of the disease. For example, the motor neuron loss caused by SOD1G85R mutation is still present despite the absence of NFL in transgenic mice [83, 84], but the animal's lifespan is prolonged by approximately 15%, suggesting an increased neuron toxicity when NFs are present in SOD1-mediated disease.

The mechanisms governing the formation of IF aggregates in ALS remain unclear because multiple factors can potentially induce the accumulation of NIFs. Firstly, these accumulations could result from perturbations of NIF transport through their abnormal phosphorylation, leading to accumulation in cell bodies and in proximal axons. Glutamate excitotoxicity could be involved in this process by activating mitogen-activated protein kinases and protein kinase N1 [85, 86]. Direct disruption of the transport motors themselves could also result in NIF accumulation, as it has been demonstrated in transgenic mice harbouring mutations or modified expression in kinesin and dynein genes [87]. Finally, one of the emerging hypotheses is that the aggregation of NIFs in ALS could result from their altered stoichiometry. Indeed, overexpression of NFL, NFM or NFH in mice provokes NF aggregations and morphological alterations similar to those found in ALS [74–76]. Remarkably, the motor neuron disease caused by excess of human NFH in transgenic mice can be rescued by a correct stoichiometry with the co-expression of human NFL transgene in a dosage-dependent fashion [88]. In a similar way, the onset of peripherin-mediated disease in transgenic mice overexpressing *PRPH* is accelerated by the deficiency of *NEFL* [82], peripherin interacting with NFM and NFH to form disorganised NIF structures. Another interesting point supporting this hypothesis is that NFL mRNA level is 70% decreased in degenerating motor neurons from ALS patients [89]. This could be due to reduced transcript stability, with a possible involvement of mutated SOD1 and TAR DNA-binding protein (TDP-43) that can bind and destabilise NFL mRNA [90, 91].

2.4. The paradox concerning perikaryal versus axonal aggregation of NIF, and the protective effect of perycarial NFH accumulation

Transgenic mice carrying mutant SOD1 transgenes develop neuronal, clinical and pathological features similar to those observed in ALS [92]. Surprisingly, the removal of axonal NIF by crossing the SOD1 transgenic mice with the NFH-LacZ transgenic mice does not affect the pathogenesis induced by SOD1 suggesting that axonal neurofilament aggregation is not the cause of ALS [93]. On the other side, overexpression of mouse NFL and NFH in SOD1G93A mice and overexpression of human NFH in SOD1G37R mice increase their lifespan by, respectively, 15 and 65%, associated with an increase of perycarial NF inclusions and a decrease of axonal spheroids (**Table 4**). Taken together, these last results suggest a protective effect of perikaryal accumulation of NFH proteins in motor neuron disease caused by mutant SOD1. Several hypotheses have been proposed to explain this protective effect. One possibility is that NF proteins may act as calcium chelators thanks to their multiple calcium-binding sites [94]. It also cannot be excluded that the accumulation of NFs could interfere with glutamate receptors and prevent glutamate excitotoxicity [95]. Finally, NF inclusions may act as a phosphorylation sink for cyclin-dependent kinase 5 or for toxic oxygen radical species induced by mutant SOD1, thereby reducing damage to other essential cellular components [96].

Mice	Lifespan	Perycarial NF inclusions	References
SODG85R – NFL -/-	Increased by 15%	No change	[84]
SODG93A – NFL overexpression	Increased by 15%	Increased	[97]
SODG93A – NFH overexpression	Increased by 15%	Increased	[97]
SODG37R – human NFH overexpression	Increased by 65%	Increased	[98]

Table 4. Effects of NF changes in SOD1-mediated disease.

3. Future directions

Implications of NIF abnormalities in the pathogenesis of ALS remain unclear. Despite extensive studies over the past 20 years, it is still unknown how these abnormalities occur and what are their exact contributions to the disease pathogenesis. Understanding how they are formed remains an important objective in the study of both sporadic and familial forms of the disease. Perhaps, the analysis of future generation of mouse models with new familial ALS mutations or conditional control of abnormal NIF proteins will help to address this issue.

Author details

Philippe Codron[1,2,3], Julien Cassereau[2,3], Joël Eyer[4*] and Franck Letournel[1,4]

*Address all correspondence to: joel.eyer@univ-angers.fr

1 Neurobiology and Neuropathology Laboratory, University Hospital of Angers, Angers, France

2 Department of Neurology, University Hospital of Angers, Angers, France

3 UMR INSERM, U771-CNRS6214, University Hospital of Angers, Angers, France

4 UPRES-EA3143, University Hospital of Angers, Angers, France

References

[1] Izmiryan A, Cheraud Y, Khanamiryan L, Leterrier JF, Federici T, Peltekian E, et al. Different expression of synemin isoforms in glia and neurons during nervous system development. Glia. 2006 Aug 15;54(3):204–13.

[2] Julien JP, Mushynski WE. Neurofilaments in health and disease. Prog Nucleic Acid Res Mol Biol. 1998;61:1–23.

[3] Kaplan MP, Chin SS, Fliegner KH, Liem RK. Alpha-internexin, a novel neuronal intermediate filament protein, precedes the low molecular weight neurofilament protein (NF-L) in the developing rat brain. J Neurosci. 1990 Aug;10(8):2735–48.

[4] Lendahl U, Zimmerman LB, McKay RD. CNS stem cells express a new class of intermediate filament protein. Cell. 1990 Feb 23;60(4):585–95.

[5] Portier MM, de Néchaud B, Gros F. Peripherin, a new member of the intermediate filament protein family. Dev Neurosci. 1983–1984;6(6):335–44.

[6] Perrot R, Berges R, Bocquet A, Eyer J. Review of the multiple aspects of neurofilament functions, and their possible contribution to neurodegeneration. Mol Neurobiol. 2008 Aug;38(1):27–65.

[7] Liu Q, Xie F, Siedlak SL, Nunomura A, Honda K, Moreira PI, et al. Neurofilament proteins in neurodegenerative diseases. Cell Mol Life Sci. 2004 Dec;61(24):3057–75.

[8] Hurst J, Flavell D, Julien JP, Meijer D, Mushynski W, Grosveld F. The human neurofilament gene (NEFL) is located on the short arm of chromosome 8. Cytogenet Cell Genet. 1987;45(1):30–2.

[9] Lees JF, Shneidman PS, Skuntz SF, Carden MJ, Lazzarini RA. The structure and organization of the human heavy neurofilament subunit (NF-H) and the gene encoding it. EMBO J. 1988 Jul;7(7):1947–55.

[10] Myers MW, Lazzarini RA, Lee VM, Schlaepfer WW, Nelson DL. The human mid-size neurofilament subunit: a repeated protein sequence and the relationship of its gene to the intermediate filament gene family. EMBO J. 1987 Jun;6(6):1617–26.

[11] Moncla A, Landon F, Mattei MG, Portier MM. Chromosomal localisation of the mouse and human peripherin genes. Genet Res. 1992 Apr;59(2):125–9.

[12] Foley J, Ley CA, Parysek LM. The structure of the human peripherin gene (PRPH) and identification of potential regulatory elements. Genomics. 1994 Jul 15;22(2):456–61.

[13] Hisanaga S, Gonda Y, Inagaki M, Ikai A, Hirokawa N. Effects of phosphorylation of the neurofilament L protein on filamentous structures. Cell Regul. 1990 Jan;1(2):237–48.

[14] Sihag RK, Jaffe H, Nixon RA, Rong X. Serine-23 is a major protein kinase A phosphorylation site on the amino-terminal head domain of the middle molecular mass subunit of neurofilament proteins. J Neurochem. 1999 Feb;72(2):491–9.

[15] Ackerley S, Thornhill P, Grierson AJ, Brownlees J, Anderton BH, Leigh PN, et al. Neurofilament heavy chain side arm phosphorylation regulates axonal transport of neurofilaments. J Cell Biol. 2003 May 12;161(3):489–95.

[16] Nixon RA, Brown BA, Marotta CA. Posttranslational modification of a neurofilament protein during axoplasmic transport: implications for regional specialization of CNS axons. J Cell Biol. 1982 Jul;94(1):150–8.

[17] Zheng Y-L, Li B-S, Veeranna null, Pant HC. Phosphorylation of the head domain of neurofilament protein (NF-M): a factor regulating topographic phosphorylation of NF-M tail domain KSP sites in neurons. J Biol Chem. 2003 Jun 27;278(26):24,026–32.

[18] Saito T, Shima H, Osawa Y, Nagao M, Hemmings BA, Kishimoto T, et al. Neurofilament-associated protein phosphatase 2A: its possible role in preserving neurofilaments in filamentous states. Biochemistry. 1995 Jun 6;34(22):7376–84.

[19] Veeranna null, Shetty KT, Link WT, Jaffe H, Wang J, Pant HC. Neuronal cyclin-dependent kinase-5 phosphorylation sites in neurofilament protein (NF-H) are dephosphorylated by protein phosphatase 2A. J Neurochem. 1995 Jun;64(6):2681–90.

[20] Dong DL, Xu ZS, Chevrier MR, Cotter RJ, Cleveland DW, Hart GW. Glycosylation of mammalian neurofilaments. Localization of multiple O-linked N-acetylglucosamine moieties on neurofilament polypeptides L and M. J Biol Chem. 1993 Aug 5;268(22): 16,679–87.

[21] Shah JV, Flanagan LA, Janmey PA, Leterrier JF. Bidirectional translocation of neurofilaments along microtubules mediated in part by dynein/dynactin. Mol Biol Cell. 2000 Oct;11(10):3495–508.

[22] Yabe JT, Pimenta A, Shea TB. Kinesin-mediated transport of neurofilament protein oligomers in growing axons. J Cell Sci. 1999 Nov;112(Pt 21):3799–814.

[23] Roy S, Coffee P, Smith G, Liem RK, Brady ST, Black MM. Neurofilaments are transported rapidly but intermittently in axons: implications for slow axonal transport. J Neurosci. 2000 Sep 15;20(18):6849–61.

[24] Trivedi N, Jung P, Brown A. Neurofilaments switch between distinct mobile and stationary states during their transport along axons. J Neurosci. 2007 Jan 17;27(3):507–16.

[25] Wang L, Ho CL, Sun D, Liem RK, Brown A. Rapid movement of axonal neurofilaments interrupted by prolonged pauses. Nat Cell Biol. 2000 Mar;2(3):137–41.

[26] Motil J, Chan WK-H, Dubey M, Chaudhury P, Pimenta A, Chylinski TM, et al. Dynein mediates retrograde neurofilament transport within axons and anterograde delivery of NFs from perikarya into axons: regulation by multiple phosphorylation events. Cell Motil Cytoskeleton. 2006 May;63(5):266–86.

[27] Angelides KJ, Smith KE, Takeda M. Assembly and exchange of intermediate filament proteins of neurons: neurofilaments are dynamic structures. J Cell Biol. 1989 Apr;108(4): 1495–506.

[28] Heins S, Wong PC, Müller S, Goldie K, Cleveland DW, Aebi U. The rod domain of NF-L determines neurofilament architecture, whereas the end domains specify filament assembly and network formation. J Cell Biol. 1993 Dec;123(6 Pt 1):1517–33.

[29] Hirokawa N, Glicksman MA, Willard MB. Organization of mammalian neurofilament polypeptides within the neuronal cytoskeleton. J Cell Biol. 1984 Apr;98(4):1523–36.

[30] Beaulieu JM, Robertson J, Julien JP. Interactions between peripherin and neurofilaments in cultured cells: disruption of peripherin assembly by the NF-M and NF-H subunits. Biochem Cell Biol. 1999;77(1):41–5.

[31] Yuan A, Sasaki T, Kumar A, Peterhoff CM, Rao MV, Liem RK, et al. Peripherin is a subunit of peripheral nerve neurofilaments: implications for differential vulnerability of CNS and PNS axons. J Neurosci. 2012 Jun 20;32(25):8501–8.

[32] Yuan A, Rao MV, Sasaki T, Chen Y, Kumar A, Veeranna null, et al. Alpha-internexin is structurally and functionally associated with the neurofilament triplet proteins in the mature CNS. J Neurosci. 2006 Sep 27;26(39):10,006–19.

[33] Szaro BG, Strong MJ. Post-transcriptional control of neurofilaments: new roles in development, regeneration and neurodegenerative disease. Trends Neurosci. 2010 Jan; 33(1):27–37.

[34] Sternberger LA, Sternberger NH. Monoclonal antibodies distinguish phosphorylated and nonphosphorylated forms of neurofilaments in situ. Proc Natl Acad Sci USA. 1983 Oct;80(19):6126–30.

[35] Kowalczyk AP, Bornslaeger EA, Norvell SM, Palka HL, Green KJ. Desmosomes: intercellular adhesive junctions specialized for attachment of intermediate filaments. Int Rev Cytol. 1999;185:237–302.

[36] Ruhrberg C, Hajibagheri MA, Simon M, Dooley TP, Watt FM. Envoplakin, a novel precursor of the cornified envelope that has homology to desmoplakin. J Cell Biol. 1996 Aug;134(3):715–29.

[37] Stappenbeck TS, Green KJ. The desmoplakin carboxyl terminus coaligns with and specifically disrupts intermediate filament networks when expressed in cultured cells. J Cell Biol. 1992 Mar;116(5):1197–209.

[38] Yang Y, Dowling J, Yu QC, Kouklis P, Cleveland DW, Fuchs E. An essential cytoskeletal linker protein connecting actin microfilaments to intermediate filaments. Cell. 1996 Aug 23;86(4):655–65.

[39] Lariviere RC, Julien J-P. Functions of intermediate filaments in neuronal development and disease. J Neurobiol. 2004 Jan;58(1):131–48.

[40] Goldstein ME, Sternberger NH, Sternberger LA. Phosphorylation protects neurofilaments against proteolysis. J Neuroimmunol. 1987 Mar;14(2):149–60.

[41] Gou JP, Leterrier JF. Possible involvement of ubiquitination in neurofilament degradation. Biochem Biophys Res Commun. 1995 Dec 14;217(2):529–38.

[42] Fuchs E, Cleveland DW. A structural scaffolding of intermediate filaments in health and disease. Science. 1998 Jan 23;279(5350):514–9.

[43] Helfand BT, Chang L, Goldman RD. Intermediate filaments are dynamic and motile elements of cellular architecture. J Cell Sci. 2004 Jan 15;117(Pt 2):133–41.

[44] Chang L, Goldman RD. Intermediate filaments mediate cytoskeletal crosstalk. Nat Rev Mol Cell Biol. 2004 Aug;5(8):601–13.

[45] Toivola DM, Tao G-Z, Habtezion A, Liao J, Omary MB. Cellular integrity plus: organelle-related and protein-targeting functions of intermediate filaments. Trends Cell Biol. 2005 Nov;15(11):608–17.

[46] Kim S, Wong P, Coulombe PA. A keratin cytoskeletal protein regulates protein synthesis and epithelial cell growth. Nature. 2006 May 18;441(7091):362–5.

[47] Frappier T, Stetzkowski-Marden F, Pradel LA. Interaction domains of neurofilament light chain and brain spectrin. Biochem J. 1991 Apr 15;275(Pt 2):521–7.

[48] Haddad LA, Smith N, Bowser M, Niida Y, Murthy V, Gonzalez-Agosti C, et al. The TSC1 tumor suppressor hamartin interacts with neurofilament-L and possibly functions as a novel integrator of the neuronal cytoskeleton. J Biol Chem. 2002 Nov 15;277(46):44,180–6.

[49] Friede RL, Samorajski T. Axon caliber related to neurofilaments and microtubules in sciatic nerve fibers of rats and mice. Anat Rec. 1970 Aug;167(4):379–87.

[50] Hoffman PN, Griffin JW, Price DL. Control of axonal caliber by neurofilament transport. J Cell Biol. 1984 Aug;99(2):705–14.

[51] Nguyen MD, Larivière RC, Julien JP. Reduction of axonal caliber does not alleviate motor neuron disease caused by mutant superoxide dismutase 1. Proc Natl Acad Sci USA. 2000 Oct 24;97(22):12,306–11.

[52] Elder GA, Friedrich VL, Bosco P, Kang C, Gourov A, Tu PH, et al. Absence of the mid-sized neurofilament subunit decreases axonal calibers, levels of light neurofilament (NF-L), and neurofilament content. J Cell Biol. 1998 May 4;141(3):727–39.

[53] Rao MV, Campbell J, Yuan A, Kumar A, Gotow T, Uchiyama Y, et al. The neurofilament middle molecular mass subunit carboxyl-terminal tail domains is essential for the radial growth and cytoskeletal architecture of axons but not for regulating neurofilament transport rate. J Cell Biol. 2003 Dec 8;163(5):1021–31.

[54] Kiernan MC, Vucic S, Cheah BC, Turner MR, Eisen A, Hardiman O, et al. Amyotrophic lateral sclerosis. Lancet. 2011 Mar 12;377(9769):942–55.

[55] Hirano A. Neuropathology of ALS An overview. Neurology. 1996 Oct 1;47(4 Suppl 2): 63S–66S.

[56] Letournel F, Bocquet A, Dubas F, Barthelaix A, Eyer J. Stable tubule only polypeptides (STOP) proteins co-aggregate with spheroid neurofilaments in amyotrophic lateral sclerosis. J Neuropathol Exp Neurol. 2003 Dec;62(12):1211–9.

[57] Munoz DG, Greene C, Perl DP, Selkoe DJ. Accumulation of phosphorylated neurofilaments in anterior horn motoneurons of amyotrophic lateral sclerosis patients. J Neuropathol Exp Neurol. 1988 Jan;47(1):9–18.

[58] Troost D, Sillevis Smitt PA, de Jong JM, Swaab DF. Neurofilament and glial alterations in the cerebral cortex in amyotrophic lateral sclerosis. Acta Neuropathol. 1992;84(6): 664–73.

[59] Corbo M, Hays AP. Peripherin and neurofilament protein coexist in spinal spheroids of motor neuron disease. J Neuropathol Exp Neurol. 1992 Sep;51(5):531–7.

[60] He CZ, Hays AP. Expression of peripherin in ubiquinated inclusions of amyotrophic lateral sclerosis. J Neurol Sci. 2004 Jan 15;217(1):47–54.

[61] Al-Chalabi A, Andersen PM, Nilsson P, Chioza B, Andersson JL, Russ C, et al. Deletions of the heavy neurofilament subunit tail in amyotrophic lateral sclerosis. Hum Mol Genet. 1999 Feb;8(2):157–64.

[62] Figlewicz DA, Krizus A, Martinoli MG, Meininger V, Dib M, Rouleau GA, et al. Variants of the heavy neurofilament subunit are associated with the development of amyotrophic lateral sclerosis. Hum Mol Genet. 1994 Oct;3(10):1757–61.

[63] Gros-Louis F, Larivière R, Gowing G, Laurent S, Camu W, Bouchard J-P, et al. A frameshift deletion in peripherin gene associated with amyotrophic lateral sclerosis. J Biol Chem. 2004 Oct 29;279(44):45,951–6.

[64] Leung CL, He CZ, Kaufmann P, Chin SS, Naini A, Liem RKH, et al. A pathogenic peripherin gene mutation in a patient with amyotrophic lateral sclerosis. Brain Pathol. 2004 Jul;14(3):290–6.

[65] Boylan KB, Glass JD, Crook JE, Yang C, Thomas CS, Desaro P, et al. Phosphorylated neurofilament heavy subunit (pNF-H) in peripheral blood and CSF as a potential prognostic biomarker in amyotrophic lateral sclerosis. J Neurol Neurosurg Psychiatr. 2013 Apr;84(4):467–72.

[66] Tortelli R, Ruggieri M, Cortese R, D'Errico E, Capozzo R, Leo A, et al. Elevated cerebrospinal fluid neurofilament light levels in patients with amyotrophic lateral sclerosis: a possible marker of disease severity and progression. Eur J Neurol. 2012 Dec; 19(12):1561–7.

[67] Eyer J, Peterson A. Neurofilament-deficient axons and perikaryal aggregates in viable transgenic mice expressing a neurofilament-beta-galactosidase fusion protein. Neuron. 1994 Feb;12(2):389–405.

[68] Letournel F, Bocquet A, Perrot R, Dechaume A, Guinut F, Eyer J, et al. Neurofilament high molecular weight-green fluorescent protein fusion is normally expressed in neurons and transported in axons: a neuronal marker to investigate the biology of neurofilaments. Neuroscience. 2006;137(1):103–11.

[69] Zhu Q, Couillard-Després S, Julien JP. Delayed maturation of regenerating myelinated axons in mice lacking neurofilaments. Exp Neurol. 1997 Nov;148(1):299–316.

[70] Elder GA, Friedrich VL, Margita A, Lazzarini RA. Age-related atrophy of motor axons in mice deficient in the mid-sized neurofilament subunit. J Cell Biol. 1999 Jul 12;146(1): 181–92.

[71] Jacomy H, Zhu Q, Couillard-Després S, Beaulieu JM, Julien JP. Disruption of type IV intermediate filament network in mice lacking the neurofilament medium and heavy subunits. J Neurochem. 1999 Sep;73(3):972–84.

[72] Levavasseur F, Zhu Q, Julien JP. No requirement of alpha-internexin for nervous system development and for radial growth of axons. Brain Res Mol Brain Res. 1999 May 21;69(1):104–12.

[73] Larivière RC, Nguyen MD, Ribeiro-da-Silva A, Julien J-P. Reduced number of unmyelinated sensory axons in peripherin null mice. J Neurochem. 2002 May;81(3):525–32.

[74] Xu Z, Cork LC, Griffin JW, Cleveland DW. Increased expression of neurofilament subunit NF-L produces morphological alterations that resemble the pathology of human motor neuron disease. Cell. 1993 Apr 9;73(1):23–33.

[75] Wong PC, Marszalek J, Crawford TO, Xu Z, Hsieh ST, Griffin JW, et al. Increasing neurofilament subunit NF-M expression reduces axonal NF-H, inhibits radial growth, and results in neurofilamentous accumulation in motor neurons. J Cell Biol. 1995 Sep; 130(6):1413–22.

[76] Marszalek JR, Williamson TL, Lee MK, Xu Z, Hoffman PN, Becher MW, et al. Neurofilament subunit NF-H modulates axonal diameter by selectively slowing neurofilament transport. J Cell Biol. 1996 Nov;135(3):711–24.

[77] Julien JP, Tretjakoff I, Beaudet L, Peterson A. Expression and assembly of a human neurofilament protein in transgenic mice provide a novel neuronal marking system. Genes Dev. 1987 Dec;1(10):1085–95.

[78] Gama Sosa MA, Friedrich VL, DeGasperi R, Kelley K, Wen PH, Senturk E, et al. Human midsized neurofilament subunit induces motor neuron disease in transgenic mice. Exp Neurol. 2003 Nov;184(1):408–19.

[79] Côté F, Collard JF, Julien JP. Progressive neuronopathy in transgenic mice expressing the human neurofilament heavy gene: a mouse model of amyotrophic lateral sclerosis. Cell. 1993 Apr 9;73(1):35–46.

[80] Lee MK, Marszalek JR, Cleveland DW. A mutant neurofilament subunit causes massive, selective motor neuron death: implications for the pathogenesis of human motor neuron disease. Neuron. 1994 Oct;13(4):975–88.

[81] Ching GY, Chien CL, Flores R, Liem RK. Overexpression of alpha-internexin causes abnormal neurofilamentous accumulations and motor coordination deficits in transgenic mice. J Neurosci. 1999 Apr 15;19(8):2974–86.

[82] Beaulieu JM, Nguyen MD, Julien JP. Late onset of motor neurons in mice overexpressing wild-type peripherin. J Cell Biol. 1999 Nov 1;147(3):531–44.

[83] Larivière RC, Beaulieu J-M, Nguyen MD, Julien J-P. Peripherin is not a contributing factor to motor neuron disease in a mouse model of amyotrophic lateral sclerosis caused by mutant superoxide dismutase. Neurobiol Dis. 2003 Jul;13(2):158–66.

[84] Williamson TL, Bruijn LI, Zhu Q, Anderson KL, Anderson SD, Julien JP, et al. Absence of neurofilaments reduces the selective vulnerability of motor neurons and slows disease caused by a familial amyotrophic lateral sclerosis-linked superoxide dismutase 1 mutant. Proc Natl Acad Sci USA. 1998 Aug 4;95(16):9631–6.

[85] Ackerley S, Grierson AJ, Brownlees J, Thornhill P, Anderton BH, Leigh PN, et al. Glutamate slows axonal transport of neurofilaments in transfected neurons. J Cell Biol. 2000 Jul 10;150(1):165–76.

[86] Manser C, Stevenson A, Banner S, Davies J, Tudor EL, Ono Y, et al. Deregulation of PKN1 activity disrupts neurofilament organisation and axonal transport. FEBS Lett. 2008 Jun 25;582(15):2303–8.

[87] Chevalier-Larsen E, Holzbaur ELF. Axonal transport and neurodegenerative disease. Biochim Biophys Acta. 2006 Dec;1762(11–12):1094–108.

[88] Meier J, Couillard-Després S, Jacomy H, Gravel C, Julien JP. Extra neurofilament NF-L subunits rescue motor neuron disease caused by overexpression of the human NF-H gene in mice. J Neuropathol Exp Neurol. 1999 Oct;58(10):1099–110.

[89] Wong NK, He BP, Strong MJ. Characterization of neuronal intermediate filament protein expression in cervical spinal motor neurons in sporadic amyotrophic lateral sclerosis (ALS). J Neuropathol Exp Neurol. 2000 Nov;59(11):972–82.

[90] Ge W-W, Wen W, Strong W, Leystra-Lantz C, Strong MJ. Mutant copper-zinc superoxide dismutase binds to and destabilizes human low molecular weight neurofilament mRNA. J Biol Chem. 2005 Jan 7;280(1):118–24.

[91] Strong MJ, Volkening K, Hammond R, Yang W, Strong W, Leystra-Lantz C, et al. TDP43 is a human low molecular weight neurofilament (hNFL) mRNA-binding protein. Mol Cell Neurosci. 2007 Jun;35(2):320–7.

[92] Tu PH, Raju P, Robinson KA, Gurney ME, Trojanowski JQ, Lee VM. Transgenic mice carrying a human mutant superoxide dismutase transgene develop neuronal cytoskeletal pathology resembling human amyotrophic lateral sclerosis lesions. Proc Natl Acad Sci USA. 1996 Apr 2;93(7):3155–60.

[93] Eyer J, Cleveland DW, Wong PC, Peterson AC. Pathogenesis of two axonopathies does not require axonal neurofilaments. Nature. 1998 Feb 5;391(6667):584–7.

[94] Roy J, Minotti S, Dong L, Figlewicz DA, Durham HD. Glutamate potentiates the toxicity of mutant Cu/Zn-superoxide dismutase in motor neurons by postsynaptic calcium-dependent mechanisms. J Neurosci. 1998 Dec 1;18(23):9673–84.

[95] Ehlers MD, Fung ET, O'Brien RJ, Huganir RL. Splice variant-specific interaction of the NMDA receptor subunit NR1 with neuronal intermediate filaments. J Neurosci. 1998 Jan 15;18(2):720–30.

[96] Nguyen MD, Larivière RC, Julien JP. Deregulation of Cdk5 in a mouse model of ALS: toxicity alleviated by perikaryal neurofilament inclusions. Neuron. 2001 Apr;30(1):135–47.

[97] Kong J, Xu Z. Overexpression of neurofilament subunit NF-L and NF-H extends survival of a mouse model for amyotrophic lateral sclerosis. Neurosci Lett. 2000 Mar 3;281(1):72–4.

[98] Couillard-Després S, Zhu Q, Wong PC, Price DL, Cleveland DW, Julien JP. Protective effect of neurofilament heavy gene overexpression in motor neuron disease induced by mutant superoxide dismutase. Proc Natl Acad Sci USA. 1998 Aug 4;95(16):9626–30.

Travail Complémentaire N°3

Direction du travail de recherche de Mlle Alexia Bodin

Master 1 parcours Neurobiologie Cellulaire et Moléculaire, Université d'Angers

Année universitaire 2018-2019

Augmentation de la production de collagène dans les fibroblastes en culture issus de patients atteints de Sclérose Latérale Amyotrophique sporadique

A. Bodin[1], P. Codron[1,2,3]

1. UMR CNRS 6015, INSERM U1083, University of Angers, Angers Cedex 9, France.

2. Service de Neurologie, CHU d'Angers, Angers Cedex 9, France.

3. Service de Neuropathologie et de Neurobiologie, CHU d'Angers, Angers Cedex 9, France.

Augmentation de la production de collagène dans les fibroblastes en culture issus de patients atteints de Sclérose Latérale Amyotrophique sporadique.

Alexia BODIN[1], Philippe CODRON[1, 2, 3]

[1] Unité MitoLab, Institut MITOVASC, CNRS 6017, INSERM U1083, Université d'Angers, Angers Cedex 9, France.
[2] Département de Neurologie, Centre SLA, CHU d'Angers, Angers Cedex 9, France.
[3] Département de Neurologie et Neuropathologie, CHU d'Angers, Angers Cedex 9, France.

Abstract

Introduction: Amyotrophic Lateral Sclerosis (ALS) is a neurodegenerative disease affecting central and peripheral motor neurons. One of the main challenges of this pathology is that there is no diagnostic and prognostic marker for the disease. The purpose of this study is to investigate collagen production of cultured fibroblasts from patients with sporadic ALS in order to identify a potential biomarker for the disease. **Methods:** Fibroblasts from 4 ALS patients (1 fast, 1 slow, 2 classic forms) and 4 control subjects were used. Collagen production was quantified using a collagen staining kit with Sirius Red/Fast Green. Structural analysis of collagen was performed by fluorescence microscopy using Sirius Red fluorescence. Similar experiments were conducted on spinal cord samples from an ALS patient and a control subject. **Results:** A significant increase of collagen production in ALS patients' fibroblasts was observed. Similarly, an increase in the amount of collagen was found in the spinal cord of ALS patients. However, no structural difference or localization of collagen was observed between the two groups. **Conclusion:** The increase of collagen production in ALS patients' fibroblasts may constitute a potential diagnostic and prognostic marker for the disease. These results must be confirmed in a larger patient population and by other collagen quantification techniques.

Mots clés : Sclérose Latérale Amyotrophique, Collagène, Fibroblastes

Introduction

La Sclérose Latérale Amyotrophique (SLA), également connue sous le nom de maladie de Charcot en raison du neurologue français l'ayant décrit pour la première fois en 1865, est une maladie neurodégénérative affectant les neurones moteurs du cortex cérébral (centraux) et de la moelle épinière (périphériques). Avec une incidence de 2,5 cas pour 100 000 individus, la SLA survient généralement aux alentours de 60 ans, plus souvent chez l'homme que la femme (1,5/1) [1]. Près de 7000 personnes sont atteintes par la maladie en France, et 2500 nouveaux cas sont diagnostiqués chaque année. Dans 90% des cas la maladie se déclare chez des individus isolés pour des raisons inconnues, elle est alors dite sporadique (sSLA). Plus rarement, les patients sont atteints de la forme héréditaire, dite familiale (fSLA), causée par la transmission de mutations portant sur des gènes de mieux en mieux connus. Cliniquement la dégénérescence des neurones moteurs responsables du mouvement se traduit par une paralysie d'aggravation progressive. En moyenne le décès survient 24 à 36 mois après le diagnostic, et 70% des décès sont causés par une insuffisance respiratoire restrictive sévère [2]. Toutefois la rapidité d'évolution de la pathologie est très hétérogène entre les patients (de quelques mois à plusieurs dizaines d'années), et ne peut être prédite au moment du diagnostic [3]. Aucun traitement curatif de la maladie n'est disponible pour les patients atteints de SLA. Le seul traitement ayant obtenu une autorisation de mise sur le marché est le Riluzole [4], dont l'efficacité reste modeste.

L'absence de traitement et les difficultés à faire émerger des pistes thérapeutiques peuvent s'expliquer par deux faits [5]. D'une part, les mécanismes expliquant la dégénérescence des motoneurones restent incertains. Si deux acteurs semblent se détacher - les inclusions cytoplasmiques de la protéine TDP-43 au sein des neurones et les anomalies de la matrice extracellulaire, en particulier du collagène - la physiopathologie de la SLA demeure mal comprise malgré l'importance des travaux scientifiques

réalisés à ce sujet. D'autre part, il n'existe pas de marqueur diagnostique et pronostic fiable de la maladie. En effet, c'est la réunion d'arguments cliniques, paracliniques et évolutifs qui permettent de retenir le diagnostic [3]. Les essais thérapeutiques conduits pour tester l'efficacité de traitements candidats sont donc difficiles à mettre en place et à interpréter compte tenu de l'hétérogénéité clinique des patients inclus dans ces études. L'identification de biomarqueurs fiable et spécifique de la maladie constitue donc un élément central dans la recherche sur la SLA, tant pour avancer dans la compréhension de la physiopathologie de la maladie que pour mieux diagnostiquer et caractériser la maladie en pratique clinique et homogénéiser les groupes de patients dans les essais.

Ces dernières années, l'identification de biomarqueurs à partir de prélèvements cutanés est devenu un champ important dans la recherche en neurosciences. En effet, les cellules de peau et les cellules neuronales dérivent toutes deux du neuroectoderme. Cette origine embryologique commune a suggéré l'idée que les atteintes neuronales observées dans les maladies neurodégénératives pourraient être retrouvées au niveau des cellules la peau des patients (facilement accessible aux prélèvements), en particulier au sein des fibroblastes. Dans le domaine de la SLA, des études ont démontrées que la peau des patients présente des anomalies de TDP-43, et notamment une augmentation de l'expression de cette dernière [6]. Une augmentation de la densité des fibrilles de collagène a également été retrouvée dans des biopsies de peau de patient touchés par la maladie [7]. Plus récemment, une équipe de recherche a réussi à mettre au point un modèle de peau reconstituée et cultivée en 3D dérivé de cellules cutanées de patients atteints de SLA [8]. Ce modèle d'étude in vitro reproduit les anomalies caractéristiques de la maladie décrites précédemment. Cependant la mise en place de ce model requiert des techniques de culture complexes et onéreuses. Des travaux ont donc été réalisés sur des cultures primaires de fibroblastes en monocouche afin de voir si ces anomalies pouvaient être retrouvées. Cette étude n'a pas permis d'identifier la présence d'agrégats protéiques de TDP-43 dans les fibroblastes de patients atteints de SLA [9]. Malgré un nombre important de paramètres analysés dans cette étude, le collagène au sein des fibroblastes n'a pas été étudié.

Ce travail vise donc à étudier le collagène de fibroblastes en culture monocouche issus de patients atteints de SLA et de sujets contrôles, afin d'identifier un potentiel biomarqueur de la maladie.

Matériel et méthode

Sujets

Les fibroblastes issus de 4 patients atteints de SLA (deux formes classiques, une forme rapide et une forme lente) et de 4 sujets contrôles ont été utilisés. Les fibroblastes ont été obtenus par Punch (biopsie cutanée simple) au niveau de l'avant-bras des sujets sous anesthésie locale, puis congelés et conservés au Centre de Ressources Biologiques (CRB) du CHU d'Angers. Les échantillons utilisés pour cette étude ont été prélevés en 2017 au CHU d'Angers dans le cadre de l'étude FibrALS (ClinicalTrials NCT02969759, CPP 2016/36, ANSM 2016-102600243). En parallèle, des prélèvements de moelle épinière cervicale d'un patient atteint de SLA et d'un sujet contrôle provenant de la banque du laboratoire de Neuropathologie du CHU d'Angers ont été utilisés pour des analyses tissulaires. Les caractéristiques cliniques des sujets sont reportées dans le tableau 1.

Culture cellulaire

Les cultures ont été réalisées dans un laboratoire de culture cellulaire de niveau L2. Après décongélation, les fibroblastes ont étés cultivés en flasques T25 dans du milieu de culture DMEM F-12 avec du SVF décomplémenté, de l'uridine et du pyruvate, et incubées à 37°C + 5% CO_2. Le passage des cellules a été réalisé tous les 2-3 jours et les flasques ont été remplacées tous les 3 passages. Afin de s'affranchir des artéfacts liés à la sénescence, toutes les expériences ont étés effectuées à passage inférieur à 20. Toutes les expérimentations ont été réalisées plusieurs fois (n>3) afin de s'assurer de la reproductibilité et de la constance des résultats.

Etude de la cinétique de croissance cellulaire

La cinétique de croissance des cellules a été étudiée à l'aide du système IncuCyte (ZOOM Essen Biosciences, Ann Arbor, MI). Après ensemencement dans une plaque 24 puits, les cellules ont été placées dans un incubateur équipé d'un portique de microscope connecté à un disque dur externe en réseau. Cet automate a permis

Tableau 1 Caractéristiques cliniques des patients et des témoins. *Abréviations : ALSFRS = Amyotrophic Lateral Sclerosis Functional Rating Scale : Ce score noté sur 48 est utilisé pour évaluer la gravité de l'atteinte motrice des patients atteints de SLA en prenant en compte plusieurs paramètres cliniques.*

	Age à l'inclusion	Sexe	Durée de la maladie (mois)	Evolution clinique	Antécédents médicaux	Traitements	Exposition aux toxiques	Score ALSFRS
SLA 1	54	F	6	Rapide	Non	Non	Non	31/48
SLA 2	65	M	18	Classique	Non	Non	Non	43/48
SLA 3	62	F	24	Classique	Non	Riluzole Anti-dépresseurs	Non	40/48
SLA 4	66	M	144	Lente	Traumatisme crânien bénin, embolisme pulmonaire	Riluzole Baclofène	Non	38/48
Ctrl 1	52	M	-	-	Syndrome Anxio-Dépressif	Anti-dépresseurs	Non	-
Ctrl 2	72	F	-	-	Hypertension artérielle	Anti-hypertenseurs	Non	-
Ctrl 3	69	M	-	-	-	-	Non	-
Ctrl 4	46	F	-	-	-	-	Non	-

d'acquérir à l'aide d'un objectif 10X, 4 images à contraste de phase par puits toutes les 2 heures pendant 100 heures. Puis à l'aide du logiciel de l'automate, un masque a été réalisé afin de mesurer le pourcentage de confluence cellulaire sur chaque photo prise par l'IncuCyte.

Analyse quantitative du collagène

Le kit de coloration du collagène au Sirius Red/Fast Green permet de déterminer le ratio Collagène/Protéines (Co/P) d'un échantillon. En effet, le Sirius Red se lie spécifiquement aux structures hélicoïdales du collagène fibrillaire, indépendamment des différents types de collagène. Le Fast Green en revanche se lie à toutes les protéines qui ne sont pas du collagène. Le Sirius Red et Fast Green ont des longueurs d'ondes d'absorption différentes, 540 nm et 605 nm respectivement, mesurables à l'aide d'un spectrophotomètre.

Pour l'étude du collagène sécrété par les fibroblastes, après ensemencement dans une plaque 24 puits, les cellules ont été fixées au Khale Fixative (eau distillée, éthanol 96%, formaldéhyde 37%, acide acétique glacial) pendant 10 minutes à température ambiante, puis rincées au PBS 1X. Les fibroblastes ont ensuite été colorés à l'aide du Kit de coloration du collagène Sirius Red/ Fast Green (Chondrex, Washington, USA).

Pour l'étude des coupes de moelle épinière, des coupes d'environ 20 micromètres d'épaisseur ont été réalisées à l'aide d'un microtome à lame vibrante Leica VT1000S (Wetzlar, Germany). Les coupes de moelle épinière ainsi obtenues ont été conservées dans du PBS 1X. Puis, les coupes ont été colorées en free floating à l'aide du kit de coloration du collagène Sirius Red/Fast Green.

Les absorbances à 540 et 605 nm des suspensions de colorant élué récoltées ont été mesurées à l'aide d'un spectrophotomètre CLARIOstar, BMG LABTECH (Ortenberg, Germany), et le ratio Co/P a été calculé à partir des densités optiques (DO) obtenues à l'aide des équations suivantes :

Calcul de la quantité de collagène produit :

$$Collagène\ (\mu g/section) = \frac{DO_{540\,nm} - (DO_{605\,nm} \times 0{,}291)}{0{,}0378}$$

Calcul de la quantité de protéines produites :

$$Protéines\ autres\ (\mu g/section) = \frac{DO_{605\,nm}}{0{,}00204}$$

Rapport Collagène/Autres protéines :

$$Rapport\ Co/P = \frac{Quantité\ de\ collagène}{Quantité\ de\ protéines\ autres}$$

Analyse structurelle du collagène par microscopie

Le Sirius Red est également détectable en microscopie à fluorescence dans les longueurs d'onde rouges. Cette propriété a été utilisée pour l'étude structurelle du collagène. Ainsi, les fibroblastes ont étés cultivés dans une plaque 12 puits contenant une lamelle de microscopie dans le fond de chaque puit. Ces fibroblastes ont étés fixés au Khale fixative comme décris précédemment puis colorés au Sirius Red/Fast Green et au DAPI. Le DAPI colore le noyau des cellules et fluoresce en bleu. Les lamelles se trouvant dans le fond des puits, recouvertes par les fibroblastes, ont ensuite étés montées sur des lames de microscopies. De la même manière, les coupes de moelle épinière ont été colorées au Sirius Red/Fast Green en free floating. Une fois colorées, ces coupes ont été montées sur des lames de microscopie.

La microscopie à fluorescence a été réalisée à l'aide d'un microscope inversé NIKON ECLIPSE Ti-E équipé d'un objectif CFI SR APO TIRF 100X ON1.49 et du système Perfect Focus (Nikon Instruments Europe, Amsterdam, Pays-Bas). La microscopie photonique en champ clair a été réalisée à l'aide d'un microscope Zeiss Axioscop40 équipé d'une caméra Axio-cam MRC5 et du logiciel Axiovision (Carl Zeiss Imaging Solutions).

Analyses Statistiques

Les analyses statistiques ont été réalisées à l'aide du logiciel Prism 5 (GraphPad Software, California, USA). Le test non paramétrique de Mann-Whitney a été utilisé pour comparer deux échantillons indépendants de petite taille. L'analyse de la variance ANOVA 1 voie a été utilisée pour comparer les moyennes de plus de 2 groupes, d'échantillons indépendants à 1 facteur d'influence. Le niveau de significativité a été fixé à priori à 5% (0,05).

Résultats

Validation de la méthode

Dans un premier temps, afin de mettre au point un protocole de mesure optimal, l'influence de la confluence des cellules sur la production de collagène a été étudiée. Pour cela des fibroblastes de sujets témoins ont été ensemencés dans une plaque 24 puits en quantité croissante de cellules de façon à créer une gamme de confluence comprise entre $3x10^3$ et $2,5x10^5$ cellules/mL. Après 24 heures de culture, les cellules ont été fixées et colorées à l'aide du kit Sirius Red/Fast Green. Les absorbances à 540 et 605 nm ont été mesurées (Figure 1A). Afin d'évaluer qualitativement la confluence de chaque puit, en parallèle ces cellules ont étés ensemencées aux mêmes concentrations dans une plaque 12 puits puis fixées à 24 heures et colorées au DAPI, pour observation au microscope (Figure 1C). Cette première expérience a permis d'évaluer l'impact de la confluence cellulaire sur la production de collagène, en s'affranchissant du temps de culture. Au vu des résultats, la confluence a un impact sur la production de collagène avec un pic de production à 80% de confluence, puis une diminution de cette production pouvant être en lien avec une surpopulation cellulaire.

Suite à l'obtention de ces premiers résultats, la cinétique de production de collagène en fonction du temps de culture a été étudiée. Des fibroblastes témoin ont été mis en culture à T=0h dans 4 plaques 12 puits. Puis la fixation et la coloration des cellules au Sirius Red/ Fast Green a été réalisée à T=24h, T=48h, T=72h, T=96h. Les absorbances à 540 et 605 nm des suspensions de colorant élué ainsi récoltées ont été mesurées (Figure 1B). Cette approche a permis de déterminer que la production de collagène augmentait avec le temps puis diminuait après 72h, correspondant au seuil de 80% de confluence observé dans l'étude de la production de collagène en fonction de la confluence.

Une gamme de confluence de cellules issues d'un sujet témoin a été ensemencée dans une plaque 24 puits (entre $2x10^4$ et $2x10^5$ cellules par puit contenant 1,5 mL de milieu). L'IncuCyte a permis de déterminer que la quantité de suspension cellulaire à inoculer dans les plaques de culture afin d'avoir une croissance homogène sur 96 heures était comprise entre $2x10^4$ et $4x10^4$ cellules/mL (Figure 1D).

La cinétique de croissance des fibroblastes de témoins de patients SLA a déjà été étudiée précédemment et ne montrait pas de différence en termes de croissance et de morphologie [9]. Compte tenu des résultats obtenus, afin de comparer la production de collagène entre les lignées, nous avons choisi d'ensemencer entre $2x10^4$ et $4x10^4$ cellules par puit et de les fixer et colorer à 72h pour atteindre les conditions optimales.

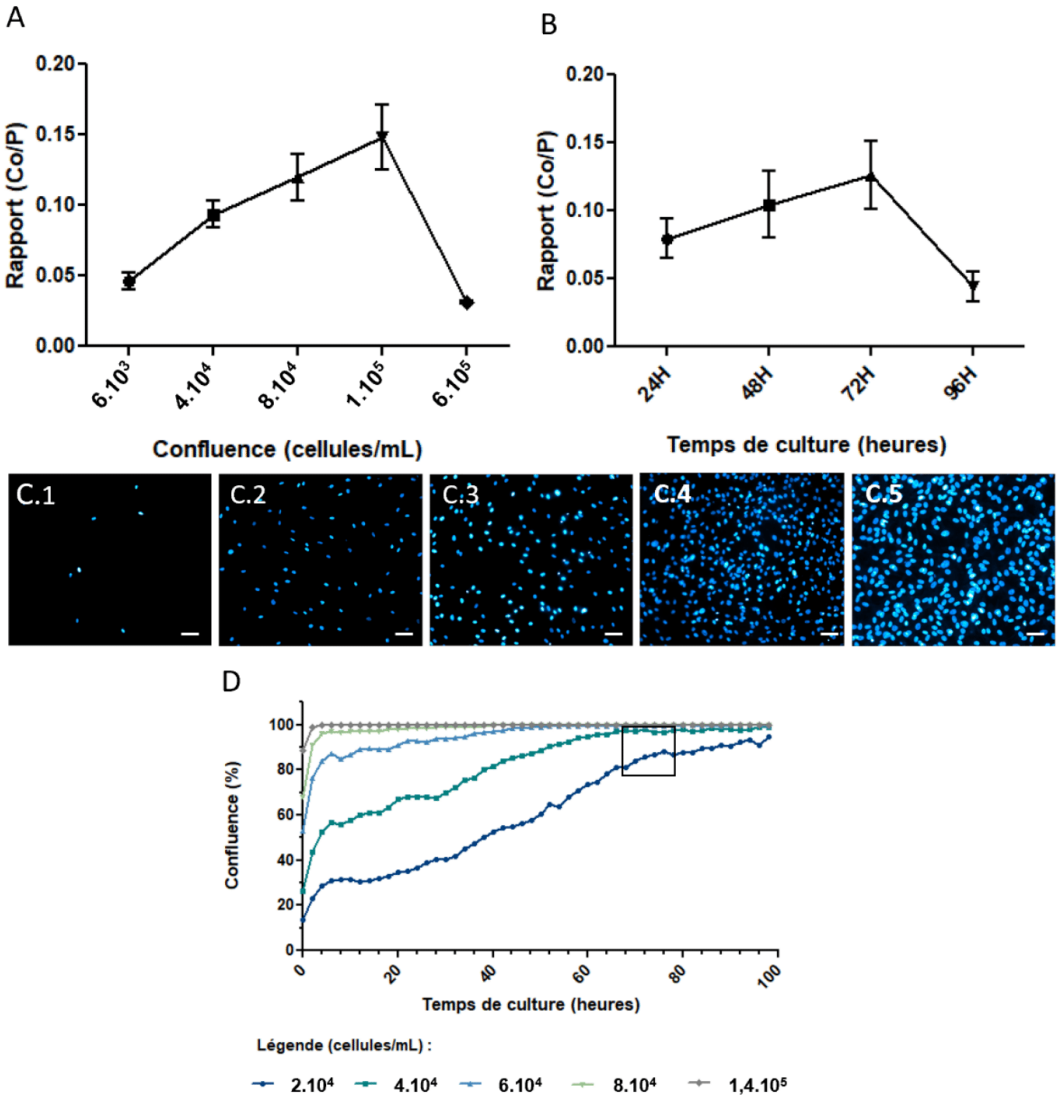

Figure 1 Production de collagène en fonction du temps de culture et de la confluence des fibroblastes. *(A) Rapport de la quantité de collagène sur la quantité de protéines autres (Co/P) en fonction de la confluence des fibroblastes témoins. (B) Rapport Co/P en fonction du temps de culture des fibroblastes témoins. (C) Observation de la confluence des cellules en microscopie à fluorescence : (1) 6.10³cellules/mL = 20% ; (2) 4.10⁴cellules/mL = 40% ; (3) 8.10⁴ cellules/mL = 60% ; (4) 1.10⁵ cellules/mL = 80% ; (5) 6.10⁵ cellules/mL = 90%. Barre d'échelle 50 µm. (D) Confluence des cellules en fonction du temps de culture et en fonction de la quantité de cellules ensemencées.*

Analyse quantitative et structurelle du collagène dans les fibroblastes de patients SLA

L'analyse du collagène produit par les fibroblastes après 72 heures de culture a révélé une augmentation significative du rapport Co/P dans les fibroblastes issus de patients atteints de SLA ($p<0,0001$) (Figure 2A). Plus la forme de SLA était lente, plus le rapport Co/P était augmenté ($p=0,0006$) (Figure 2B). Afin de déterminer si une atteinte structurale du collagène existait dans les fibroblastes de patients atteints de SLA, une imagerie par microscopie à fluorescence a été réalisée sur les fibroblastes fixés et colorés au DAPI et au Sirius Red. L'analyse du collagène dans les fibroblastes ne montrait pas de différence significative entre les sujets témoins (Figure 2C) et les patients atteint de SLA (Figure 2D). Le collagène était réparti uniformément dans le cytoplasme des fibroblastes, et n'a pas été observé dans le milieu extracellulaire.

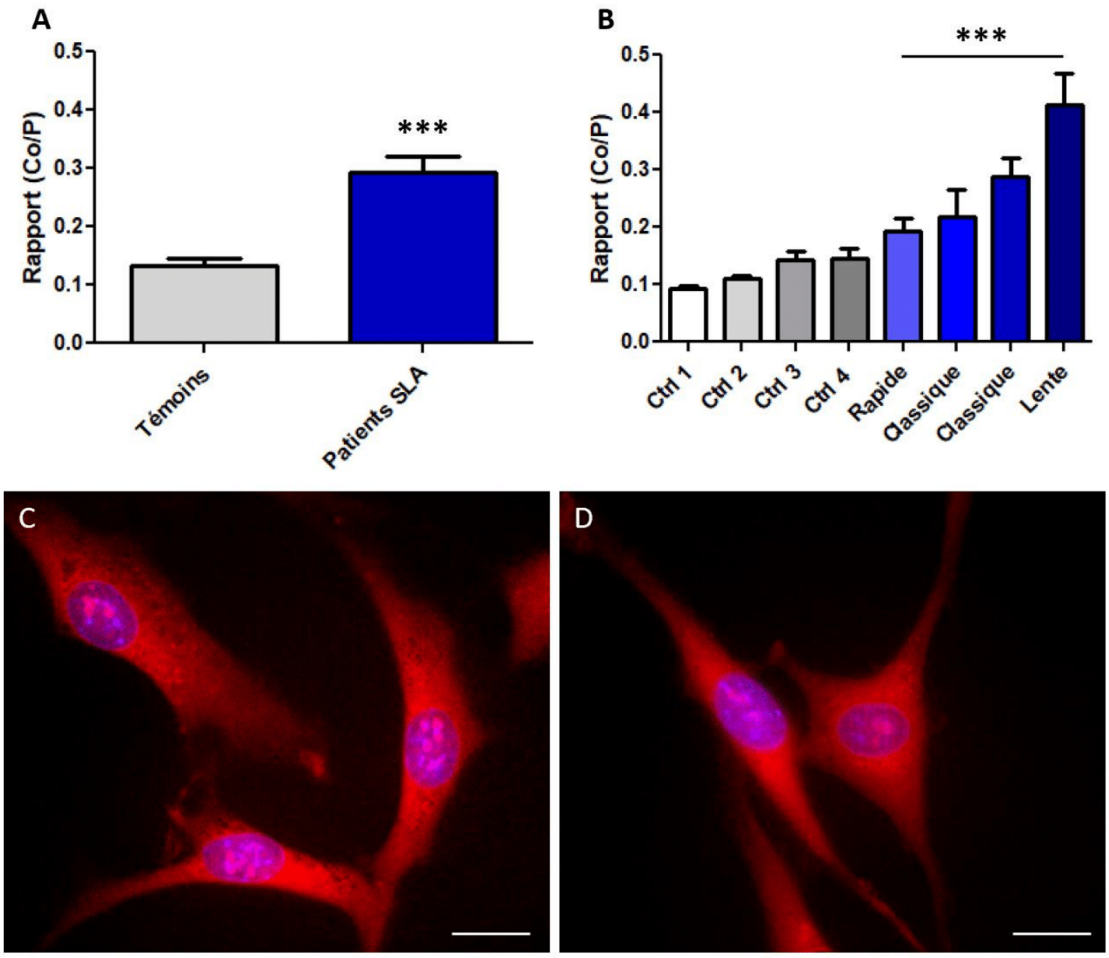

Figure 2 Analyse quantitative et structurelle du collagène dans les fibroblastes de témoins et de patients SLA. *(A) Rapport Co/P dans les fibroblastes de patients SLA comparé aux fibroblastes de témoins (p<0,0001). (B) Rapport Co/P en fonction de la forme de SLA (p=0,0006). Fibroblastes de sujet témoin (C) et de patients SLA (D) colorés au DAPI (bleu) et au Sirius Red (rouge) observés en microscopie à fluorescence. Barre d'échelle 10 µm.*

Analyse quantitative et structurelle du collagène dans la moelle épinière de patients SLA

Les coupes de moelle épinière du patient SLA (Figure 4A) et du témoin (Figure 4B) ont été observées en microscopie photonique en champ clair afin de s'assurer de la présence au sein des coupes de substance blanche et de substance grise (en particulier corne antérieure). L'analyse quantitative du collagène dans les coupes de moelle épinière démontrait une augmentation significative (p=0,0175) du rapport Co/P chez le patient atteint de SLA (Figure 4A). L'analyse structurelle du collagène en microscopie à fluorescence n'a pas été possible compte tenu de l'importance des artéfacts d'autofluorescence (Figure 4D).

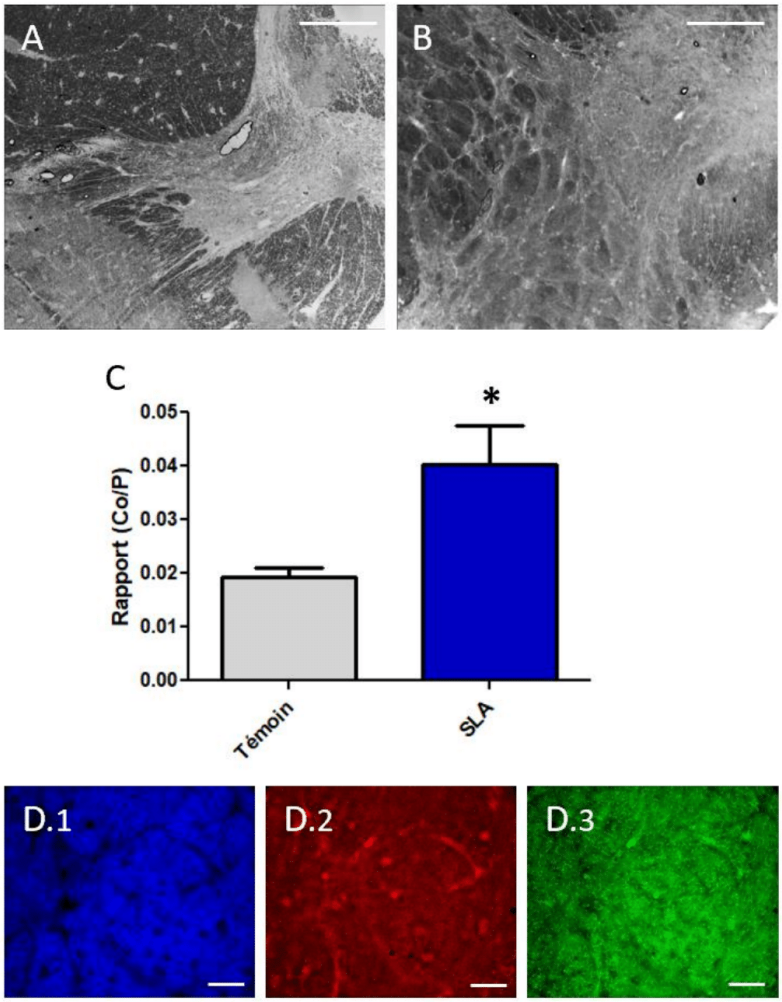

Figure 3 Analyse quantitative et structurelle du collagène dans des coupes de moelle épinière de témoin et de patient atteint de SLA. *Coupe de moelle épinière de patient atteint de SLA (A) et de sujet contrôle (B), colorées au DAPI et au Sirius Red/Fast Green observées au microscope photonique en champ clair, grossissement 5x. (C) Rapport Co/P dans des coupes de moelle épinière de témoin comparé à des coupes de patient atteint de SLA (p=0,0175). (D) Auto-fluorescence de la moelle épinière du sujet contrôle observée en microscopie à fluorescence (1) DAPI, (2) RFP, (3) GFP. (Images similaires obtenues avec la moelle du patient SLA). Barres d'échelle 500 µm (A, B) et 10 µm (D).*

Discussion

Cette étude démontre une augmentation de la production de collagène dans des fibroblastes en culture issus de patients atteints de SLA, en accord avec ce qui a été retrouvé au niveau du système nerveux central (SNC). De plus, cette augmentation de collagène semblait être corrélée à la forme de la maladie, avec une augmentation proportionnelle à la durée de cette pathologie.

A notre connaissance, cette étude est la première portant sur l'analyse du collagène dans les fibroblastes en culture issus de patients atteints de SLA. Même si peu d'études sont réalisées sur le collagène dans la SLA, nos résultats sont en accord avec l'augmentation de la densité des fibrilles de collagène dans le derme des patients SLA observée par *Ono et al* [7]. De plus, les auteurs de cet article avaient également observé une augmentation de la densité des fibrilles en lien avec la durée de la maladie. En revanche, l'augmentation de la quantité de collagène retrouvée dans les prélèvements de moelle épinière de patients SLA est en contraction avec une autre étude menée par la même équipe, et qui démontre une diminution de la quantité de collagène dans la moelle épinière de patients SLA

[10]. Cependant la méthode utilisée pour la quantification du collagène dans cette étude est différente de celle que nous avons utilisés.

L'augmentation du collagène observée dans les fibroblastes de patients SLA peut amener à avancer deux hypothèses. La première étant que cette augmentation de la production de collagène est un mécanisme de défense à la fois au niveau du SNC contre la neurodégénérescence, mais également au niveau de la peau contre la perte motrice. Ces résultats peuvent également nous permettent de penser que l'augmentation de collagène est un mécanisme pathologique central de la SLA, actif au niveau du SNC et dont on observerait le reflet au niveau de la peau compte tenu de leur proximité embryologique.

Afin d'obtenir des résultats les plus fiables possible, notre travail a d'abord consisté à mettre au point une technique de mesure dans le but d'obtenir un protocole optimal. Nous avons utilisé des lignées cellulaires dérivant de patients recrutés prospectivement selon des critères d'inclusion strictes. Toutefois, cette étude n'a été menée que sur 4 patients atteints de SLA et 4 sujets contrôles ce qui en constitue la principale limite, il est donc indispensable d'augmenter l'effectif de patients afin de pouvoir tirer des conclusions fiables. Il serait également important de diversifier les techniques d'étude du collagène, telles que le Western Blot et l'immunofluorescence pour étudier quantitativement et structurellement les différents types de collagène (I, III, VI) dans les fibroblastes. De même, l'étude du métabolisme du collagène par les métalloprotéinases pourrait fournir des informations supplémentaires.

Si la diversification des techniques de quantification du collagène dans les fibroblastes d'un grand effectif de patients atteints de SLA confirme nos premiers résultats, le collagène dans les fibroblastes pourrait alors devenir un potentiel marqueur diagnostique et pronostic de la pathologie. De plus, ceci permettrait également de confirmer l'utilisation de cultures primaires en monocouches de fibroblastes issus de patients comme modèle in vitro de la pathologie, moins couteux et contraignant que le modèle de culture en 3D développé par *Paré et al* [8]. Enfin, ceci permettra de placer le collagène en tant que nouvel acteur dans la physiopathologie de la SLA, permettant d'ouvrir de nouvelles pistes thérapeutiques.

Bibliographie

[1] Association ARSLA, [En ligne], https://www.arsla.org/ (consulté le 8 janvier 2019).

[2] Cintas, P., Corcia, P., Couratier, P., Danel-brunaud, V., Desnuelle, C., Perez, T., Salachas, F., Soriani, M.-H. (2015). Protocole national de diagnostic et de soins (PNDS) Sclerose laterale amyotrophique (ALD9). Haute Autorité de Santé (Has Santé).

[3] Swinnen, B., and Robberecht, W. (2014). The phenotypic variability of amyotrophic lateral sclerosis. Nature Reviews Neurology *10*, 661–670.

[4] Miller, R., Mitchell, J., Lyon, M., and Moore, D. (2002). Riluzole for amyotrophic lateral sclerosis (ALS)/motor neuron disease (MND). In Cochrane Database of Systematic Reviews, The Cochrane Collaboration, ed. (Chichester, UK: John Wiley & Sons, Ltd), CD001447.

[5] Mitsumoto, H., Brooks, B.R., and Silani, V. (2014). Clinical trials in amyotrophic lateral sclerosis: why so many negative trials and how can trials be improved? The Lancet Neurology 13, 1127–1138.

[6] Suzuki, M., Mikami, H., Watanabe, T., Yamano, T., Yamazaki, T., Nomura, M., Yasui, K., Ishikawa, H., and Ono, S. (2010). Increased expression of TDP-43 in the skin of amyotrophic lateral sclerosis. Acta Neurologica Scandinavica.

[7] Ono, S., Toyokura, Y., Mannen, T., and Ishibashi, Y. (1988). Increased dermal collagen density in amyotrophic lateral sclerosis. Journal of the Neurological Sciences 83, 81–92.

[8] Paré, B., Touzel-Deschênes, L., Lamontagne, R., Lamarre, M.-S., Scott, F.-D., Khuong, H.T., Dion, P.A., Bouchard, J.-P., Gould, P., Rouleau, G.A., et al. (2015). Early detection of structural abnormalities and cytoplasmic accumulation of TDP-43 in tissue-engineered skins derived from ALS patients. Acta Neuropathologica Communications *3*.

[9] Codron, P., Cassereau, J., Vourc'h, P., Veyrat-Durebex, C., Blasco, H., Kane, S., Procaccio, V., Letournel, F., Verny, C., Lenaers, G., et al. (2018). Primary fibroblasts derived from sporadic amyotrophic lateral sclerosis patients do not show ALS cytological lesions. Amyotrophic Lateral Sclerosis and Frontotemporal Degeneration *19*, 446–456.

[10] Ono, S., Imai, T., Munakata, S., Takahashi, K., Kanda, F., Hashimoto, K., Yamano, T., Shimizu, N., Nagao, K., and Yamauchi, M. (1998). Collagen abnormalities in the spinal cord from patients with amyotrophic lateral sclerosis. J. Neurol. Sci. 160, 140–147.

[11] Kiernan, M.C., Vucic, S., Cheah, B.C., Turner, M.R., Eisen, A., Hardiman, O., Burrell, J.R., and Zoing, M.C. (2011). Amyotrophic lateral sclerosis. The Lancet *377*, 942–955.

IMPLICATION TECHNIQUE PERSONNELLE

CHAPITRE 1 : COMPREHENSION DES MECANISMES PHYSIOPATHOLOGIQUES.

Étude du cerveau humain à l'échelle nanoscopique par microscopie super-résolutive

- Conception du schéma expérimental, rédaction du projet, des demandes d'autorisation et des appels d'offre pour financement (investigateur principal).
- Contact avec les équipes de recherches pour partenariat.
- Sélection des patients (échantillons) sur dossier médical et neuropathologique.
- Lecture de lames archivées. Microscope : Zeiss Axioscop40 (Carl Zeiss). Logiciel d'acquisition : AxioVisio 4.6 software (Carl Zeiss).
- Récupération des échantillons au centre de ressource biologique et coupe au cryostat Leica CM3050 S (Leica Biosystems).
- Immunomarquage conventionnel ou en free floating des coupes, montage pour analyse.
- Paramétrage du microscope et acquisitions en imagerie conventionnelle ou super-résolutive STORM. Microscope : NIKON ECLIPSE Ti-E (Nikon Instruments). Logiciel d'acquisition : Metamorph (Molecular Devices).
- Traitement d'images (reconstruction 3D et STORM, Z projection, overlay, mesures). Logiciels : Metamorph (Molecular Devices, CA, USA), WaveTracer (Roper Scientific), Imaris 8.0 software (Bitplane).
- Méthodologie et analyse statistique. Logiciel : PRISM version 5.0 (GraphPad).
- Communications orales et affichées des résultats lors de réunions et de congrès nationaux.
- Rédaction du manuscrit (article scientifique en Anglais) et composition des figures. Logiciel de montage : Illustrator (Adobe).

CHAPITRE 2 : MODELES ET BIOMARQUEURS.

Étude de l'ultrastructure et du métabolisme de fibroblastes issues de patients atteints de Sclérose Latérale Amyotrophique sporadique

- Conception du schéma expérimental, rédaction du projet, des demandes d'autorisation et des appels d'offre pour financement (investigateur principal).
- Contact avec les équipes de recherches pour partenariat.
- Étude des dossiers médicaux des patients sélectionnés par les médecins du centre SLA (Dr Cassereau, Dr Pautot, Dr Vieillard).
- Entretien avec patient et entourage pour inclusion dans l'étude, examen clinique et signature du consentement. Tenue du dossier de l'étude.
- Biopsie cutanée par punch après anesthésie locale.
- Culture cellulaire (L2) de fibroblastes obtenus, traitement, induction de stress.
- Étude de la croissance cellulaire par système IncuCyte (Essen Biosciences).
- Analyses biochimiques par Western Blot et Oxygraphie.
- Traitement par sondes (live imaging) ou immunomarquage (cellules fixées) et montage pour analyse en imagerie. Paramétrage du microscope et acquisitions en imagerie épifluorescence 3D, vidéomicroscopie (live imaging) et microscopie super-résolutive STORM. Microscope : NIKON ECLIPSE Ti-E (Nikon Instruments). Logiciel d'acquisition : Metamorph (Molecular Devices).
- Traitement d'images (reconstruction 3D et STORM, Z projection, overlay, mesures). Logiciels : Metamorph (Molecular Devices), WaveTracer (Roper Scientific), Imaris 8.0 software (Bitplane).
- Direction du travail de recherche d'une étudiante en Master 1 parcours Neurobiologie Cellulaire et Moléculaire, Université d'Angers.
- Méthodologie et analyse statistique. Logiciel : PRISM version 5.0 (GraphPad).
- Communications orales et affichées des résultats lors de réunions et de congrès nationaux.
- Rédaction du manuscrit (article scientifique en Anglais) et composition des figures. Logiciel de montage : Illustrator (Adobe). Soumission au journal Amyotrophic Lateral Sclerosis and Frontotemporal Degeneration.

CHAPITRE 3 : PISTES THERAPEUTIQUES.

Injection intrathécale d'une immunoglobuline monoclonale dirigée contre le domaine RRM1 de la protéine TDP-43

- Demande de mobilité auprès du Pr Jean-Pierre Julien pour effectuer un travail de recherche au sein du centre CERVO.
- Participation à la conception du schéma expérimental.
- Culture cellulaire (L1) des lignées HEK293 et Neuro2A.
- Traitements, induction de stress et transfection des lignées.
- Suivi des souris : identification, pesée, performances motrices (Rotarod, Grid test, Wire hanging test, pole test) et cognitives (novel object recognition test, Step-through passive avoidance test).
- Sacrifice des souris après injection létale IP, perfusion, et prélèvement des tissus.
- Préparation des tissus congelés pour analyses biochimiques.
- Préparation des tissus fixés et coupe par microtome SM2000 R (Leica) pour analyses en immunofluorescence.
- Analyses biochimiques (culots cellulaires et échantillons SNC) par Western Blot.
- Immunomarquage conventionnel ou en free floating (culots cellulaires et échantillons SNC), montage pour analyse.
- Paramétrage des microscopes et acquisitions en imagerie conventionnelle par épifluorescence. Microscopes : DM5000 B (Leica Microsystems) et Axio Imager Z1 (Carl Zeiss). Logiciel d'acquisition : Leica Application Suite (Leica Microsystems) et AxioVision (Carl Zeiss).
- Traitement d'images (Z projection, overlay, mesures). Logiciel : ImageJ.
- Méthodologie et analyse statistique. Logiciel : PRISM version 6.0 (GraphPad).
- Communications orales et affichées des résultats lors de réunions et congrès de nationaux et internationaux.
- Rédaction du manuscrit (article scientifique en Anglais) et composition des figures. Logiciel de montage : Illustrator (Adobe).

ABRÉVIATION

AAV : adeno associated virus.

Aβ : Amyloid-β.

ac.p65 : acetylated-p65.

AD : Alzheimer's disease.

ADN : acide désoxyribonucléique.

ADNmt : ADN mitochondrial.

AF : Alexa Fluor.

ALS : amyotrophic lateral sclerosis.

ALSFRS : amyotrophic lateral sclerosis functional rating scale.

AMOF: acute multiple organ failure.

AMP : atrophie musculaire progressive.

ANG : angiogénine.

ANOVA : analysis of variance.

AO : adaptive optics.

APOE : Apolipoproteine E.

ARN : acide ribonucléique.

ARNm : ARN messager.

ARNnc : ARN non codant.

ATP : adénosine triphosphate.

BBB : blood-brain barrier.

BH : brain hemorrhage.

BHE : barrière hémato-encéphalique.

BSA : bovine serum albumin.

CIHR : Canadian institutes of health research.

CLB : cortical Lewy body.

CNRS : **centre national de la recherche scientifique.**

CTF : fragments d'extrémité C-terminale.

DER : dépense énergétique de repos.

DLB : dementia with Lewy bodies.

DMEM : Dulbecco’s modified eagle medium.

STORM : stochastic optical reconstruction microscopy.

DTT : dithiothreitol.

ECAS : Edinburgh cognitive and behavioural ALS screen.

EMCCD : Electron Multiplying Charge Coupled Device.

ES : effet secondaire.

FcR : fragment Fc.

FCS : fetal calf serum.

FI : filaments intermédiaires.

fSLA : sclérose latérale amyotrophique familiale.

FTLD : frontotemporal lobar degeneration.

GRD : Glycin Rich Domain.

GST : glutathione S-transferase.

HEK293 : human embryonic kidney cells.

ICV : intra cérébroventriculaire.

IgG : immunoglobuline G.

IN : intranasal.

INSERM : institut national de la santé et de la recherche médicale.

IP : intrapéritonéal.

iPSC : cellules souches pluripotentes induites.

IT : intrathécal.

IV : intraveineux.

LB : Lewy body.

LCS : liquide cérébro-spinal.

LN : Lewy neurite.

lncARN : long ARN non codant.

LV : Lentivirus.

MAPK : mitogen-activated protein kinase.

MBP : Myelin Basic Protein.

MEF : fibroblastes embryonnaires murins.

MET : microscopie électronique à transmission.

miARN : micro-ARN.

mIgG2A : immunoglobuline G2A murine.

MMPs : Métalloprotéases matricielle.

NES : nuclear export sequence.

Neuro2A : mouse neuroblastoma cells.

NF : neurofilament.

NFH : neurofilament heavy chain.

NFκB : nuclear factor kappa-light-chain-enhancer of activated B cells.

NFL : neurofilament light chain.

NFM : neurofilament medium chain.

NFT : neurofibrillary tangle.

NLS : nuclear localization sequence.

Nrf2 : nuclear factor erythroid 2-related factor 2

PBS : phosphate buffered saline.

PD : Parkinson's disease

PFA : paraformaldehyde.

PRR : pattern-recognition receptor.

PSF : point spread function.

pTau : hyperphosphorylated tau protein

RBP : RNA-binding-protein.

ROS : espèces réactives de l'oxygène.

RRM : RNA recognition motifs.

RT : room temperature.

scFv : fragment monocaténaire recombinant.

SD : standard deviation.

SELFI : self-interference.

SG : granules de stress.

SLA : sclérose latérale amyotrophique.

SLP : sclérose latérale primitive.

SMN : survie des motoneurones.

SNC : système nerveux central.

sSLA : sclérose latérale amyotrophique sporadique.

TDP-43 : Transactive Response DNA-binding protein-43.

TEM : Transmission Electron Microscopy.

TGF-β : transforming growth factor-β.

TIRF : total internal reflection fluorescence.

TLB : typical Lewy body.

UMR : unité mixte de recherche.

VCP : valosin containing protein.

VEGF : vascular endothelial growth factor.

FIGURES

TABLEAUX

UNIVERSITE BIOLOGIE BRETAGNE SANTE LOIRE

université angers

Marqueurs Pathologiques et Pistes Thérapeutiques dans la Sclérose Latérale Amyotrophique Sporadique

Mots clés : SLA, TDP-43, Dynamique mitochondriale, Cytosquelette, Microscopie STORM, Fibroblastes, Immunothérapie.

Résumé : La sclérose latérale amyotrophique (SLA) sporadique est une pathologie neurodégénérative affectant les motoneurones, responsable d'une paralysie diffuse d'aggravation rapidement progressive aboutissant au décès des patients dans les 5 années suivant le diagnostic. Il n'existe à ce jour aucun traitement de la maladie. L'étude des lésions neuronales à l'origine de la maladie, l'identification de biomarqueurs de la SLA, et la mise au point de nouvelles approches thérapeutiques sont les domaines de recherche sur lesquels les efforts sont actuellement concentrés. Le premier objectif de ce travail de thèse a été d'optimiser l'analyse histologique des lésions neuronales observées chez les patients atteints de maladies neurodégénératives grâce à l'utilisation des nouvelles techniques d'imagerie super-résolutive, qui permettent un immunomarquage spécifique à l'échelle nanoscopique. Nos premiers résultats obtenus à partir de la banque de cerveaux du département de Neuropathologie du CHU d'Angers ont permis de caractériser avec précision les agrégats protéiques observés dans les processus de neurodégénérescence, ouvrant un nouveau champ pour l'exploration du tissu cérébral et médullaire des patients atteints de SLA. Le second travail de cette thèse a porté sur l'identification de biomarqueurs de la SLA à partir des hypothèses physiopathologiques impliquant la protéine TDP-43, des déficits mitochondriaux et les anomalies du cytosquelette. Grâce à l'expertise de l'équipe MitoLab (Angers), nous avons exploré l'ultrastructure cellulaire, le métabolisme énergétique et protéique, l'architecture du réseau mitochondrial, et la réponse au stress d'une biocollection de fibroblastes issue de patients atteints de SLA sporadique constituée prospectivement. Nos données ont permis d'objectiver une altération de certaines voies métaboliques, ainsi qu'une augmentation de la synthèse du collagène. Ces résultats font de ces deux paramètres de potentiels marqueurs diagnostique et pronostique de la maladie. La 3ème approche expérimentale de cette thèse a été menée au sein de l'équipe du Professeur J.-P. JULIEN (Institut CERVO Canada). Nous avons étudié l'adressage et l'action d'anticorps ciblant les agrégats de protéine TDP-43 au niveau du système nerveux central. Nos résultats obtenus par immunomarquages fluorescents et études histologiques ont montré l'efficacité de l'adressage du traitement ainsi qu'une diminution des lésions chez des souris transgéniques porteuses de la mutation TDP-43^{A315T}. Sur la base de ces résultats, des projets complémentaires ont été initiés dans la perspective de tester l'efficacité cette nouvelle approche chez l'homme.

Pathological markers and therapeutic prospects in Sporadic Amyotrophic Lateral Sclerosis

Keywords : ALS, TDP-43, Mitochondrial dynamics, Cytoskeleton, STORM imaging, Fibroblasts, Immunotherapy

Abstract : Amyotrophic lateral sclerosis (ALS) is a neurodegenerative disorder affecting both upper and lower motor neurons. The disease is responsible for a progressive paralysis leading to death within 5 years after the symptom onset, with no curative treatment available so far. Studying pathophysiological processes, identifying new biomarkers of the disease, and developing new therapeutic prospects are currently the three main fields of ALS research. In this work, we first aimed to develop a new microscopy technique allowing super-resolutive imaging of the human brain, with the aim of studying tissue samples at the nanoscale level with specific immunostaining. Our results on brain samples from the Neuropathology Department of the University Hospital of Angers allowed us to characterize precisely the architecture of pathological protein aggregates observed in neurodegenerative disorders. Extending this approach to brain and spinal cord samples from patients affected with ALS will contribute to characterize the composition and organization of intra-neuronal lesions, and reveal underlying mechanisms involved in the diseases. Concomitantly, we aimed to identify new ALS biomarkers on the basis of pathophysiological mechanisms involved in the disease. Thanks to the expertise of the research unit MitoLab (Angers), we analyzed the ultrastructural organization, mitochondrial metabolism, stress response and collagen synthesis of controls- and patients-derived skin fibroblasts. Our results highlighted alterations of purine and pyrimidine metabolisms, and an increase of the collagen synthesis in fibroblasts derived from ALS patients. These parameters could be used as markers for ALS diagnosis and prognosis, and may turn out to be valuable tools in clinical practice and therapeutic research. Finally, joining the Canadian research team of Pr Jean-Pierre JULIEN (CERVO Institute, Qc), we participated in the development of a new therapeutic approach in ALS based on the use of monoclonal antibodies targeting pathological TDP-43 aggregates in neurons. The treatment decreased TDP-43 proteinopathy in vitro in cultured neuronal cells, and in vivo in TDP-43^{A315T} transgenic mice models. On the basis of these results, a new research project has started with the aim of humanizing the antibodies to consider immunotherapy for future therapeutic trials